**The Thesis Committee for Julia Liu Jin**
**Certifies that this is the approved version of the following Thesis:**

# An Investigation of Viscoelastic Polymer Flooding in High Permeability Sandstones

**APPROVED BY**

**SUPERVISING COMMITTEE:**

Kishore K. Mohanty Supervisor

Matthew T. Balhoff, Co-Supervisor

# An Investigation of Viscoelastic Polymer Flooding in High Permeability Sandstones

**by**

**Julia Liu Jin**

**Thesis**

Presented to the Faculty of the Graduate School of

The University of Texas at Austin

in Partial Fulfillment

of the Requirements

for the Degree of

**Master of Science in Engineering**

**The University of Texas at Austin**

**August 2019**

# Dedication

To my parents, who always push me and want the best for me; to my brother and wibbs, who always keep me grounded; and to my friends, who always remind me to never give up.

## Acknowledgements

I want to thank my supervisors, Dr. Kishore K. Mohanty and Dr. Matthew T. Balhoff for their mentorship and their endless patience and advice. Their guidance allowed me to constantly learn and improve myself as a researcher and as an engineer.

The entire laboratory staff at the University of Texas at Austin provided an opportunity to work in a collaborative space with like-minded people. Their expertise and support was extremely helpful and I always appreciated their insight. They were always available whenever I had questions, or concerns, or was just stuck on anything. I will always be grateful to Pengpeng Qi, who had the patience and the generosity to introduce me to everything in the labs from the first day I started. A special thanks goes to my undergraduate student, Marc Ponghunsa, who was extremely helpful and always responsible. His help made it possible for me to finish the work in this thesis.

A big thanks goes to the Chemical EOR project sponsors in the Center for Petroleum and Geosystems Engineering for funding this research and the research of so many graduate students like me. As students, we are always grateful for their support.

To my parents: thank you for always standing by and supporting me, regardless of my career goals. To my brother: thank you for always helping me destress with wibbs.

And finally, to my friends who remind me to take care of myself, work hard, and have a little bit of fun while doing it.

**Abstract**

# An Investigation of Viscoelastic Polymer Flooding in High Permeability Sandstones

Julia Liu Jin, MSE

The University of Texas at Austin, 2019

Supervisors: Kishore K. Mohanty, Matthew T. Balhoff

Recovery of oil is the key consideration of oil production in underground reservoirs. The correlated decline in oil discoveries and increase in demand for oil have created a scenario in which enhanced oil recovery (EOR) technologies have become increasingly necessary to compensate for the growing energy demand. Polymer flooding has been used as one EOR technique to increase oil recovery. Several authors have observed reduction of residual oil in porous media using polymers that are viscoelastic.

Five coreflood experiments were completed using aqueous hydrolyzed polyacrylamide (HPAM) and scleroglucan (EOR-grade) polymer solutions. HPAM polymers were solubilized in low salinity brine which created viscoelastic solutions. All experiments were completed in high-permeability (>1000mD) Bentheimer and Boise sandstones. Two Bentheimer cores were chemically treated to be considered oil-wet. Three other water-wet Boise cores were also used. All experiments were completed using light (4-6 cP) oil. The elastic polymer floods were

formulated so that they would have high relaxation times, and therefore high Deborah numbers. Each elastic flood was followed by an inelastic polymer flood with a similar viscosity. The Deborah number for the inelastic polymer floods were less than or close to 1.

Following the successful experiments using alternating elastic and inelastic polymer floods in Bentheimer sandstones, these experiments were conducted in different mediums to see if this phenomenon could be replicated under different circumstances. Experiment #1 replicated previous work completed using viscoelastic polymers and alternating elastic and inelastic floods. The results in coreflood #1 showed extremely promising results in the comparatively more heterogeneous Boise sandstone. After alternating between elastic and inelastic polymer floods, the residual oil saturation decreased to lower than 6%. The viscoelastic polymer floods following a waterflood decreased residual oil saturation. In four of the five experiments, the residual saturation after viscoelastic polymer floods closely matched the predicted saturation given by the Elastic Desaturation Curve (EDC) developed by Qi (2018). Except for one flood, the actual experimental $S_{orp}$ values were within 1-3% of the predicted $S_{orp}$.

## Table of Contents

## List of Tables

## List of Figures

# Chapter 1: Introduction

## 1.1 BACKGROUND AND MOTIVATION

Oil and natural gas are undeniably connected to the United States economy. It is currently the largest energy source, and global energy consumption has been steadily growing each year. Recovery of oil is the key consideration of oil production in underground reservoirs. The correlated decline in oil discoveries and increase in demand for oil have created a scenario in which enhanced oil recovery (EOR) technologies have become increasingly necessary to compensate for the growing energy demand. Primary and secondary recovery methods, such as artificial lift or waterflooding, target mobile oil in the reservoir.

Waterflooding as a secondary recovery method that can greatly improve recovery factors beyond primary recovery methods, but can still leave over 50% of the original oil in place (OOIP).The injected water, a low-viscosity displacing fluid, bypasses some of the oil and is referred to as unswept or bypassed oil, other remaining oil is referred to as residual oil, which is trapped due to capillary forces. EOR methods are employed to recover some the remaining oil when the target of recovery is substantial and it is financially worth pursuing (Sorbie, 1991; Abidin, 2012). Polymer flooding has been used as one EOR technique to increase oil recovery. Polymers increase injectant viscosity, lowering the mobility ratio, and thus improving volumetric sweep efficiency (Lake, 1989; Sheng 2010).

Further studies (Wreath, 1989; Ranjbar, 1992; Garrouch, 1999; Kamal, 2015; Sheng, 2015; Erincik, 2018; Qi, 2018) have shown that residual oil saturation can be reduced by using polymers, and in particular, viscoelastic polymers that exhibit non-Newtonian rheological behavior. Ranjbar et al. (1992) proposed a viscoelastic model that described the flow of

viscoelastic polymers through porous media. To quantify viscoelastic effects, they derived a model based on Maxwell-Fluid-Relation. Their model index, $\dot{E}$, represented the viscoelasticity within the pore space and they found a relationship between viscoelasticity and displacement efficiency. They used natural and artificial cores and partially hydrolyzed acrylamide polymers to examine the influence of viscoelasticity of polymers on flow and oil recovery. In one of their experiments, after a waterflood, a 0.5 PV slug of polyethylenglycol reduced oil saturation. They determined that a critical injection rate is dependent on the polymer concentration, core permeability, salinity, temperature, and polymer molecular weight. Garrouch et al. (1999) described a polymer viscosity model that used an average porous media power-law constant and polymer elasticity. Steady-state flow experiments using polysaccharides and partially hydrolyzed polyacrylamides in bead pack and Berea sandstone showed a non-linear flow relationship similar to the capillary-tube model. They developed a "viscosity number" that was calculated from the power-law exponent, rock permeability, porosity, fluid flow velocity, and found that it correlated with the pressure gradient inside the porous medium. It has also been hypothesized that viscoelastic polymers can reduce residual oil saturation by creating areas of higher stresses at pore throats that can potentially mobilize trapped oil (Afsharpoor and Balhoff, 2013; Ehrenfried 2013), or that viscoelastic polymers can prevent oil droplets from "snapping" (Huh and Pope, 2008).

Several authors have observed reduction of residual oil in porous media using polymers that are viscoelastic. Wang et al. (2000, 2001, 2007) used HPAM polymers to reduce residual oil saturation in Daqing oilfield cores. They found that polymers with higher concentrations (and subsequently higher relaxation times) reduced residual oil saturation the most. Vermolen et al.

(2014) completed four core floods that showed a reduction in residual oil saturation in lower viscosity crude oil. They only noted this reduction when there is an increase in polymer viscosity or flow rate, and when the polymer is highly viscoelastic. Clarke et al. (2016) also observed a reduction in residual oil saturation at lower capillary numbers in elastic HPAM floods in Bentheimer cores. Qi et al. (2017) performed corefloods using homogenous Bentheimer cores and viscous (~150 cp) oil and demonstrated a reduction in residual oil saturation with increasing elasticity (characterized by the dimensionless Deborah number), supporting the hypothesis that viscoelastic polymers can significantly impact residual oil saturation. Further investigations by Erincik et al. (2017) and Erincik (2017) showed that after reduction of residual oil by polymers that were viscoelastic (and relatively low salinity), injection of less elastic polymers (with higher salinity) could recover additional oil. Erincik (2017) and Qi (2018) completed many coreflood experiments investigating the effects of viscoelastic polymers primarily in homogenous Bentheimer cores using both high and low viscosity oils at relatively high pressure gradients. The key objectives of this work are to expand upon these experiments by working with lower pressure gradients, different polymers and molecular weights, and alternative mediums, such as Boise and oil-wet sandstones.

## 1.2 CHAPTER DESCRIPTIONS

This thesis contains five chapters. Chapter 2 includes background information about chemical EOR and a literature review of polymer flooding, viscoelasticity and other relevant experiments. Chapter 3 describes the materials and methods of the experiments that are performed. The experimental results are presented in Chapter 4 for five different corefloods using Boise and chemically modified oil-wet Bentheimer sandstones using viscoelastic

polymers. Chapter 5 summarizes conclusions from the experiments and suggestions for future work.

# Chapter 2: Background and Literature Review

## 2.1 BACKGROUND

Recovery of oil is the key consideration of oil production in underground reservoirs. As the need for oil increases, and as global energy consumption steadily grows, it has become increasingly necessary to develop new enhanced oil recovery (EOR) technologies in order to supply enough oil to meet the increasing energy demand. As the number of new reservoirs being discovered decreases, improving EOR technology can help produce additional oil beyond waterflooding or other primary recovery techniques.

## 2.2 EOR TECHNIQUES

Reservoirs undergo up to three different stages of recovery as defined by the Society of Petroleum Engineers (SPE) and shown in Figure 2.1 (Lake, 2014). Primary and secondary recovery methods, such as artificial lift or waterflooding can target mobile oil in the reservoir (Sorbie, 1991). Tertiary recovery is considered EOR, and targets the oil that cannot be produced due to capillary and viscous forces. EOR recovery methods comprise of thermal, gas, chemical or other alternative injections. These oil production methods progress in a fashion from primary to tertiary/EOR or whenever it is no longer economical to produce hydrocarbon. Thus, EOR methods are employed when the target of recovery is substantial and it is financially worth pursuing.

EOR is capital and resource intensive, due to high injectant costs. Optimization of EOR usage in oil recovery is necessary to efficiently produce oil at a productive cost. In chemical enhanced oil recovery (CEOR), the primary goal is to recover additional oil after primary and secondary recovery by either reducing the mobility of the water injection, or reducing the

interfacial tension of the oil through surfactants or alkalis. CEOR methods include polymer flooding, surfactant-polymer flooding (SP), and alkaline-surfactant-polymer (ASP) flooding. Surfactants can be used to recover residual oil primarily by reducing interfacial tension (IFT) while polymers are used to improve displacement and volumetric sweep efficiency. For example, in sandstone formations, chemical EOR methods have been implemented as these types of reservoirs have shown the highest potential to be implemented and correlated in good field examples (Alvarado, 2010). In particular, chemical EOR methods have been used mostly in sandstone reservoirs, with the number of active projects increasing over the years. As the experiments in this research focus solely on polymer flooding, this thesis focuses primarily on that particular chemical EOR method.

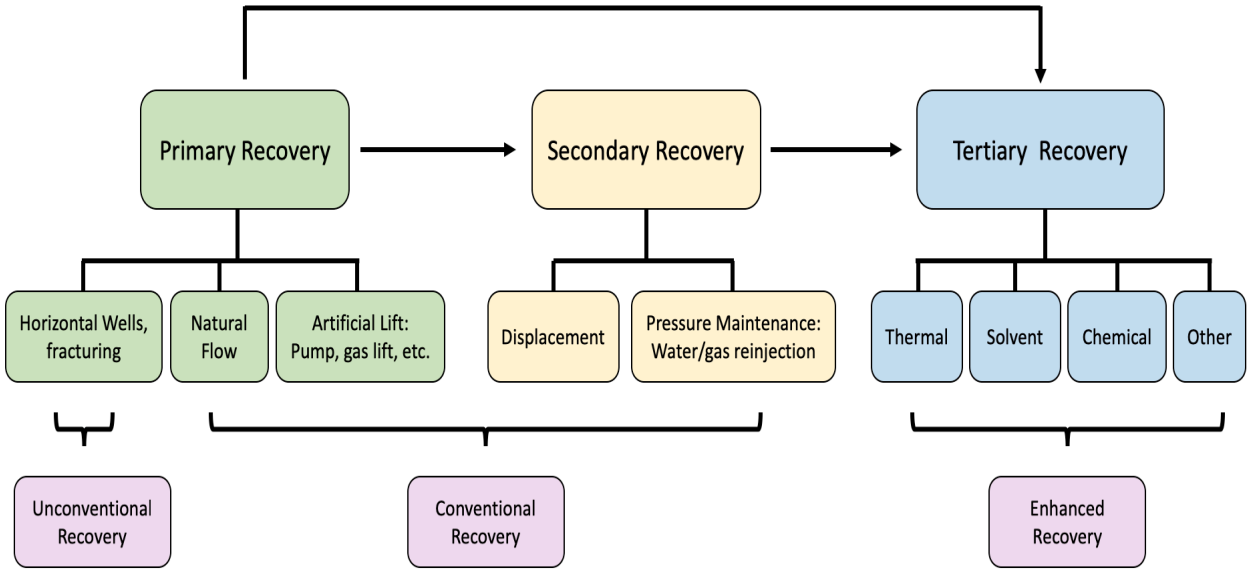


Figure 2.1: Classification breakdown of oil recovery (adapted from Lake et al. 2014).

### 2.2.1 POLYMER FLOODING

Polymer flooding in enhanced oil recovery is a method that is usually used to recover unswept or bypassed oil left in reservoirs. When conducting a polymer flood, a viscosity enhancing polymer is added in water to decrease the fluid mobility and subsequently improve the sweep efficiency of the injection flood (Lake, 1989). While the primary objective for polymer flooding is to alter the fluid viscosity, oil recovery can become more efficient through the effect of polymers on fractional flow, altering water/oil mobility, and/or diverting injected water thus increasing sweep efficiency (Needham, 1987). Most polymer floods have been implemented in sandstones, while carbonates remain a major challenge (Kokal, 2010). The most common polymer used in experiments are the polyacrylamide group (Abidin, 2012). Recent laboratory and field work have suggested that these polymers, which are often viscoelastic, can help reduce the residual oil saturation in reservoir rocks.

## 2.3 UNSWEPT AND RESIDUAL OIL

### 2.3.1 Unswept Oil

Remaining oil can be defined as oil that has just been unswept. The amount of unswept oil is dependent upon the mobility ratio (which is dependent on the fluid properties such as viscosity) and could theoretically be recovered if given enough time or enough injected pore volumes of displacing fluid. It is different from residual oil in that residual oil is oil that is trapped by capillary forces and can only be produced by either increasing the capillary number, or by the reduction of interfacial tension (IFT).

### 2.3.2 Residual Oil Saturation

Residual oil is defined as oil ganglia trapped in various pore throats by capillary forces. Saturation of residual oil can depend on variables such as pore size distribution, interfacial tension, or wettability. At smaller pore throats, capillary forces are balanced by viscous forces from displaced fluids, and the isolated oil droplets become trapped (Green and Willhite, 1998). The trapped droplets are held in place by the capillary forces (Figure 2.2).

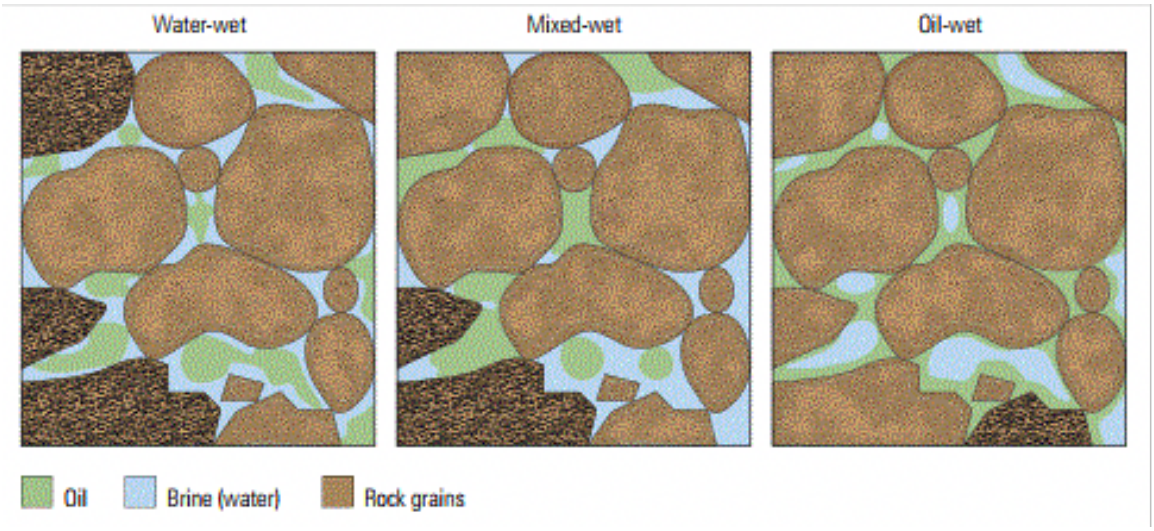


Figure 2.2: Trapped oil in various mediums. Oil droplet distribution vary between different wettability environments (Ziauddin et al. 2007).

## 2.4 MOBILITY CONROL AND CAPILLARY FORCES

Two parameters that are important in the evaluation of EOR research are the mobility ratio and the capillary number.

### 2.4.1 Mobility Ratio

The mobility ratio (M) is defined as the ratio of the mobility ($\lambda$) of the displacing fluid to the displaced fluid, represented as:

$$M = \frac{\lambda_{displacing\ fluid}}{\lambda_{displaced\ fluid}} = \frac{\left(\frac{k_{r_{displacing}}}{\mu_{displacing}}\right)}{\left(\frac{k_{r_{displaced}}}{\mu_{displaced}}\right)} = \frac{k_{r_{displacing}}\mu_{displaced}}{k_{r_{displaced}}\mu_{displacing}} \quad (2.1)$$

where $k_r$ is the relative permeability of various fluid phases (water, oil, polymer) and $\mu$ is the viscosity of the fluid (Lake et al. 2014; Green and Willhite, 2018). Displacement is considered stable or favorable when mobility is less than one (<1) and can improve sweep efficiency and oil recovery. As seen in Equation 2.1, mobility can be controlled directly by increasing the viscosity of the injected/displacing fluid. When mobility is unfavorable, it can result in unstable displacement and viscous fingering can occur, resulting in unswept oil. As previously discussed, this unswept oil could theoretically be recovered and produced if given enough time or injected displacing fluid. While unswept oil is mobility ratio and time dependent, residual oil saturation is independent of those factors.

### 2.4.2 Capillary Number

The capillary number ($N_c$) is a dimensionless number representing the ratio of viscous forces to interfacial forces (Stegemeier, 1977; Chatiz and Morrow, 1984; Lake et al. 2014) and is defined as:

$$N_c = \frac{k\nabla\Phi}{\sigma} = \frac{k\left(\frac{\Delta P}{L}\right)}{\sigma} \quad (2.2)$$

where $k$ is the single-phase permeability of brine, $\nabla\Phi$ is the flow potential gradient, and σ is the interfacial tension between fluids (usually brine/polymer and oil).

The trapping number ($N_T$) is a generalized version of the capillary number which includes the viscous, capillary, and buoyance forces together into one "trapped phase" (Jin, 1995; Pope et al. 2000).

$$N_T = \frac{\left|\vec{\vec{k}}\left(\vec{\nabla}\Phi + g(\rho_w - \rho_o)\vec{\nabla}D\right)\right|}{\sigma} \tag{2.3}$$

where $g$ is the gravitational acceleration, $D$ is the depth, $\rho_w$ is the density of water (or the displacing fluid), $\rho_o$ is the density of the oil (or displaced fluid), and $\sigma$ is the IFT between the displacing and displaced fluid.

In the absence of gravitational forces, the potential gradient in equation 2.2 can be simplified to the pressure gradient. The experiments in this thesis are completed in a linear core and in a way so that gravitational forces are ignored. Capillary number has been defined by others as:

$$N_c = \frac{\mu u}{\sigma} \tag{2.3}$$

where $u$ is the Darcy flow velocity (q/A). In this work we primarily used equation (2.2) for calculations.

It has been observed that when capillary numbers are low, the residual oil saturation is nearly constant with capillary number, but residual oil saturation decreases with $N_c$ beyond a critical capillary number. This relationship can be observed in a capillary desaturation curve (CDC). A general CDC is represented in Figure 2.3.

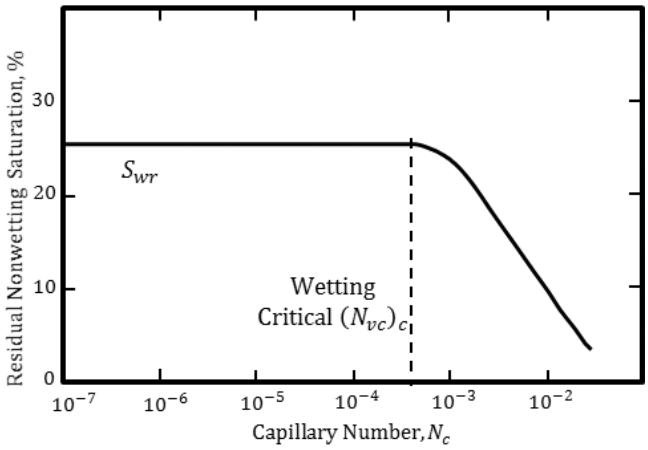

Figure 2.3: Example of CDC (adapted from Lake, 2014).

The CDC and critical capillary number for a particular porous medium depends on the pore size distribution, wettability, and rock type. Generally speaking, in most sandstones, the critical $N_c$ is around $10^{-4}$ to $10^{-6}$. At reservoir conditions where the frontal velocity is on the order of 1 ft/day and pressure gradients are generally below 1 psi/ft, the capillary number is usually well below he critical capillary number unless the interfacial tension is decreased significantly (e.g. using surfactants). However, in laboratory conditions, it may be possible to exceed the critical value. In the experiments studied in this work, it is important for the $N_c$ to remain below the critical $N_c$ so that any reduction in residual saturation is not due to capillary desaturation. Capillary desaturation curves for both Bentheimer sandstones and Boise sandstones were developed experimentally by Qi et al. (2017) and Chatiz and Morrow (1984), respectively, in Figures 2.4 and 2.5.

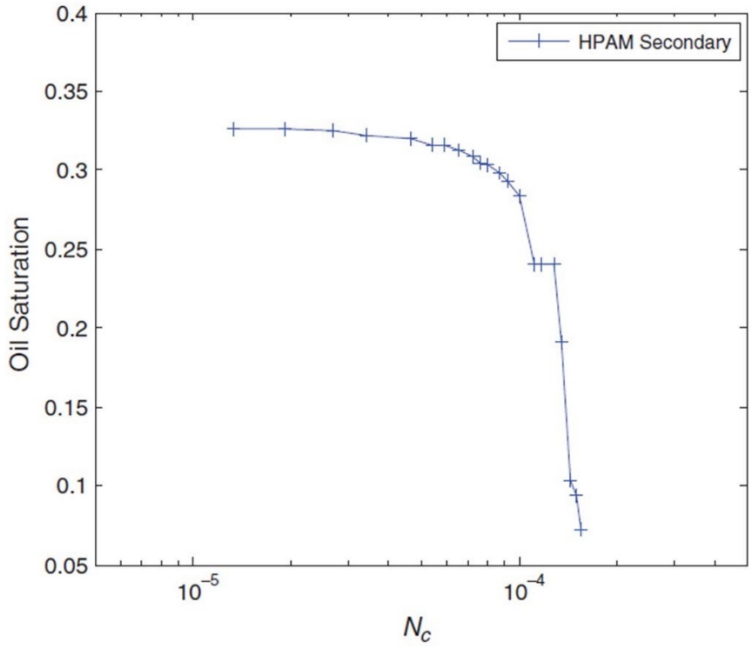


Figure 2.4: CDC for Bentheimer sandstone (Qi et al. 2017).

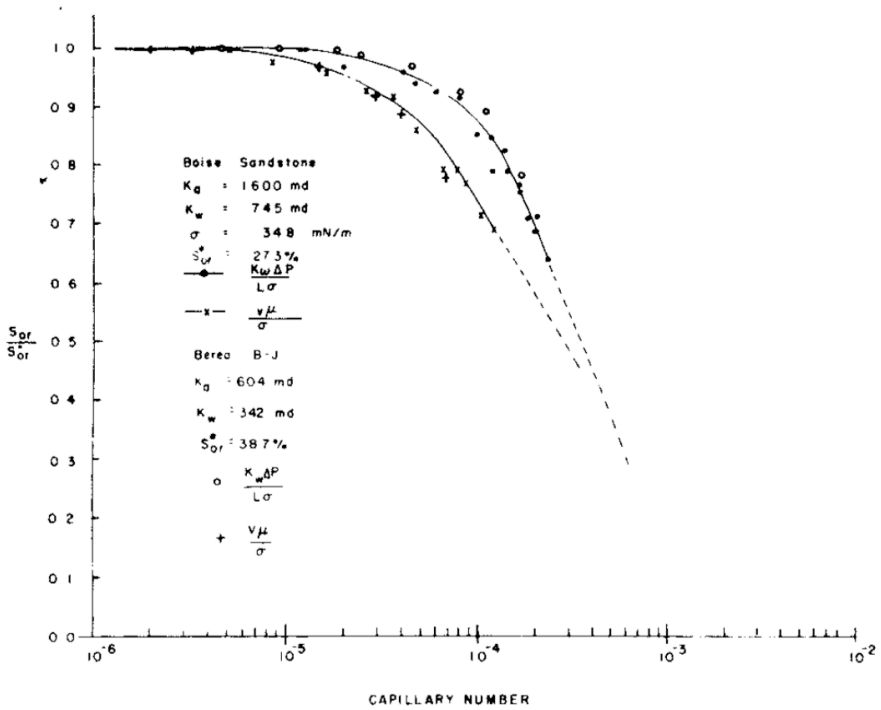


Figure 2.5: Comparison of normalized residual oil vs. capillary number in Boise and Berea sandstones (Chatiz and Morrow, 1984).

The CDC and subsequently critical $N_c$, will change if wettability is altered. Humphry et al. (2014) investigated the effect of wettability on residual oil saturation and CDC in outcrop Berea sandstones. Rock wettability was characterized by spontaneous imbibition and measured using the centrifuge technique. Humphry et al. (2014) determined that as a rock system (in this case, a sandstone) became less water wet, the residual oil saturation decreases and the critical $N_c$ increases to at least one order of magnitude higher (Figure 2.6).

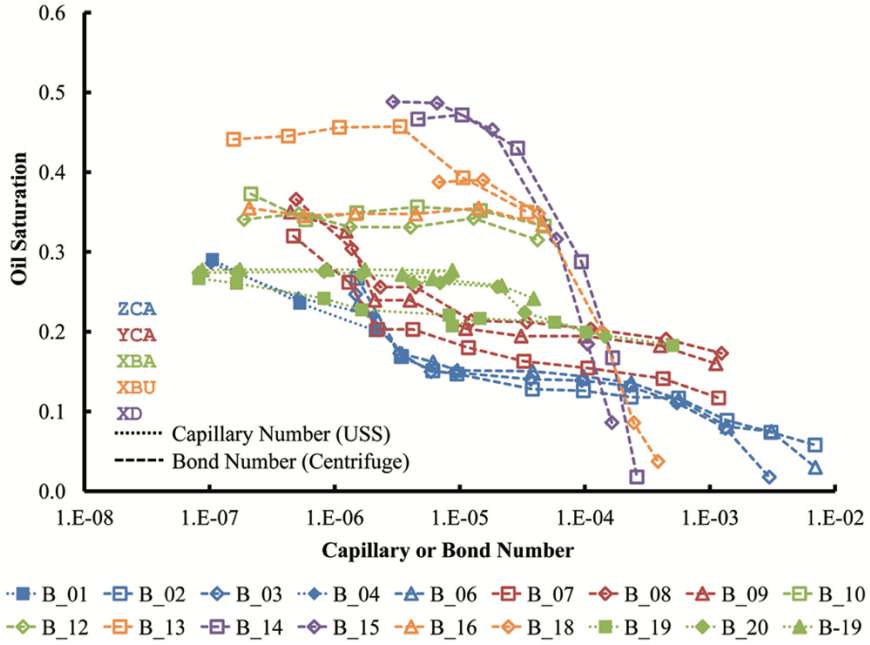


Figure 2.6: CDC curves on Berea sandstones of varying wettability (Humphry et al. 2014). The cores from most water-wet to least water-wet are ordered as XD, XBU, XBA, ZCA/YCA.

### 2.4.3 Deborah Number

The Deborah number ($N_{De}$) is a dimensionless number that represents the relative elasticity of a fluid. It represented by the ratio of a polymer's relaxation time to the residence time of the fluid in the rock pores (Delshad et al. 2008).

$$N_{De} = \frac{\tau_r}{\tau_\varepsilon} \tag{2.4}$$

where $\tau_r$ is the relaxation time and $\tau_\varepsilon$ is the characteristic residence time which can be estimated as the inverse of the stretching rate (Hirasaki and Pope, 1974; Durst et al. 1981; Delshad et al. 2008), or shear rate (Koh, 2015; Qi, 2018). The Deborah number has also been characterized as:

$$N_{De} = \tau_r \dot{\gamma}_{eq} \tag{2.5}$$

where $\dot{\gamma}_{eq}$ is the equivalent shear rate defined as:

$$\dot{\gamma}_{eq} = C\left(\frac{3n+1}{4n}\right)^{\frac{n}{n-1}} \frac{4u}{\sqrt{8kk_{rw}\phi S_w}} \tag{2.6}$$

where $C$ represents the shear correction factor, $n$ is the power law exponent, $u$ is Darcy velocity, $k$ is single-phase brine permeability, $k_{rw}$ is the relative permeability of brine, $\phi$ is porosity, and $S_w$ is aqueous phase saturation (Canella et al. 1988; Koh, 2015). When the Deborah number exceeds values above 1, the effect of viscoelasticity is considered significant (Hirasaki and Pope, 1974; Durst et al. 1981; Delshad et al. 2008; Masuda, et al. 1992).

## 2.5 WETTABILITY

Wettability the measure of a fluid's ability to adhere and spread on a solid surface when in the presence of an immiscible fluid (Peters, 2012). If a fluid prefers to spread on a surface, it is the wetting fluid. The degree of wetting is defined by the interaction between repulsive and cohesive forces. Generally, water is the primary fluid that occupies the pore space in reservoirs, and minerals have typically high energy surfaces, resulting in water-wet reservoirs. However, it has been noted that crude oil can have properties that can affect surface wettability. Wetting phases generally can be water/brine or oil, and occupies the smaller pore throats. Wettability impacts how fluids flow through porous media and ultimately oil recovery processes.

Reservoir wettability can affect rock-fluid properties such as relative permeability, fluid distribution, capillary pressure, and residual oil saturation. During immiscible floods, the wetting fluid will attach to the rock surface more than the non-wetting fluid. The wetting preference of a reservoir can reduce the relative permeability of the wetting phase at corresponding saturations (Owens and Archer, 1971). Figure 2.7 shows the significant difference of relative permeability in rocks of different wettability.

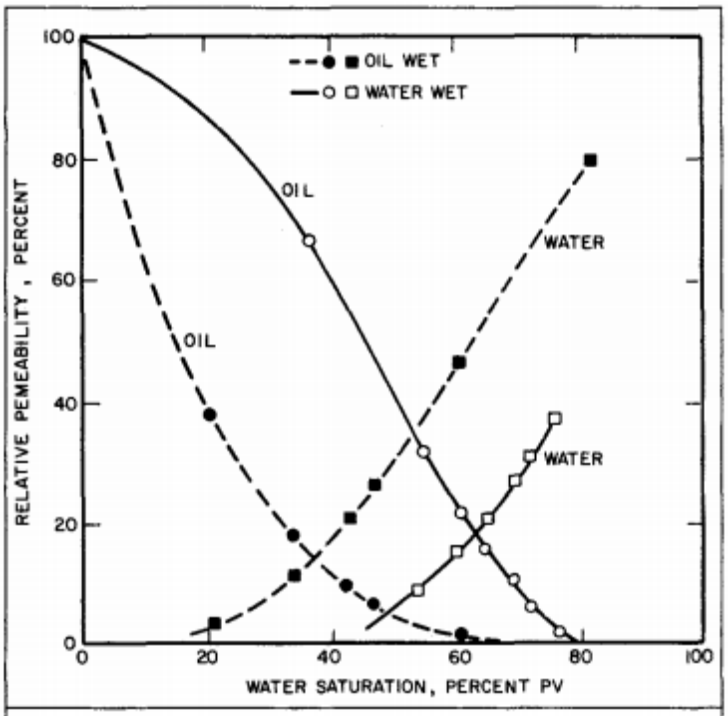


Figure 2.7: Relative permeability curves measured with heptane and brine in water-wet and oil-wet cores (Anderson, 1987).

Wettability can affect chemical flood performance due to its impact on flow and spatial distribution of fluids in the porous medium. As seen in Figure 2.1, in water-wet rocks, the injected water can imbibe into the smaller pore spaces while the oil can move to larger pores, and as a result the oil is more easily displaced in the water-wet system. Owen and Archer (1971) also compared waterflood efficiencies in reservoirs of varying wettability (Figure 2.8).

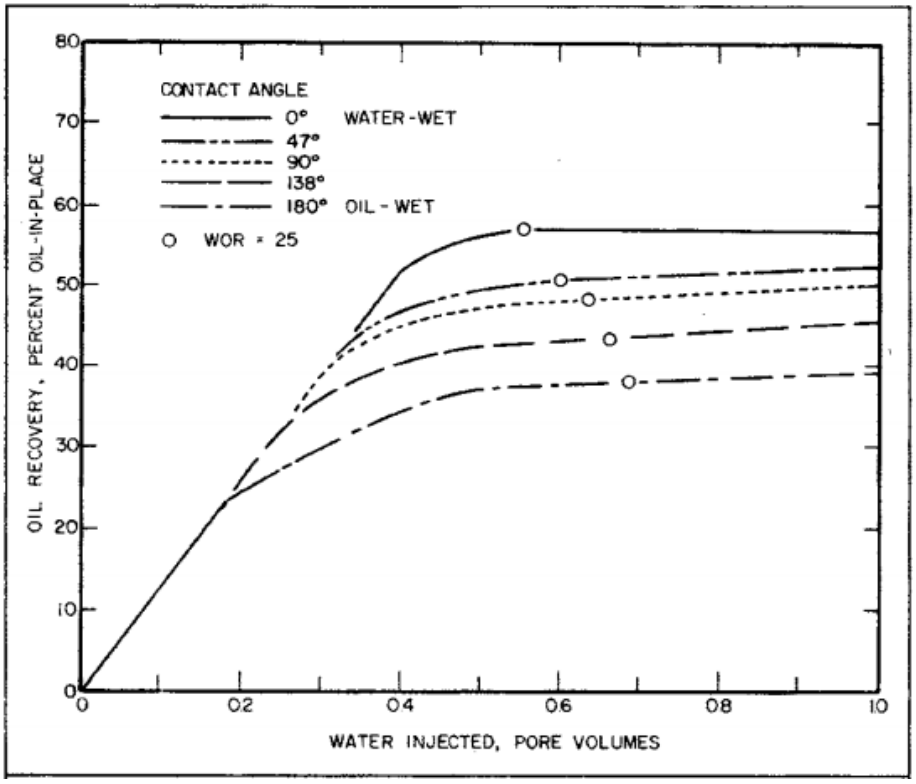

Figure 2.8: Effect of wettability on waterflood in a 20-acre five-spot pattern (Owen and Archer 1971).

## 2.6 HPAM POLYMER PROPERTIES AND RHEOLOGY

Synthetic polymers, such as hydrolyzed polyacrylamide (HPAM) polymers, are commonly available commercial EOR polymers (Sorbie, 1991; Azad and Trivedi, 2019). These synthetic polymers can have flexible chains that allow it to exhibit viscoelastic behaviors. HPAM polymer viscosity is dependent on properties such as polymer concentration, polymer molecular weight, brine salinity, and shear rate.

### 2.6.1 Chemical Structure and Molecular Weight

HPAM is a commonly used synthetic polymer made up of acrylamide monomers in a random coil structure (Sorbie, 1991). This coil allows HPAM to exhibit viscoelastic behavior. The chemical structure of HPAM is seen in Figure 2.9.

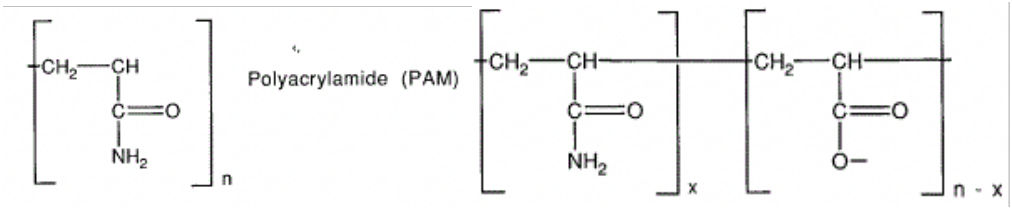


(a) (b)

Figure 2.9: Chemical structure of (a) a primary chain monomer and (b) a partially hydrolyzed PAM (Sorbie, 1991).

Different HPAM molecules can be synthesized by increasing the size of the chains by adding more monomer units. The double helix structure of HPAM has been noted to allow the molecule to have a less rigid structure when compared to xanthan gum (Qi, 2018). As the number of monomers grow, the molecular weight of the polymers will increase. Both viscosity and elasticity will increase with the polymer molecular weight. Very large HPAM polymers can be synthesized, and thus are more viscoelastic. Sheng et al. (2015) has reported that the typical HPAM molecular weight ranges between 2-25 million g/mole. At higher molecular weights, the same mass of polymer can be more elastic, and thus recover more oil (Sheng, 2010). Limitations on higher molecular weight polymers do exist, as lower permeability reservoirs may experience pore throat plugging with larger polymers. Examples of the different HPAM polymers of different molecular weights include HPAM FP6040 (35 million Daltons), HPAM FP3630s (18-20 million Daltons), and HPAM FP3330s (8-10 million Daltons).

### 2.6.2 Salinity

As seen in Figure 2.10, HPAM molecules contain negatively charged units. When the aqueous solution contains minimal positively charged ions, the negative charges on the polymer chain repel each other, leading to larger polymer hydro-diameters (Sorbie, 1990). Subsequently, the viscosity and relaxation times are higher in low salinity polymer solutions. When cations are present in the solution, ions will attract to the negatively charged carboxyl groups. The repulsion

between molecules in the polymer chain are reduced and the molecules will "curl up," reducing viscosity and relaxation time (Figure 10).

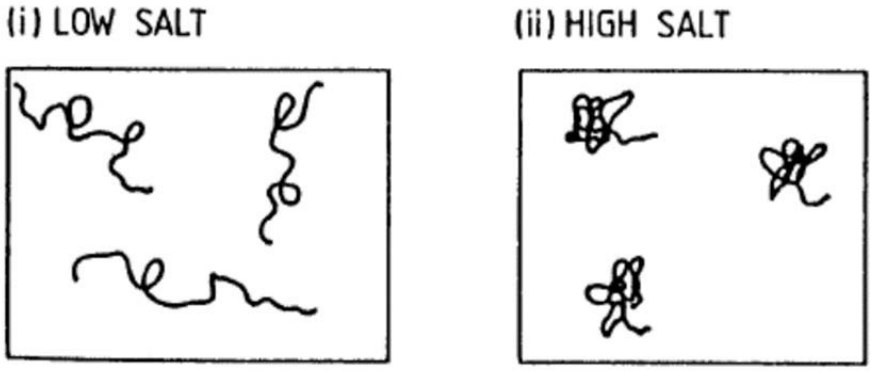


Figure 2.10: HPAM molecules in (i) low salinity and (ii) high salinity aqueous solutions (Sorbie, 1990).

**2.6.3 Bulk Rheology**

The bulk rheology of HPAM polymers experiences different behavioral regions as the molecules are entangled and randomly oriented in aqueous solutions. As shear forces are applied, the tangled molecules begin to orient in the direction of shear forces, which can reduce viscosity. Viscoelastic polymers generally have four flow regimes: (1) Newtonian at low shear rates, (2) shear thinning at medium shear rates, (3) shear thickening at higher shear rates, and (4) mechanical degradation (Figure 2.11).

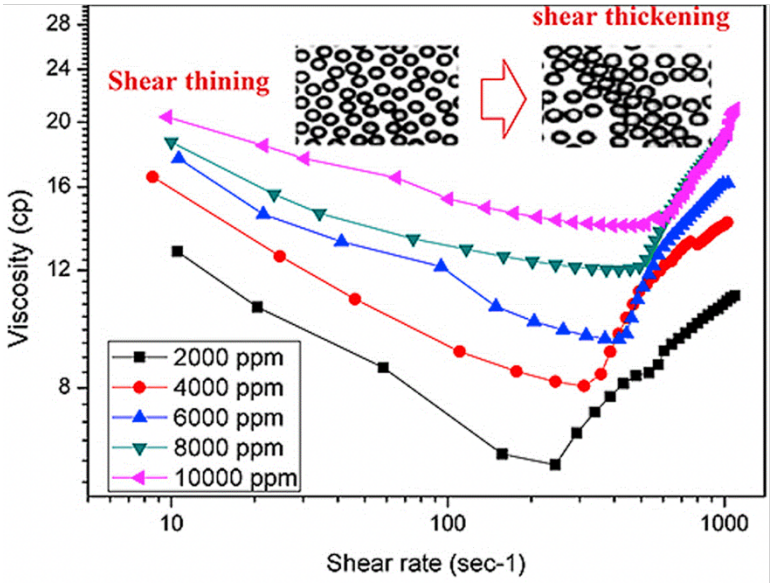


Figure 2.11: Behavior of viscoelastic polymers with shear-thinning and shear-thickening regimes (Kumar and Mandal, 2017).

The typical way to observe polymer rheological behavior can be observed is through a steady sweep rheology test (Figure 2.12). Figure _ shows the viscosity versus shear rate, and the shear thinning regime can be observed.

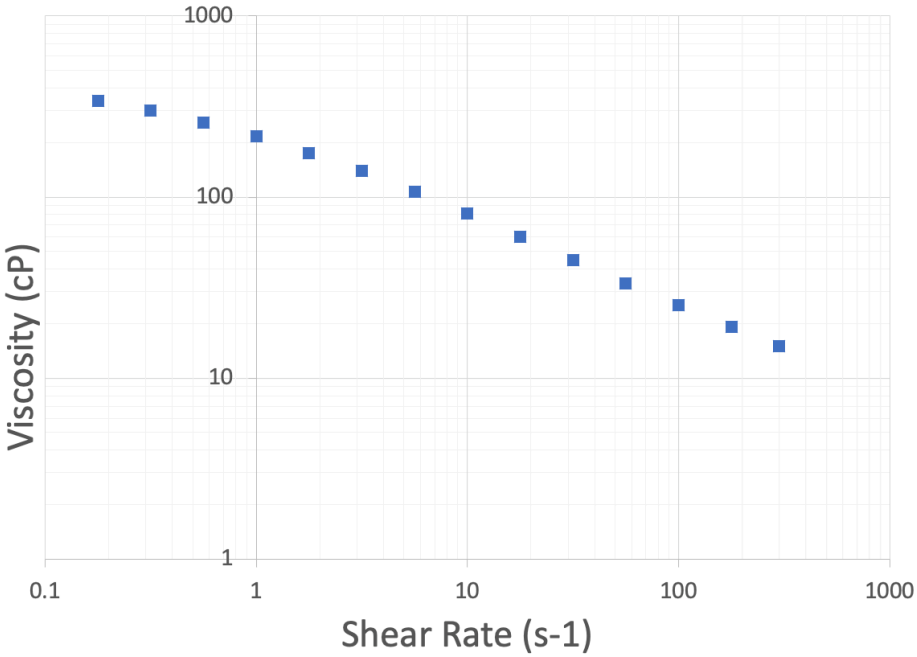


Figure 2.12: Example of viscosity profile of a sample polymer solution (2000 ppm FP3330s in 1000 ppm NaCl + 400 ppm $NaHCO_3$).

Polymer viscosity is shear rate dependent, and the most commonly used model is the power-law model which can help model the shear thinning region:

$$\mu_{apparent} = K\dot{\gamma}^{n-1} \tag{2.7}$$

where $K$ is the power law coefficient (Pa-s$^n$) and $n$ is the shear-thinning index.

Another polymer viscosity model that also models the shear-thinning regime is the Meter model (Meter and Bird, 1964):

$$\mu_{app} - \mu_w = \frac{{\mu_p}^0 - \mu_w}{1 + \left(\frac{\dot{\gamma}}{\dot{\gamma}_{\frac{1}{2}}}\right)^{P_\alpha - 1}} \tag{2.8}$$

where $\mu_{app}$ is the apparent viscosity, $\dot{\gamma}_{1/2}$ is the shear rate where the viscosity is half of the sum of ${\mu_p}^0$ and $\mu_w$ and $P_\alpha$ is an empirical fitting parameter.

Another model for modeling polymer regime that can account for the Newtonian regime is the Carreau model:

$$\mu(\dot{\gamma}) = \mu_\infty + (\mu_0 - \mu_\infty)[1 + (\lambda\dot{\gamma})^2]^{\frac{(n-1)}{2}} \tag{2.9}$$

where $\mu_0$ is the viscosity at zero shear rate and $\mu_\infty$ is the shear rate at infinity, and $n$ is the shear thinning index (same as the power law model index).

The relaxation time for polymers is considered as the time it takes for a polymer to "relax" back to its original state. Many models have been used to predict relaxation time. Volpert et al. (1998) predicted relaxation time by using the G' (elastic component of viscoelasticity) and G'' (viscous component) modulus cross-over point model on linear viscoelastic fluids. The Rouse model (Rouse, 1953) and Generalized Maxwell Model (GMM) (Kim et al. 2010), have

been adapted to fit non-linear viscoelastic models. Further studies (Kim et al. 2010; Qi, 2017; Erincik, 2017) reviewed the accuracy of the modulus cross-over model to the GMM and Rouse non-linear models and found that the cross-over model were acceptable fits for the non-linear models. Thus, the relaxation time of a viscoelastic fluid was considered the inverse of the angular frequency at which the two moduli cross. This value can be obtained simply from a dynamic frequency sweep test. An example of a viscoelastic polymer undergoing the dynamic frequency sweep test is seen in Figure 2.13. The modulus crossover was identified at an angular frequency of 0.6696 rad/sec which gives a corresponding relaxation time of almost 1.5 sec.

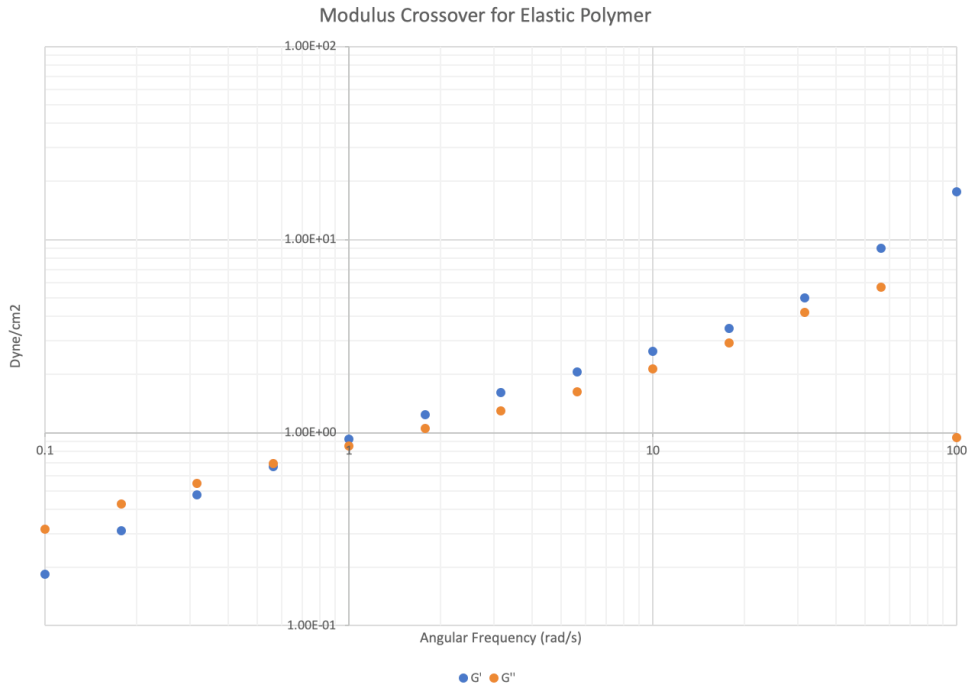


Figure 2.13: Example of dynamic frequency sweep test of a viscoelastic fluid (1000ppm 3630s in 1000ppm NaCl and 400ppm $NaHCO_3$).

### 2.6.4 Polymer Rheology in Porous Media

**Rheology and Viscoelasticity**

Polymer viscosity is often shear-thickening in converging-diverging geometries, such as pore throats. Polymer in porous media can encounter similar regimes as discussed in section 2.6.3, but with the addition of a shear-thickening regime (Figure 2.14).

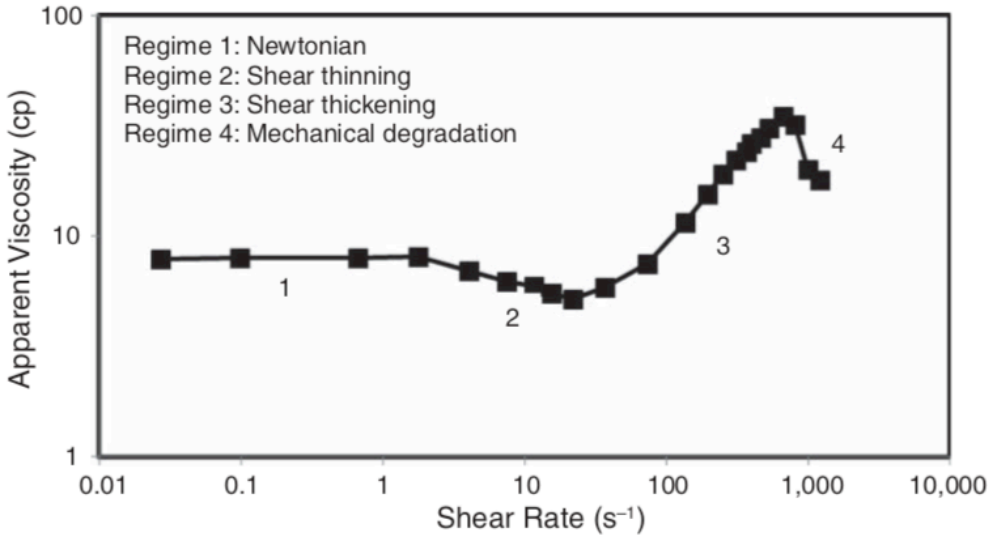


Figure 2.14: Synthetic polymer viscosity behavior demonstrating different behaviors in varying flow regimes (Azad and Trivedi, 2019).

A power-law regression can still be applied to the rheological data, specifically in the shear-thinning region of the curve to fit the power-law model:

$$\mu_{apparent} = K\dot{\gamma}_{eq}{}^{n-1} \tag{2.10}$$

where $\mu_{apparent}$ represents the viscosity of the fluid, $K$ is the power law constant, $n$ is the bulk power law index, and $\dot{\gamma}_{eq}$ is the equivalent shear rate. of the polymer as shown in equation 2.6.

Hirasaki and Pope (1974) proposed a similar apparent viscosity model using Darcy velocity instead of equivalent shear rate.

$$\mu_{apparent} = Hu^{n-1} \tag{2.11}$$

$$H = K\left(\frac{3n+1}{n}\right)^{n-1}(8kk_{rw}\phi S_w)^{\left(\frac{1-n}{2}\right)} \tag{2.12}$$

where $H$ is a function of wetting phase permeability, $\phi$ is porosity, and water/brine saturation.

The apparent viscosity of the polymer can also be obtained by rearranging Darcy's Law. Darcy's law is the relationship between volumetric flow rate ($Q$), viscosity ($\mu$), geometry ($L$ as length and $A$ for cross-sectional area), and permeability ($k$).

$$k = \frac{\mu QL}{A\Delta P} \tag{2.13}$$

$$\mu_{apparent} = \frac{kA\Delta P}{QL} \tag{2.14}$$

Polymer molecules experience coil-stretching cycles which can lead to lower or higher viscosity values, creating shear-thickening regimes (Bird et al. 1987; Delshad et al. 2008). The shear-thickening regime is related to polymer elasticity, which can be related to the polymer relaxation time previously discussed (Delshad et al. 2008) in Figure 2.13. Equivalent shear rate and subsequent apparent shear rate (equation 2.10) can then be related to the rheological lab viscosity data that was obtain through bulk rheology analysis (Figure 2.12 and equation 2.7).

It is also important to obtain rheological data of polymers before and after injection in porous media to compare potential changes in solution viscosity after traveling through the rock. Polymers can be adsorbed, snapped off, or trapped in small or disconnected pores. Polymer

retention on rock surfaces is dependent on polymer type, size, weight, brine composition, mineral composition, flow rate, and temperature (Sorbie, 1991; Lake et al. 2014).

## 2.7 BIOPOLYMERS

Biopolymers such as xanthan gum, and scleroglucan, also exhibit viscoelastic behavior similar to synthetic polymers (Azad and Trivedi, 2019). The primary rheological difference between synthetic and biopolymers are that synthetic polymers often exhibit viscoelastic properties due to the flexible molecular chain. A combination of synthetic and biopolymers can be used to help maintain certain viscosity profiles without changing the salinity of aqueous solutions.

## 2.8 VISCOELASTIC POLYMER FLOODING LITERATURE REVIEW

Past studies of the effect of viscoelastic polymers on reducing residual oil saturation have varied in their results. Geometries used to experimentally study the effect of oil displacement by polymers include glass bead packs, microfluidics, or rock core samples.

Azad and Trivadi (2019) more recently gave a comprehensive review different viscoelastic experiments and the quantification of viscoelastic polymer flooding. They discuss the existing methods for quantifying viscoelastic floods such as Deborah number, pore-scale models, and continuum viscoelastic models. They observed that while the Deborah number can successfully represent the viscoelastic effect in porous media, they claimed that the conventional Deborah number that is calculated from residence time is not universal. Their main issue with the Deborah number is that different researchers have used both shear and strain rates to calculate polymer residence time, and there is no unifying definition to calculate for residence time.

Wreath (1989) suggested secondary polymer flooding in heterogenous media may lower residual saturation and found that HPAM polymers (Pusher 700, NalFlo 3837) decreased residual oil saturation 7% after waterflooding in Antolini sandstones (~2900mD at around 2 psi), although those results were not replicated in lower permeability Berea sandstones (~800mD).

Wang et al. (2010) used mathematical simulations to look at how micro-forces drive displacement efficiency at the pore scale. They determined these micro-forces were made up of normal forces caused by the change in the shape of the flow patterns in the pores and kinetic forces caused by the change in momentum. The difference in velocity profiles are seen in Figure 2.15. Ultimately, they determined that these micro-forces influence the change in flow lines. For viscoelastic fluids, they found that micro-forces in pores are larger when compared to Newtonian fluids. The enhanced micro-forces caused oil droplets that were protruding to change shape and mobilize.

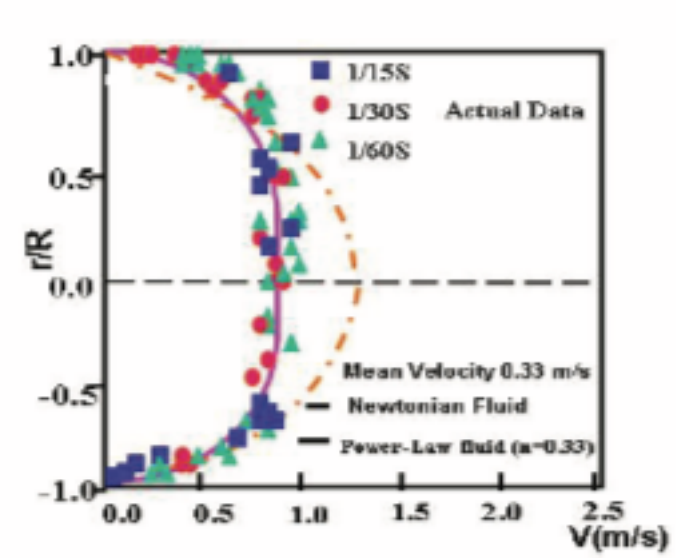


Figure 2.15: Comparison of velocity profile acting on oil droplet (Wang et al. 2010).

Jung et al. (2013) investigated the polymer flooding characteristics of partially hydrolyzed polyacrylamide (HPAM) solution (A-132PH) in a homogenous glass-bead pack and its efficacy in displacing heavy oils. Their experimental results showed that the HPAM polymer was sensitive to temperature, salinity and alkali changes. In their homogenous glass-bead pack, they found that over 60% of the original oil in place (OOIP) was produced from the polymer flood, versus only 40% of OOIP from the waterflood (Figure 2.16). The polymer flood was 21.7% more efficient than waterflooding.

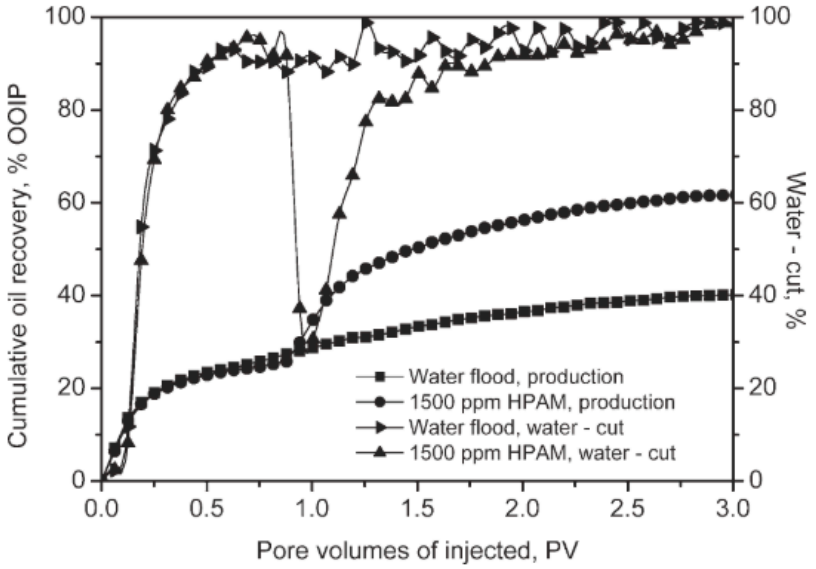


Figure 2.16: Comparison of waterflood and polymer flood in oil recovery (Jung et al. 2013).

Nilsson et al. (2013) investigated the effect of fluid rheology in a microfluidic sandstone chip. They specifically utilized microfluidic devices (Figure 2.17) to examine how shear-thinning, shear thickening, and viscoelastic fluids affect oil recovery. Initial baseline experiments were performed by displacing oil with both water and a water-surfactant solution over a variety of flow rates. The polymer (0.1wt% FP3630s with a relaxation time of 0.1 sec) was found to

displace more oil than either water or surfactant solutions in the model and have a higher oil recovery.

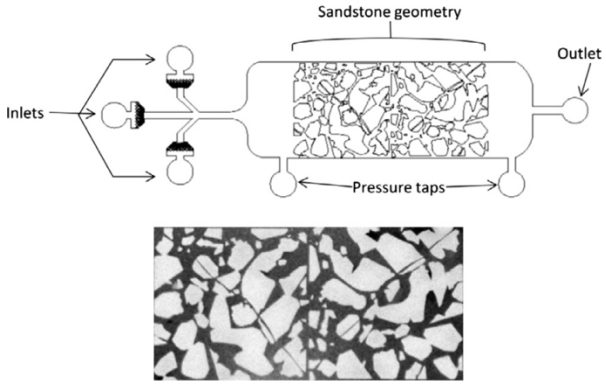


Figure 2.17: Microfluidic device design from Nilsson et al. (2013).

Clarke et al. (2015) created micromodel networks to compare fluid flow from xanthan gum to HPAM polymer. The specifically observed the temporal velocity fluctuation and saw how the viscoelastic polymer solutions displaced the trapped oil phase at a lower than expected capillary number. The onset of temporal flow fluctuations correlated with the desaturation of their porous medium. The flow fluctuations they observed have the same behavior as elastic turbulence. They noted that as the Deborah number of the flow increased, the fluctuations began generating additional forces that disrupted the ganglia of the trapped oil. They saw that for HPAM flow, there were more significant fluctuations than in xanthan flow (Figure 2.18).

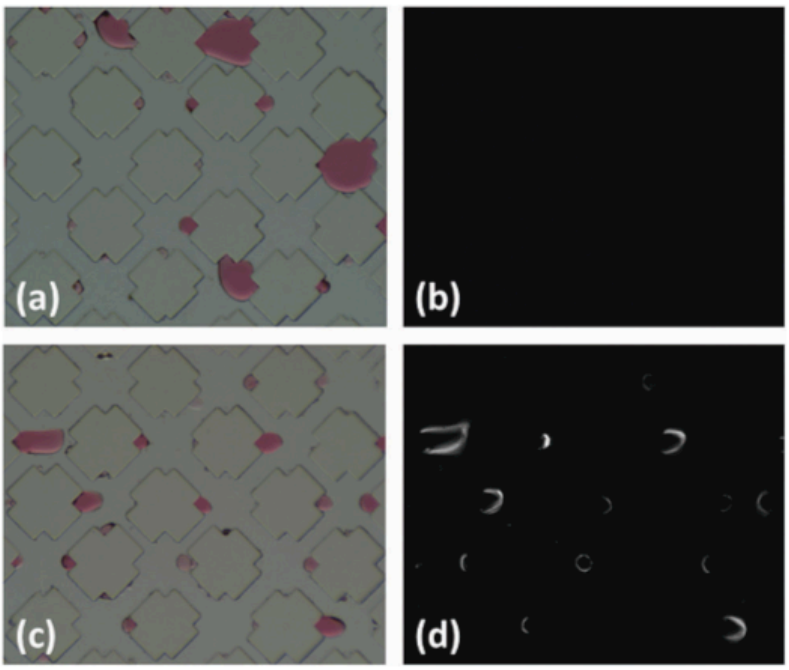


Figure 2.18: Oil ganglia remaining after polymer flow from Clarke et al. 2015. (a) and (b) is the xanthan flood and (c) and (d) is the HPAM flood. (b) and (d) show the integrated difference images from video sequences. (Clarke et al. 2015).

While microfluidic chips can help visualize pore scale behaviors, true reservoirs can also contain other minerals, such as clay, which can alter the permeability and porosity of a reservoir which would not be modeled in a glass bead pack model (Jung et al. 2013) or micromodels (Nilsson et al. 2013; Clarke et al. 2015). However, these studies can help set up future studies using more developed models with more appropriate heterogeneities and mineralogy.

Laboratory coreflood studies have been completed by various researchers through the years, and in recent studies. Vermolen et al. (2014) completed four core floods in Bentheimer outcrop cores. The cores were flooded with both heavier oil (300 cp) and light oil (9 cp). HPAM polymers were used for the viscoelastic floods. The core floods showed a reduction in residual oil saturation in lower viscosity crude oil, but no significant reduction in higher viscosity crude oil. They only noted this reduction when there is an increase in polymer viscosity or flow rate,

and when the polymer is highly viscoelastic. They suggested that the oil recovery during increasing pressure was not due to the viscous stripping of the oil, because when the inelastic polymer was injected at similar pressure gradients, there was no additional oil recovery.

Sandengen et al. (2017) completed short Bentheimer core plugs experiments in a micro-CT imaging system. Polymer injection following the waterflood did not produce any additional oil and did not change oil saturation. They noted that the general "spatial location" of the oil was unaltered by the polymer floods. When reinjecting oil back into the core, and then subsequently injecting more oil, the final residual oil saturation was actually higher than the final saturation in the previous flood.

Ehrenfried (2013) produced inconclusive results on whether viscoelastic polymers could reduce residual oil saturation in water-wet sandstones. Bentheimer sandstones showed that HPAM 3630s did reduce residual oil saturation, while his experiments using Berea cores did not produce strong results. Qi et al. (2017) performed six coreflood experiments at constant pressure gradient (3-11 psi/ft) using high permeability (~1500-2000 mD) Bentheimer sandstones saturated with viscous oil (~150 cp). Since the oil was viscous and the mobility ratio with water was poor, they followed the waterflood with a viscous, aqueous glycerin flood to ensure the core was at residual oil saturation before injecting polymer. The apparent in-situ viscosity of the polymer was approximately equal to the glycerin viscosity so there was very little change in the mobility ratio, pressure gradient, or capillary number. They showed significant improvement in oil recovery using HPAM polymer solutions that were viscoelastic and concluded the residual saturation had decreased. CT scans in one coreflood confirmed that the improved recovery from the viscoelastic polymer flood was residual oil and not bypassed oil (Figure 2.19).

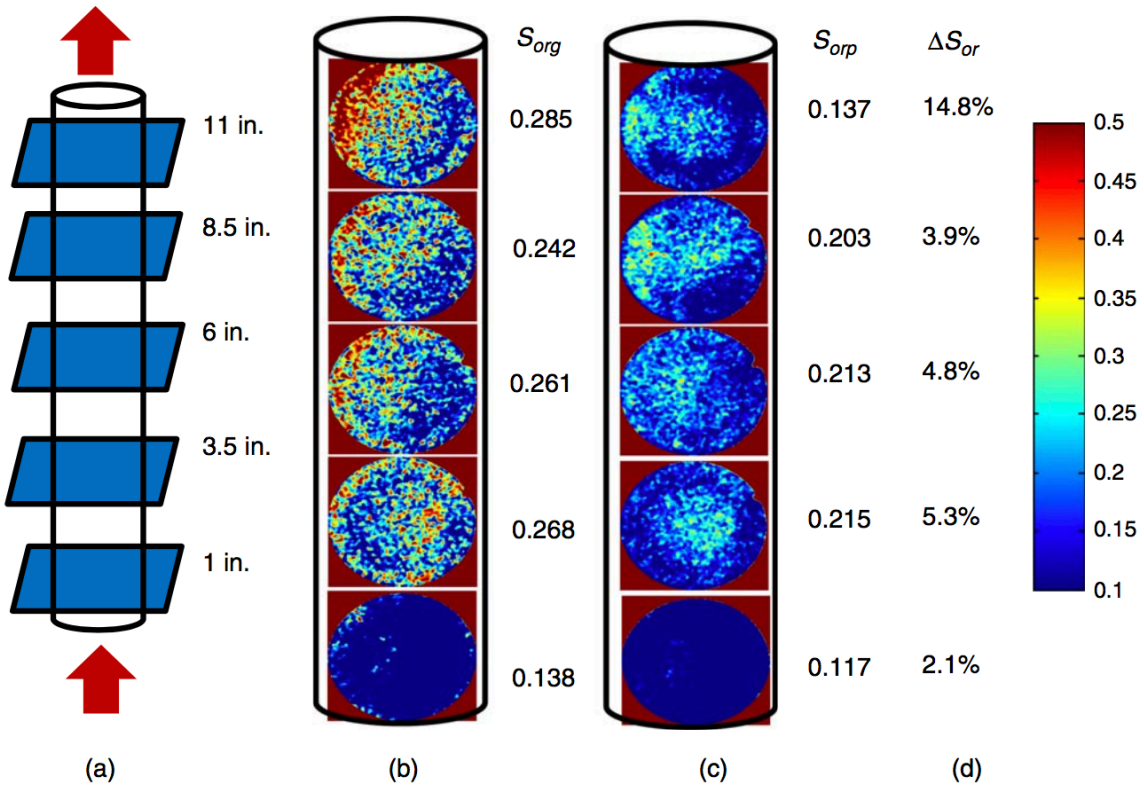


Figure 2.19: CT scans of oil saturation in Bentheimer sandstone after glycerin and polymer floods (Qi et al. 2017).

Erincik et al. (2018) performed coreflood experiments with the original objective of expanding upon Qi et al. (2017)'s studies in Bentheimer cores. They found a significant decrease in residual oil saturation by a viscoelastic solution of HPAM that had relatively low salinity. There most notable discovery, however, was that by performing a high salinity, low viscoelasticity polymer flood after the low salinity, high viscoelasticity polymer flood on Bentheimer sandstones produced significantly more amounts of oil (Figure 2.20). In all, Erincik et al.'s experiments showed an average reduction of nearly 24% in oil saturation from polymer floods, about 12% from each polymer flood. They also showed that continuous alternating of the polymer floods sometimes showed continued improved recovery, but with diminishing returns.

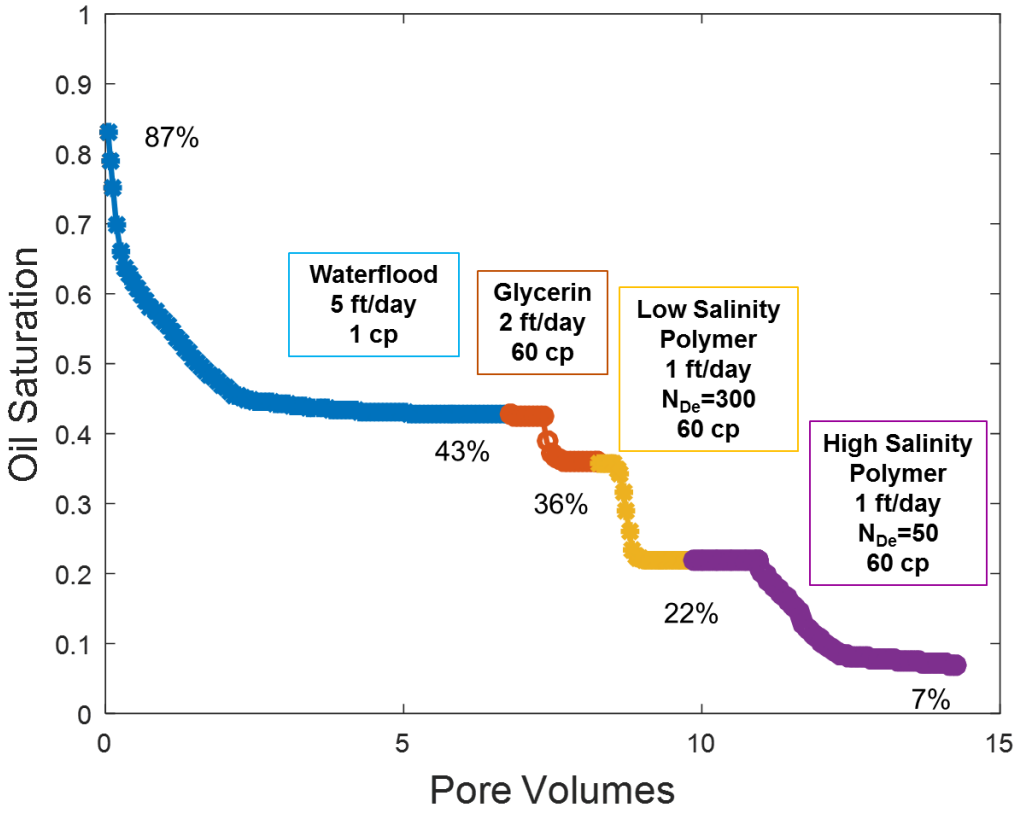


Figure 2.20: Oil saturation versus injected pore volumes of polymer (Erincik et al. 2018).

These experiments demonstrated high success in viscoelastic polymer flooding from polymers alone, with no reduction in IFT, and capillary numbers below the critical threshold, although there were still questions about the mechanisms behind the success.

In addition, Qi (2018) also completed six corefloods; five in Bentheimer cores and one in a Berea core. All cores used light viscosity oil. Viscoelastic polymer floods were designed to have high Deborah numbers. Qi (2018) found that there as an average oil saturation reduction of 11.8% OOIP from the second high salinity inelastic polymer flood. Twenty viscoelastic core floods were compiled to develop a correlation between the Deborah number and the ratio of residual oil saturation after polymer flood, and residual oil saturation before polymer flood (after

waterflood). This relationship was referred to as an Elastic Desaturation Curve (EDC) and seen in Figure 2.21.

$$\frac{S_{orp}}{S_{orw,\infty}} = \begin{cases} 1 & \text{if } N_{De} < 1 \\ 1 - 0.133 \log N_{De} & \text{if } N_{De} \geq 1 \end{cases}$$

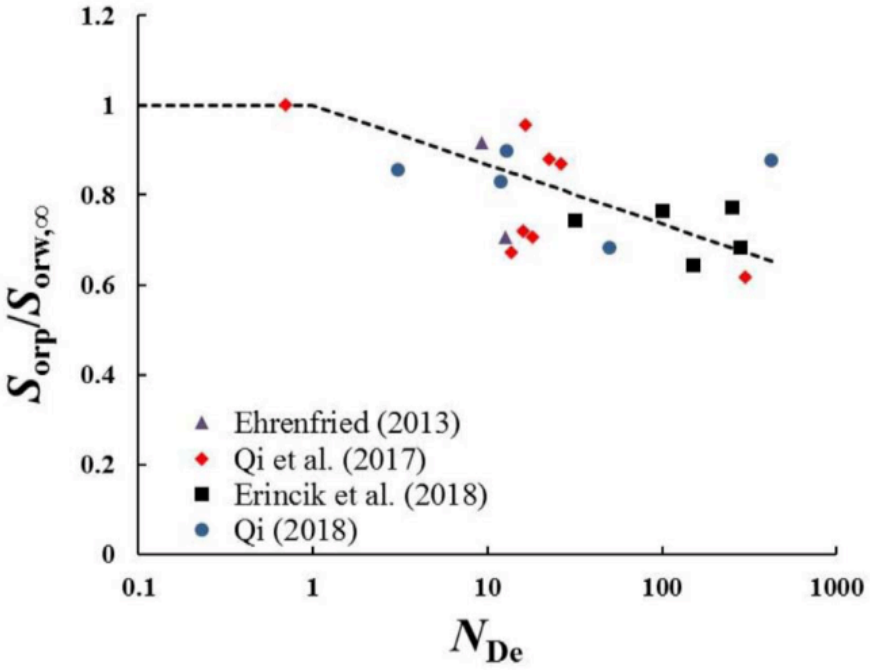


Figure 2.21: Elastic desaturation curve developed from twenty different corefloods (Qi 2018).

The EDC shows a general trend of decreasing residual oil saturation to an increasing Deborah number. In addition, this correlation was implemented into a reservoir simulator (UTCHEM) to see the effect of viscoelastic polymers at the reservoir scale. When the correlation was used on a pilot field, the simulator showed an additional 12% of oil was recovered (Figure 2.22).

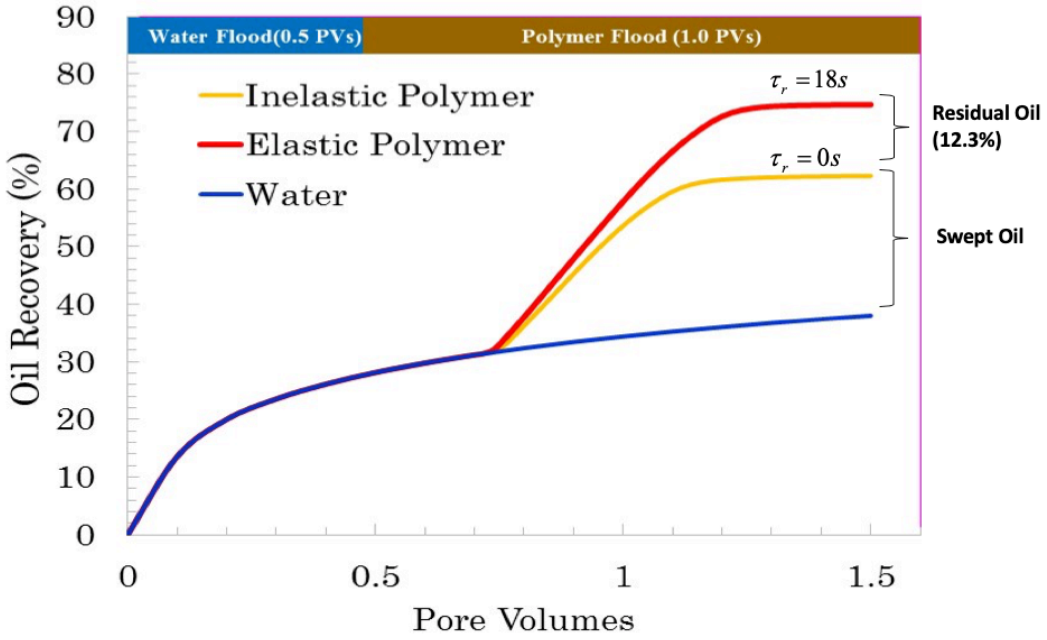


Figure 2.22: Predicted oil recovery of pilot field after polymer flood using UTCHEM simulation with EDC implemented (Qi 2018).

Afsharpoor and Balhoff (2013) suggested that normal forces in elastic fluid flow could mobilize trapped oil droplets in both water-wet and oil-wet porous media. Clarke et al. (2015) also suggested that these normal forces could improve the viscoelastic effect of the polymers by stretching the polymer more frequently, causing an increase in elasticity and elastic turbulence. Huh and Pope (2008) proposed that flowing oil filaments are less likely to snap in polymer solutions and that this allowed the oil filaments to be "protected." Qi (2018) showed oscillations of HPAM FP3330s and polyethylene oxide (PEO) in microfluidic devices. The polymer solution began to experience periodic oscillations at the pore throat entrance in the microfluid device. These oscillations became more evident as flow rate increased.

It is hoped that polymers can play an important role in increasing the production of oil wells as more recent polymer flood applications in EOR has shown to recover more than 20% of additional oil from OOIP. The most commonly used polymer in injection, HPAM, has been

found to be effective, although its properties vary significantly in changing salinity or temperature. While many experiments have been done in homogenous glass packs, or homogenous Bentheimer outcrop cores, it was important to explore the effects of viscoelastic polymers in other rock types, such as Boise sandstones, or oil-wet mediums. Key objectives for this work were to expand upon these experiments in literature by working with lower pressure gradients in the core, different polymers and molecular weights, and alternative porous mediums. Higher molecular weight HPAM polymers (such as FP6040) have the potential to have even higher relaxation times, thus further increasing Deborah numbers. Using a lower molecular weight polymer (such as FP3330s) or a biopolymer (such as scleroglucan) as the inelastic flood can help prevent the change in salinities between the viscoelastic and inelastic polymer floods. Further studies need to be completed so that the most economic and efficient methods for oil recovery can be completed.

# Chapter 3: Experimental Materials and Approaches

Core flood experiments were conducted to study the effect of viscoelastic polymers on the residual oil saturation in sandstones. This chapter discusses the experimental approaches, materials, equipment, methods, and calculations in conducting the core flood experiments in this thesis.

## 3.1 FLUID PREPARATION

### 3.1.1 Low Viscosity Oil

Experiments were performed using a low viscosity dead oil (18 cp). Water was removed from low viscosity oil through a separation funnel and stored at 25$^{o}$C. The separated crude oil was diluted with toluene (17 wt%) to bring the oil viscosity to around 6 cp. The diluted oil was filtered to remove residual solids with 1.2 μm filter paper under 15 psi of compressed air.

### 3.1.2 Brine Solutions

All brine solutions are prepared by dissolving salts in deionized water. Salts were measured out using weight by volume. Deionized (DI) water and the appropriate salts were mixed using a magnetic stir plate and magnetic stirrer bars. All brines are degassed with argon gas for at least two hours prior to use. A low salinity brine used for the waterflood and low salinity polymer solution has a composition of 1000 ppm NaCl + 400 ppm $NaHCO_3$. 400 ppm $Na_2S_2O_4$ was added to the low salinity brine during waterflood as a reducing agent in the brine, but left out of polymer solutions as it was found to reduce the viscosity and relaxation time of the polymers. The high salinity brine used in the high salinity, inelastic, polymer has a composition of 20,000 ppm NaCl + 400 ppm $NaHCO_3$. All brines were filtered by vacuum filtration through a 0.4 μm filter.

### 3.1.3 HPAM Polymer Solution Preparation

#### 3.1.3.1 Polymer Dilution

Polymers used in this work were hydrolyzed polyacrylamide (HPAM), FLOPAAM (FP) 6040 (molecular weight 35 million Daltons), 3630s (molecular weight 20 million Daltons) or 3330s (molecular weight 10 million Daltons) in dry powder. The pure dry powder polymers were diluted into an initial stock solution of 6000 ppm HPAM FP3630s or FP6040 in deionized (DI) water or 8,000 ppm HPAM 3330s in DI water. To mix the initial stock solution, the powder was dissolved into DI water under an argon gas blanket with a magnetic stir bar rotating at 175 rpm. Solutions were allowed to hydrolyze for at least 48 hours at room temperature before being allowed to rest in the fridge (7$^{o}$C). Before allowing the stock solution to rest in the fridge, no undissolved polymer powder was observed in the stock solution.

A commercially available, EOR-grade, biopolymer (scleroglucan) was also used in an experiment. Scleroglucan was prepared and diluted in low salinity brine (1000 ppm NaCl + 400 ppm $NaHCO_3$) and provided by Cargill. The initial concentration of the scleroglucan in low salinity brine was 2000 ppm scleroglucan which was eventually diluted down into different concentrations before use. The solution was stored similar to the HPAM polymers in the fridge.

Diluted polymer solutions used for experimental core flood injections were diluted from these stock solutions. While the final diluted solution can have varying salinities and concentrations in different experiments, the procedures for diluting them to desired concentrations are similar. All salts were dissolved in DI water to ensure no remaining solids were undissolved before being mixed into the polymer. Diluted polymer solutions were calculated by weight, mixed for at least 3 hours with a magnetic stir bar, and bubbled with argon.

Polymer solutions were all filtered under 15 psi of argon gas through a 1.2μm filter paper and must pass the filtration test (described in section 3.1.3.2). Samples of the diluted polymer are taken for rheological studies, as described in section 3.1.3.3 (dynamic frequency sweep, and steady sweep tests). Diluted polymer solutions are de-oxygenated with argon for at least 2 hours before being used in experiments.

### 3.1.3.2 Filtration Test

All solutions were filtered before injecting into the core to remove impurities or any unwanted solids that may plug up any pores in the core. For brine filtration, a simple vacuum filtration set-up using a bucher funnel, and vacuum pump were used. For polymer solutions, a more complex filtration set-up was used to make sure the polymer was properly mixed and hydrated. 15 psi of argon gas was passed through filter bells in order to filter the polymer solutions through a "filter press unit," as shown in Figure 3.1.

Figure 3.1: Polymer filtration set up.

Each filter bell was filled with the polymer solution and then placed into the filter press unit. As the argon gas passed through the bell, it pushed the polymer solution through a 1.2 μm filter (Millipore mixed cellulose ester membrane). The solution passed through the membrane into a graduated cylinder and the time that it takes to filter 200 mL was recorded. A filtration

ratio (FR) is defined as the ratio of the time to filter 20 mL at the end of the filtration to the time it filter 20 mL at the beginning of filtration. For a filter bell of 250 mL of polymer solution, the FR can be calculated as:

$$FR = \frac{t_{200mL} - t_{180mL}}{t_{80mL} - t_{60mL}} \tag{3.1}$$

A polymer solution is considered acceptable for injection if the FR is less than 1.2. Ideally, the time it takes for a volume of solution to pass through the filter near the end of the filtration should be close to the time it would take at the beginning of the filtration. An acceptable FR suggests that a diluted solution is homogenously mixed, and has appropriately hydrated. All polymers used in core flood experiments passed the filtration test.

#### 3.1.3.3 Rheological Properties Measurements

The TA instruments Advanced Rheometric Expansion System Low Shear-1 (ARES LS-1) was used for analyzing rheological properties of fluid solutions. The rheometer was designed for fluids rheology testing, and the low-shear (LS) motor has both dynamic and steady sweep modes. The dynamic mode can measure strain and torque, while the steady mode can measure rotations, torque, and normal forces. To evaluate the rheological fluid properties, the dynamic frequency sweep test and steady rate sweep test were used. A double wall couette geometry (34 mm outer diameter (OD) and 27.95 mm inner diameter (ID)) was used for analysis of polymers, and a 34 mm OD couette geometry for crude oil viscosity analysis.

***Dynamic Frequency Sweep Test (DFST)***

The dynamic frequency sweep test analyzed the frequency and time dependent behavior of polymer solutions at a constant strain. It plotted the storage modulus and loss modulus over a specific range of oscillatory frequencies at a constant strain (20% in these experiments) and a

constant temperature (25°C room temperature). The relaxation time of the polymer solution was calculated as the inverse of the frequency at which the G' and G" intersected (the modulus crossover point). It was noted that when the loss modulus (G") is larger than the storage modulus (G'), then the solution is considered more "liquid-like." The range of frequencies tested ranged from an initial frequency of 0.1 rad/s to a final frequency of 100 rad/s. Figure 3.2 shows an example of an elastic polymer (825 ppm FP6040 in 1000 ppm NaCl + 400 ppm $NAHCO_3$) with a higher relaxation time. If the moduli never crossed over, the range of frequencies were adjusted until a crossover was observed.

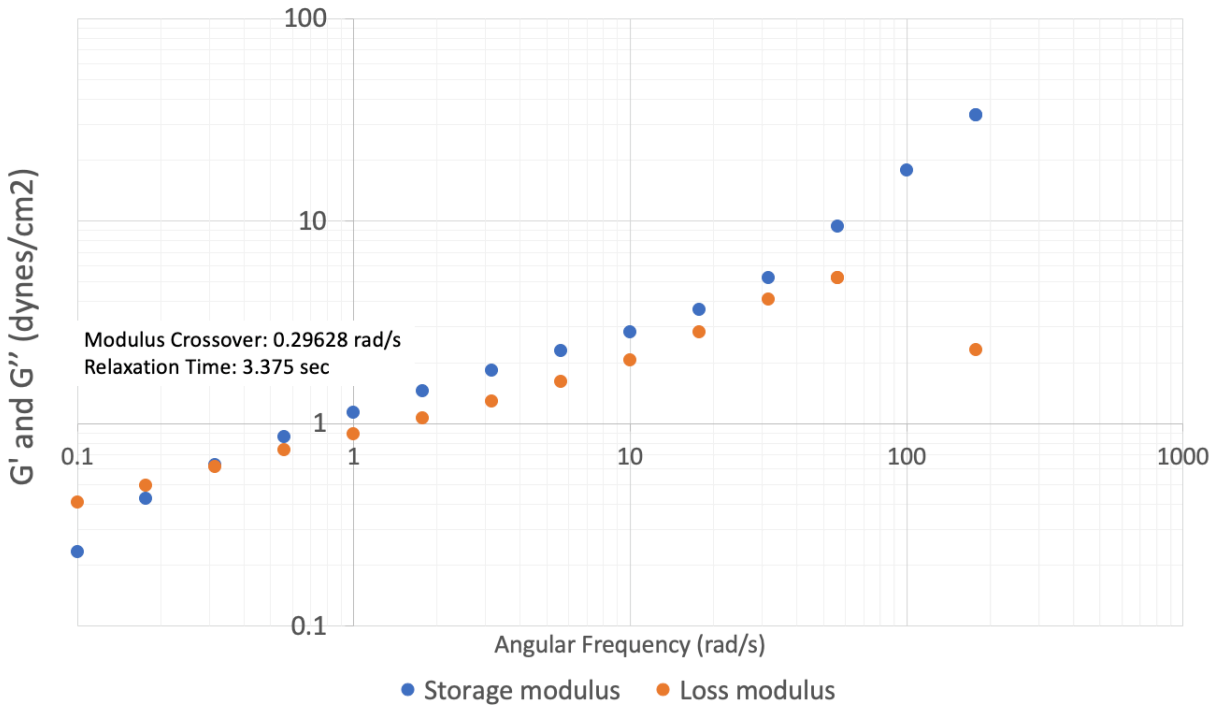


Figure 3.2: Example of elastic polymer DFST. G' and G'' modulus crossover is observed and relaxation time is calculated to be almost 3.4 sec.

***Steady Rate Sweep Test (SRST)***

The steady rate sweet test analyzes the shear viscosity (μ) of the solution as a function of shear rate (γ) at a constant temperature (25°C). The shear rates ranged from $0.1s^{-1}$ to $300s^{-1}$. The shear thinning region of the curve was fitted to a power-law model to determine the polymer power-law constants. This region was generally between the shear rates of 1 $s^{-1}$ to 100 $s^{-1}$ as seen in Figure 3.3.

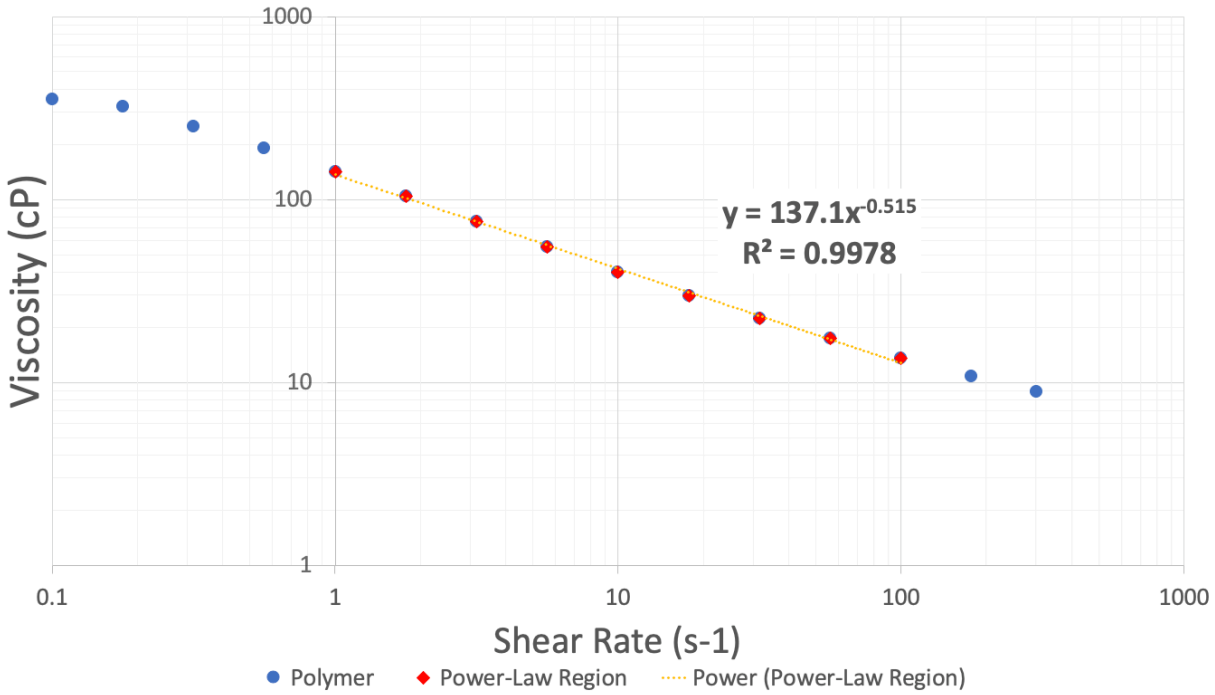


Figure 3.3: Example of elastic polymer SRST. Viscosity is plotted versus shear rate. The shear thinning region is fitted with a power-law regression.

The viscosity shown in Figure 3.3 can be fitted to the power law model, i.e.,

$$\mu_{app} = K\dot{\gamma}^{1-n} = 137.1\dot{\gamma}^{0.515} \tag{3.2}$$

where *K* is then 137.1, and *n* is 0.485.

## 3.2 CORE FLOOD EQUIPMENT

### 3.2.1 Pump

All core flood experiments were performed at constant flow rates. A Teledyne Instrument Specialties Company (ISCO) pump (Figure 3.4) was used to inject a fluid at a desired flow rate. The pump has a capacity that can vary from 500 mL to 1000 mL (dependent on column size). Pumps held mineral oil that was used to displace fluids into the core, and were refilled immediately when emptied to prevent long periods of inactive time during chemical floods. Effluent fractions were collected based on the set flow rate on the pump.

Figure 3.4: Pump used to inject fluids in experiments.

### 3.2.2 Brine and Polymer Solution Columns

Custom polycarbonate columns, shown in Figure 3.5, were used to hold brine and polymer solutions that were injected into the core. These columns were custom designed to hold different volumes of solution. Mineral oil was injected into these columns, and would displace

the brine or polymer out into the core. The exact volume of mineral oil injected was carefully determined so that only brine or polymer would be displaced and no mineral oil enters the core.

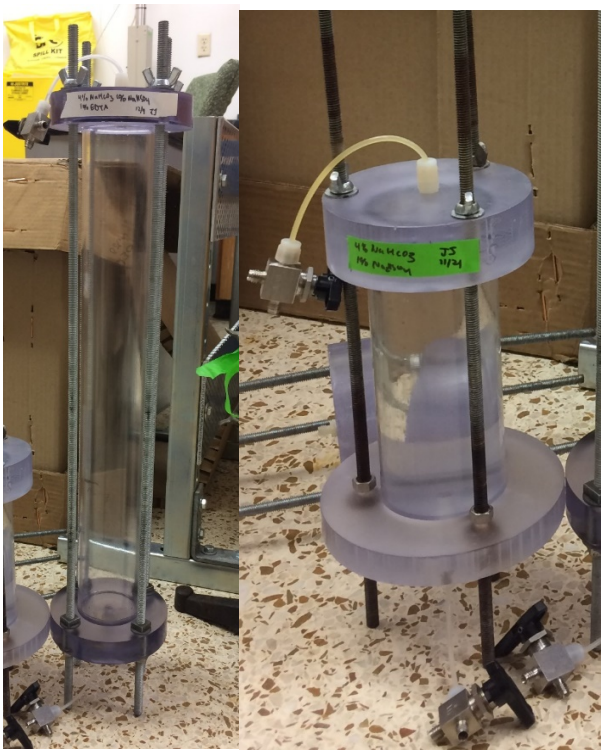

Figure 3.5: Polycarbonate columns used to hold injection solutions.

### 3.2.3 Oil Stainless Steel Column

Stainless steel cylinders with stainless steel Swagelok fittings were used to inject oil into the core at higher pressures (>40 psi).

### 3.2.4 Pressure Transducers

Pressure transducers (Rosemount 3051T) were connected to the core in all experiments. There were four sectional pressure transducers that record a pressure range of 0-30 psi. There were two additional whole pressure transducers that record pressures from 0-150 psi. The hydraulic connection between the pressure tap and the pressure transducer pressure drop was

recorded by a data acquisition software (National Instruments LabView™). Figure 3.6 shows a generalized set up of the pump, core, columns, and pressure transducers.

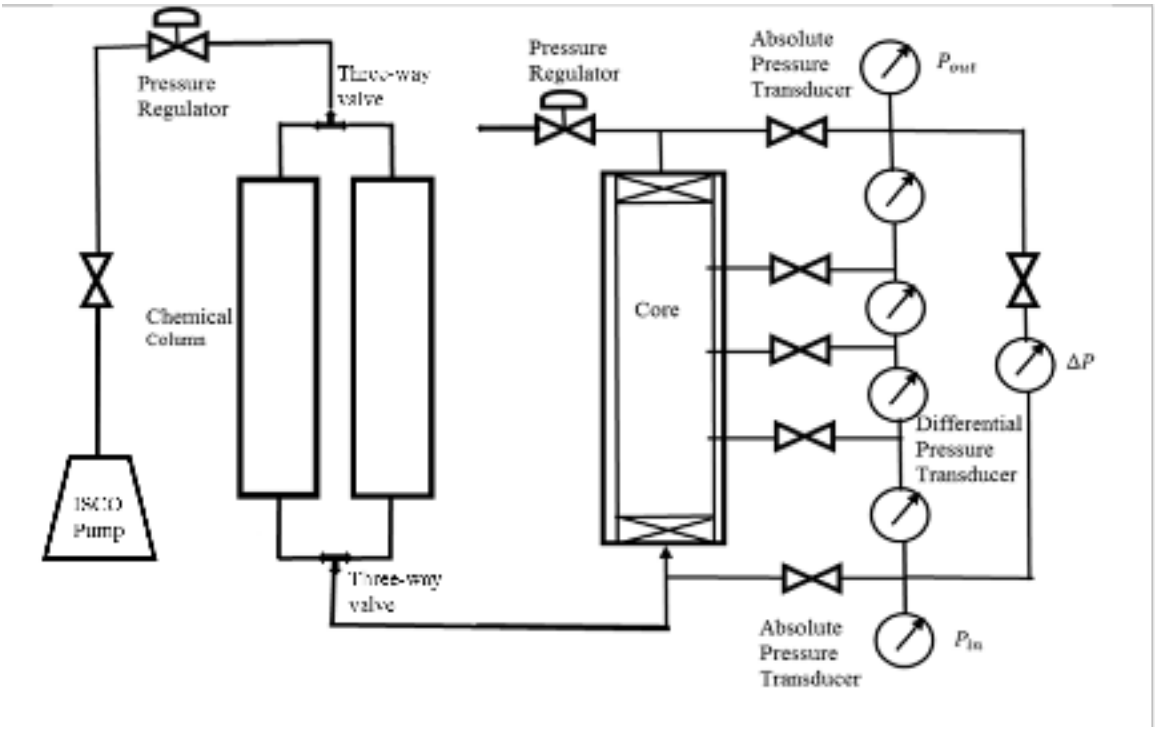


Figure 3.6: General core flood schematic showing pump, core, and pressure transducer set up.

### 3.2.5 Fractional Sample Collector

A Teledyne ISCO Retriever 500 fraction collector (Figure 3.7) was used to collect effluent samples from each experiment. The fraction collector was programmed to move every set time interval as determined by the flow rate and desired fraction size. For example, for a flow rate of 0.1mL/min and a fraction size of 9 mL, the appropriate time interval was calculated to be $\frac{9ml}{0.1ml/min}$ or 90 minutes. In this example, after 90 minutes, the fraction collector would move to the next tube, and have collected 9 mL of effluent.

Figure 3.7: Fraction collector used to collect effluent samples in experiments.

### 3.2.6 Refractometer

A hand-held portable refractometer (Figure 3.8) was used for reading the refractive index/salinity index of solutions. The refractometer measures salinity from 0 parts per thousand (% ppt) to 100 ppt. It also measures specific gravity (d 20/20) from 1-1.070. To measure the salinity index of effluent samples, the refractometer was used to determine the salinity of the effluents in parts per thousand.

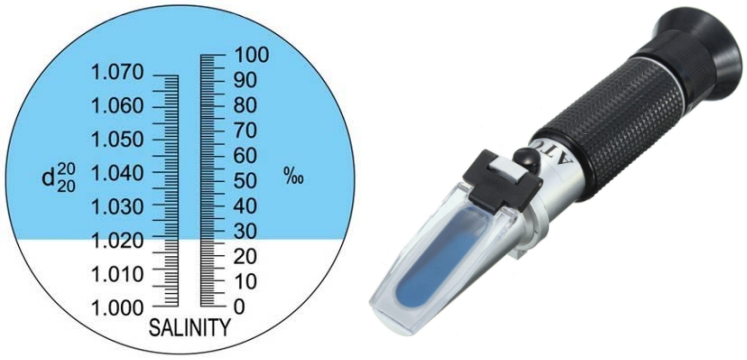


Figure 3.8: Refractometer and salinity index.

## 3.3 CORE PREPARATION AND SET-UP

Cores used in these experiments were all 2 inches in diameter and 12 inches in length.

Both Bentheimer and Boise sandstone blocks (1ft$^3$) were provided by Kocurek Industries. Cores were drilled out from the original sandstone blocks and dried in a high temperature oven (at least 70 ºC) overnight.

### 3.3.1 Core Epoxy Preparation

Sandstone cores were taken from the oven after being dried, and left to cool to room temperature. The dimensions of the core (diameter, length, mass) were measured and recorded. Bulk Volume ($V_B$) of the core was determined in equation 3.3 as:

$$V_B = hA = h\pi\frac{D^2}{4} \tag{3.3}$$

where $h$ is the core height, $A$ is the area, and $D$ is the diameter of the core.

The density of the core can be determined in equation 3.4 as:

$$\rho_B = \frac{m}{V_B} \tag{3.4}$$

where $\rho_B$ is the density of the core, and $m$ is the mass of the core.

Two end caps (Figure 3.9) were placed on the ends of the core and connected to the core with quick 5-minute curing epoxy (Grainger). The end caps were custom made from polycarbonate or ULTEM if using corrosive chemicals that react with polycarbonate (such as silanes or acetone). The epoxy was only used to secure the end caps to the end of the core, but it was important to leave the flat end of the core clear of any epoxy to prevent any blockage.

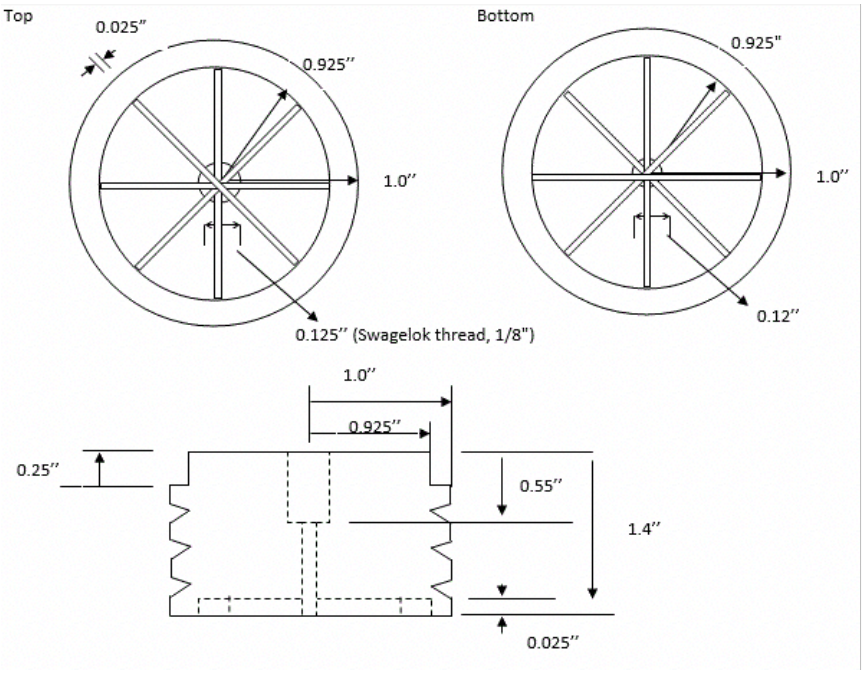


Figure 3.9: Custom polycarbonate end cap pieces

Additional 5-minute epoxy was then coated all over the side of the core, which was used to seal the core surface face. The quicker curing epoxy created a protective coat that will prevent the imbibition of the slow curing epoxy into the sandstone. Once the quick 5-minute curing epoxy has set, the core was placed in the middle of a larger polycarbonate tube (2.5-inch diameter and 15-inch length). The inlet and outlet of the end pieces should be protected with tape to prevent epoxy from leaking in and blocking the inlet or outlet of the core.

The slow curing, 24-hour epoxy was prepared by mixing the epoxy base (EPON Resin 828) with the curing agent (Versamid 125) in a 2:1 ratio by weight. The epoxy was mixed in a disposable plastic container until it becomes a homogenous mixture. This slow curing epoxy was poured into the annular space between the core and the polycarbonate tube. The epoxy was poured slowly to prevent the formation of large air bubbles. The core was left to cure overnight, at minimum. The epoxy must have solidified completely before moving on to drilling the

pressure taps.

The cores were then drilled in three evenly spaced out holes for pressure taps. The pressure taps should be on the same vertical line. The taps were secured with more epoxy and connected to 3-way Swagelok valves. To make sure the taps have been drilled properly, high pressure (95 psi) air was injected into the core and used to make sure all taps are flowing properly. The cores were submerged in a water bath while air was being injected into the core. If there were any leaks or points of weakness in the epoxy, bubbles should appear in the water. The integrity of the core must be confirmed before moving on to any next steps.

### 3.3.2 Wettability Alteration

The sandstones used in these experiments were all initially water-wet; two experiments were performed in oil-wet media, so the wettability of Bentheimer cores was altered for those experiments. Organosilane compounds, such as dichlorodiphenylsilane (DCDPS) and chlorotrimethylsilane (CTMS) consist of silicon molecules with chlorines and hydrophobic organic groups were the main chemicals for the oil-wet core treatment. The general formula of this type of silane is $R_nSiCl_{4-n}$ where R is typically methyl or phenyl and n is equal to 0, 1, 2, or 3. After the reaction with the hydroxyl group (OH) on silicon dioxide surfaces of sandstones, the organic groups are exposed on the surface, thus generating non-hydrophilic wettability (Figure 3.10).

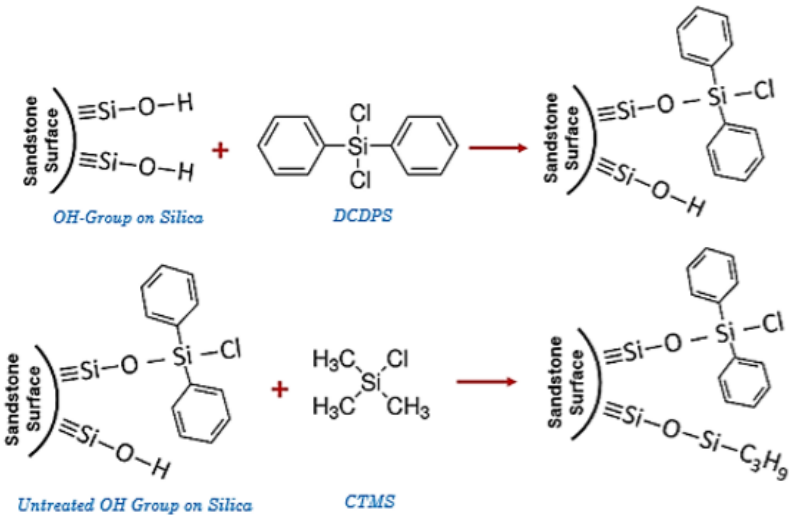


Figure 3.10: Chemical reaction on sandstone surface to produce an oil-wet surface.

The following method was followed to generate an oil-wet surface at Bentheimer sandstone cores in these experiments. The cores were dried in the oven at temperature 120°C for 24 hours. After the cores were cooled down at the room temperature, cores were put into a stainless core holder and connected to a vacuum pump in order to remove any fluid inside dry cores. A confining pressure was applied at 650 psi. The dry core was then imbibed with 7% dichlorodiphenylsilane (DCDPS) at 150 psi at constant pressure. Once the core was sufficiently imbibed with DCDPS, the core was allowed to age for at least 1 hour. The core was then flushed with at least 1.5 PV of dried 100% hexane, at 20 ml/min constant flow rate to remove any remaining DCDPS. Dried hexane was then injected at 150 psi constant pressure and allowed to age for at least 1 hour, or even overnight. At least 1 PV of 7% chlorotrimethylsilane (CTMS) was then used to flush out the hexanes at 20ml/min constant flow rate, and then injected under constant pressure at 150 psi. The CTMS was allowed to age in the core for at least 1 hour. After the cores were sufficiently aged, the cores were cleaned of chemicals by injecting 100% hexane.

All wastes were collected in the fume hood and the injected solvents were stored in the stainless-steel accumulator. After the chemical treatment process, the cores were placed in the oven for 24 hours.

This method could also be completed in an epoxy core set up, as long as the end caps were made of chemically resistant material (such as ULTEM or PEEK). For cores in stainless steel core-holders, an overburden of 650 psi was held prior to the injection of silanes. The constant pressure injection of the chemicals were increased to 350 psi of constant pressure. All tubing should be stainless-steel. As previously discussed, it was important to remove as much water from all materials when working with the organosilanes. Any glass jars or tubing washed with water or chemicals were completely dried in 100$^{o}$C before being used. It was assumed that the pore structure of the core such as pore-size distribution and connectivity was not changed after the process.

To determine the wettability of the surface, water droplets were placed on the surface of the dry core. Originally, water instantly imbibed into the dry core (water-wet core) because dry pore spaces contained gas which was the most non-wetting fluid. After oil-wet treatment, as shown in Figure 3.11, water drops could not imbibe into the dry core. These results suggest that the wettability of the core was strongly oil-wet.

Figure 3.11: Water droplets on a Bentheimer core surface.

After becoming oil-wet, cores were allowed to dry completely before proceeding with the experiments.

### 3.3.3 Core Saturation

The pore volume (PV) of the core was estimated by the volume of brine that was imbibed into a vacuumed core. PV was defined as the aqueous volume the core has when 100% saturated with brine. The dry core was first vacuumed with a vacuum pump for at 2-3 hours at minimum. An initial volume ($V_i$) of waterflood brine was recorded in a graduated cylinder. The core inlet was connected to the graduated cylinder and the waterflood brine was allowed to be imbibed into the vacuumed core. When no change in volume of the graduated cylinder was observed, a final volume ($V_f$) was recorded and PV was calculated by:

$$PV = V_i - V_f \tag{3.5}$$

The estimated PV was then used to determine porosity of the core in equation 3.6, which was the ratio of pore volume to bulk volume ($V_b$):

$$\phi = \frac{PV}{V_b} \tag{3.6}$$

The PV in this case was considered an estimate that was confirmed after the salinity tracer test.

### 3.3.4 Salinity Tracer Test

The salinity tracer tests that were completed in these studies were done by injecting two brines with different salinities. The tracer test can show rock homogeneity and determine pore volume. In these experiments, the cores were initially saturated with a low salinity waterflood brine (1000 ppm NaCl + 400 ppm $NaHCO_3$), and it was displaced with high salinity brine (4% NaCl and 1% NaHCO3) at a flow rate of 2mL/min. Effluents were collected every 4 minutes, and the salinity of the tubes were measured using a refractometer. The refractive index (RI) values were read from the refractometer were normalized in Equation 3.7 as:

$$RI_{normalized} = \frac{RI_{effluent} - RI_{minimum}}{RI_{maximum} - RI_{minimum}} \tag{3.7}$$

The normalized salinity was plotted against effluent volume. The aqueous volume was considered the area above the curve, shaded in the example in Figure 3.12.

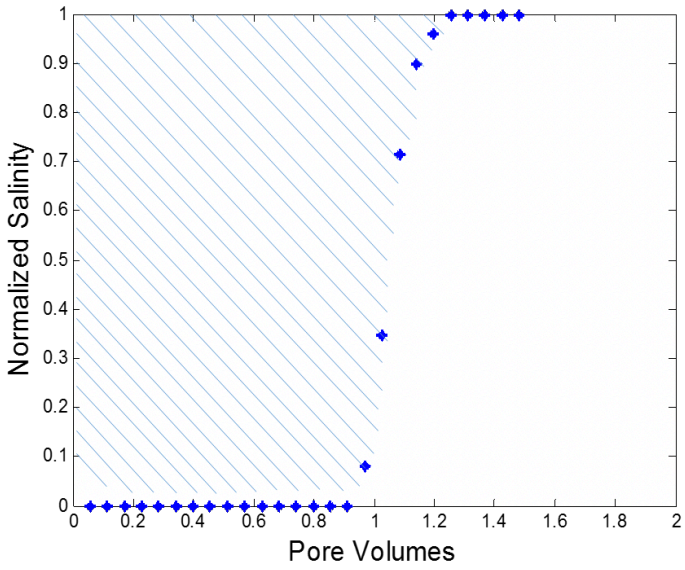


Figure 3.12: Tracer test in core going from low salinity brine to high salinity brine. PV of core is calculated as the area above the curve.

Bentheimer cores were considered very homogeneous, and a sharp salinity gradient was

observed. The displacement of the brine was stable, and the volume of the displaced brine was considered equal to the total core PV. This PV was compared to the PV estimated during the saturation of the core, and the porosity of the core was confirmed.

### 3.3.5 Brine Permeability of the Core

Waterflood brine was used to measure single phase brine permeability. Brine permeability was calculated from Darcy's Law in Equation 3.8:

$$k = \frac{\mu q L}{\mathrm{A}\Delta P} \tag{3.8}$$

where $k$ is the brine permeability, $L$ is the core length, $A$ is the core cross-sectional area, $\Delta P$ is the change in pressure, $q$ is the volumetric flow rate, and $\mu$ is the fluid viscosity.

Brine was injected into the core at different flow rates and the pressure drop was recorded. Permeabilities were calculated from the pressure gradients and flow rates at steady state. The average of these permeabilities was used and considered the brine permeability. Figure 3.13 shows an example of a plot of different pressure values during the different brine injection rates.

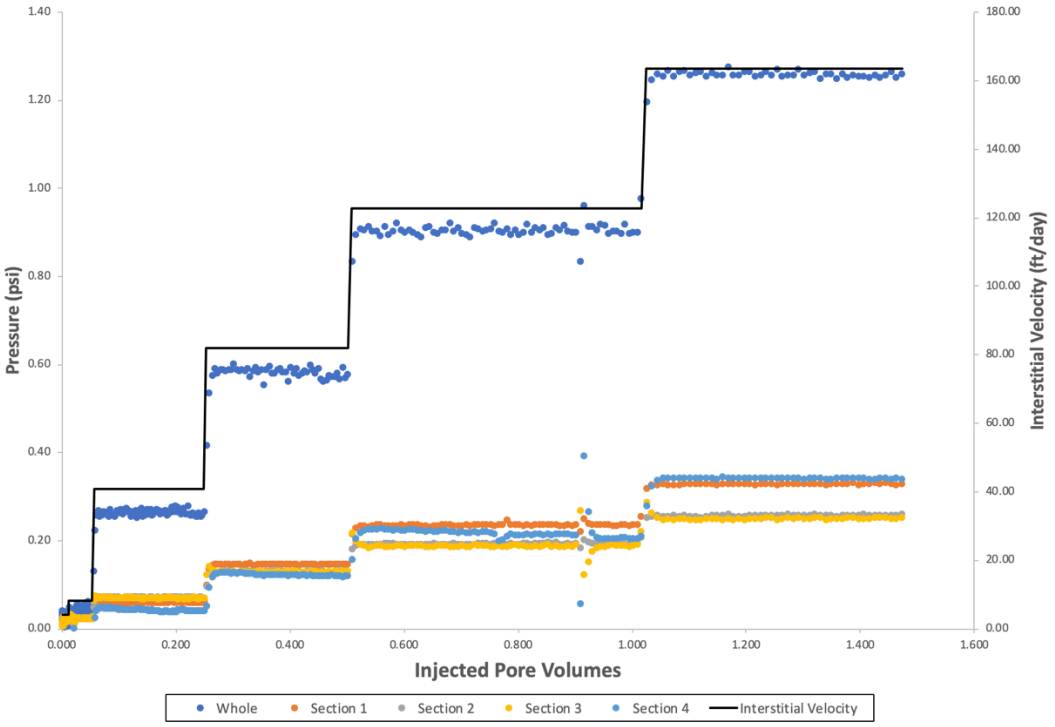


Figure 3.13: Pressure values during different brine injection rates used to calculate brine permeability.

### 3.3.6 Iron Reduction in the Core

The sandstones used in these experiments (Bentheimer and Boise) contain significant amounts of iron ions, which could degrade the polymers chemically. Ferric ions have been found to crosslink some HPAM polymers, prevent good polymer transport, and also degrade polymers in the presence of oxygen. Thus, all cores were flushed with a reducing iron brine (4% $NaHCO_3$, 1% $Na_2S_2O_4$, 1% tetra-sodium EDTA) to remove amorphous oxidized iron. The cores were flooded with this reduction brine, and continuously flooded at about 1mL/min (10.4 ft/day) in order to reduce the iron in the core. This was continued until a steady state iron concentration of 3 or less ppm as measured by the MQuant Iron Test Strips (0, 3, 10, 25, 50, 100, 250, 500 mg/l $Fe^{2+}$). Once the effluent was measured to be below 3 ppm, the core was flushed with brine (4% $NaHCO_3$ + 1% $Na_2S_2O_4$) to clear the core of EDTA, and the iron concentration measured on the

strip was 0 ppm. It was noted that far more reduction solution was needed to reduce the Boise sandstone cores to acceptable iron levels in comparison to the Bentheimer sandstone cores.

### 3.3.7 Oil Flood

After the core has been reduced of ferric ions, cleared of EDTA, and saturated with waterflood brine, the core can be flooded with filtered crude oil. Stainless steel columns were filled with low viscosity oil as previous described. These columns were connected to compressed air lines. The gas was set at a constant pressure (20-40 psi) and used to displace the oil into the core. Two large burettes (100 mL) collected effluent, and the oil saturation was determined by the amount of brine that was displaced by the oil. Oil flooding was continued until the oil cut has reached 99% and steady state pressure drop has been reached. As the oil was collected in the burette, the volume was recorded as well as the time per volume increment which can be used to calculate flow rate. The core was allowed to age with oil for at least 48 hours prior to subsequent floods. Initial oil saturation ($S_{oi}$) was the ratio of total displaced brine as observed in the burettes ($V_{brine\ in\ burette}$), to the core pore volume (PV) as determined previously.

$$S_{oi} = \frac{V_{brine\ in\ burette}}{PV} \tag{3.9}$$

Residual water saturation ($S_{wr}$) was determined in Equation 3.10:

$$S_{wr} = 1 - S_{oi} \tag{3.10}$$

The end point oil relative permeability (Equation 3.10) can be back-calculated using Darcy's Law (3.8):

$$k_{ro}{}^{o} = \frac{k_o}{k} = \frac{\mu_{oil} q L}{A \Delta P k} \tag{3.11}$$

where $k_o$ is effective oil permeability, $k_{ro}{}^{o}$ is endpoint oil relative permeability, and $\mu_{oil}$ is oil

viscosity.

### 3.3.8 Water Flood

After the core was aged in oil, a waterflood was performed by injecting desired brine at a constant flow rate (interstitial velocity of 1ft/day) until steady state pressure is observed and oil cut is zero. Oil cut was considered the ratio of the oil volume to the total effluent volume. The interstitial velocity ($v$ ft/day), also referred to as the frontal velocity, can be defined as the volumetric flow rate ($q$) divided by porosity ($\phi$) and the cross-sectional area of the core ($A$) (Equation 3.12). The Darcy velocity ($u$), also referred to as the superficial velocity, can be defined as the ratio of the volumetric flow rate to the cross-sectional area of the core.

$$v = \frac{u}{\phi} = \frac{q}{A\phi} \tag{3.12}$$

The oil cut of an effluent was the ratio of oil versus the total volume of the effluent sample. Once steady state was reached, and oil cut was low, the water flood was continued or flow rate was increased (interstitial velocity of 2ft/day or 5ft/day) for an additional 2-3 PVs. Oil saturation was measured from mass balance based on oil cuts. The end point water relative permeability can be back-calculated using Darcy's Law (3.8):

$$k_{rw}{}^{o} = \frac{k_w}{k} = \frac{\mu_{brine} q L}{A \Delta P k} \tag{3.13}$$

where $k_w$ is effective brine permeability, $k_{rw}{}^{o}$ is endpoint brine relative permeability, and $\mu_{brine}$ is brine viscosity. The mobility of the flood is calculated in equation 3.14 as:

$$M = \frac{\frac{k_{rw}{}^{o}}{\mu_w}}{\frac{k_{ro}{}^{o}}{\mu_o}} = \frac{k_{rw}{}^{o} \mu_o}{k_{ro}{}^{o} \mu_w} \tag{3.14}$$

### 3.3.9 Polymer Flood

All waterfloods were followed by an elastic polymer flood. Polymer floods were prepared as previously described. Stock solutions were diluted to target concentrations and salinities. All solutions were filtered in the method previously mentioned and degassed in argon for at least an hour. Solutions were transferred into the accumulator columns through a vacuum to prevent additional gasses from being trapped in the solution. All solutions were injected at constant flow rate and effluents were collected. Effluents were collected and analyzed in a similar manner to the brine flood effluent samples. Residual oil saturation ($S_{orp}$) was calculated:

$$S_{orp} = S_{or} - \frac{V_o}{PV} \tag{3.14}$$

where $V_o$ is the volume of total oil produced in the polymer flood as measured through the oil cut fractions, and $S_{or}$ is the residual oil saturation after the previous flood (could be brine or another polymer flood).

#### 3.3.9.1 First Polymer Flood (Viscoelastic)

The waterflood was succeeded by a low-salinity, viscoelastic polymer flood. Four out of the five experiments used FP3630s as the viscoelastic polymer flood. The stock solution of 6000 ppm FP3630s was diluted in low-salinity brine for a final concentration of 1000 ppm 3630s in 1000 ppm NaCl + 400 ppm $NaHCO_3$. One of the experiments used a higher molecular weight polymer (FP6040). The stock solution of 6000 ppm FP6040 was diluted in low-salinity brine for a final concentration of 1000 ppm 3630s in 1000 ppm NaCl + 400 ppm $NaHCO_3$. All of the polymer solutions were injected at a constant flow rate until steady state was reached and oil cut was zero. All viscoelastic floods were designed to have high Deborah numbers. The Deborah

number was defined as Equation 2.5, or the equivalent shear rate (equation 2.6) multiplied by the relaxation time obtained through the dynamic frequency sweep test (DFST) (Figure 3.2).

The volume of the oil that was produced during the polymer flood was collected in glass test tubes and measured. Effluent samples were collected in fractions of 9-10 mL and the total volume of oil and polymer were read. The total volume of the effluent was recorded, and the oil-water interface was also recorded. The volume of oil ($V_o$) was the oil-water interface volume subtracted from the total effluent volume. The oil saturation was calculated as described in equation 3.14. Effluent samples were kept and the effluent polymers were used to measure rheological properties as well as effluent salinity if needed. The effective permeability ($k_{rp}$) of the low-salinity, elastic flood was calculated through iterations of Darcy's law, apparent viscosity of the polymer, and the equivalent shear rate. Darcy's law can be rearranged to equation 3.15

$$k_{rp} = \frac{\mu_{app} q L}{\mathrm{A}\Delta P} \tag{3.15}$$

and apparent viscosity ($\mu_{app}$) as seen in equation 3.2. Because the apparent viscosity was dependent upon the equivalent shear rate ($\dot{\gamma}_{eq}$), and the equivalent shear rate was determined by flow rate and relative permeability, iterations were completed between equations 3.2, 3.15, and 2.6 to determine polymer relative permeability. End point relative permeability ($k_{rp}{}^{o}$) was determined as the effective permeability to the brine permeability. End point mobility ratio ($M_{o\ viscoelastic\ polymer}$) of the viscoelastic polymer flood was calculated from equation 3.16:

$$M_{o\ visoelastic\ polymer} = \frac{\left(\frac{k_{rp}{}^{o}}{\mu_{polymer}}\right)}{\left(\frac{k_{ro}{}^{o}}{\mu_{o}}\right)} = \frac{k_{rp}{}^{o}\,\mu_{o}}{k_{ro}{}^{o}\,\mu_{polymer}} \tag{3.16}$$

Capillary numbers during the polymer flood was calculated as shown in equation 2.2 by using the maximum pressure drops.

**3.3.9.2 Second Polymer Flood (Inelastic)**

The viscoelastic polymer flood was succeeded by an inelastic polymer flood. The inelastic polymer flood was composed of either a high-salinity, inelastic FP3630s solution, a salinity, low molecular weight inelastic FP3330s solution, or low salinity, inelastic scleroglucan solution. All polymer solutions were formulated as described previously using the same methods of dilution, and filtration. All of the polymer solutions were injected at a constant flow rate until steady state was reached and oil cut was zero. The inelastic polymer floods were designed to have low Deborah numbers (below or around 1). The Deborah number was defined as Equation 2.5, or the equivalent shear rate (equation 2.6) multiplied by the relaxation time obtained through the dynamic frequency sweep test (DFST) (Figure 3.2).

Effluent samples were collected similar to the previous floods. The volume of the oil that was produced during the polymer flood was collected in glass test tubes and measured. The total volume of the effluent was recorded, and the oil-water interface was also recorded. The volume of oil ($V_o$) was the oil-water interface volume subtracted from the total effluent volume. The oil saturation was calculated as described in equation 3.14. The effective permeability ($k_{rp}$) of the inelastic flood was calculated through the same iterations of Darcy's law, apparent viscosity of the polymer, and the equivalent shear rate as the viscoelastic polymer flood as previously described in equation 3.15. End point relative permeability ($k_{rp}{}^{o}$) and end point mobility ratio ($M_{o\ viscoelastic\ polymer}$) were also iterated in the same calculations as the previous polymer flood as

described (equation 3.16). Capillary numbers during the inelastic polymer flood was calculated as shown in equation 2.2 by using the maximum pressure drops.

# Chapter 4: Core Flood Experimental Results

In this chapter, the results and analysis of five coreflood experiments will be discussed. The purpose of these experiments was to isolate and determine the mechanisms behind the reduction of residual oil saturation in sandstones by viscoelastic polymers .

## 4.1 CORE FLOOD EXPERIMENTS

Corefloods completed in the past by Erincik (2017) and Qi (2018) were done with high viscosity oil in water-wet high permeability Bentheimer sandstone cores. Qi (2018) also completed six additional core floods with light viscosity oil in Bentheimer sandstones. In the current experiments, low viscosity oil was used and some of the cores were oil-wet. Three experiments (#1, #2, #3) were conducted in high permeability Boise sandstones, and two experiments (#4, #5) were conducted in homogenous, high permeability oil-wet Bentheimer sandstones. Residual oil saturation was measured after consecutive injection of a brine, an elastic polymer, and an inelastic polymer. The elastic/inelastic polymer floods were sequentially alternated until steady state and a final residual oil saturation was reached. All experiments used the same (batch and dilution) low viscosity crude oil (4-6cP). Four different types of polymer were used in these experiments: Flopaam™ (FP) 6040, 3630s, 3330s, as well as EOR-grade scleroglucan. All percentage dilution values are based upon weight, or weight parts per million (ppm). Viscous glycerin was chosen not to be injected directly after the waterflood in these core floods. The end point mobility ratios of waterfloods were less than or close to 1 because of low oil viscosity and small waterflood injection flow rates.

Boise sandstones are relatively more heterogenous in comparison to Bentheimer sandstones. Salinity tracer tests were conducted in both Boise and Bentheimer cores. The change

of salinity in the Bentheimer core is sharper than that in the Boise sandstone (Figure 4.1) indicating lower dispersity and less heterogeneity. The Boise sandstone cores in general had a much higher permeability (3800-4200mD) in comparison to the Bentheimer sandstone cores (1000-1300 mD).

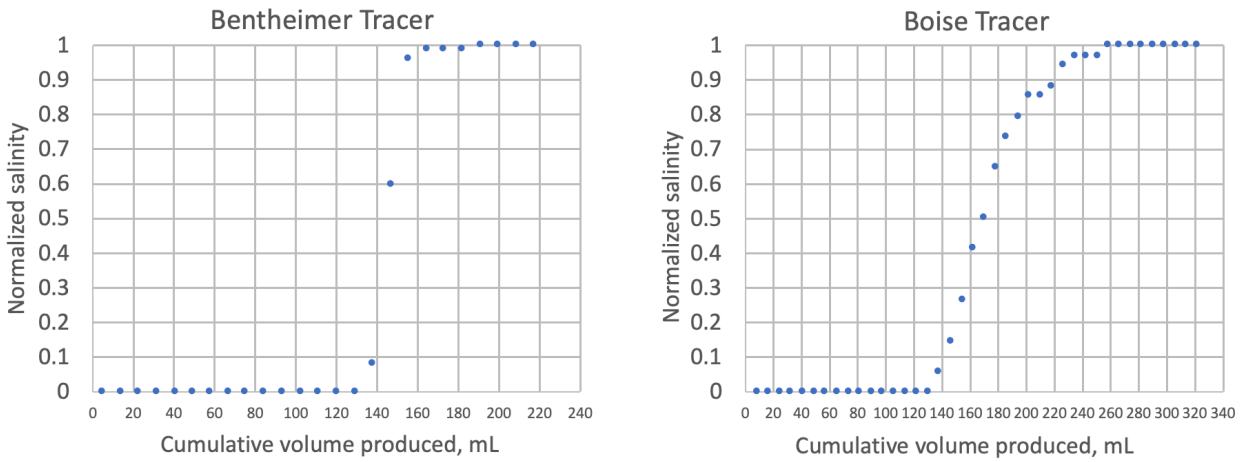


Figure 4.1: Comparison of salinity tracer tests between Bentheimer sandstone and Boise sandstone.

The main purpose of these experiments were to determine if alternating viscoelastic and inelastic polymer floods would reduce residual oil saturation in Boise core floods, and if these polymer floods would also reduce saturation in oil-wet cores. Different inelastic polymers were used to test if the change in elasticity or change in salinity was the reason for the further reduction of saturation. Experiments were completed at low pressure gradients to see if the alternating polymer floods would still succeed. Elastic polymer floods were also made with a higher molecular weight polymer to see if increasing relaxation number (and as a result, Deborah number) would improve oil recovery.

## 4.2 EXPERIMENT #1: BOISE CORE #1

### 4.2.1 Core Preparation and Conditioning

The purpose of this coreflood was to test the effect of viscoelasticity on residual oil saturation when a high-salinity polymer flood was performed following a low-salinity polymer flood repeatedly. These cycles were conducted until a steady state residual saturation was achieved. The polymer floods were designed to keep the capillary number lower than the critical capillary number in Boise sandstone cores (~$1x10^{-4}$). Table 4.1 summarizes the general properties of the core and the fluids.

Table 4.1: Core and experimental fluid properties for experiment #1

| | |
|---|---|
| **Core Name** | BS 1-2 |
| **Rock Type** | Boise Sandstone |
| **Brine permeability (mD)** | 4000 |
| **Crude Oil Viscosity (cP)** | 4.5 |
| **Temperature ($^oC$)** | 23 |
| **Diameter (cm)** | 5.0 |
| **Length (cm)** | 28.575 |
| **Area ($cm^2$)** | 19.66 |
| **Bulk Volume (cc)** | 561.92 |
| **Pore Volume (mL)** | 175 |
| **Porosity** | 0.31 |
| **Bulk Density (g/cc)** | 2.00 |
| **Brine Composition** | 1000 ppm NaCl + 400 ppm $NaHCO_3$ + 400 ppm $Na_2S_2O_4$ |
| **Elastic Polymer Composition** | 1000 ppm FP3630s HPAM polymer in 1000 ppm NaCl + 400 ppm $NaHCO_3$ aqueous solution |
| **Inelastic Polymer Composition** | 2200 ppm FP3630s HPAM polymer in 20,000 ppm NaCl + 400 ppm $NaHCO_3$ aqueous solution |

The Boise sandstone core was dried in a 100°C oven overnight and then potted in epoxy in preparation for core flooding as described in Chapter 3. The estimated pore volume from brine imbibition was 180 mL. The iron reducing fluid was injected at varying rates (1, 5, 10, 15, 20 ml/min) to determine brine permeability which was estimated to be ~4000mD using Darcy's Law. Figure 4.2 shows the pressure drop values of the different brine injection rates.

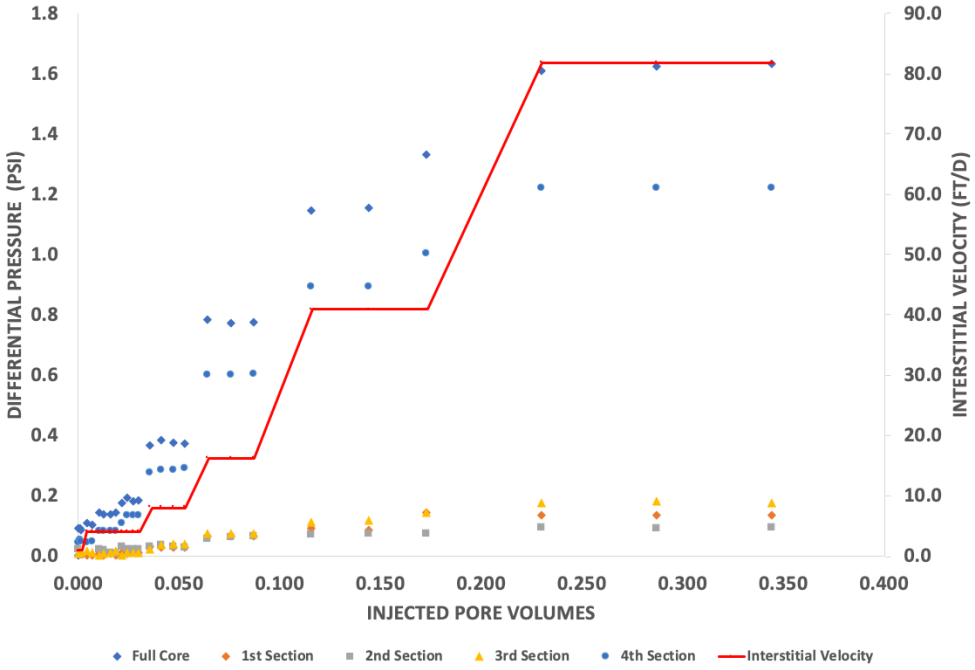


Figure 4.2: Pressure drop during brine injection experiment #1.

Following the iron reduction test, a salinity tracer test was performed to calculate the pore volume and heterogeneity of the core. A low salinity brine (1000 ppm NaCl + 400 ppm $NaHCO_3$ + 400 ppm $Na_2S_2O_4$) (0.0 normalized salinity) was injected at 1.5 ml/min to displace the iron reduction solution previously existing in the core (1.0 normalized salinity) as shown in Figure 4.3. Figure 4.3 shows the salinity of the effluent samples decreasing as the low salinity brine displaces the higher salinity brine solution present in the core. The pore volume of the core was calculated to be 175 mL.

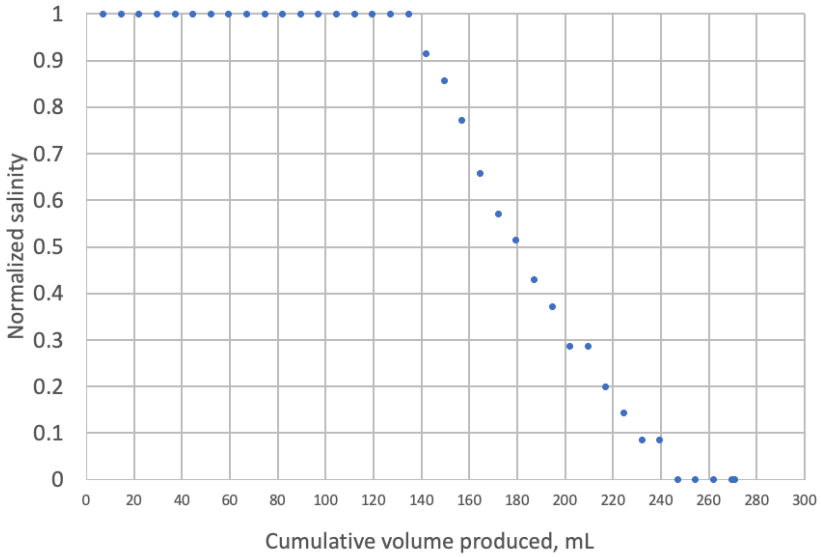

Figure 4.3: Salinity tracer test for experiment #1

### 4.2.2 Oil Flood

Diluted dead crude oil (with 13% toluene) was filtered through 1.2 μm filter paper under 20 psi of air at 23ºC. The diluted oil was found to have a viscosity of 4.5 cP. The low viscosity oil was injected into the core at a constant pressure using argon at 30 psi. At least 1.5 PV of oil was injected. Volumetric calculations were used to determine initial oil saturation ($S_{oi}$) by observing the volume of water and oil produced in burettes during the oil floods. The displaced brine volume was used to calculate initial oil saturation. Oil flood continued until there was a consistent water cut of 0%. The core was allowed to age with the oil for at least 48 hours. Initial oil saturation was determined to be 65%.

### 4.2.3 Waterflood

An aqueous solution of 1000 ppm NaCl + 400 ppm $NaHCO_3$ + 400 ppm $Na_2S_2O_4$ was injected at constant flow rate of 0.125 ml/min, (1 ft/day). This brine was injected until steady state pressure was reached and the oil cut was zero. Oil saturation (Figure 4.4) after waterflood

was calculated to be 34.1%. The pressure gradient at steady state was recorded to be 0.75 psi/ft (Figure 4.5).

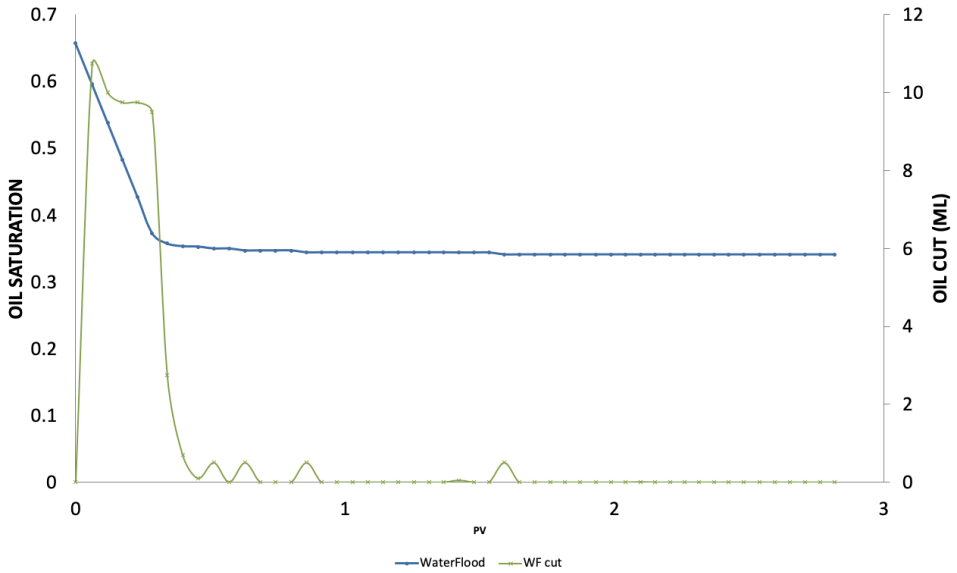


Figure 4.4: Oil saturation after waterflood in experiment #1.

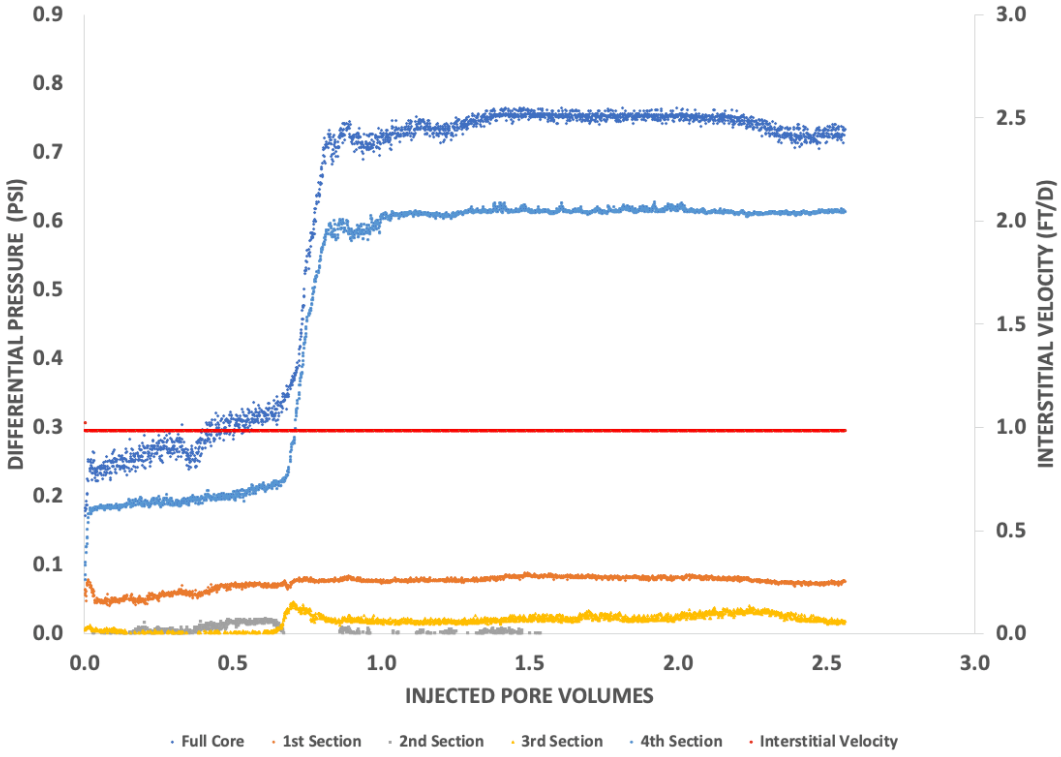


Figure 4.5: Waterflood pressure data for experiment #1.

### 4.2.4 Polymer Floods for Experiment #1

A high molecular weight polymer (FP3630s) was prepared in the same low salinity brine as the waterflood (1000 ppm NaCl + 400 ppm $NaHCO_3$). This solution produced a polymer with a high relaxation time (1.45 sec) and referred to as the "elastic polymer". After hydrating for 24 hours, the solution was filtered under 15 psi of argon gas at 23°C through a 1.2 μm filter paper. The polymer solution was allowed to degas with argon for at least two hours before being transferred into the injection column. The same high molecular weight polymer (FP3630s) was prepared in a high salinity brine (2200 ppm FP3630s HPAM polymer in 20,000 ppm NaCl + 400 ppm $NaHCO_3$) in a similar manner. This solution produced a polymer with a very low relaxation time (0.02 sec) and referred to as the "inelastic polymer." Multiple batches of these polymer solutions were made as the floods were planned to be alternated until a steady state was reached. The dynamic frequency sweep test (DFST) was performed as previously discussed in Chapter 3 to determine relaxation times. The steady rate sweep test (SRST) was also performed as previously discussed in Chapter 3 to obtain the viscosity profiles of each polymer solution. The power-law viscosity region was used to fit an equation to create the power law model for the solutions.

The viscosities of the polymer solutions were compared to make sure that they were similar to avoid oil displacement due to viscosity differences (Figure 4.6). It can be noted that the high salinity, inelastic polymer had slightly lower viscosities at lower shear rates, but were nearly identical at a shear rate of 20 $s^{-1}$, the rate at which the core floods were conducted. Multiple batches of polymer slugs were made when steady state was not reached within a few cycles, but

the general relaxation time and viscosity profiles were all similar. Each batch was tested on the rheometer for quality control.

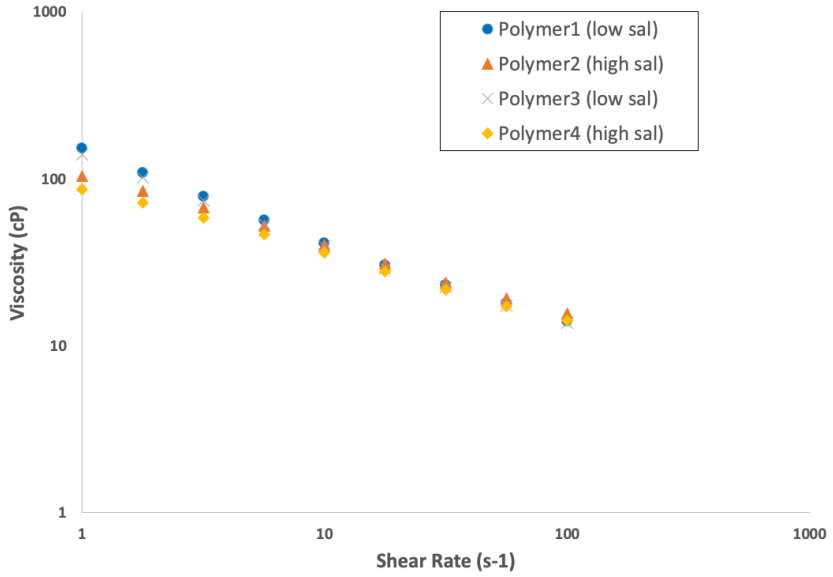


Figure 4.6: Polymer viscosities for experiment #1

#### 4.2.4.1 Polymer Flood #1 (Viscoelastic)

The low-salinity, elastic, polymer was injected at a constant flow rate of 0.12 ml/min (0.96 ft/day) until steady state (steady pressure drop for all four sections and zero oil cut). Figure 4.7 shows the pressure drops. The steady state was reached after almost 4 pore volumes. The pressure gradient at steady state was 6.75 psi/ft. The equivalent shear rate at steady state was 20.85 $sec^{-1}$. Oil saturation and oil cut during the waterflood and the first elastic polymer flood are shown in Figure 4.7. Residual oil saturation (Figure 4.8) was decreased from 34.1% to 24.3%, and the corresponding Deborah number was 39.61. The change in residual oil saturation was 9.8% for the first elastic polymer flood.

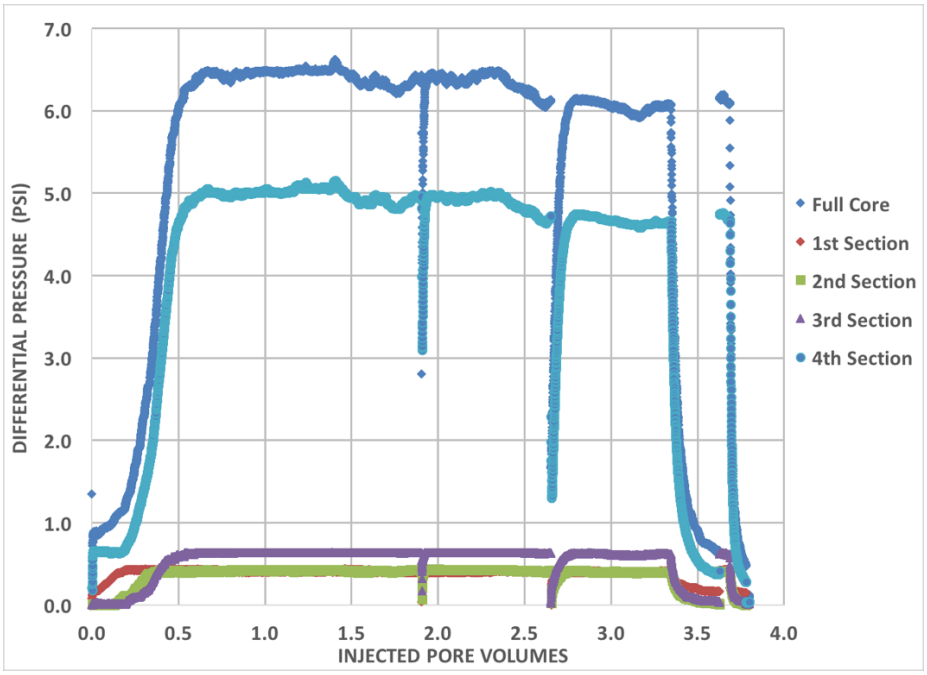


Figure 4.7: Pressure data during the first polymer flood (viscoelastic) during experiment #1.

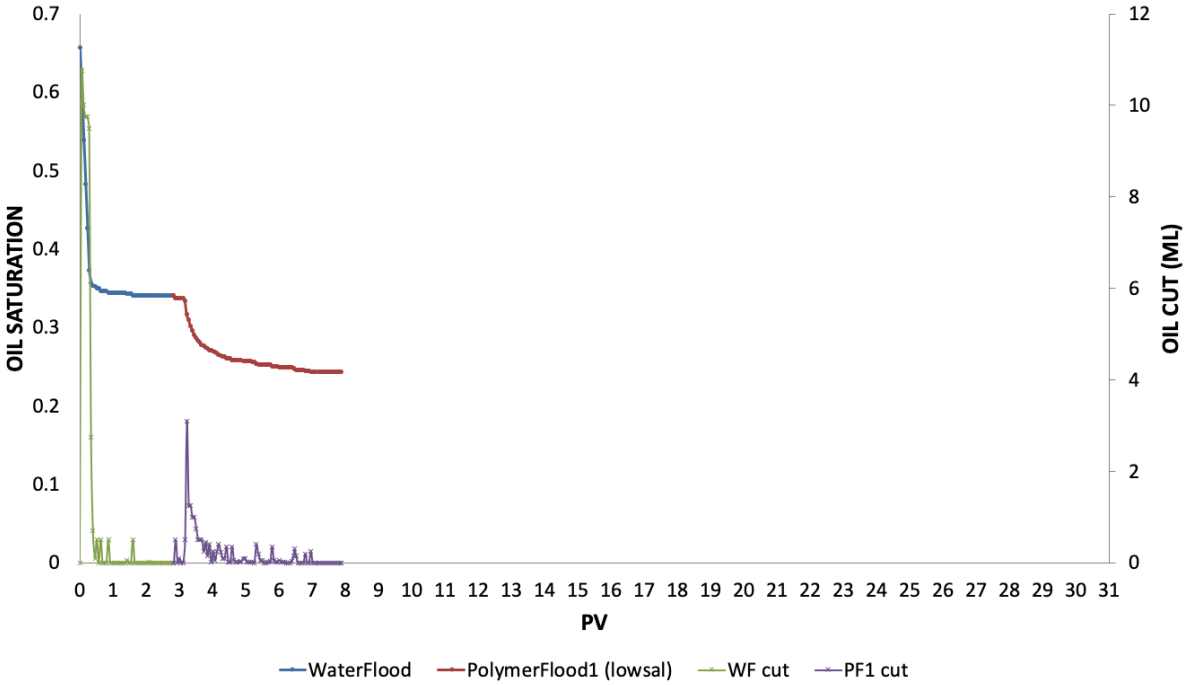


Figure 4.8: Oil saturation after the first polymer flood (viscoelastic) during experiment #1.

The cumulative oil recovery at the end of the polymer flood was 62.6% of the original oil in place. The maximum capillary number for the elastic polymer flood was 3.96 X $10^{-5}$, which was below the critical capillary number (1 X $10^{-4}$ as discussed in Chapter 2).

#### 4.2.4.2 Polymer Flood #2 (Inelastic)

The high-salinity, inelastic, polymer was injected at a constant flow rate of 0.12 ml/min (0.96 ft/day) until a steady state was reached and zero oil cut. Figure 4.9 shows the pressure drops in the core flood. The steady state was reached after almost 9 pore volumes. The pressure gradient at the steady state was lower than the previous flood, at 3.5 psi/ft. The equivalent shear rate at steady state was 13.08 $sec^{-1}$. Oil saturation and oil cut up to the first inelastic polymer flood are shown in Figure 4.10. Residual oil saturation was decreased from 24.3% to 19.8% during the inelastic polymer flood, and the corresponding Deborah number was 0.73. The change in residual oil saturation was 4.5% for the inelastic polymer flood.

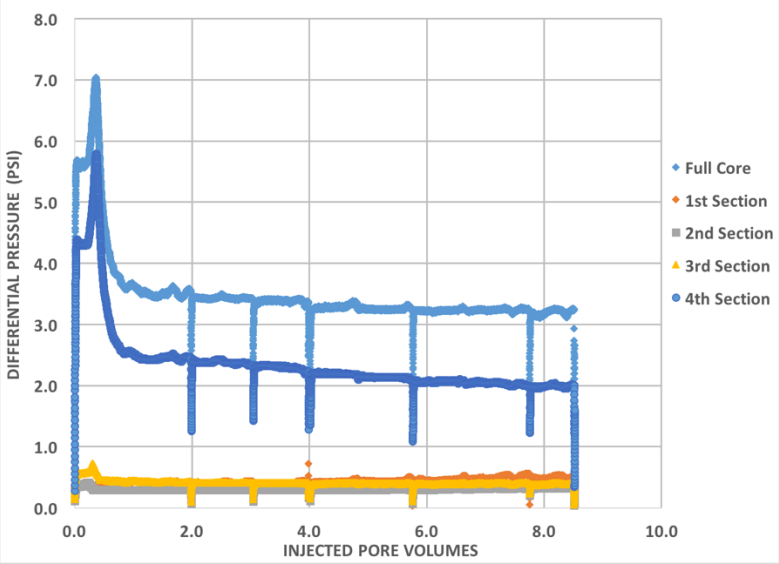


Figure 4.9: Pressure data during the second polymer flood (inelastic) during experiment #1.

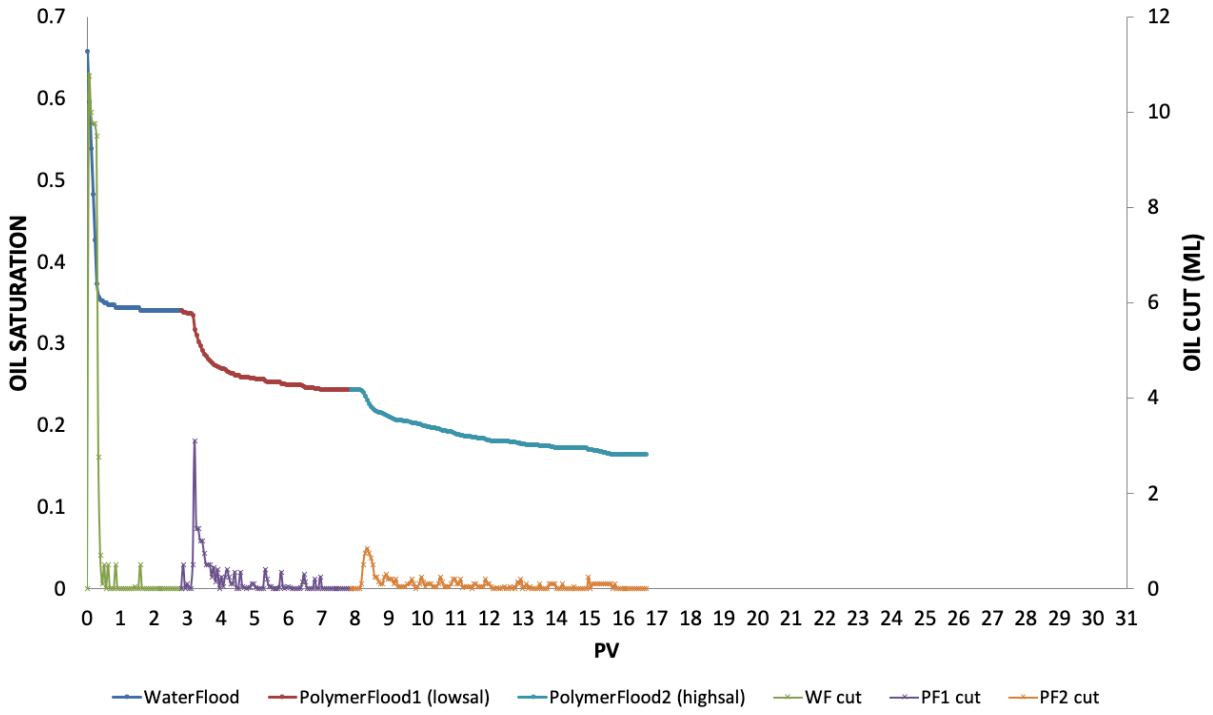


Figure 4.10: Oil saturation after the second polymer flood (inelastic) during experiment #1.

The cumulative oil recovery at the end of the polymer flood was 69.5% of the original oil in place. The maximum capillary number for the elastic polymer flood was 2.05 X $10^{-5}$, which was below the critical capillary number (1 X $10^{-4}$).

#### 4.2.4.3 Polymer Flood #3 (Viscoelastic)

The low-salinity, elastic, polymer was injected again at a constant flow rate of 0.12 ml/min (0.96 ft/day) until steady state was reached and zero oil cut. Figure 4.11 shows the pressure drops. The steady state was reached after almost another 9 pore volumes. The pressure gradient at steady state was 7.9 psi/ft. The equivalent shear rate at steady state was 20.26 $sec^{-1}$. Oil saturation and oil cut during the waterflood and the first elastic polymer flood are shown in Figure 4.11. Surprisingly, the residual oil saturation continued to decrease from 19.8% to 7.5%,

as shown in Figure 4.12, and the corresponding Deborah number was 29.81. The change in residual oil saturation was 12.3% from the elastic polymer flood.

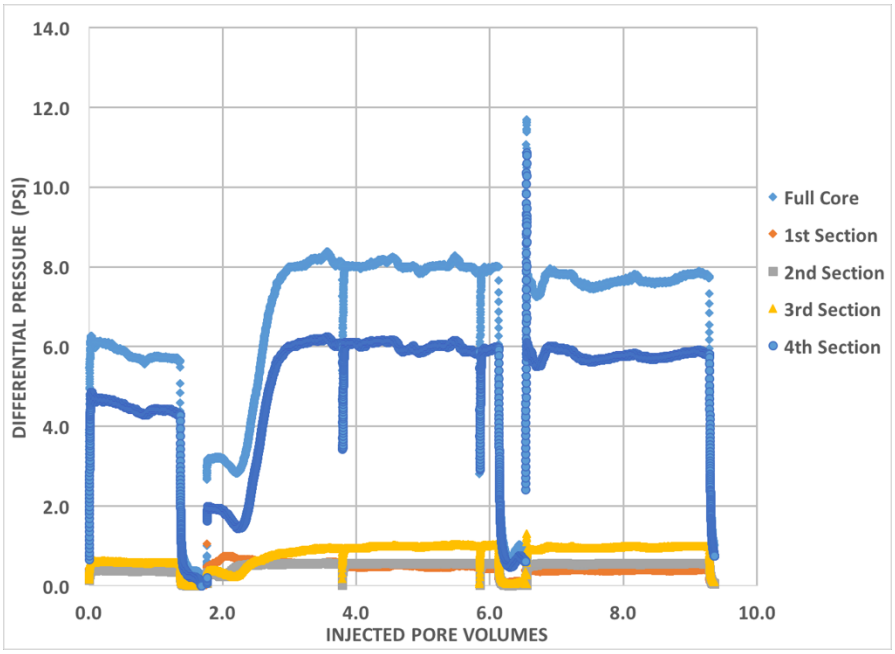


Figure 4.11: Pressure data during the third polymer flood (viscoelastic) during experiment #1.

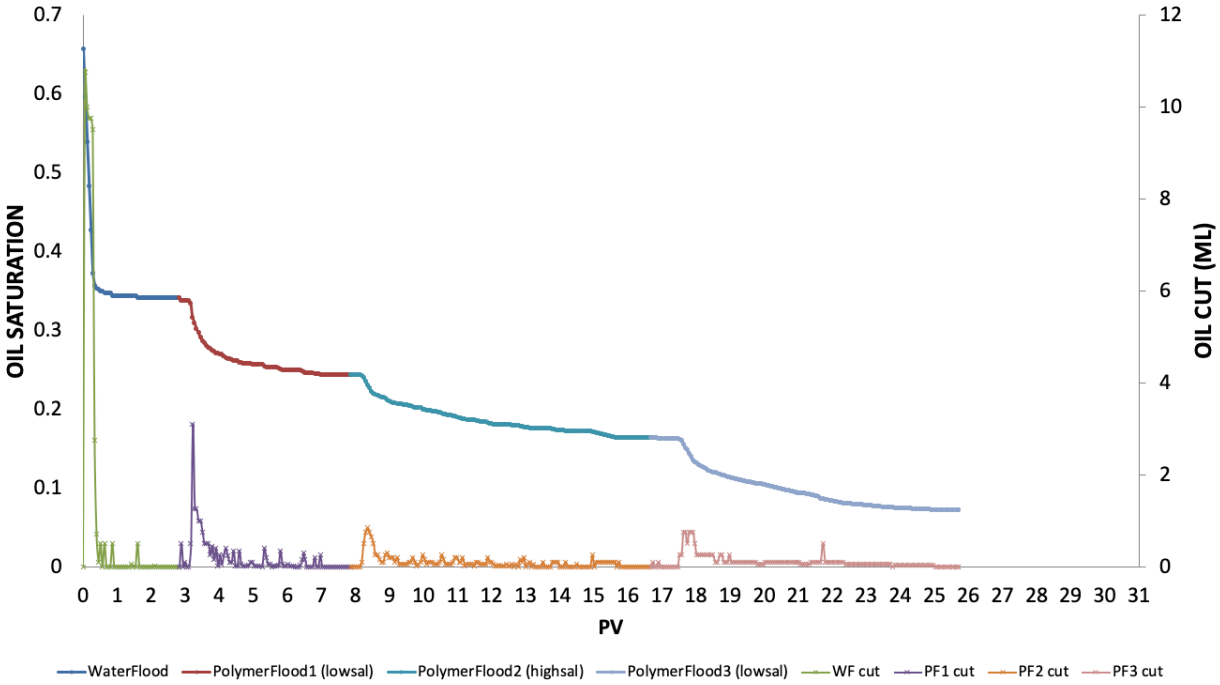


Figure 4.12: Oil saturation after the third polymer flood (viscoelastic) during experiment #1.

The cumulative oil recovery at the end of the polymer flood was 88.5% of the original oil in place. The maximum capillary number for the elastic polymer flood was 4.23 X $10^{-5}$, which was still below the critical capillary number (1 X $10^{-4}$).

#### 4.2.4.4 Polymer Flood #4 (Inelastic)

The final high-salinity, inelastic, polymer was injected at a constant flow rate of 0.12 ml/min (0.96 ft/day) until steady state was reached and zero oil cut. Figure 4.13 shows the pressure drops. The steady state was reached after just 2 pore volumes but the flood was continued for another pore volume. The pressure gradient at steady state was lower than the previous flood again, at 4.1 psi/ft. The equivalent shear rate at steady state was 13.86 $sec^{-1}$. Residual oil saturation was decreased from 7.5% to 5.3% as shown in Figure 4.14 and the corresponding Deborah number is 0.28. The change in residual oil saturation was 2% for the inelastic polymer flood.

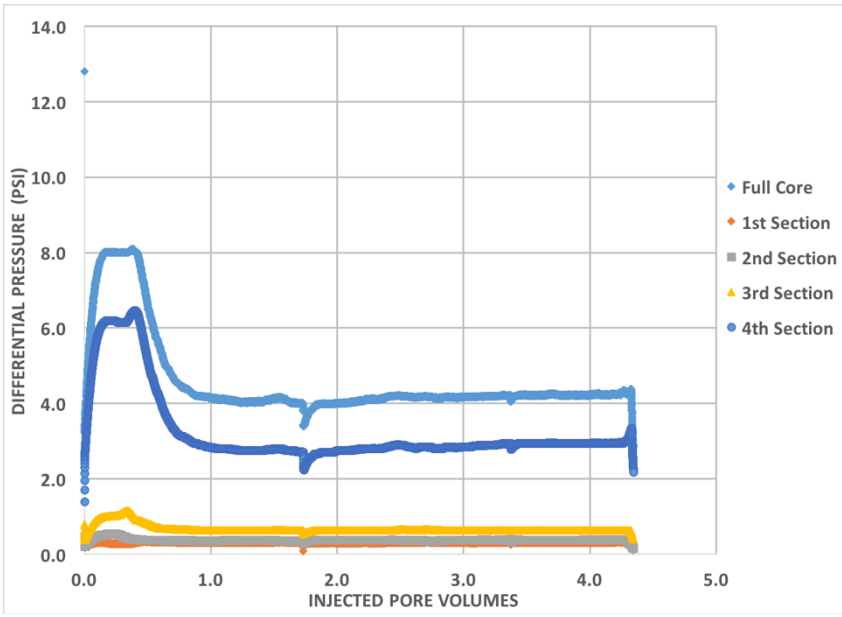


Figure 4.13: Pressure data during the fourth polymer flood (inelastic) during experiment #1.

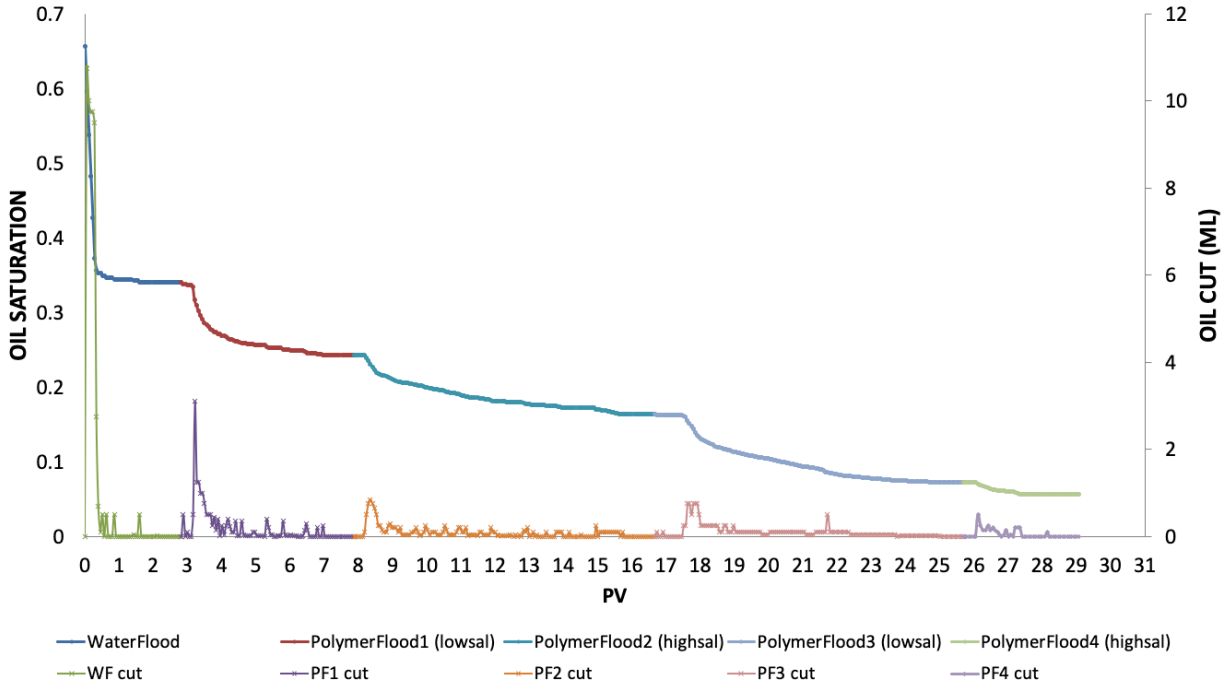


Figure 4.14: Oil saturation after all polymer floods during experiment #1.

The maximum capillary number for the inelastic polymer flood was 2.35 X $10^{-5}$, which was still below the critical capillary number (1 X $10^{-4}$). The cumulative oil recovery at the end of the polymer flood was 91.5% of the original oil in place from polymers alone. As the capillary number during all the floods were below the critical capillary number, the reduction in oil saturation is not due to changes in capillary pressure.

### 4.2.5 Final Salinity Gradient Tracer Test

As a confirmation of the final residual oil saturation, after the final high salinity, inelastic, polymer flood was completed, another low salinity polymer slug was injected as a tracer to estimate the available pore space available to polymer. The polymer pore volume was estimated to be 164ml, which suggests the oil occupies 11ml, or just about 6%, which confirms the oil saturation obtained through mass balance. The tracer test of the core prior to the oil flood and after chemical floods are shown for comparison in Figure 4.15.

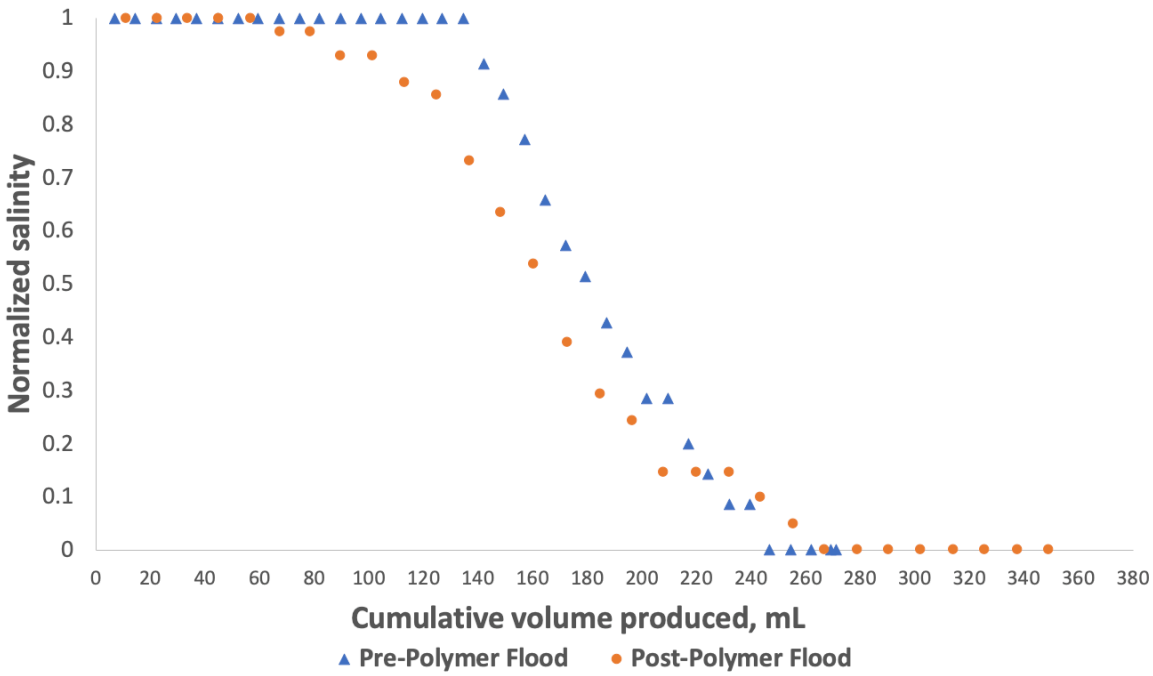


Figure 4.15: Comparison of salinity tracer tests before the oil flood and after the polymer floods in experiment #1

## 4.3 EXPERIMENT #2: BOISE CORE #2

Following the success of Experiment #1, Experiment #2 was designed to test the oil recovery due to viscoelasticity using lower pressure gradients. While the previous experiment had capillary numbers below the critical capillary number, this experiment was used to determine if pressure gradients lower than 3 psi/ft would produce similar results. This coreflood also explored using higher molecular weight polymer (FP6040) as polymers with potentially higher relaxation times. The second polymer flood was also designed to remove the variability of changing salinities between elastic and inelastic polymer floods. In the previous inelastic polymer flood experiment, the salinity was increased to decrease the relaxation time. In this experiment, a lower molecular weight polymer was used to decrease the relaxation time; the

same salinity was maintained in the inelastic polymer flood as the waterflood and the elastic polymer flood.

### 4.3.1 Core Preparation and Conditioning

The purpose of this coreflood was to test the effect of viscoelastic polymer floods on residual oil saturation when a low molecular weight polymer flood was performed following a high molecular weight polymer flood; these cycles were repeated until a steady state residual saturation was achieved. The polymer floods were designed to try to keep the capillary number lower than the critical capillary number in Boise sandstone cores ($\sim 1 \times 10^{-4}$). Table 4.2 summarizes the general properties of the core and the brine and polymer fluids.

Table 4.2: Core and experimental fluid properties for experiment #2.

| | |
|---|---|
| **Core Name** | BS 1-4 |
| **Rock Type** | Boise Sandstone |
| **Brine permeability (mD)** | 3962 |
| **Crude Oil Viscosity (cP)** | 6 |
| **Temperature ($^{o}$C)** | 23 |
| **Diameter (cm)** | 4.76 |
| **Length (cm)** | 30.32 |
| **Area (cm$^2$)** | 17.81 |
| **Bulk Volume (cc)** | 540.14 |
| **Pore Volume (mL)** | 170.4 |
| **Porosity** | 0.316 |
| **Bulk Density (g/cc)** | 2.00 |
| **Brine Composition** | 1000 ppm NaCl + 400 ppm $NaHCO_3$ + 400 ppm $Na_2S_2O_4$ |
| **Viscoelastic Polymer Composition #1** | 825 ppm FP6040 HPAM polymer in 1000 ppm NaCl + 400p pm $NaHCO_3$ aqueous solution |
| **Viscoelastic Polymer Composition #2** | 1000 ppm FP3630s HPAM polymer in 1000 ppm NaCl + 400 ppm $NaHCO_3$ aqueous solution |
| **Inelastic Polymer Composition** | 1500p pm FP3330s HPAM polymer in 1000 ppm |

| | |
|---|---|
| **#1** | NaCl + 400 ppm $NaHCO_3$ aqueous solution |
| **Inelastic Polymer Composition #2** | 2200 ppm FP3630s HPAM polymer in 20,000 ppm NaCl + 400 ppm $NaHCO_3$ aqueous solution |

The Boise sandstone core was dried in a 100ºC oven overnight and then potted in epoxy in preparation for core flooding as described in Chapter 3. The estimated pore volume from brine imbibition was 180mL. Once the core was saturated with this low salinity brine (0.0 normalized salinity), the high salinity iron reduction aqueous solution (4% $NaHCO_3$ + 1% EDTA + 1% $Na_2S_2O_4$) (1.0 normalized salinity) was injected at 2.5 ml/min to complete a salinity tracer test to calculate the pore volume and heterogeneity of the core. Figure 4.16 shows the salinity of the effluent samples increasing as the high salinity brine displaces the low salinity brine solution present in the core. The pore volume of the core was calculated to be 17.2 mL.

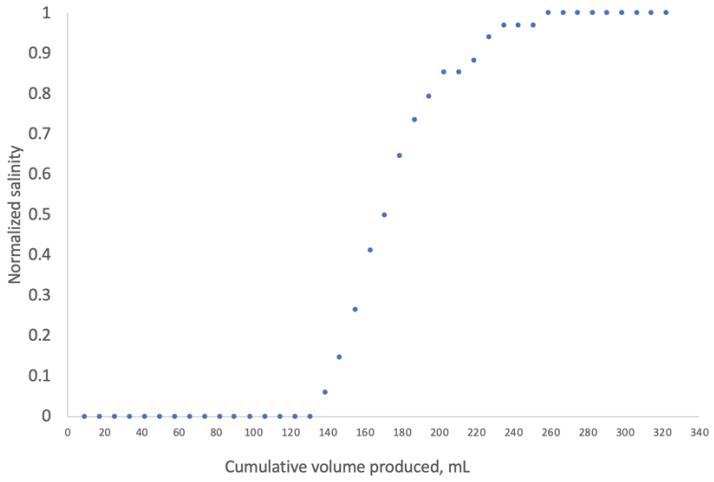


Figure 4.16: Salinity tracer test for experiment #2.

The core was continuously pumped with this iron reduction solution at 1ml/min (10.4 ft/day) in order to reduce the amorphous oxidized iron in the core. The iron reducing fluid was

injected at varying rates (1, 5, 10, 15, 20 ml/min), as seen in Figure 4.17, to determine permeability which was estimated to be 3962mD using Darcy's Law.

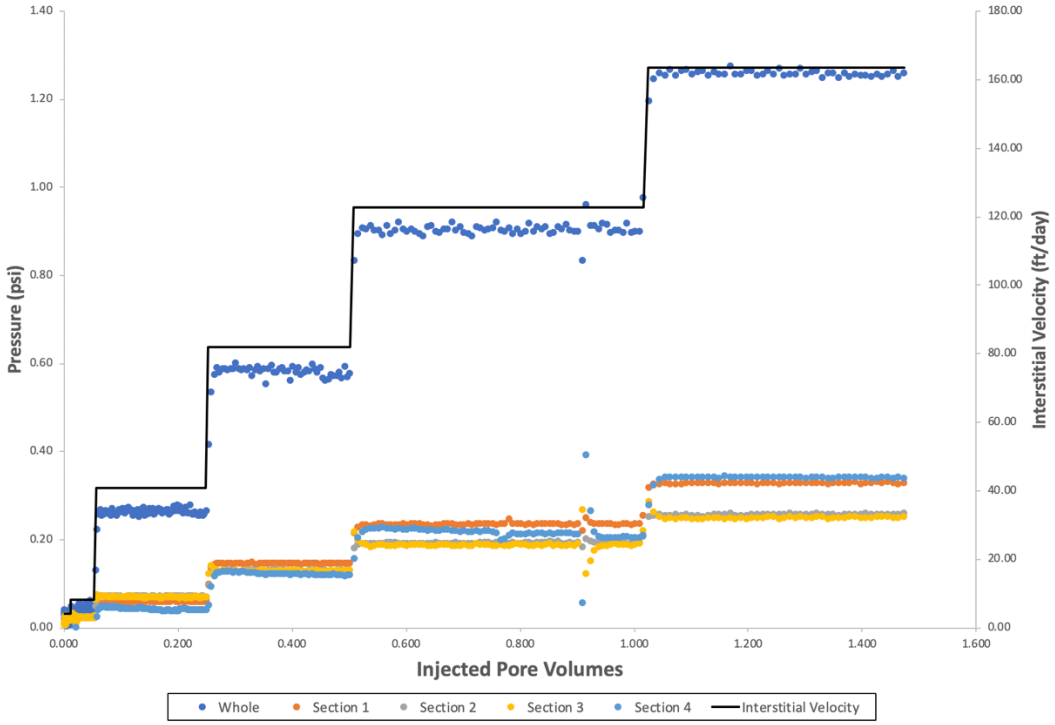


Figure 4.17: Pressure values while establishing brine permeability in experiment #2.

### 4.3.2 Oil Flood

Diluted dead crude oil (with 13% toluene) was filtered through 1.2 µm filter paper under 20 psi of air at 23ºC. The diluted oil was found to have a viscosity of 6 cP. The low viscosity oil was injected into core at a constant pressure using argon at 30 psi. At least 1.5PV of oil was injected. Volumetric calculations were used to determine initial oil saturation ($S_{oi}$) by observing the volume of water and oil produced in burettes during the oil floods. The displaced brine volume was used to calculate initial oil saturation. Oil flood continued until there was a consistent water cut of 0%. The core was aged with the oil for at least 48 hours. Initial oil saturation was determined to be 65.4%.

### 4.3.3 Waterflood

An aqueous solution of 1000 ppm NaCl + 400 ppm $NaHCO_3$ + 400 ppm $Na_2S_2O_4$ was injected at constant flow rate of 0.105ml/min, (0.887 ft/day), 0.12 ml/min (1 ft/day), and then 0.6 ml/min (5 ft/day). This increase in flow rate was to maintain that the oil saturation after waterflood was truly residual oil saturation. This brine was injected until steady state pressure was reached and the oil cut was zero. Oil saturation after waterflood was calculated to be 22%, as seen in Figure 4.18. The pressure gradient at steady state was recorded to be 0.075 psi/ft (0.887 ft/day), 0.1 psi/ft (1 ft/day), and 0.23 psi/ft (5 ft/day) (Figure 4.19).

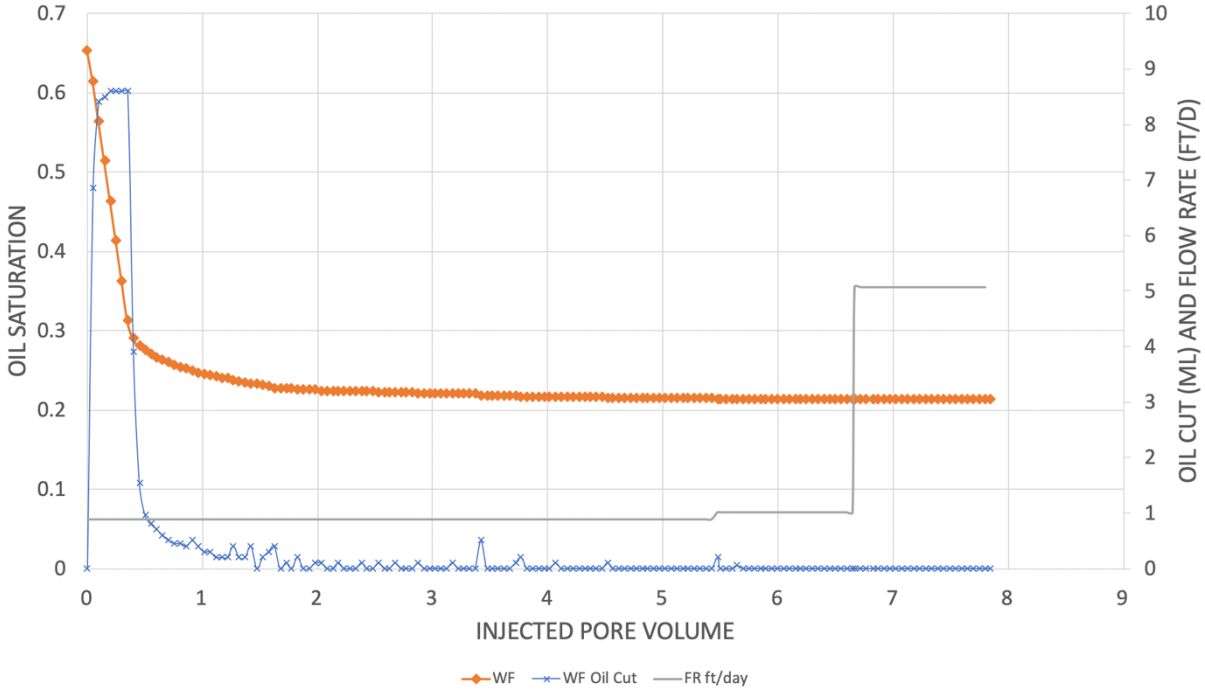


Figure 4.18: Oil saturation after waterflood in experiment #2.

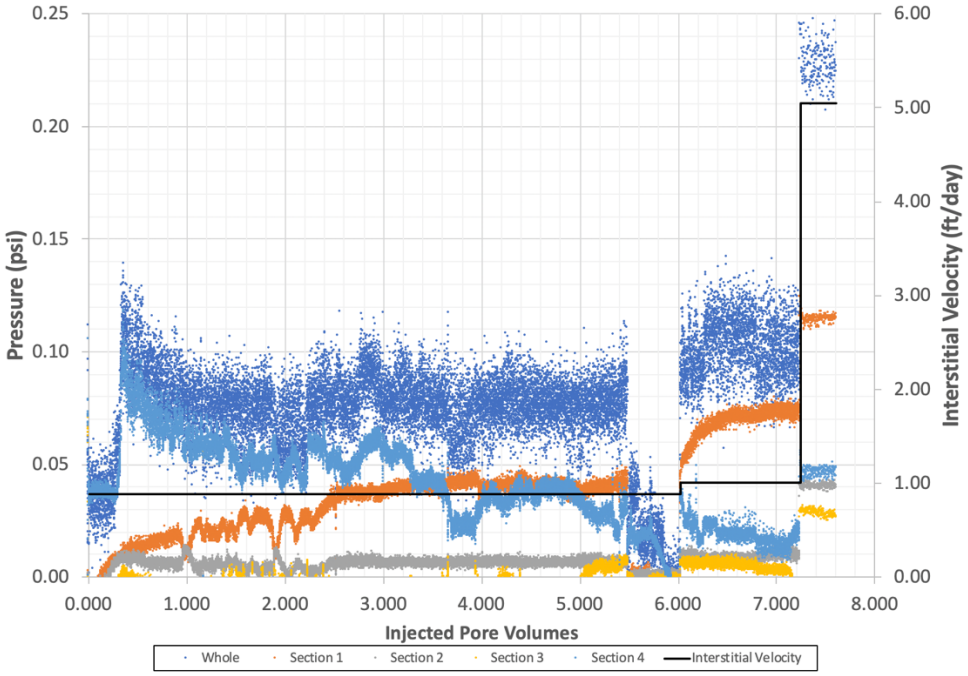


Figure 4.19: Waterflood pressure data for experiment #2.

### 4.3.4 Polymer Floods for Experiment #2

This coreflood explored the use of a higher molecular weight polymer (FP6040) as a polymer with higher relaxation time. Different concentrations of FP6040 were prepared in low salinity brine and their viscosity was measured (Figure 4.20).

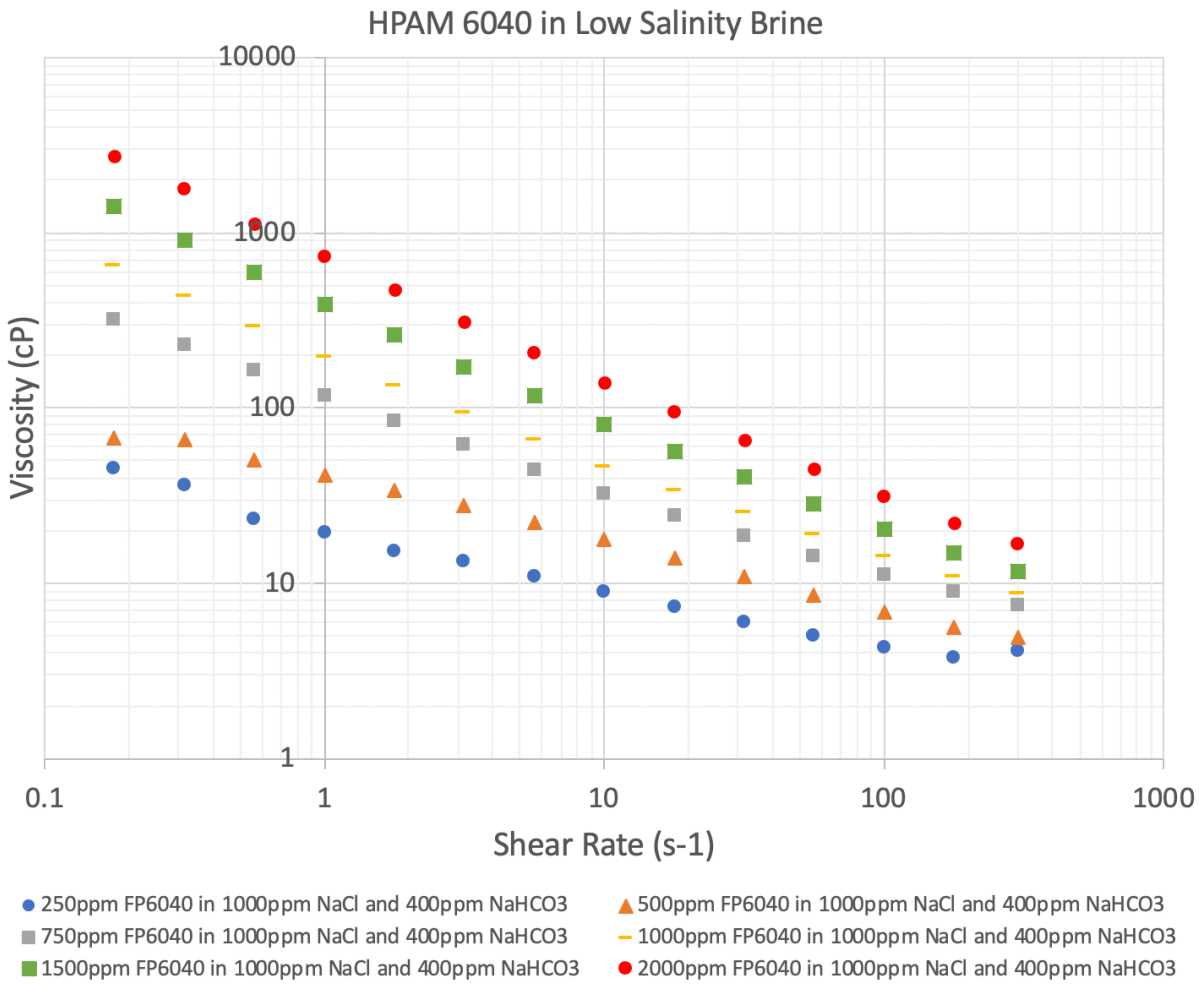


Figure 4.20: Viscosity of FP6040 in low salinity brine.

The second polymer flood was also designed to remove the variability of changing salinities between elastic and inelastic polymer floods. The previous inelastic polymer flood had increased the salinity of the flood to decrease relaxation time. In this experiment, a lower molecular weight polymer was used to decrease relaxation time, but also maintained the same salinity as the waterflood and the elastic polymer flood. Different concentrations of FP3330s were prepared in low salinity brine. The viscosity of these polymer solutions is shown in Figure 4.21.

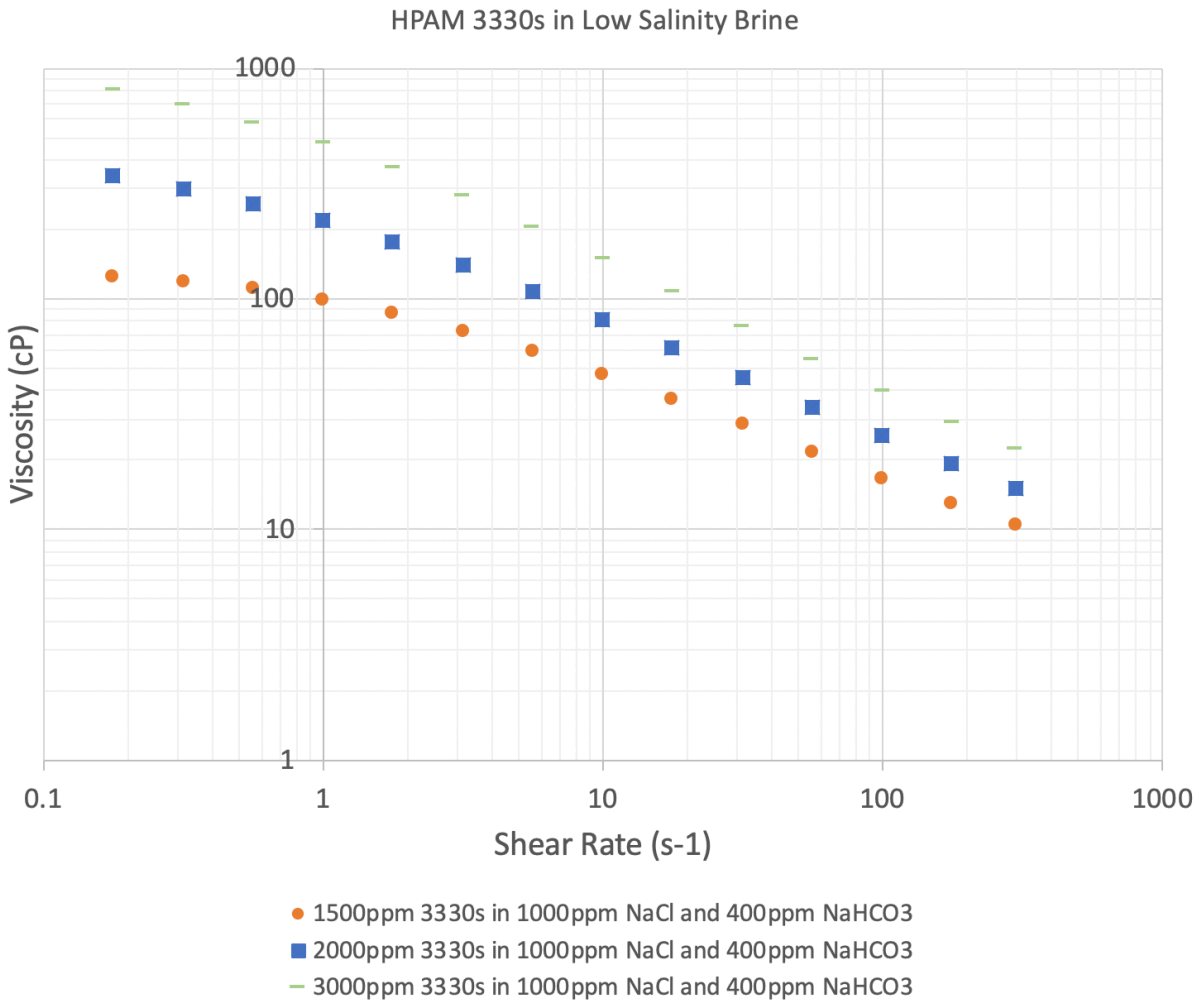


Figure 4.21: Viscosity of FP3330s in low salinity brine.

The FP6040 and FP3330s were diluted to maintain similar viscosities as the previously used 3630s. It was determined that the polymers that would fit the profile best was 825ppm FP6040 in low salinity brine (1000 ppm NaCl and 400 ppm $NaHCO_3$) as the new elastic flood and 1500 ppm FP3330s in low salinity brine (1000 ppm NaCl and 400 ppm $NaHCO_3$) as the new inelastic flood. It is important to note that the salinity of all four polymer solutions are all the same low salinity brine. Figure 4.21 shows the rheology of the elastic polymers (FP6040 and low salinity FP 3630s), and the inelastic polymers (FP3330s and high salinity FP3630s).

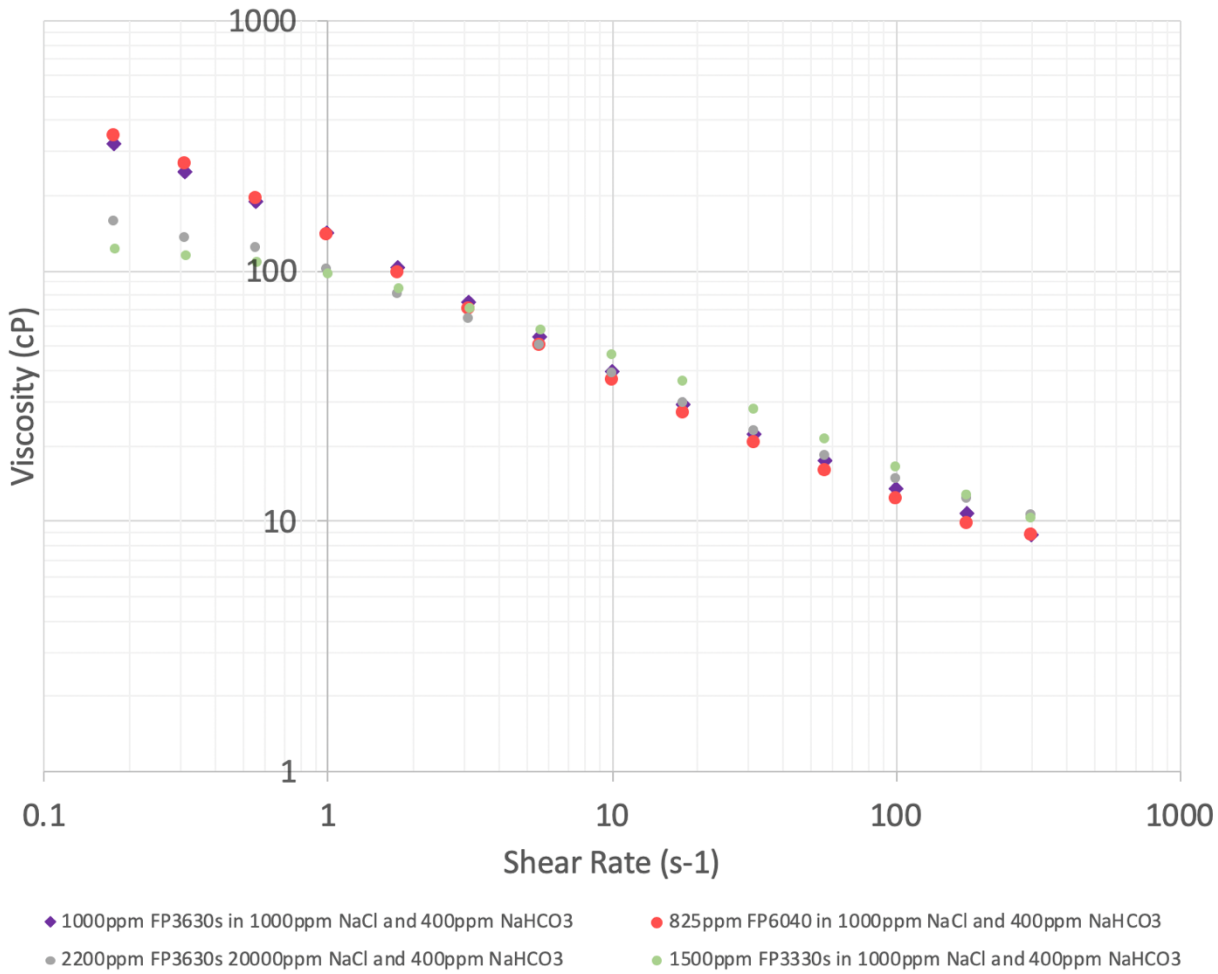


Figure 4.22: Comparison of viscosity of different HPAM polymers in low salinity brine

The elastic polymer solutions (FP6040 and FP3630s) were prepared in the same low salinity brine as the waterflood (1000 ppm NaCl + 400 ppm $NaHCO_3$). This solution produced a polymer with a high relaxation time (3.2 sec) and referred to as the "elastic polymer flood". After hydrating for 24 hours, the solution was filtered under 15 psi of argon gas at 23°C through a 1.2 μm filter paper. The polymer solution was allowed to degas with argon for at least two hours before being transferred into the injection column. The inelastic polymer solutions (FP3330s and FP3630s) were prepared in high salinity brine (2200 ppm FP3630s HPAM polymer in 20,000 ppm NaCl + 400 ppm $NaHCO_3$) in a similar manner. This solution produced a polymer with a

very low relaxation time (0.02 sec) and referred to as the "inelastic polymer flood." Multiple batches of these polymer solutions were made as the floods were planned to be alternated until steady state was reached. The dynamic frequency sweep test (DFST) was performed as previously discussed in Chapter 3 to determine relaxation times. The steady rate sweet test (SRST) was also performed as previously discussed in Chapter 3 to obtain the viscosity profiles of each polymer solution. The power-law viscosity region was used to fit an equation to create the power law model to obtain the constants for the solution.

The polymer solutions were compared to make sure that their viscosity at different shear rates were similar (Figure 4.22). It can be noted that at the high salinity, inelastic polymer had slightly lower viscosities at lower shear rates, but were nearly identical at a shear rate of $20s^{-1}$, the rate at which the core floods were completed at. Multiple batches of the polymer slugs were made when steady state was not reached, but the general relaxation time and viscosity profiles were all similar. Each batch was tested on the rheometer for quality control. The relaxation times of these polymer are significantly different. For the elastic floods, low salinity FP6040 produced a solution with a relaxation time of around 3.2 sec and low salinity FP3630s produced a solution with a relaxation time of around 1.3 sec. For the inelastic floods, both high salinity FP3630s and low salinity FP3330s produced a solution with a relaxation time of around 0.02-0.04 sec.

#### 4.3.4.1 Polymer Flood #1 (Viscoelastic)

The low-salinity, elastic, polymer (825 ppm FP6040 in 1000 ppm NaCl + 400 ppm $NaHCO_3$) was injected at a constant flow rate of 0.03 ml/min (0.25 ft/day), 0.045 ml/min (0.38 ft/day) and 0.06 ml/min (0.5 ft/day) until steady state was reached and zero oil cut. This slow injection rate was chosen to reduce the pressure gradient to be below 3 psi/ft. At 0.25 ft/day, the

pressure gradient was found to be 1.5 psi/ft (Figure 4.23). The oil saturation only decreased by 1.5% (Figure 4.24). To see if an increase of pressure or an increase of flow rate (and subsequently an increase in Deborah number) would produce more oil, the flow rate was increased. At 0.5 ft/day, the pressure gradient reached 2.5 psi/ft, but only reduced the residual oil saturation by another 0.5%.

Polymer flood was considered completed at zero oil cut, which was reached after almost 4 pore volumes. Figure 4.23 shows the pressure values during polymer flood. The maximum pressure gradient at final steady state was 2.5 psi/ft. The equivalent shear rate at steady state was 6.89 $sec^{-1}$. Figure 4.24 shows the oil saturation values up to the end of the first polymer flood. Residual oil saturation was decreased from 22% to 19.8%, and the corresponding Deborah number was 20.68. The change in residual oil saturation decreased only 2.2% from the elastic polymer flood.

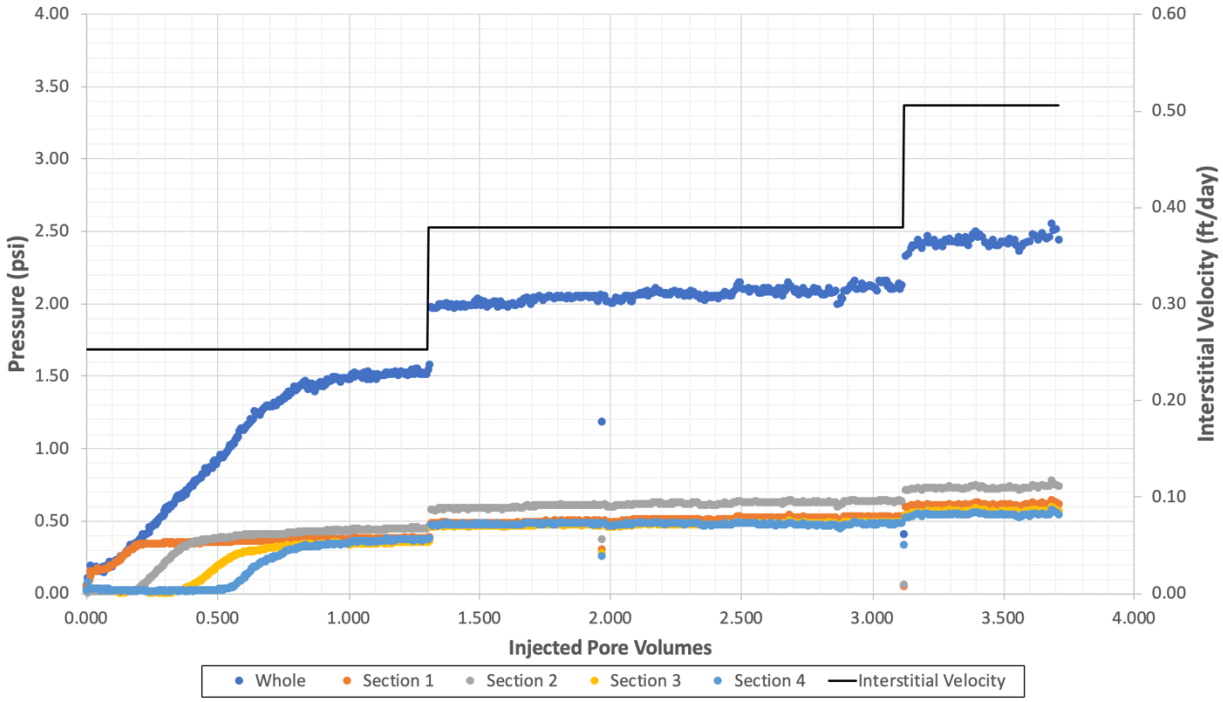


Figure 4.23: Pressure data during the first polymer flood (viscoelastic) during experiment #2.

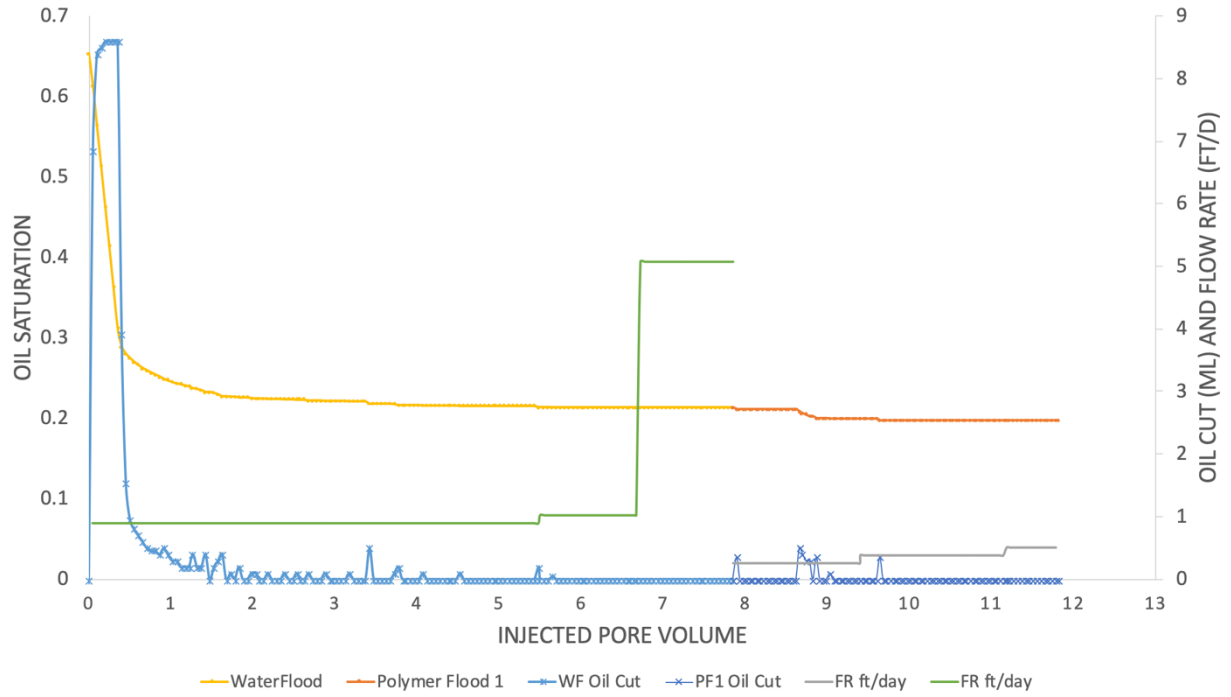


Figure 4.24: Oil saturation after the first polymer flood (viscoelastic) during experiment #2.

The cumulative oil recovery at the end of the polymer flood was 69.7% of the original oil in place. The maximum capillary number for the elastic polymer flood was 1.32 X $10^{-5}$, which was below the critical capillary number (1 X $10^{-4}$).

### 4.3.4.2 Polymer Flood #2 (Inelastic)

The low-salinity, inelastic polymer (1500 ppm FP3330s in 1000 ppm NaCl + 400 ppm $NaHCO_3$) was injected at a constant flow rate of 0.03 ml/min (0.25 ft/day), 0.045 ml/min (0.38 ft/day) and 0.06 ml/min (0.5 ft/day) until steady state was reached and zero oil cut. This slow injection rate was chosen to reduce the pressure gradient to be below 3 psi/ft. Figure 4.25 shows the pressure values for the inelastic polymer flood. The pressure gradients for the second polymer flood were similar to the preceding first elastic polymer flood. At 0.25 ft/day, the pressure gradient was found to be 1.5 psi/ft. The oil saturation did not decrease, as seen in Figure

4.26. To see if an increase of pressure or an increase of flow rate (and subsequently an increase in Deborah number) would produce more oil. At 0.5 ft/day, the pressure gradient reached 2.5 psi/ft, but there was no reduction of residual oil saturation.

Polymer flood was considered completed at zero oil cut, which was reached after almost 4.5 pore volumes. The maximum pressure gradient at final steady state was 2.5 psi/ft. The equivalent shear rate at steady state was 13.08 $sec^{-1}$. Residual oil saturation was decreased from 22% to 19.8%, and the corresponding Deborah number was 0.73. There was no change in residual oil saturation from the polymer floods alone (Figure 4.25).

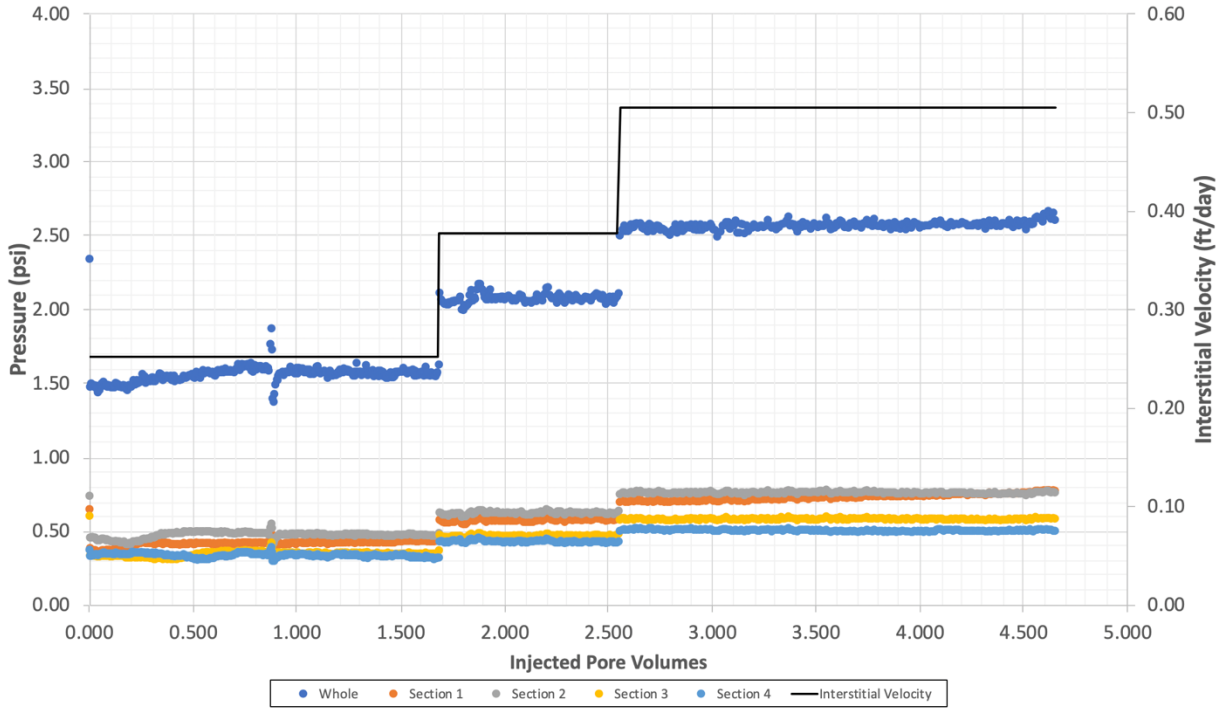


Figure 4.25: Pressure data during the second polymer flood (inelastic) during experiment #2.

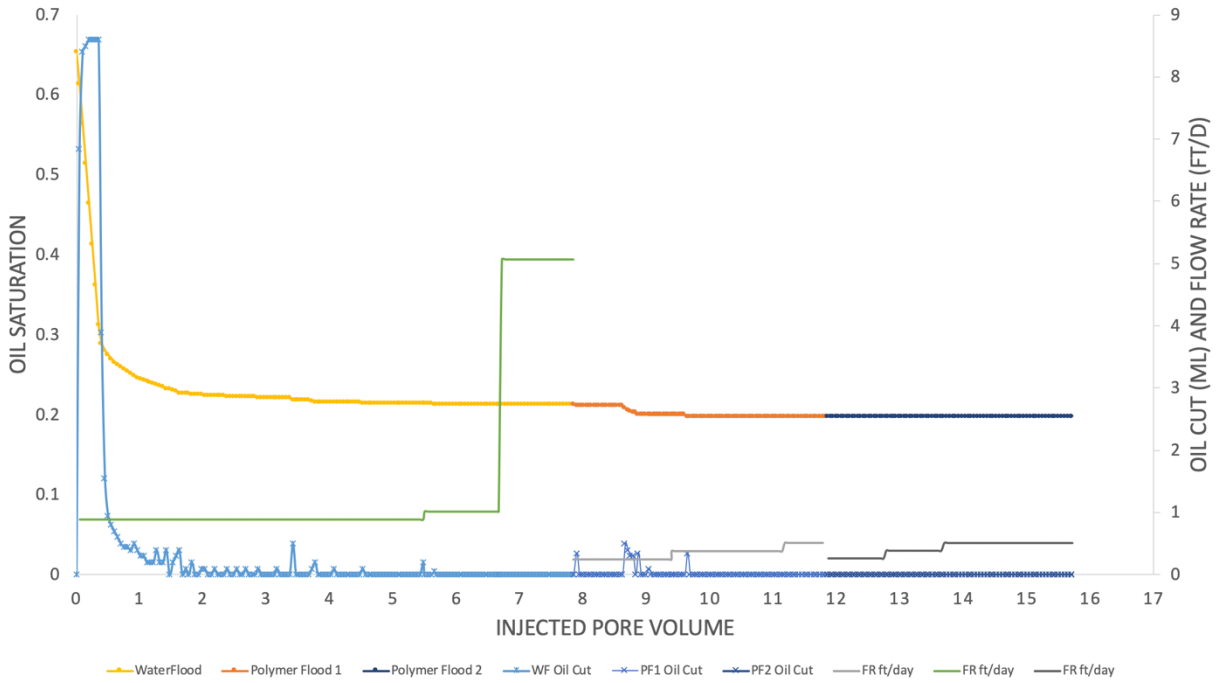


Figure 4.26: Oil saturation after the second polymer flood (inelastic) during experiment #2.

The cumulative oil recovery at the end of the polymer flood was still 69.7% of the original oil in place. The maximum capillary number for the elastic polymer flood was also 1.32 X $10^{-5}$, which was below the critical capillary number (1 X $10^{-4}$).

### 4.3.4.3 Polymer Flood #3 (Viscoelastic)

The low-salinity, elastic, polymer (825ppm FP6040 in 1000 ppm NaCl + 400 ppm $NaHCO_3$) was injected at a constant flow rate of 0.09 ml/min (0.75 ft/day), 0.12 ml/min (1 ft/day) and 0.18 ml/min (1.5 ft/day) until steady state was reached and zero oil cut. This injection rate was chosen to see if the significant increase in pressure would reduce the oil saturation and see if an increase of pressure or an increase of flow rate (and subsequently an increase in Deborah number) would produce more oil. Figure 4.27 shows the pressure values as the injection flow rate increases. At 0.75 ft/day, the pressure gradient was found to be 3.2 psi/ft. Figure 4.28 shows the oil saturation during polymer flood and it is noted that the oil saturation did not

decrease. At 1 ft/day, the pressure gradient reached 3.8 psi/ft, but again did not reduce the oil saturation. At 1.5 ft/day, the pressure gradient reached 4.8 psi/ft, but the oil saturation only reduced 0.2% to 19.6% oil saturation.

Polymer flood was considered completed at zero oil cut, which was reached after almost 4 pore volumes. The maximum pressure gradient at final steady state was 4.8 psi/ft. The equivalent shear rate at steady state was 22.63 $sec^{-1}$. Residual oil saturation was only decreased from 19.8% to 19.6%, and the corresponding Deborah number was 45.25. The change in residual oil saturation decreased only 0.2% from the elastic polymer flood.

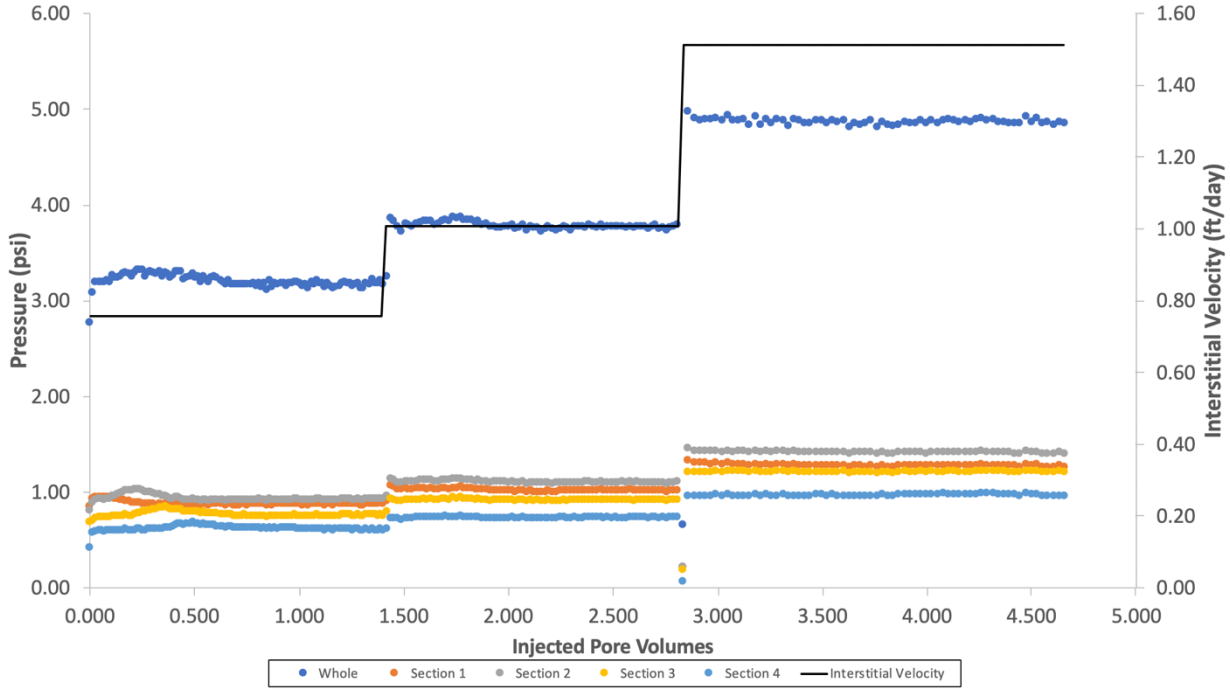


Figure 4.27: Pressure data during the third polymer flood (viscoelastic) during experiment #2.

Previous floods (Erincik, 2017; Qi, 2018) found success sometimes by letting the core equilibrate statically before restarting a chemical flood. Thus, experiment #2 was allowed to age for 30 days before allowing the elastic flood to start again. The same elastic polymer was injected again (825ppm FP6040 in 1000 ppm NaCl + 400 ppm $NaHCO_3$). The polymer was

injected at a constant flow rate of 0.12 ml/min (1 ft/day), 0.18 ml/min (1.5 ft/day) and 0.24 ml/min (2 ft/day) until steady state was reached and zero oil cut. Pressure values are shown in Figure 4.28 and saturation values are shown in 4.29.

At 1 ft/day, the pressure gradient was found to be 3.8 psi/ft. The oil saturation did decrease but only about 0.4%. At 1.5 ft/day, the pressure gradient reached 5 psi/ft, but again did not reduce the oil saturation. At 2 ft/day, the pressure gradient reached 5.8 psi/ft, but the oil saturation again did not decrease. Polymer flood was considered completed at zero oil cut, which was reached after almost 4.5 pore volumes. The max pressure gradient at final steady state was 5.8 psi/ft. The equivalent shear rate at steady state was 30.14 $sec^{-1}$. Residual oil saturation was only decreased from 19.6% to 19.2%, and the corresponding Deborah number was 57.53. The change in residual oil saturation decreased only 0.4% from the elastic polymer flood.

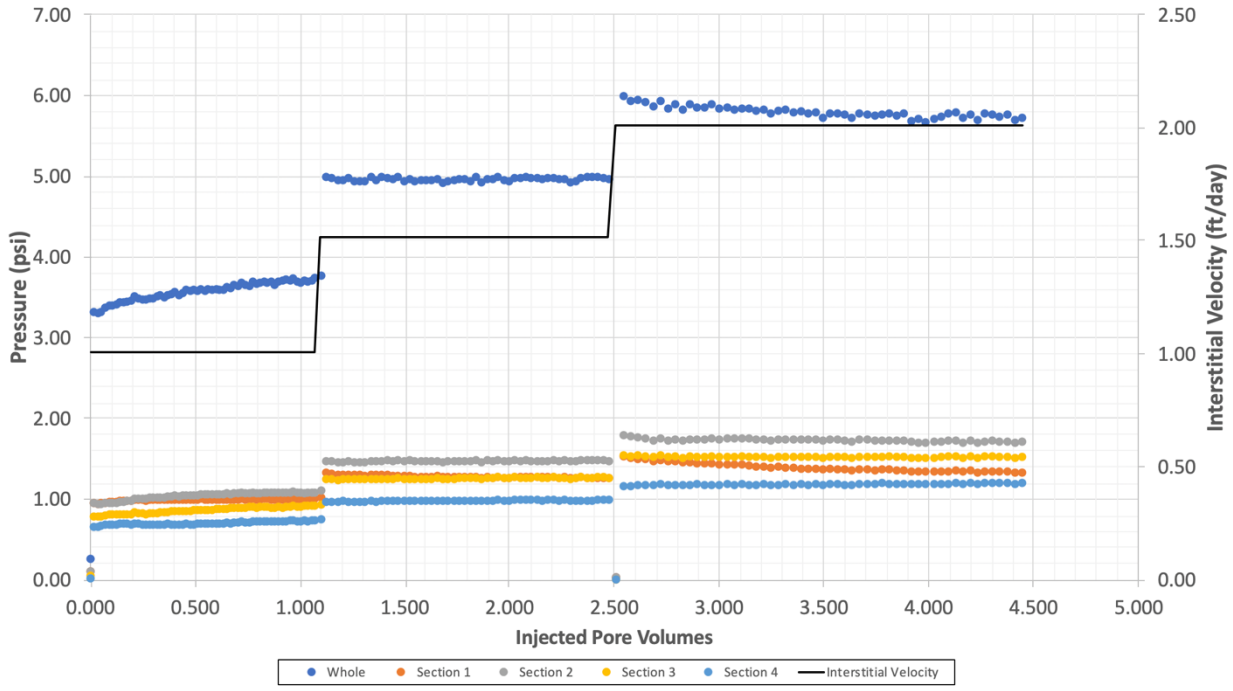


Figure 4.28: Pressure data during the third polymer flood (viscoelastic) after a 30 day equilibration period during experiment #2.

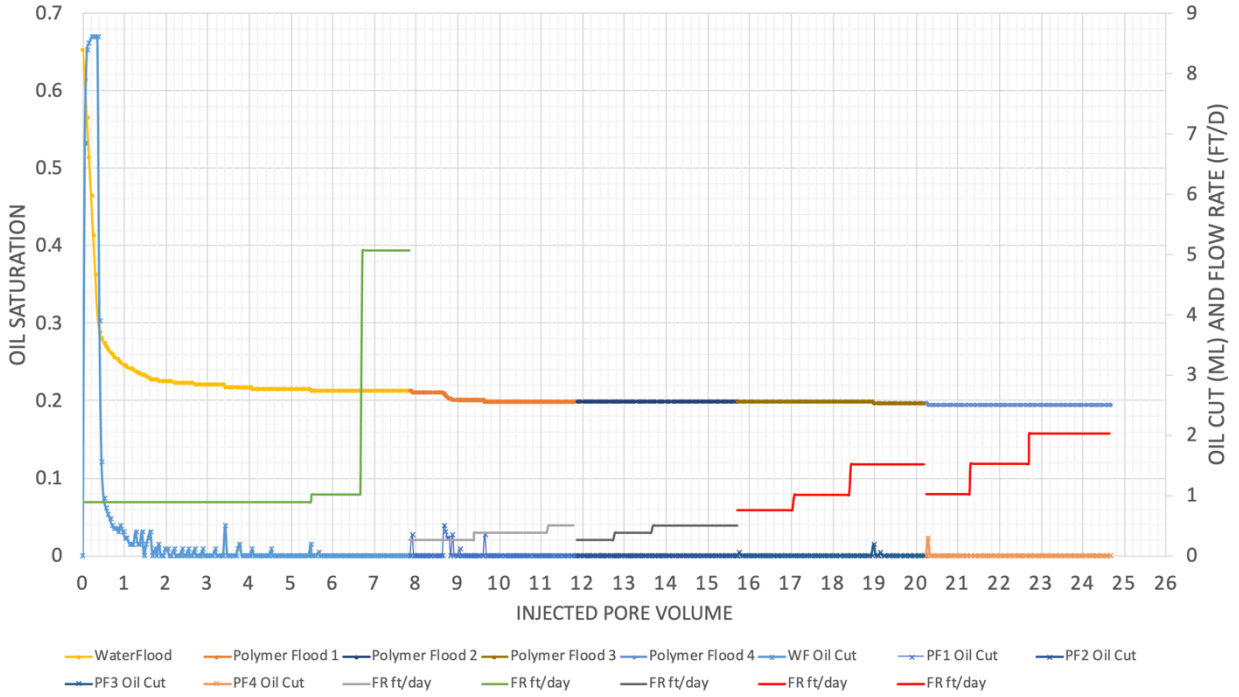


Figure 4.29: Oil saturation after the two elastic polymer floods during experiment #2. Polymer floods labelled PF3 and PF4 are the same polymer, and PF4 is the flood after 30 days of the core equilibrating.

The cumulative oil recovery at the end of the polymer flood was 70.3% of the original oil in place. The maximum capillary number for the elastic polymer flood was also 3.04 X $10^{-5}$, which was below the critical capillary number (1 X $10^{-4}$).

#### 4.3.4.4 Final Alternating Polymer Floods #4 and #5 (Inelastic and Viscoelastic)

The low-salinity, inelastic polymer (1500 ppm FP3330s in 1000 ppm NaCl + 400 ppm $NaHCO_3$) was injected at a constant flow rate of 0.18 ml/min (1.5 ft/day), and 0.24 ml/min (2 ft/day) until steady state was reached and zero oil cut. This injection rate was chosen to see if the inelastic low-salinity polymer flood would "sweep" out any remaining oil that had been trapped or disturbed by the viscoelastic polymer flood. Pressure values are shown in Figure 4.30 and the oil saturation during the course of the polymer flood is shown in Figure 4.31. At 2 ft/day, the max pressure gradient was found to be 5.2 psi/ft. The oil saturation did not experience any

significant reduction. The equivalent shear rate at steady state was 23.83 $sec^{-1}$. The corresponding Deborah number was 0.57. There was no change in residual oil saturation from the polymer floods alone. The maximum capillary number for the inelastic polymer flood was also 2.75 X $10^{-5}$, which was below the critical capillary number (1 X $10^{-4}$ ).

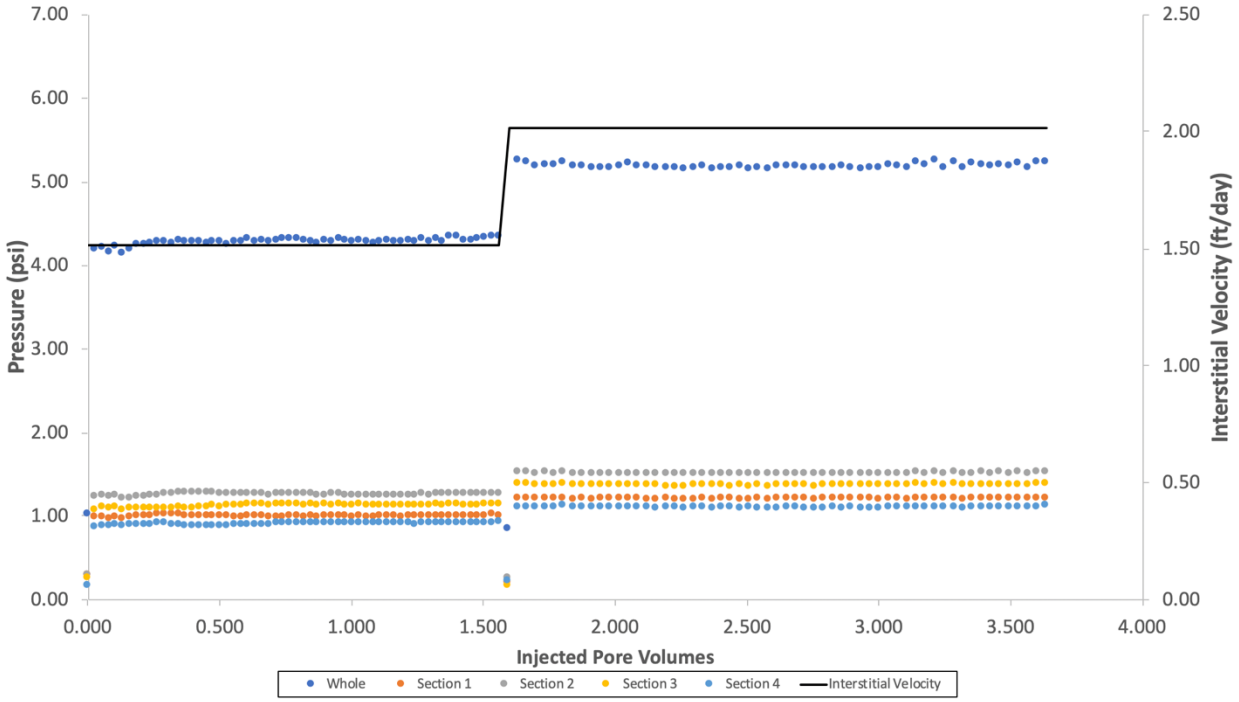


Figure 4.30: Pressure data during the fourth polymer flood (inelastic) during experiment #2.

Even though the pressure gradients were increased, there was no change in the recovery of oil. In Experiment #1, the polymer floods had significantly different salinities in order to create different relaxation times, while in Experiment #2, the salinity was kept constant throughout all the floods. Because of this change, the original polymers were made to be used in this experiment. Two polymer solutions were made: an elastic solution of 1000 ppm FP3630s in 1000 ppm NaCl + 400 ppm $NaHCO_3$ and an inelastic solution of 2200 ppm FP3630s in 20,000 ppm NaCl + 400 ppm $NaHCO_3$. Their relaxation times were 1.3 sec and 0.04 sec respectively.

The elastic polymer solution was injected in order to reestablish an elastic flow pattern within the core. The polymer was injected first at slow injections rates (0.25 ft/day, 0.5 ft/day) in order to see if there would still be recovery of oil at low pressure gradients. Figure 4.31 shows the corresponding pressure values at different polymer injection rates. At 0.25 ft/day, the pressure gradient was found to be 1.2 psi/ft and at 0.5 ft/day, the pressure gradient was found to be 1.8 psi/ft. Figure 4.32 shows the oil saturation during the polymer flood. Neither rates produced any additional oil from the core. The elastic polymer was then injected at faster flow rates (1 ft/day and 1.5 ft/day), as seen in Figure 4.31. At 1 ft/day, the pressure gradient was found to be 2.9 psi/ft and at 1.5 ft/day, the pressure gradient was found to be 4.6 psi/ft. Neither rates produced any additional oil from the core (Figure 4.32). The max pressure gradient at final steady state was 4.6 psi/ft. The equivalent shear rate at steady state was 20.67 $sec^{-1}$. The Deborah number was calculated to be 24.81. There was no change in residual oil saturation and the final oil saturation remained at 19.2%. The maximum capillary number for the elastic polymer flood was also 2.43 X $10^{-5}$, which was below the critical capillary number (1 X $10^{-4}$).

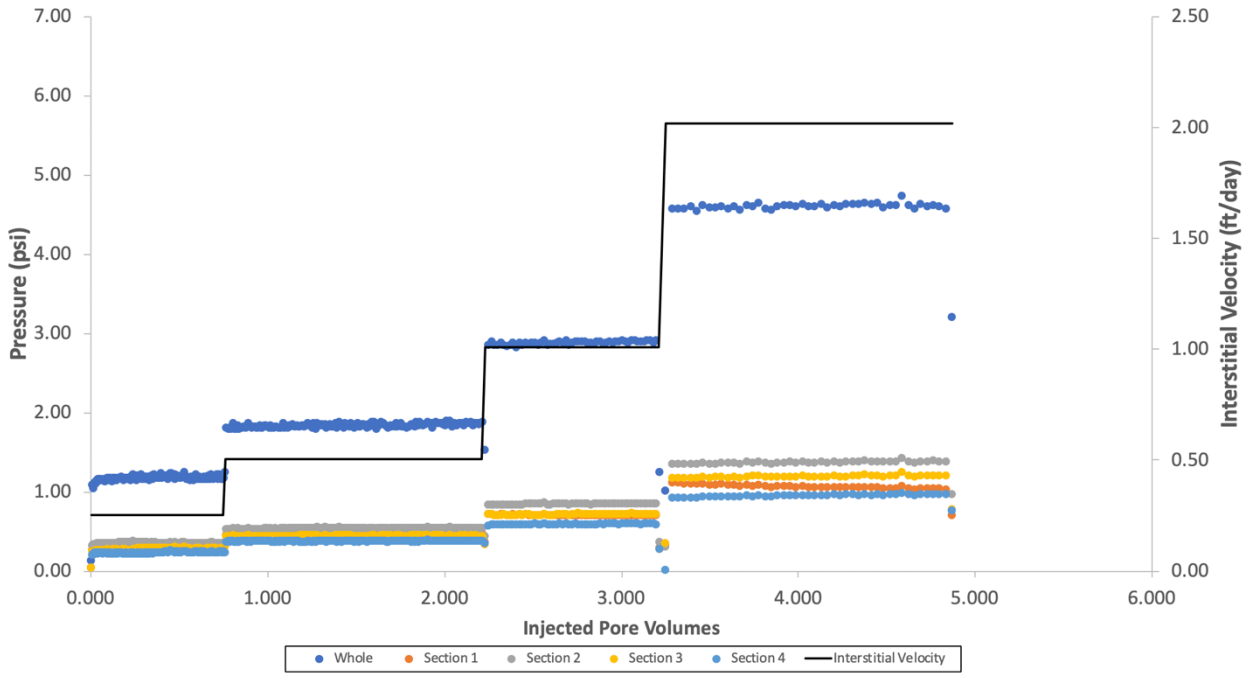


Figure 4.31: Pressure data during the final elastic polymer flood during experiment #2. The polymer used in this flood was returned back to the original elastic polymer used in experiment #3 (1000 ppm FP3630s in 1000 ppm NaCl + 400 ppm $NaHCO_3$).

The final inelastic polymer flood (2200 ppm FP3630s in 20,000 ppm NaCl + 400 ppm $NaHCO_3$) was injected into the core. The solution was made with high salinity brine in order to reduce the relaxation time in the polymer. The polymer was injected at 1.5 ft/day and the corresponding pressure values are seen in Figure 4.32. At 1.5 ft/day, the pressure gradient was found to be 3.5 psi/ft at steady state. The max pressure gradient at final steady state was 3.6 psi/ft. The equivalent shear rate at steady state was 17.32 $sec^{-1}$. The Deborah number was calculated to be 0.35. There was no change in residual oil saturation and the final oil saturation remained at 19.2%, as seen in Figure 4.33. The maximum capillary number for the elastic polymer flood was also 1.85 X $10^{-5}$, which was below the critical capillary number (1 X $10^{-4}$).

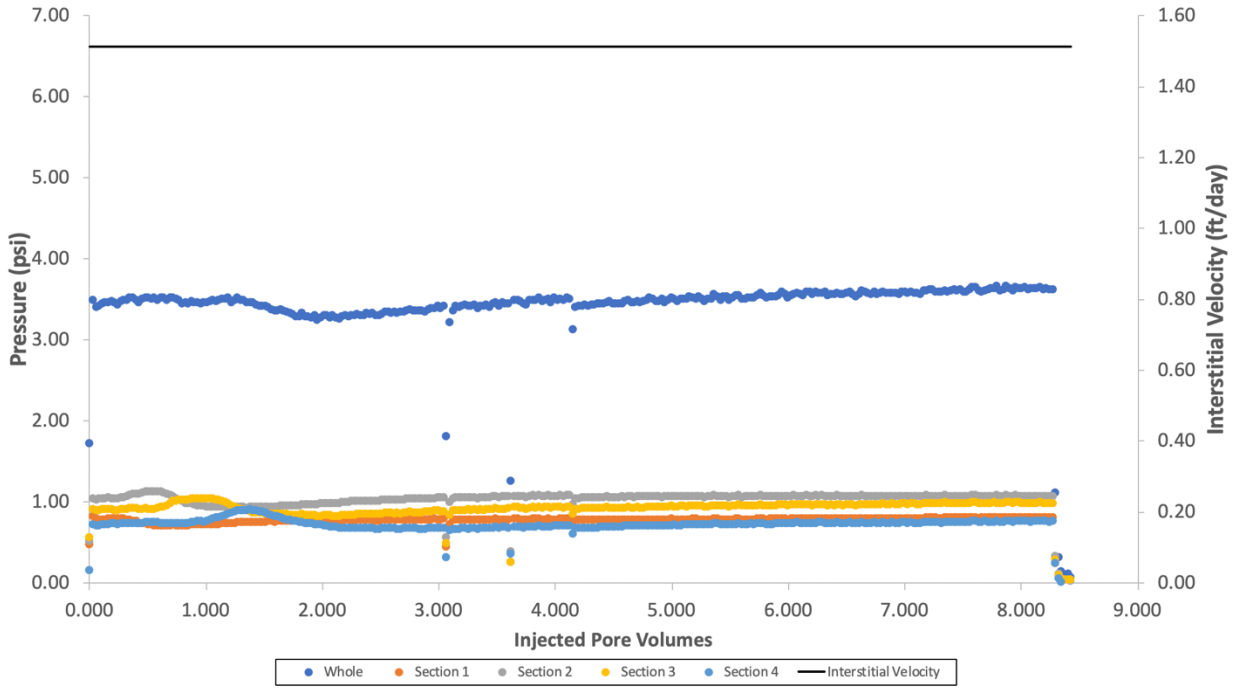


Figure 4.32: Pressure data during the final elastic polymer flood during experiment #2. The polymer used in this flood was returned back to the original inelastic polymer used in experiment #3 (2200 ppm FP3630s in 20,000 ppm NaCl + 400 ppm $NaHCO_3$).

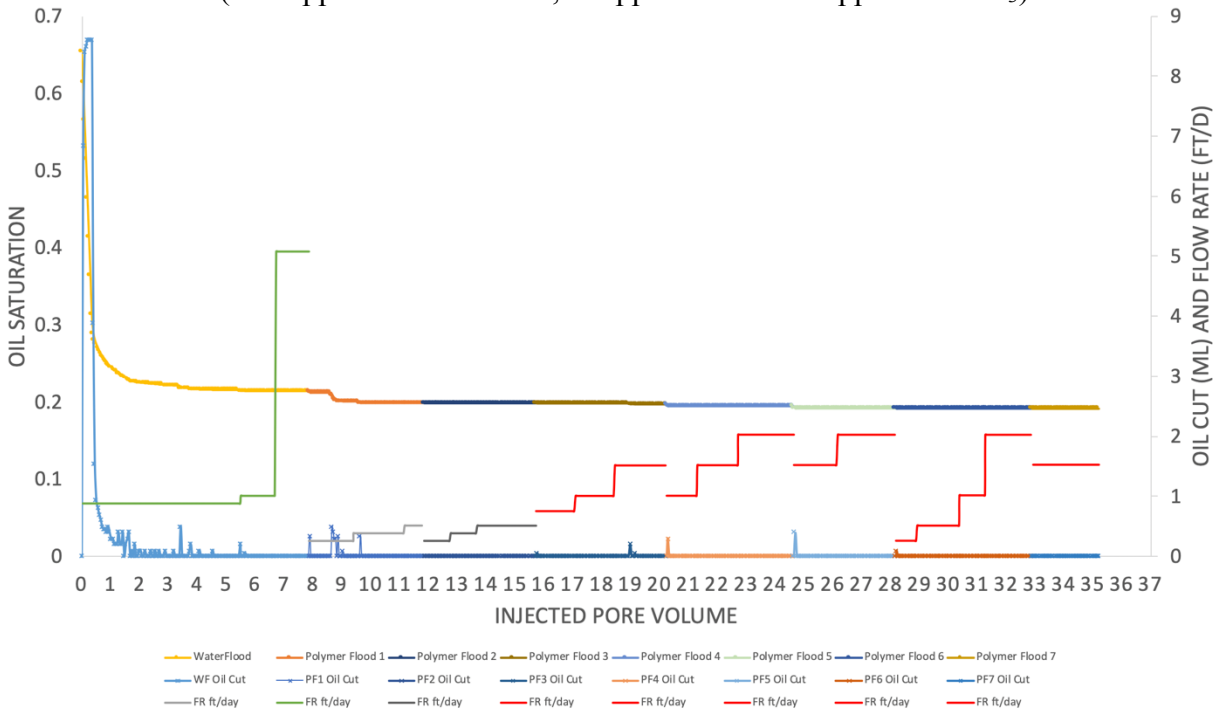


Figure 4.33: Oil saturation after multiple alternating polymer floods in experiment #2.

Figure 4.33 shows the final oil saturation after the completion of multiple polymer floods. The cumulative oil recovery at the end of the polymer flood was 70.6% of the original oil in place. Unfortunately, while this experiment did not show much oil recovery when in comparison to the previous experiment, it suggested that the significant change in salinity in polymer floods while keeping the floods below the critical capillary number might be key in reducing residual oil saturation. Multiple variables were changed during the course of this experiment such as the higher molecular weight polymer, as well as the overall lower pressure gradients in this experiment.

## 4.4 EXPERIMENT #3: BOISE SANDSTONE CORE #3

### 4.4.1 Core Preparation and Conditioning

Experiment #3 was designed to replicate the success of experiment #1 and test out an inelastic polymer, scleroglucan. The purpose of this coreflood was to again test the effect of viscoelastic polymer floods on residual oil saturation when a high-salinity polymer flood was performed following a low-salinity polymer flood and repeated these cycles until a steady state residual saturation was achieved. The polymers used were the same as experiment #1. A commercially available, EOR grade, biopolymer (scleroglucan) was used as an inelastic polymer. The polymer floods were designed to try to keep the capillary number lower than the critical capillary number in Boise sandstone cores (~$1x10^{-5}$). Table 4.5 summarizes the general properties of the core and the brine and polymer fluids.

Table 4.3: Core and experimental fluid properties for experiment #3.

| | |
|---|---|
| **Core Name** | BS 1-5 |
| **Rock Type** | Boise sandstone |

| | |
|---|---|
| **Brine permeability (mD)** | 3941 |
| **Crude Oil Viscosity (cP)** | 5 |
| **Temperature ($^oC$)** | 23 |
| **Diameter (cm)** | 4.76 |
| **Length (cm)** | 30.16 |
| **Area ($cm^2$)** | 17.81 |
| **Bulk Volume (cc)** | 537.31 |
| **Pore Volume (mL)** | 175.0 |
| **Porosity** | 0.326 |
| **Bulk Density (g/cc)** | 2.00 |
| **Brine Composition** | 1000 ppm NaCl + 400 ppm $NaHCO_3$ + 400 ppm $Na_2S_2O_4$ |
| **Viscoelastic Polymer Composition** | 1000 ppm FP3630s HPAM polymer in 1000 ppm NaCl + 400 ppm $NaHCO_3$ aqueous solution |
| **Inelastic Polymer Composition #1** | 2200 ppm FP3630s HPAM polymer in 20,000 ppm NaCl + 400 ppm $NaHCO_3$ aqueous solution |
| **Inelastic Polymer Composition #2** | 900 ppm Scleroglucan in 1000 ppm NaCl + 400 ppm $NaHCO_3$ aqueous solution |

The Boise sandstone core was dried in a 100$^o$C oven overnight and then potted in epoxy in preparation for core flooding, as described in Chapter 3. The estimated pore volume from brine imbibition was 180 mL. Once the core was saturated with this low salinity brine (0.0 normalized salinity), the high salinity iron reduction aqueous solution (4% $NaHCO_3$ + 1% EDTA + 1% $Na_2S_2O_4$) (1.0 normalized salinity) was injected at 2.5 ml/min to complete a salinity tracer test to calculate the pore volume and heterogeneity of the core. Figure 4.34 shows the salinity of the effluent samples increasing as the high salinity brine iron reduction aqueous displaced the low salinity brine solution previously existing in the core. The pore volume was calculated from the tracer test as 175 mL.

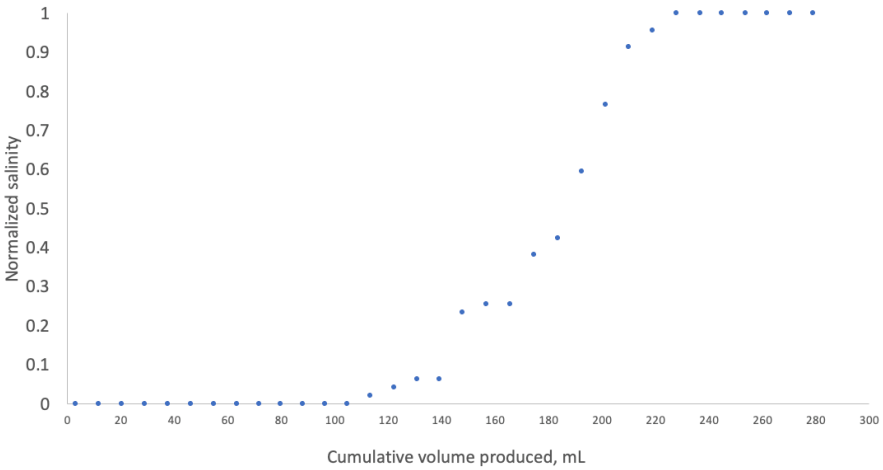


Figure 4.34: Salinity tracer test for experiment #3.

The core was continuously pumped with this iron reduction solution at 1ml/min (10.4ft/day) in order to reduce the amorphous oxidized iron in the core. The iron reducing fluid was injected at varying rates (1, 5, 10, 15, 20 ml/min) to determine permeability. The pressure values corresponding with these increasing brine injections rates are shown in Figure 4.35 and used to calculate brine permeability, which was estimated to be 3941mD using Darcy's Law.

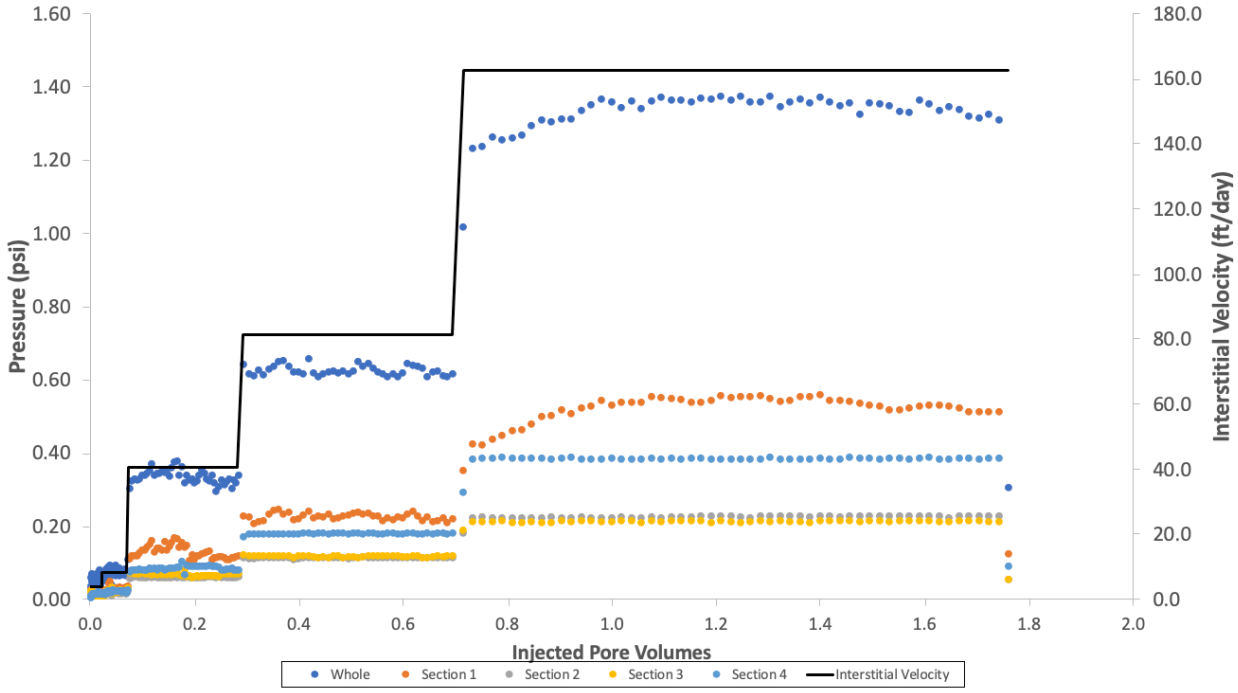


Figure 4.35: Pressure drop during brine injection experiment #3.

### 4.4.2 Oil Flood

Diluted dead crude oil (13% toluene) was filtered through 1.2 μm filter paper under 20 psi of air at 23°C. The diluted oil was found to have a viscosity of 6 cP. The low viscosity oil was injected into core at a constant pressure using argon at 30 psi. At least 1.5PV of oil was injected. Volumetric calculations were used to determine initial oil saturation ($S_{oi}$) by observing the volume of water and oil produced in burettes during the oil floods. The displaced brine volume was used to calculate initial oil saturation. Oil flood continued until there was a consistent water cut of 0%. The core was aged with the oil for at least 48 hours. Initial oil saturation was determined to be 64.6%.

### 4.4.3 Waterflood

An aqueous solution of 1000 ppm NaCl + 400 ppm $NaHCO_3$ + 400 ppm $Na_2S_2O_4$ was injected at constant flow rate of 0.12ml/min, (1 ft/day), 0.24 ml/min (2 ft/day), and then 0.6

ml/min (5 ft/day). This increase in flow rate was to maintain that the oil saturation after waterflood was truly residual oil saturation. Pressure values are shows in Figure 4.37 and the oil saturation and oil cut after waterflood are shown in Figure 4.36. Brine was injected until steady state pressure was reached and the oil cut was zero. Oil saturation after waterflood was calculated to be 30.9%. The pressure gradient at steady state was recorded to be 0.22 psi/ft (1 ft/day), 0.25 psi/ft (2 ft/day), and 0.6 psi/ft (5 ft/day) (Figure 4.62).

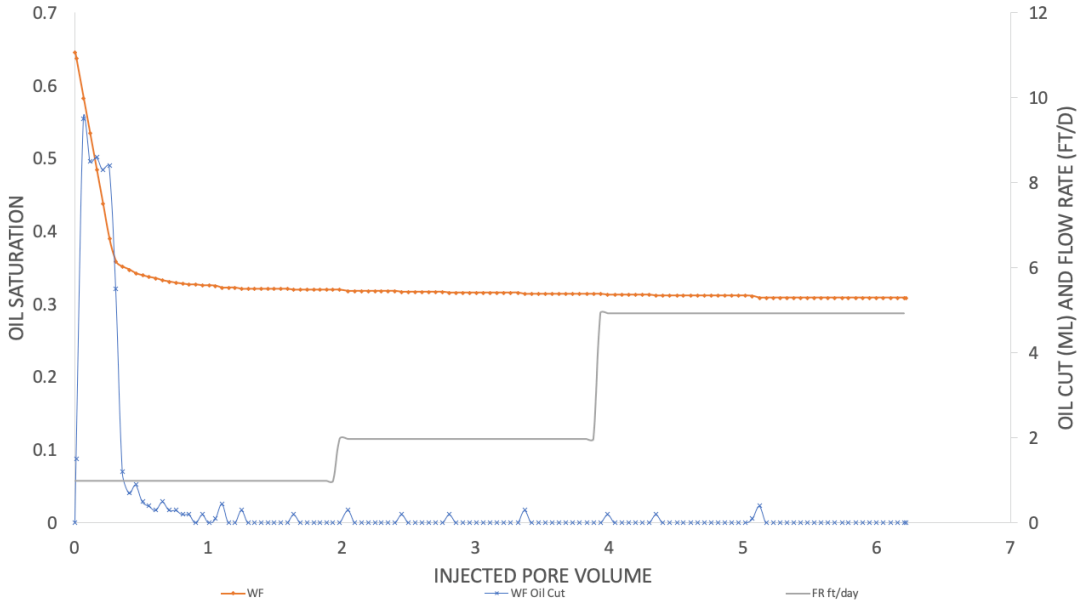


Figure 4.36: Oil saturation after waterflood in experiment #3.

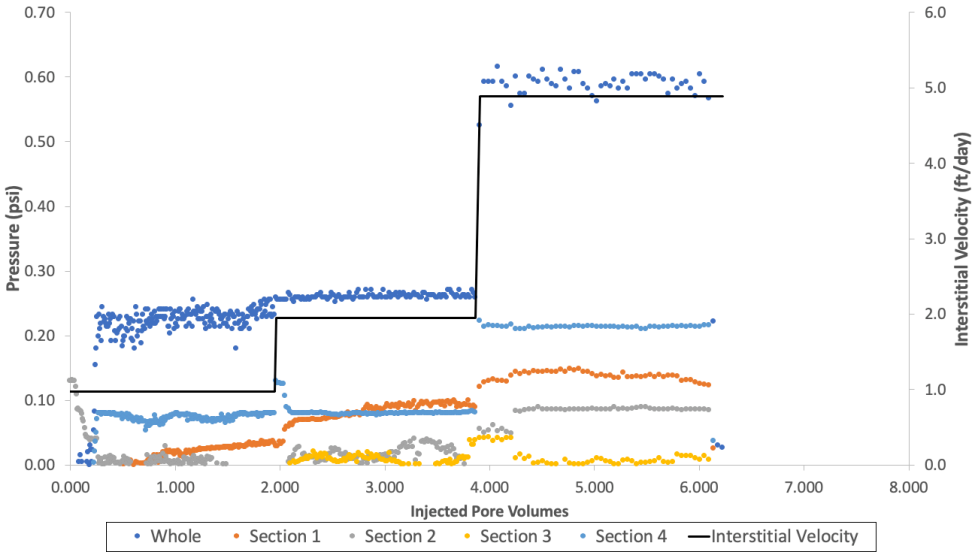


Figure 4.37: Waterflood pressure data for experiment #3.

### 4.4.4 Polymer Floods for Experiment #3

A high molecular weight polymer (FP3630s) was prepared in the same low salinity brine as the waterflood (1000 ppm NaCl + 400 ppm $NaHCO_3$). This solution produced a polymer with a high relaxation time (1.45 sec) and referred to as the "elastic polymer flood". This coreflood also explored using a commercially available, EOR-grade, biopolymer (scleroglucan). The scleroglucan was diluted into the low salinity brine in order to create an inelastic polymer flood without increasing the salinity of the polymer solution. Different concentrations of scleroglucan were prepared in low salinity brine, shown in Figure 4.38.

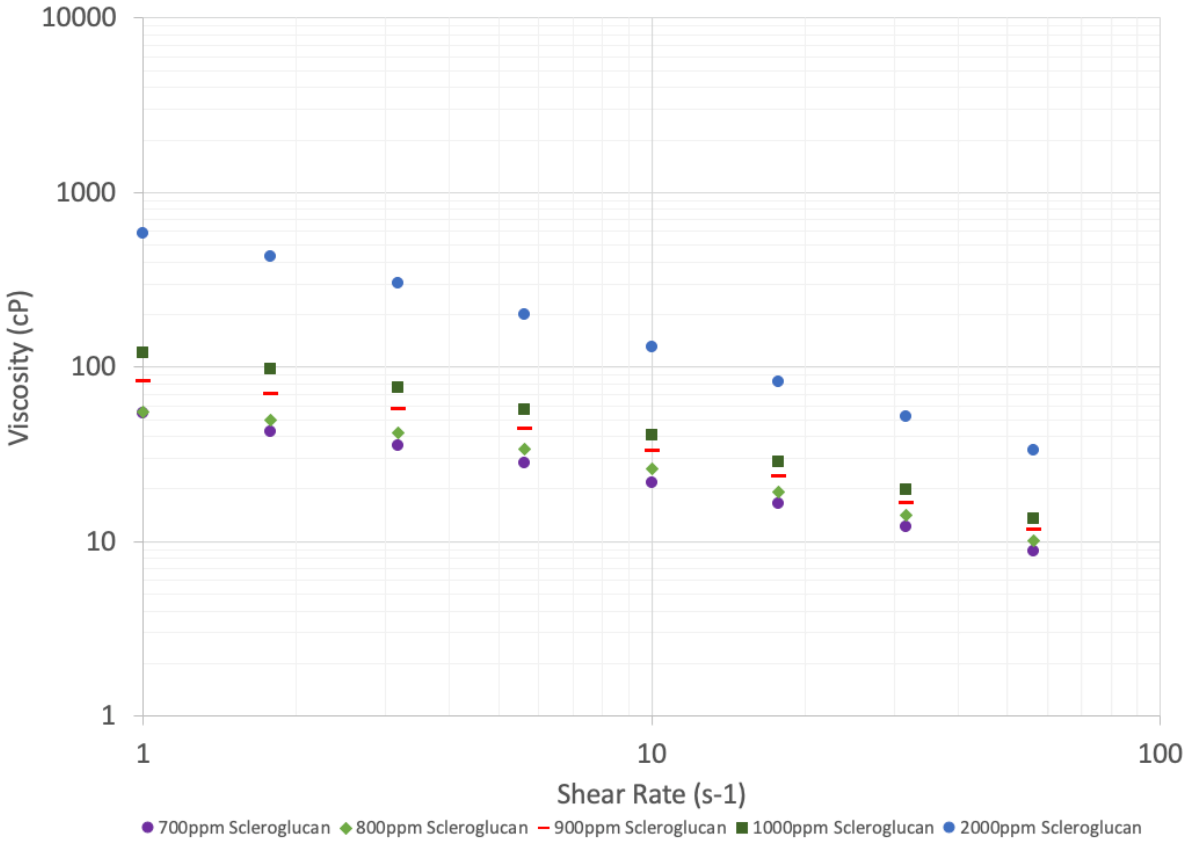


Figure 4.38: Viscosity of scleroglucan diluted in low salinity brine.

This second polymer flood was also designed to remove the variability of changing salinities between elastic and inelastic polymer floods. The previous inelastic polymer flood had increased the salinity of the flood to significantly decrease relaxation time. The scleroglucan diluted in low salinity brine provided the same viscosities and low relaxation times (0.05 sec).

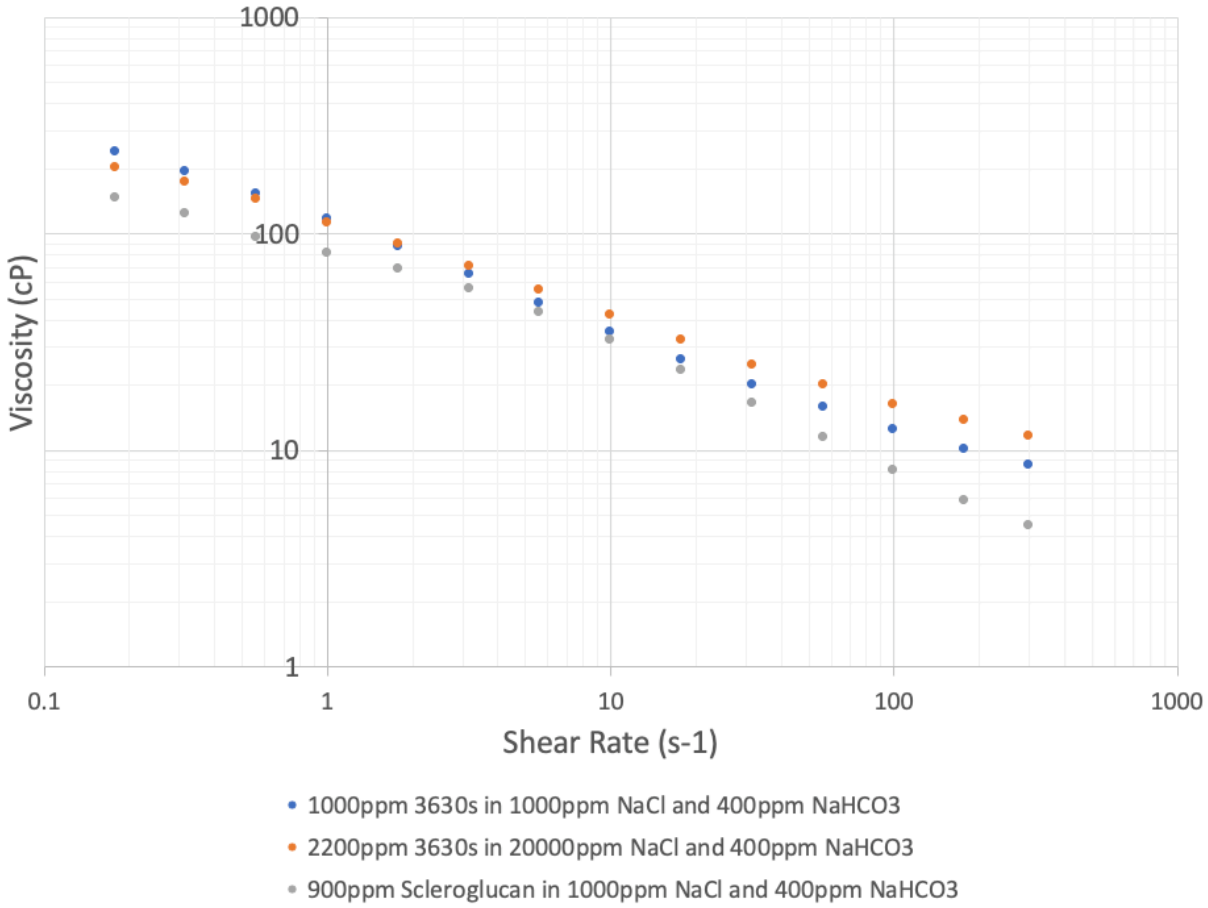


Figure 4.39: Viscosity of low salinity/elastic FP3630s, high salinity/inelastic FP3630s, and inelastic scleroglucan polymer solutions that are used in experiment #3.

The same high molecular weight polymer (FP3630s) was prepared in high salinity brine (2200 ppm FP3630s HPAM polymer in 20,000 ppm NaCl + 400 ppm $NaHCO_3$) in a similar manner. This solution produced a polymer with a very low relaxation time (0.02 sec) and referred to as the "inelastic polymer flood." The polymer solutions were compared to make sure that their viscosity at different shear rates were similar to avoid unstable displacement (Figure 4.39). It can be noted that the high salinity, inelastic polymer had slightly lower viscosities at lower shear rates, but were nearly identical at a shear rate of $20s^{-1}$, the rate at which the core floods were completed at. Each batch was tested on the rheometer for quality control.

#### 4.4.4.1 Polymer Flood #1 (Viscoelastic)

The low-salinity, elastic, polymer was injected at a constant flow rate of 0.12 ml/min (1 ft/day) until steady state was reached and zero oil cut. Polymer flood was considered completed at zero oil cut, which was reached after almost 5.5 pore volumes. Pressure values are shows in Figure 4.40 and the oil saturation and oil cut up to the elastic polymer flood are shown in Figure 4.41. The pressure gradient at steady state was 5.6 psi/ft. The equivalent shear rate at steady state was 20.5 $sec^{-1}$. As seen in Figure 4.41, residual oil saturation was decreased from 30.9% to 25.9%, and the corresponding Deborah number was 22.55. The change in residual oil saturation decreased 5% from the elastic polymer flood.

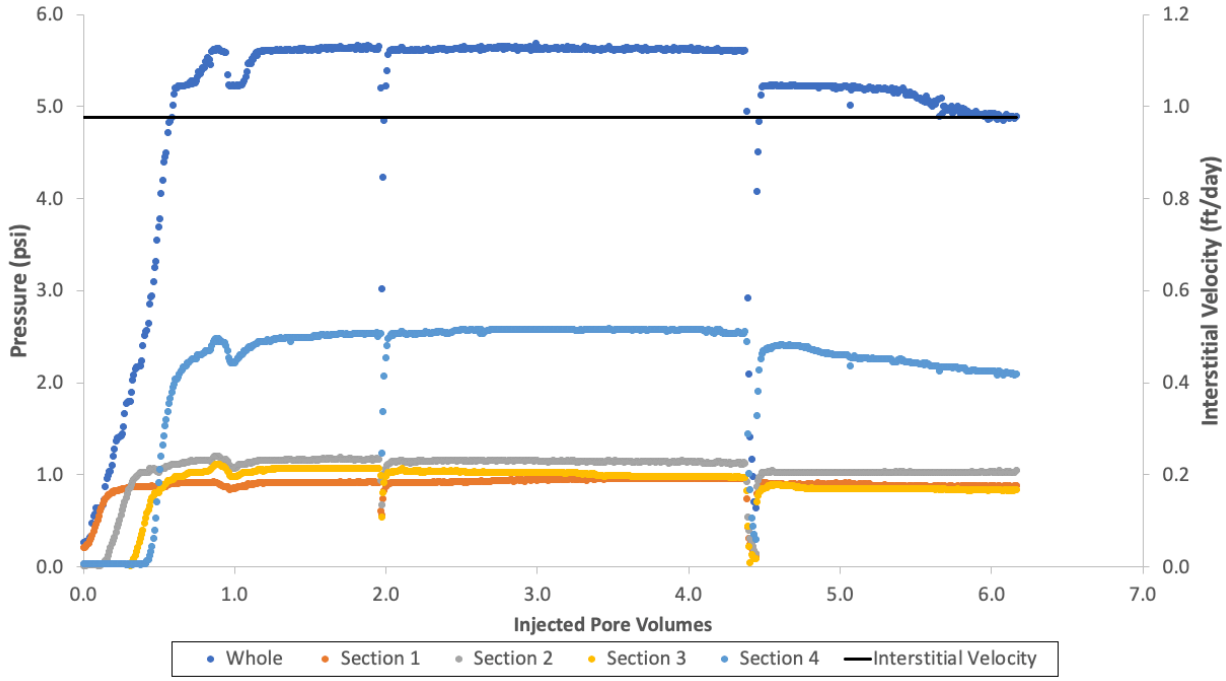


Figure 4.40: Pressure data from first polymer flood (viscoelastic) in experiment #3.

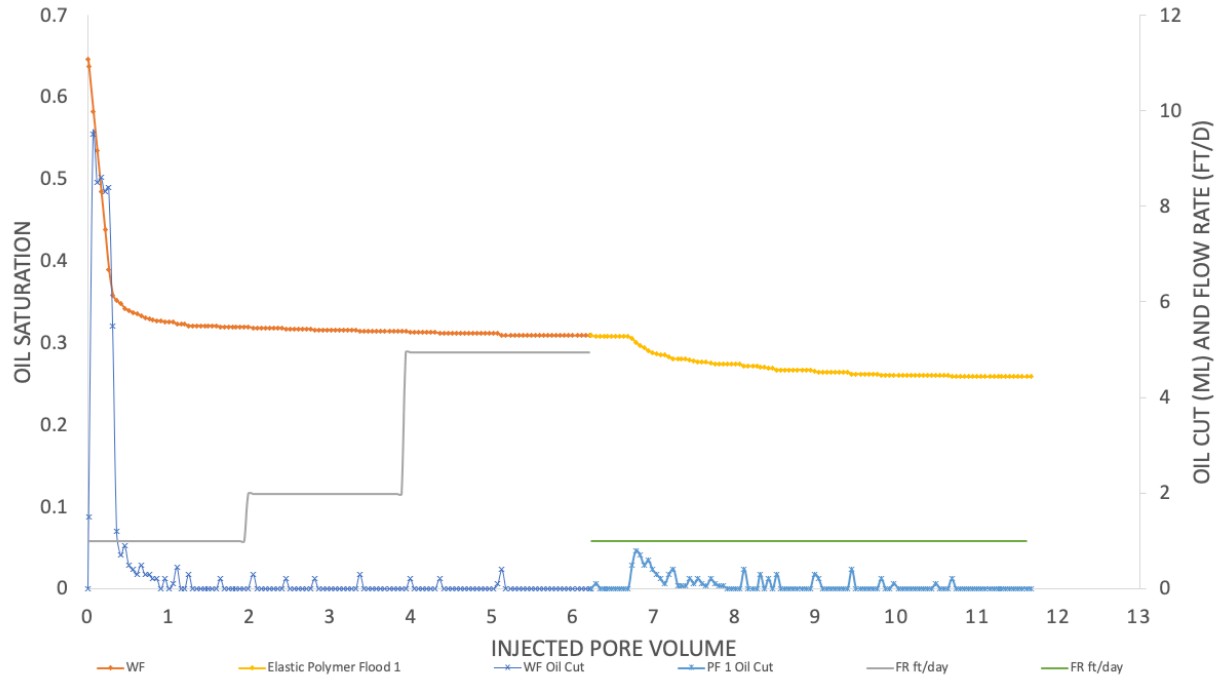


Figure 4.41: Oil saturation after first polymer flood (viscoelastic) in experiment #3.

The cumulative oil recovery at the end of the polymer flood was 60.1% of the original oil in place. The maximum capillary number for the elastic polymer flood was 2.94 X $10^{-5}$, which was below the critical capillary number (1 X $10^{-4}$).

#### 4.4.4.2 Polymer Flood #2 (Inelastic)

The scleroglucan dilution (900 ppm Scleroglucan in 1000 ppm NaCl and 400 ppm $NaHCO_3$) was prepared as previously discussed. This polymer solution had the same salinity as the previous polymer flood and the waterflood. The low-salinity, inelastic polymer was injected at a constant flow rate of 0.12 ml/min (1 ft/day) until steady state was reached and zero oil cut. Polymer flood was considered completed at zero oil cut, which was reached after 2.5 pore volumes. Pressure values are shows in Figure 4.42 and the oil saturation and oil cut after the inelastic scleroglucan polymer flood are shown in Figure 4.43. No additional oil was produced from the scleroglucan polymer flood. The pressure gradient at steady state was 3.7 psi/ft. The

equivalent shear rate at steady state was 19.09 $sec^{-1}$ and the Deborah number was 1.34. The max capillary number during the scleroglucan polymer flood was 1.95 X $10^{-5}$. There was no change in residual oil saturation after the inelastic polymer flood.

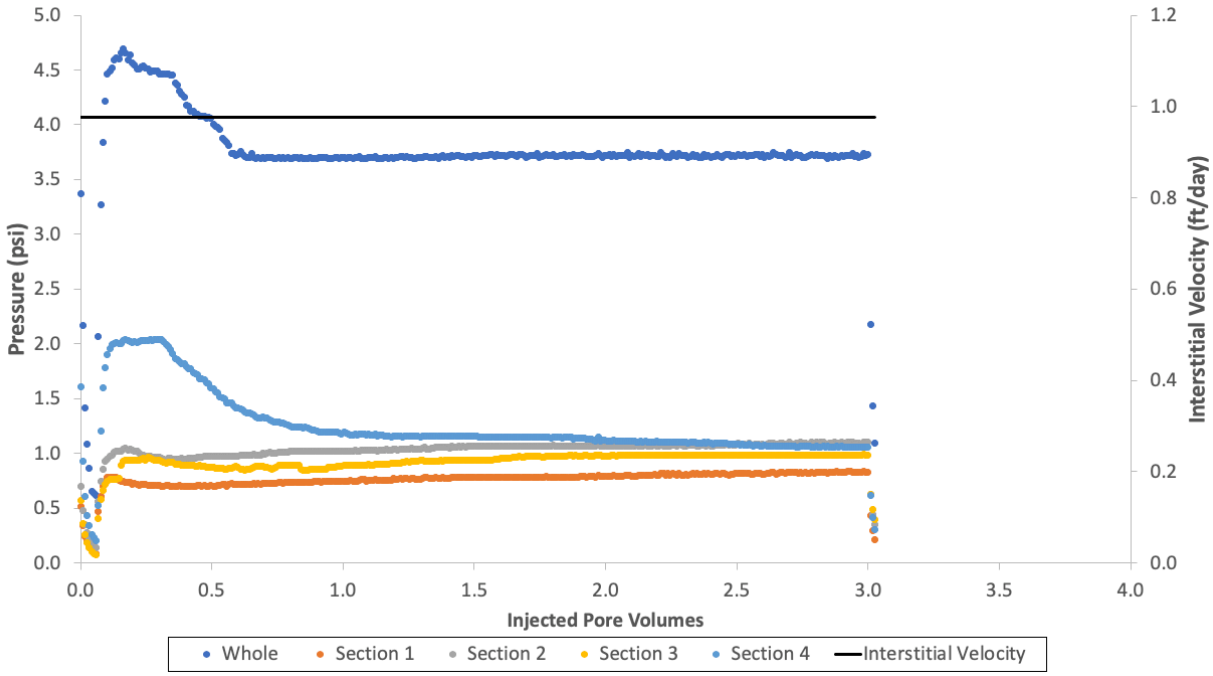


Figure 4.42: Pressure data after the inelastic scleroglucan polymer flood in experiment #3.

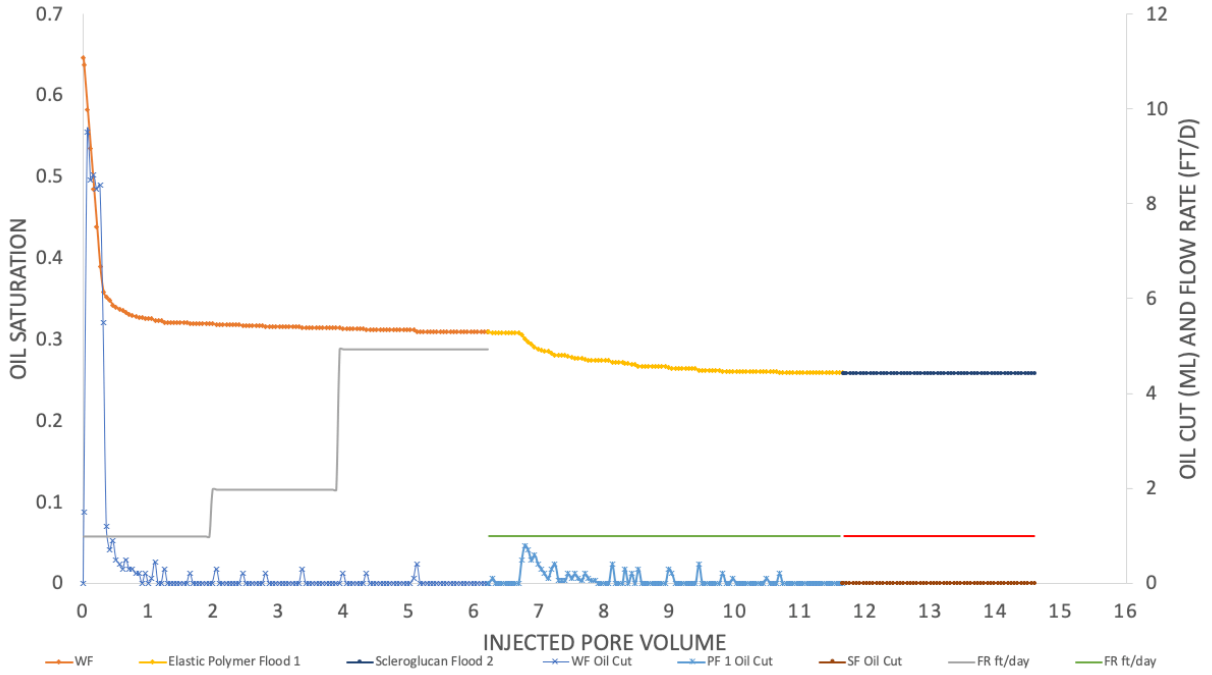


Figure 4.43: Oil saturation after the inelastic scleroglucan polymer flood in experiment #3.

#### 4.4.4.3 Final Alternating Polymer Floods #3, #4, and #5 (Viscoelastic, Inelastic, Viscoelastic)

After the scleroglucan polymer flood did not produce any significant oil recovery, the original low-salinity, elastic FP3630s polymer solution and the original high-salinity, inelastic FP 3630s polymer solution from experiment #1 was made to be used as the final cycle of polymer floods.

The elastic, low-salinity polymer solution was injected at a constant flow rate of 0.12 ml/min (1 ft/day). This polymer solution had the same salinity as the previous polymer flood and the waterflood. Polymer flood was considered completed at zero oil cut, which was reached after 1.5 pore volumes. Pressure values are shows in Figure 4.44 and the oil saturation and oil cut up to the elastic polymer flood are shown in Figure 4.45. No significant additional oil was produced from the elastic polymer flood. The pressure gradient at steady state was 4.5 psi/ft. The

equivalent shear rate at steady state was 17.92 $sec^{-1}$ and the Deborah number was 17.88. The max capillary number during the scleroglucan polymer flood was 2.37 X $10^{-5}$. There was no significant change in residual oil saturation after the elastic polymer flood.

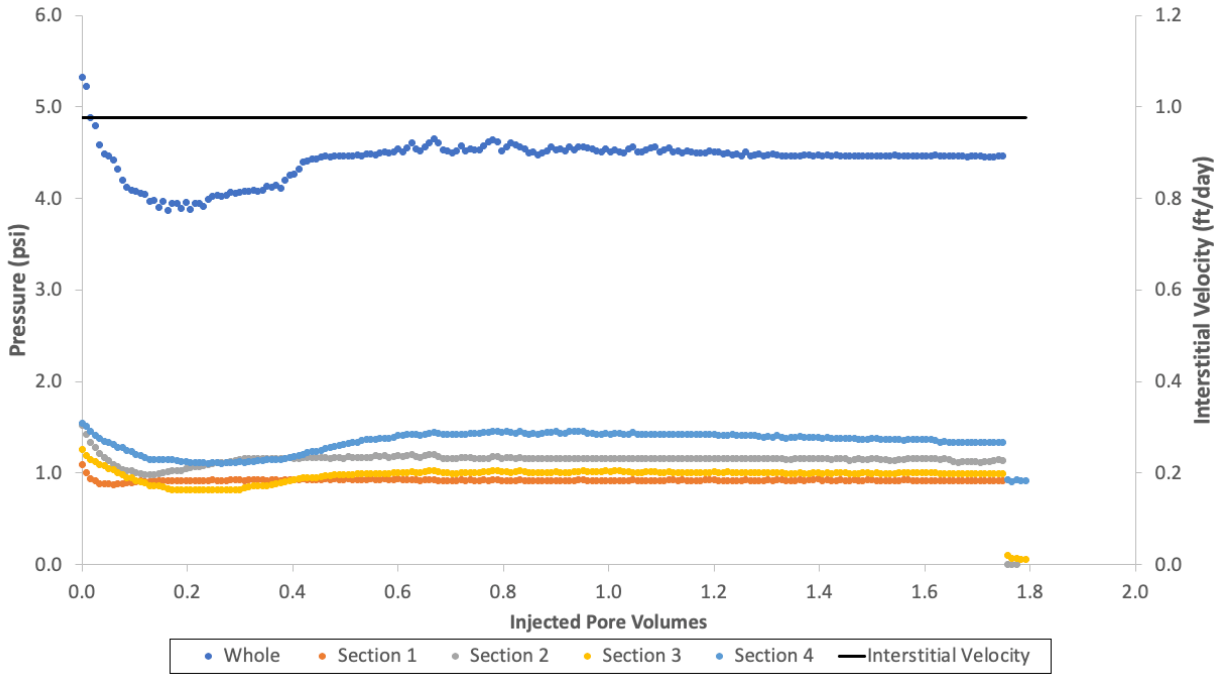


Figure 4.44: Pressure data after third polymer flood (viscoelastic) in experiment #3.

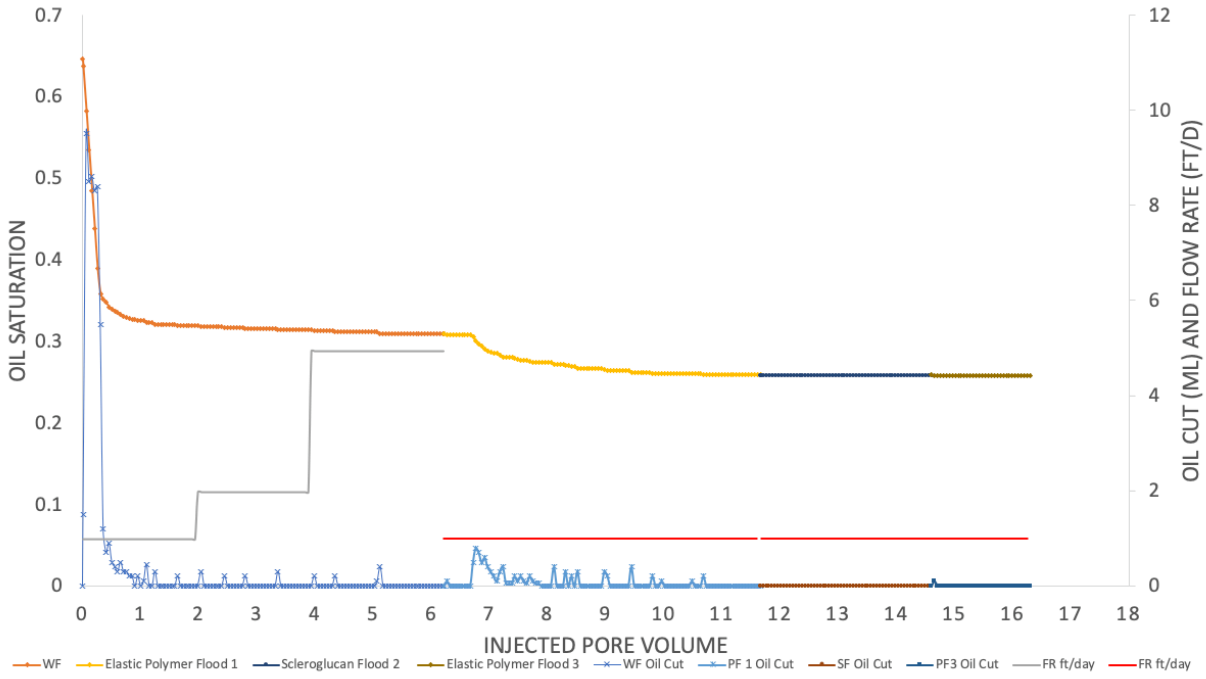


Figure 4.45: Oil saturation after third polymer flood (viscoelastic) in experiment #3.

In order to try and recover any mobilized oil droplets that might have been captured by the elastic polymer flood, the high-salinity, inelastic FP3630s was injected at a constant flow rate of 0.12 ml/min (1 ft/day). This polymer solution had the a much higher salinity as the previous polymer flood and the waterflood. Polymer flood was considered completed at zero oil cut, which was reached after 2.5 pore volumes. Pressure values are shows in Figure 4.46 and the oil saturation and oil cut after the inelastic polymer flood are shown in Figure 4.47. No significant additional oil was produced from the inelastic polymer flood. The pressure gradient at steady state was 3.5 psi/ft. The equivalent shear rate at steady state was 17.5 $sec^{-1}$ and the Deborah number was 0.84. The max capillary number during the scleroglucan polymer flood was 1.84 X $10^{-5}$. There was no significant change in residual oil saturation after the elastic polymer flood.

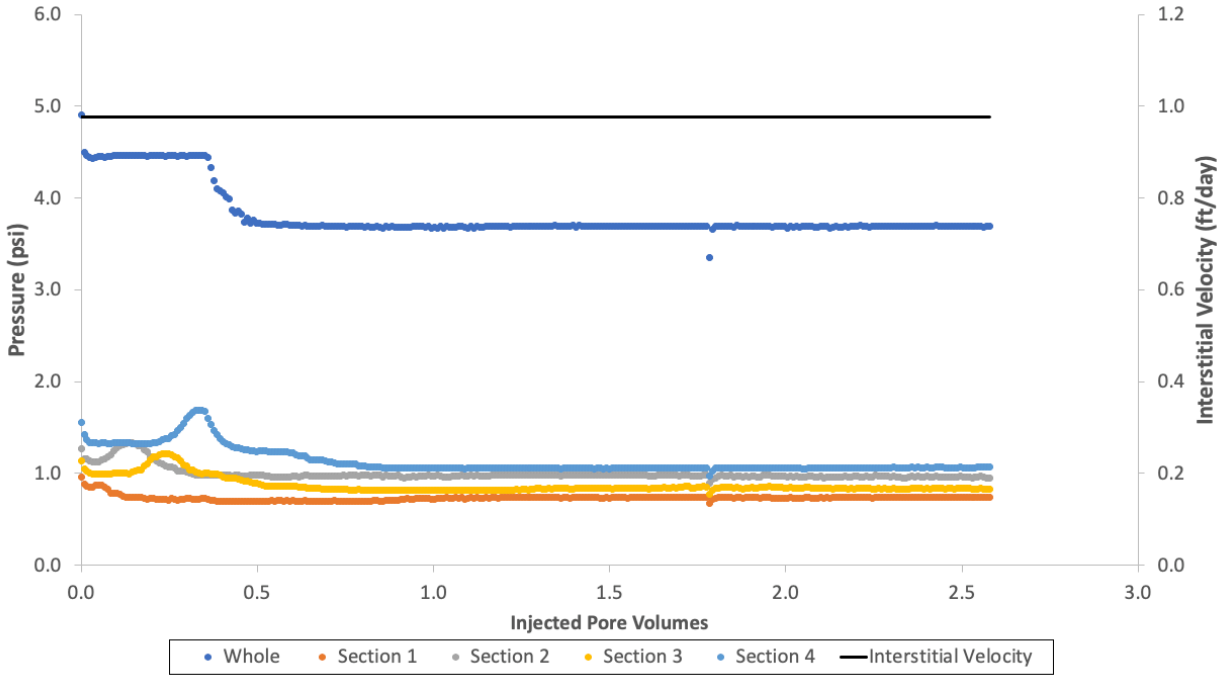


Figure 4.46: Pressure data after fourth polymer flood (inelastic) in experiment #3.

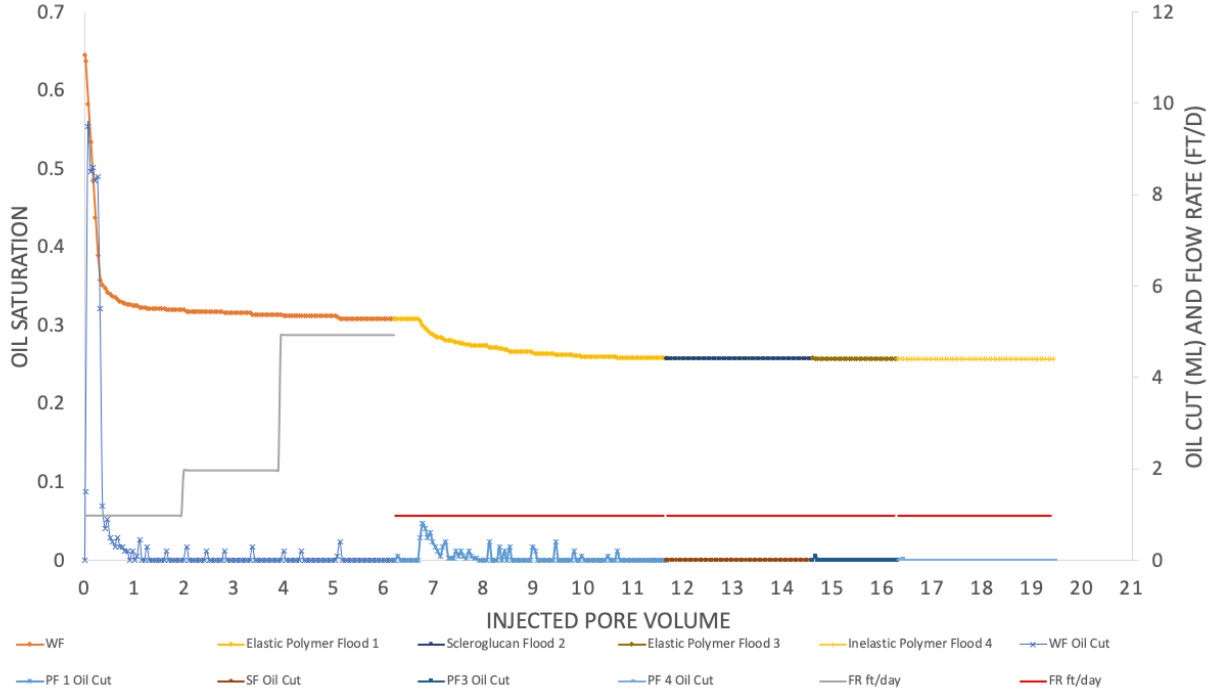


Figure 4.47: Oil saturation after fourth polymer flood (inelastic) in experiment #3.

In order to see if any additional oil could be recovered by injecting polymer at a higher rate or at higher pressure gradients, a final low-salinity, elastic polymer solution (polymer flood #5) was injected first at 1 ft/day, and then bumped up to 2 ft/day. The corresponding pressure values are seen in Figure 4.48. At 1 ft/day, the pressure gradient at steady state was 4.9 psi/ft. The equivalent shear rate at steady state was 17.55 $sec^{-1}$ and the Deborah number was 26.15. The max capillary number during the scleroglucan polymer flood was 2.58 X $10^{-5}$. The residual oil saturation is shown in Figure 4.49 after the polymer flood. There was no significant change in residual oil saturation after the elastic polymer flood.

At 2 ft/day, the pressure gradient at steady state was 4.9 psi/ft. The equivalent shear rate at steady state was 37.92 $sec^{-1}$ and the Deborah number was 56.5. The max capillary number during the scleroglucan polymer flood was 4.36 X $10^{-5}$. As seen in Figure 4.49, there was a small amount of oil that was recovered during the initial bump in flow rate, but there was no significant oil production that resulted from the significant increase in flow rate or pressure gradient.

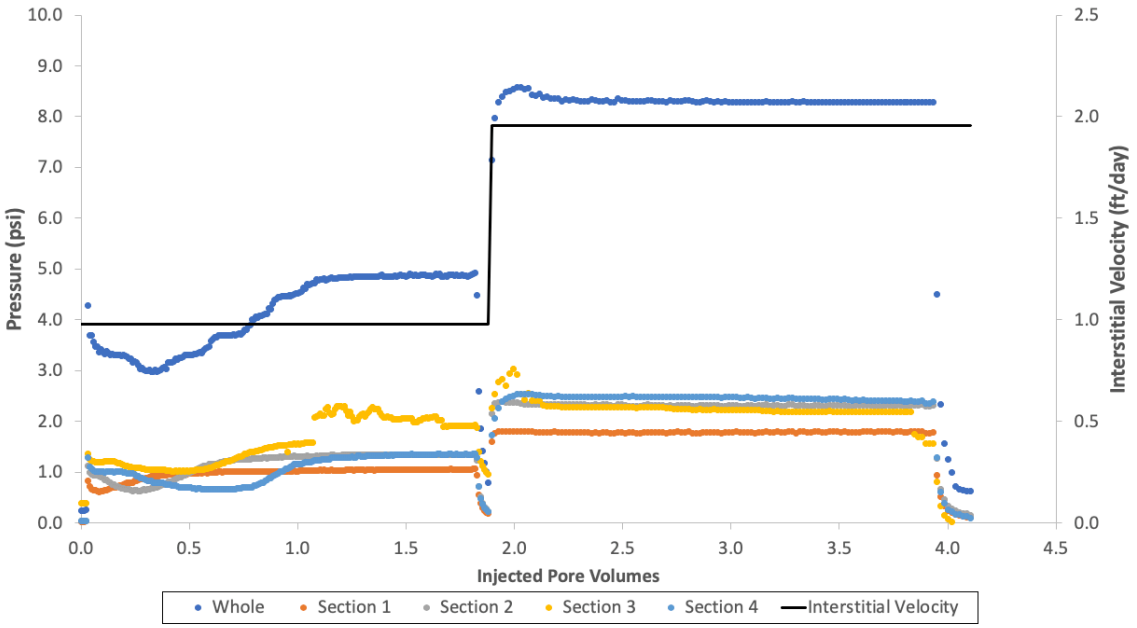


Figure 4.48: Pressure data after final elastic polymer flood in experiment #3.

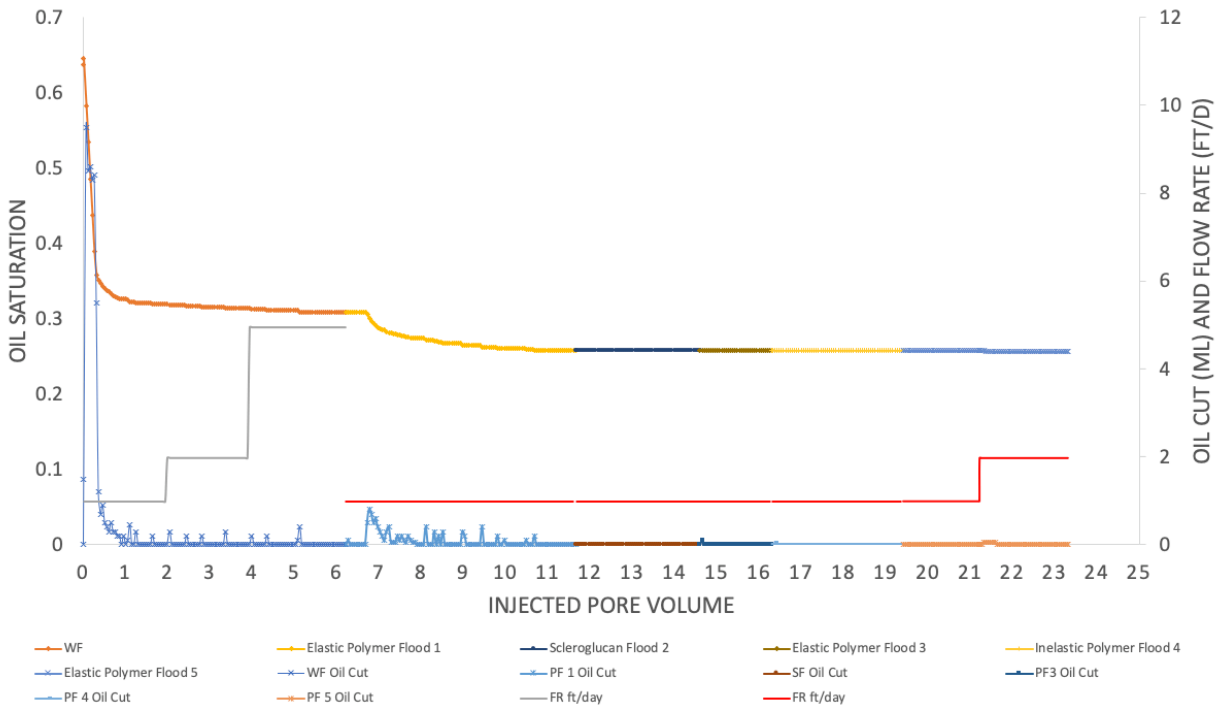


Figure 4.49: Oil saturation after all polymer floods in experiment #3.

The polymer floods were stopped after the fifth polymer flood. The cumulative oil recovery at the end of the polymer flood was 60.4% of the original oil in place. The final oil saturation of the core was 25.6%. Again, the significant increase in pressure in the last elastic polymer flood did not significantly produce more oil, suggesting that perhaps a higher pressure gradient isn't necessarily the mechanism behind the viscoelastic effect of the polymer. The recovery of oil might not be attributed to capillary effects. Similar to the previous corefloods, the pressure gradients, while higher than those in the Boise sandstone experiments, remained relatively stable throughout the injections of polymers. All polymer floods remained below the critical capillary number.

## 4.5 EXPERIMENT #4: OIL WET BENTHEIMER SANDSTONE CORE #1

Experiment #3 was designed to test viscoelastic polymer floods in oil-wet Bentheimer cores. High permeability Bentheimer sandstones were injected with organosilanes as discussed in Chapter 3 to alter the water-wet rock surfaces in the sandstone to become oil-wet.

### 4.5.1 Core Preparation and Conditioning

The purpose of this coreflood was to test the effect of viscoelastic polymer floods on residual oil saturation when a high-salinity polymer flood was performed following a low-salinity polymer flood and repeated these cycles until a steady state residual saturation was achieved. These floods were meant to be similar to the successful floods in experiment #1. The polymer floods were designed to try to keep the capillary number lower than the critical capillary number in Bentheimer sandstone cores (~$1x10^{-5}$). Table 4.4 summarizes the general properties of the core and the brine and polymer fluids.

Table 4.4: Core and experimental fluid properties for experiment #4.

| | |
|---|---|
| **Core Name** | BT 1-1 |
| **Rock Type** | Bentheimer sandstone |
| **Brine permeability (mD)** | 1323 |
| **Crude Oil Viscosity (cP)** | 5 |
| **Temperature ($^oC$)** | 23 |
| **Diameter (cm)** | 5.08 |
| **Length (cm)** | 30.48 |
| **Area ($cm^2$)** | 20.27 |
| **Bulk Volume (cc)** | 617.78 |
| **Pore Volume (mL)** | 142.9 |
| **Porosity** | 0.231 |
| **Bulk Density (g/cc)** | 2.00 |
| **Brine Composition** | 1000 ppm NaCl + 400 ppm $NaHCO_3$ + 400 ppm |

| | |
|---|---|
| | $Na_2S_2O_4$ |
| **Viscoelastic Polymer Composition** | 1000 ppm FP3630s HPAM polymer in 1000 ppm NaCl + 400 ppm $NaHCO_3$ aqueous solution |
| **Inelastic Polymer Composition** | 2200 ppm FP3630s HPAM polymer in 20,000 ppm NaCl + 400 ppm $NaHCO_3$ aqueous solution |

The Bentheimer sandstone core was dried in a 100°C oven overnight and then placed in a stainless steel core holder. It was vacuum evacuated and underwent the chemical alteration of the wettability of the core as detailed in Chapter 3. The organosilanes were injected into the core and the rock surfaces became hydrophilic and considered oil-wet. After the core was changed to oil-wet, it was cleaned with hexanes, removed from the stainless steel core holder, and allowed to completely dry in a 100°C oven overnight. The dry, clean, oil-wet core was then potted in epoxy in preparation for core flooding as described in Chapter 3. The estimated pore volume from brine imbibition was 140 mL. Once the core was saturated with this low salinity brine (0.0 normalized salinity), the high salinity iron reduction aqueous solution (4% $NaHCO_3$ + 1% EDTA + 1% $Na_2S_2O_4$) (1.0 normalized salinity) was injected at 2.5 ml/min to complete a salinity tracer test to calculate the pore volume and heterogeneity of the core. Figure 4.50 shows the salinity of the effluent samples increasing as the high salinity brine iron reduction aqueous displaces the low salinity brine solution previously existing in the core. The pore volume was calculated from the tracer test as 142.9 mL.

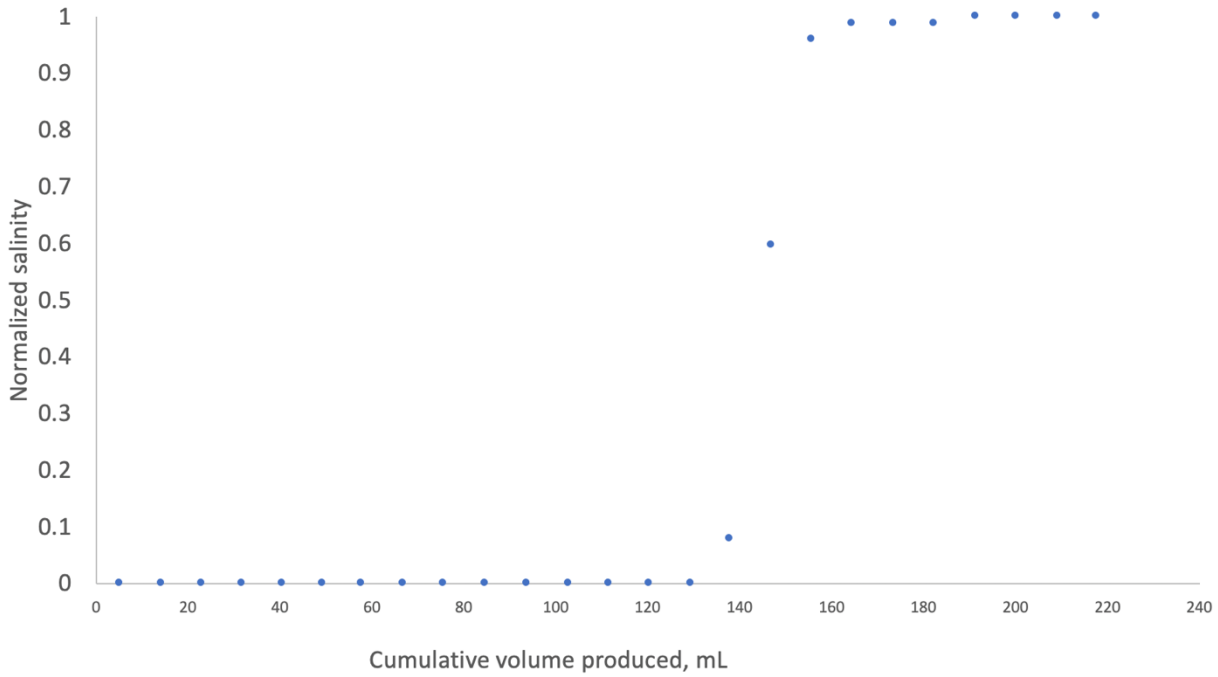


Figure 4.50: Salinity tracer test of the Bentheimer sandstone used in experiment #4.

The core was continuously pumped with this iron reduction solution at 1ml/min (10.4ft/day) in order to reduce the amorphous oxidized iron in the core. The iron reducing fluid was injected at varying rates (1, 5, 10, 15, 20 ml/min) and the corresponding pressure values recorded, as shown in Figure 4.51. These pressures were used to determine permeability which was estimated to be 1323mD using Darcy's Law.

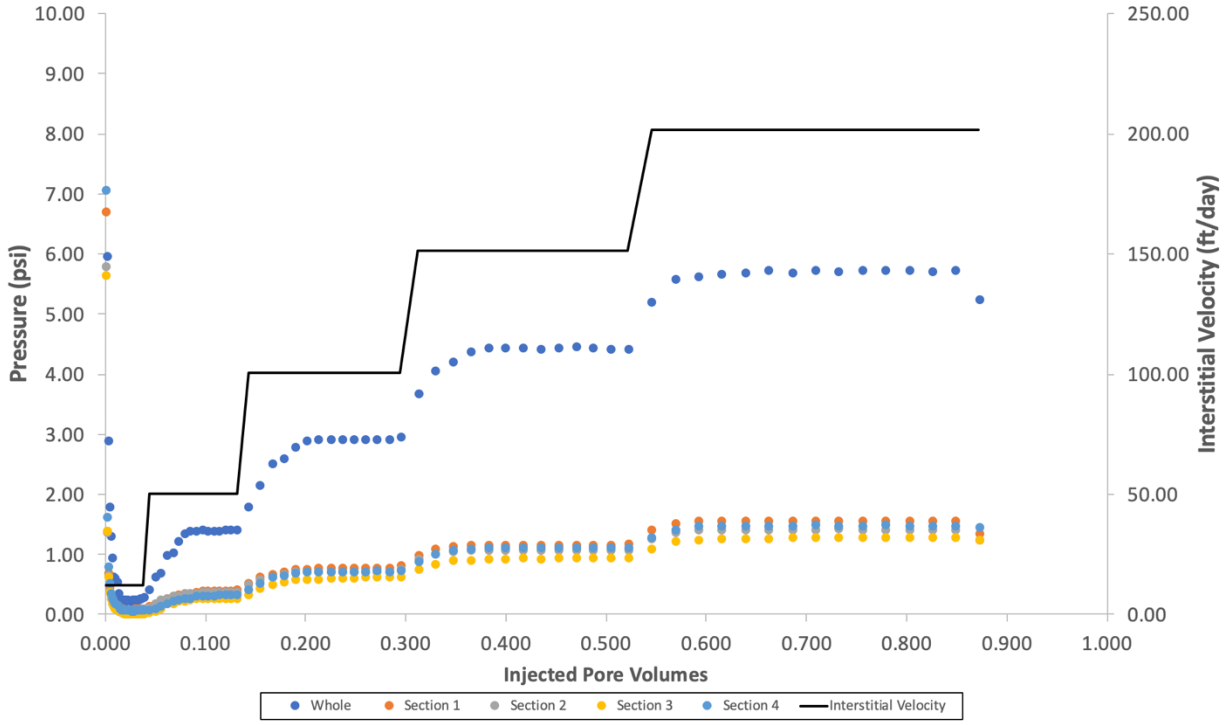


Figure 4.51: Pressure values while establishing brine permeability in experiment #4.

### 4.5.2 Oil Flood

Diluted dead crude oil (13% toluene) was filtered through 1.2 μm filter paper under 20 psi of air at 23°C. The diluted oil was found to have a viscosity of 5 cP. The low viscosity oil was injected into core at a constant pressure using argon at 40 psi. At least 1.5PV of oil was injected. Volumetric calculations were used to determine initial oil saturation ($S_{oi}$) by observing the volume of water and oil produced in burettes during the oil floods. The displaced brine volume was used to calculate initial oil saturation. Oil flood continued until there was a consistent water cut of 0%. The core was aged with the oil for at least 48 hours. Initial oil saturation was determined to be 74.2%.

### 4.5.3 Waterflood

An aqueous solution of 1000 ppm NaCl + 400 ppm $NaHCO_3$ + 400 ppm $Na_2S_2O_4$ was injected at constant flow rate of 0.1ml/min, (1 ft/day), and then 0.5 ml/min (5 ft/day). This increase in flow rate was to maintain that the oil saturation after waterflood was truly residual oil saturation. This brine was injected until steady state pressure was reached and the oil cut was zero. The pressure gradient at steady state was recorded to be 0.4 psi/ft (1 ft/day), and 0.6 psi/ft (5 ft/day) (Figure 4.52). Oil saturation after waterflood at 1 ft/day was calculated to be 18.4% (Figure 4.53). After the waterflood was increased to 5 ft/day, the oil saturation further decreased to 13.7%.

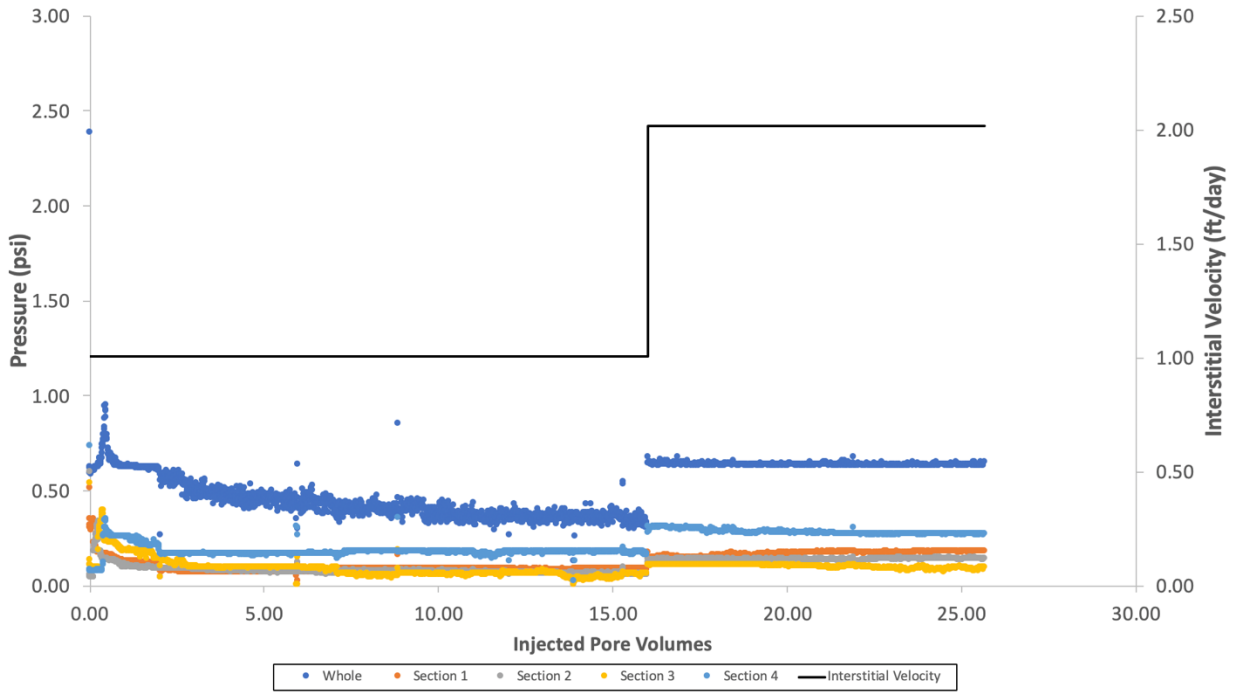


Figure 4.52: Waterflood pressure data for experiment #4.

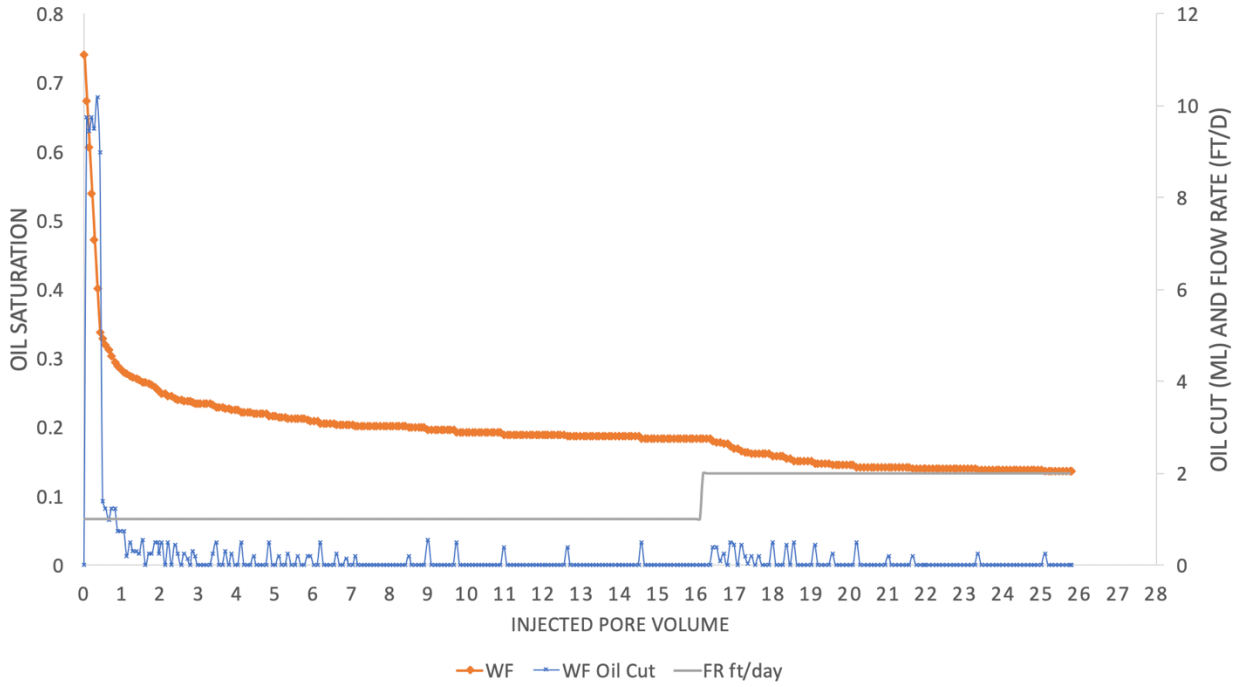


Figure 4.53: Oil saturation after waterflood in experiment #4.

Because this was the first experiment of this type to be completed in an oil-wet rock, it was important to make sure that residual oil saturation had been reached. A large amount of brine was injected during the waterflood because there was still small fractions of oil being produced even later in the flood. At the beginning of the waterflood, the oil fractions were almost 100%, although that reduced quickly within 1PV. However, the core consistently continued to produce almost 1mL in the fractions following the initial oil bank, which is why more brine was continued to be injected. The bump in the waterflood rate was chosen after no oil was produced for almost 1 PV. Even after the bump in injection rate to 5 ft/day, there was a period in which additional oil was being produced.

It was also noted that the oil saturation is already low after almost 26PV of brine was injected and that small amounts of oil are still coming out of the core, although it is not large fractions. This was suspected to be due to the distribution of oil droplets on the rock grains. As

seen in Figure 2.2, the water droplets will prefer to be in the larger pore spaces, while the oil droplets will be on the smaller pore spaces. As more water is injected, it slowly strips off oil droplets. The waterflood was considered completed since very small fractions of oil would be recovered after many pore volumes of water was injected. It was suspected that the polymer floods subsequent to the waterflood would produce oil in a similar fashion.

### 4.5.4 Polymer Floods for Experiment #4

A high molecular weight polymer (FP3630s) was prepared in the same low salinity brine as the waterflood (1000 ppm NaCl + 400 ppm $NaHCO_3$). This solution produced a polymer with a high relaxation time (1.3 sec) and referred to as the "elastic polymer flood". After hydrating for 24 hours, the solution was filtered under 15 psi of argon gas at 23$^{o}$C through a 1.2 μm filter paper. The same high molecular weight polymer (FP3630s) was prepared in high salinity brine (2200 ppm FP3630s HPAM polymer in 20,000 ppm NaCl + 400 ppm $NaHCO_3$) in a similar manner. This solution produced a polymer with a very low relaxation time (0.02-0.04 sec) and referred to as the "inelastic polymer flood." Multiple batches of these polymer solutions were made as the floods were planned to be alternated until steady state was reached. Polymer solutions 1, 3, and 5 in Figure 4.37 were elastic and polymers 2, 4, and 6 were inelastic solutions. The dynamic frequency sweep test (DFST) was performed as previously discussed in Chapter 3 to determine relaxation times. The steady rate sweet test (SRST) was also performed as previously discussed in Chapter 3 to obtain the viscosity profiles of each polymer solution. The power-law viscosity region was used to fit an equation to create the power law model to obtain the constants for the solution.

The polymer solutions were compared to make sure that their viscosity at different shear rates were similar to avoid unstable displacement (Figure 4.54). It can be noted that the high salinity, inelastic polymer had slightly lower viscosities at lower shear rates, but were nearly identical at a shear rate of $20s^{-1}$, the rate at which most of the core floods were completed at. Each batch was tested on the rheometer for quality control.

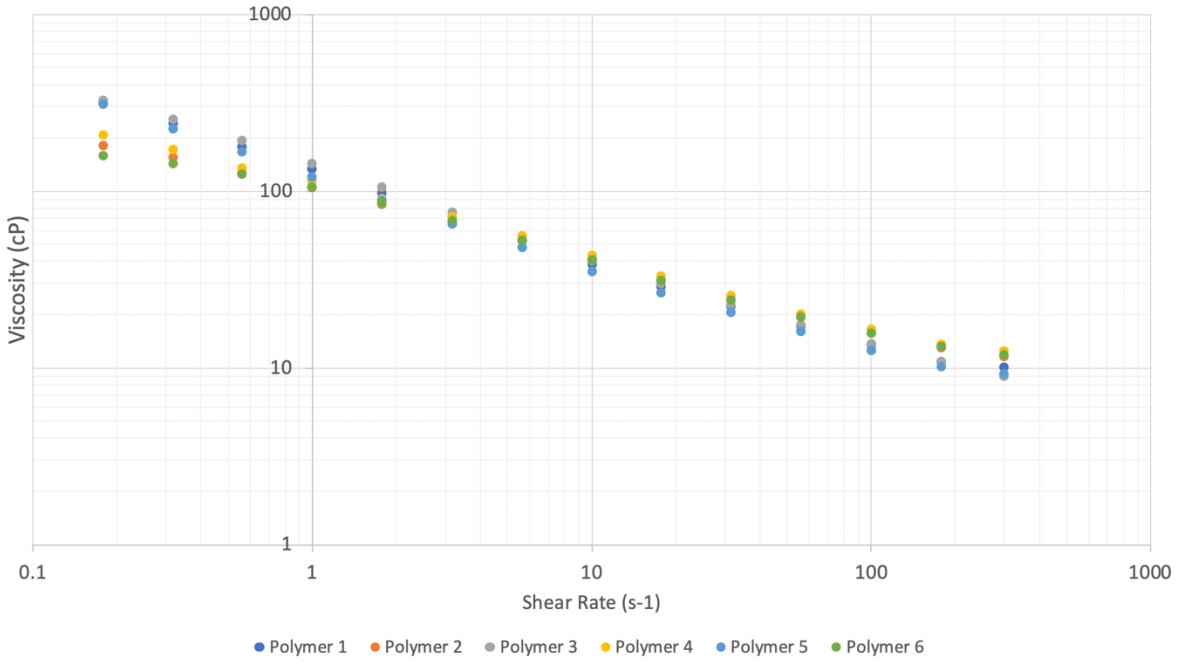


Figure 4.54: Polymer rheology for samples in experiment #4.

### 4.5.4.1 Polymer Flood #1 (Viscoelastic)

The low-salinity, elastic, polymer was injected at a constant flow rate of 0.1 ml/min (1 ft/day) until steady state was reached and zero oil cut. Polymer flood was considered completed at zero oil cut, which was reached after almost 6 pore volumes. The pressure gradient at steady state was 14 psi/ft, as seen in Figure 4.55. The equivalent shear rate at steady state was 33.46 $sec^{-1}$. Oil saturation and oil cut up to the first inelastic polymer flood are shown in Figure 4.56. Residual oil saturation was decreased from 13.7% to 10.28%, and the corresponding Deborah

number was 40.16. The change in residual oil saturation decreased 3.42% from the elastic polymer flood.

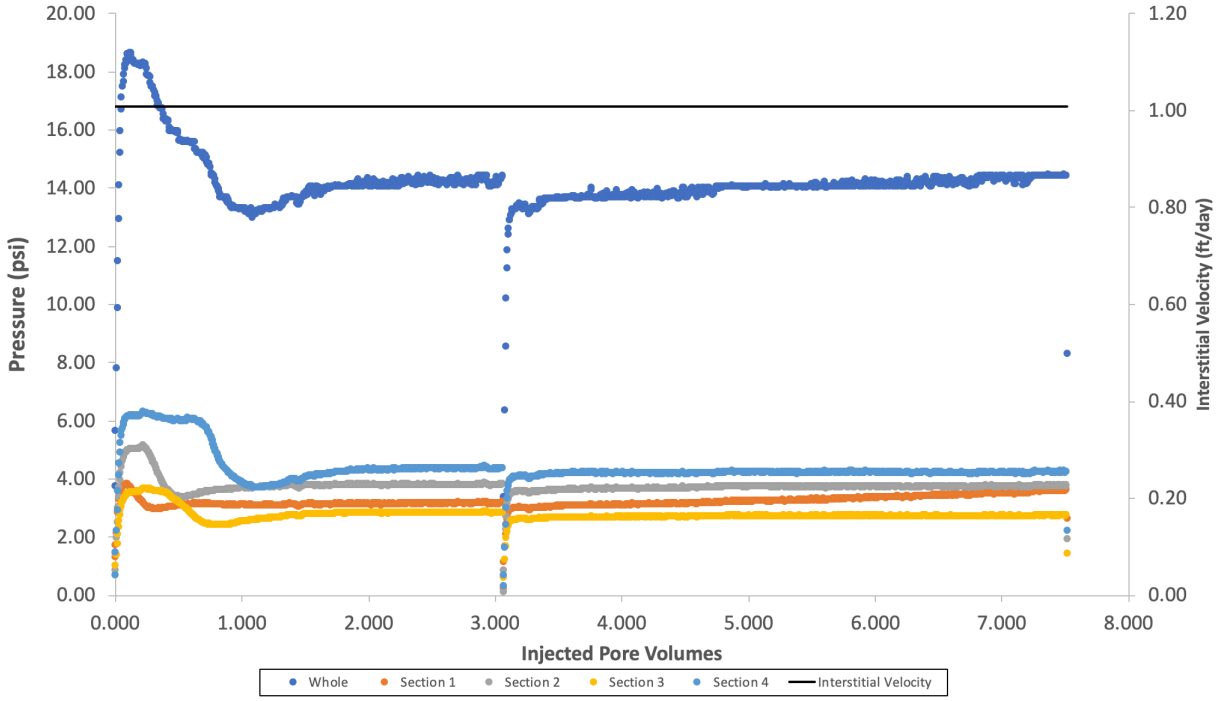


Figure 4.55: Pressure data during the first polymer flood (viscoelastic) in experiment #4.

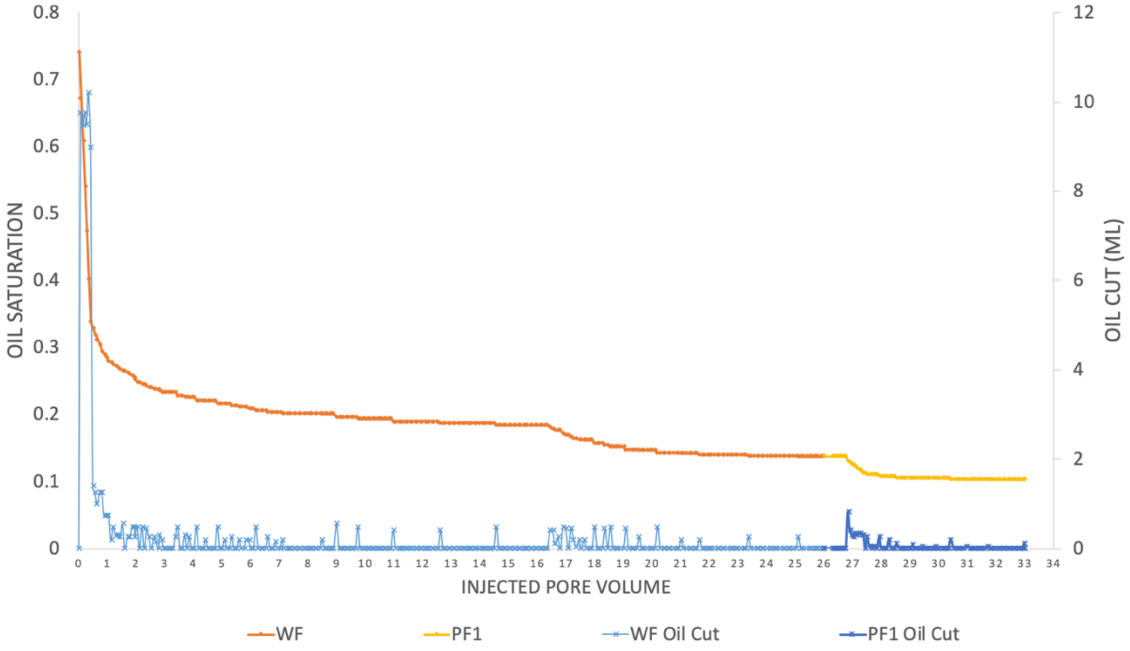


Figure 4.56: Oil saturation after first polymer flood (viscoelastic) in experiment #4.

The cumulative oil recovery at the end of the polymer flood was 86.14% of the original oil in place. The maximum capillary number for the elastic polymer flood was 2.47 X $10^{-5}$, which was below the critical capillary number (1 X $10^{-4}$).

### 4.5.4.2 Polymer Flood #2 (Inelastic)

The high-salinity, inelastic, polymer was injected at a constant flow rate of 0.12 ml/min (0.96 ft/day) until steady state was reached and zero oil cut. Polymer flood was considered completed at zero oil cut, which was reached after almost 2PV, as seen in Figure 4.58. The pressure data is shown in Figure 4.57. The pressure gradient at steady state was similar to the previous flood, at 14 psi/ft. The equivalent shear rate at steady state was 32.17 $sec^{-1}$. Residual oil saturation was decreased from 10.28% to 10.268%, and the corresponding Deborah number was 0.64. The change in residual oil saturation barely decreased 0.012% from the inelastic polymer flood.

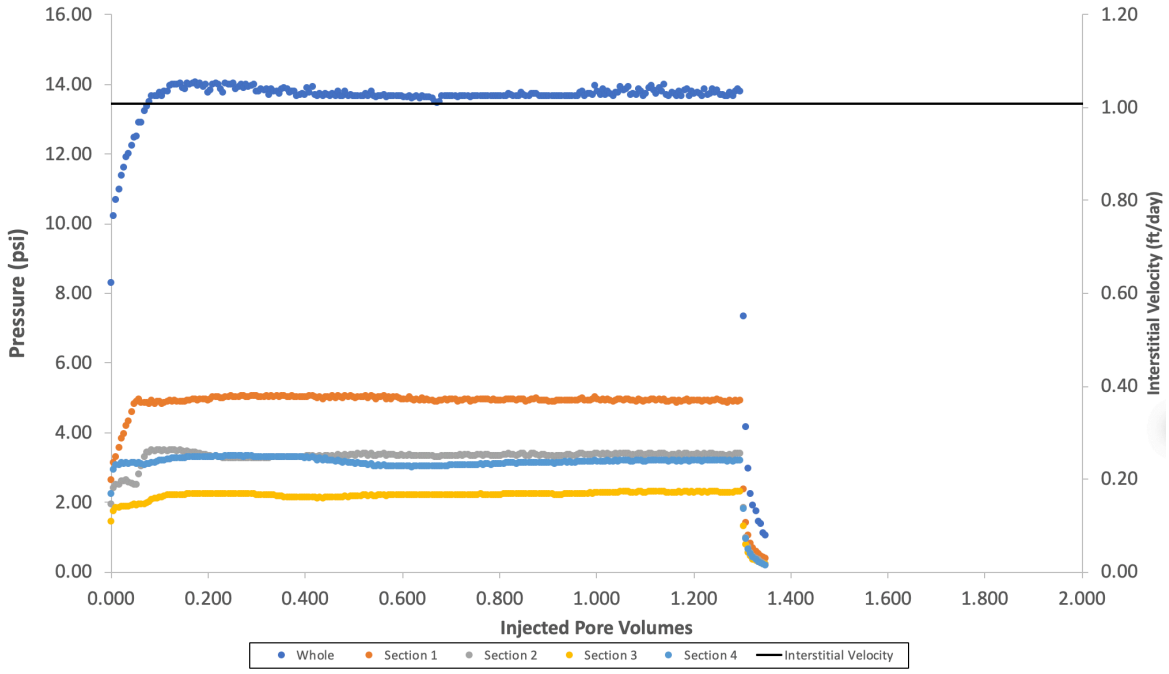


Figure 4.57: Pressure data during second polymer flood (inelastic) in experiment #4.

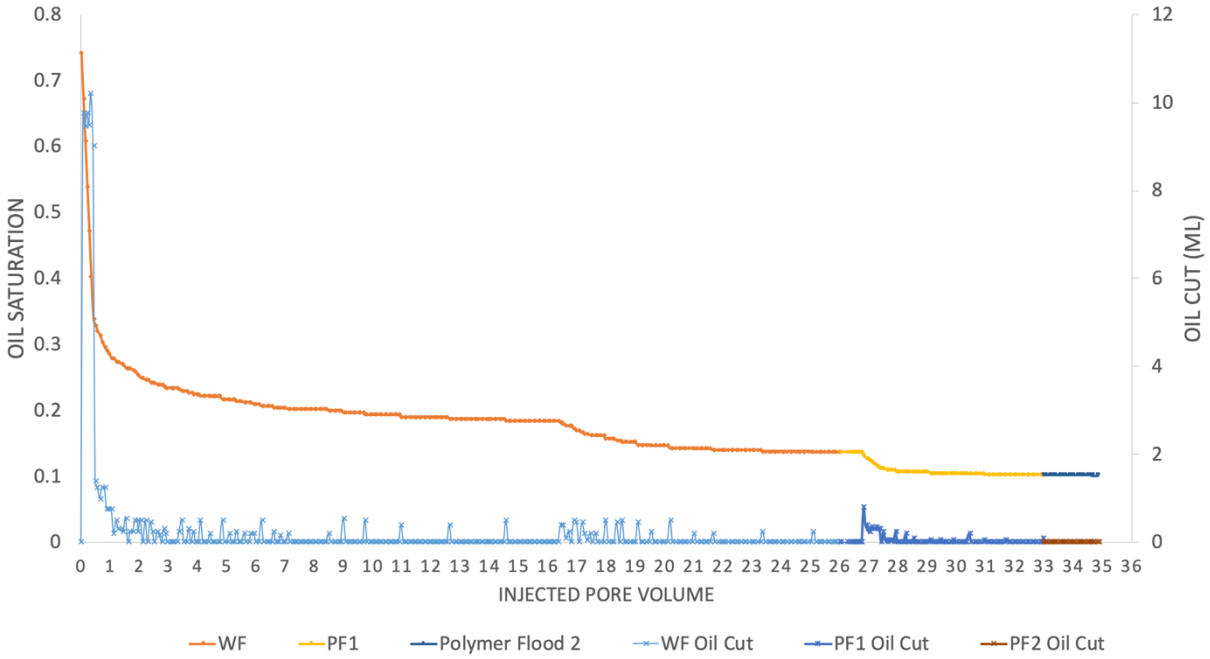


Figure 4.58: Oil Saturation after second polymer flood (inelastic) in experiment #4.

The cumulative oil recovery at the end of the polymer flood was 86.2% of the original oil in place. The maximum capillary number for the elastic polymer flood was 2.47 X $10^{-5}$, which was below the critical capillary number (1 X $10^{-4}$).

### 4.5.4.3 Polymer Flood #3 (Viscoelastic)

The low-salinity, elastic, polymer was injected at a constant flow rate of 0.1 ml/min (1 ft/day) until steady state was reached and zero oil cut. Polymer flood was considered completed at zero oil cut, which was reached after 2 pore volumes. Figure 4.59 shows the pressure values and Figure 4.60 shows the oil saturation and oil cut up to the third polymer flood. The pressure gradient at steady state was 23 psi/ft. The equivalent shear rate at steady state was 33.46 $sec^{-1}$. The Deborah number was 30.94. The residual oil saturation did not change.

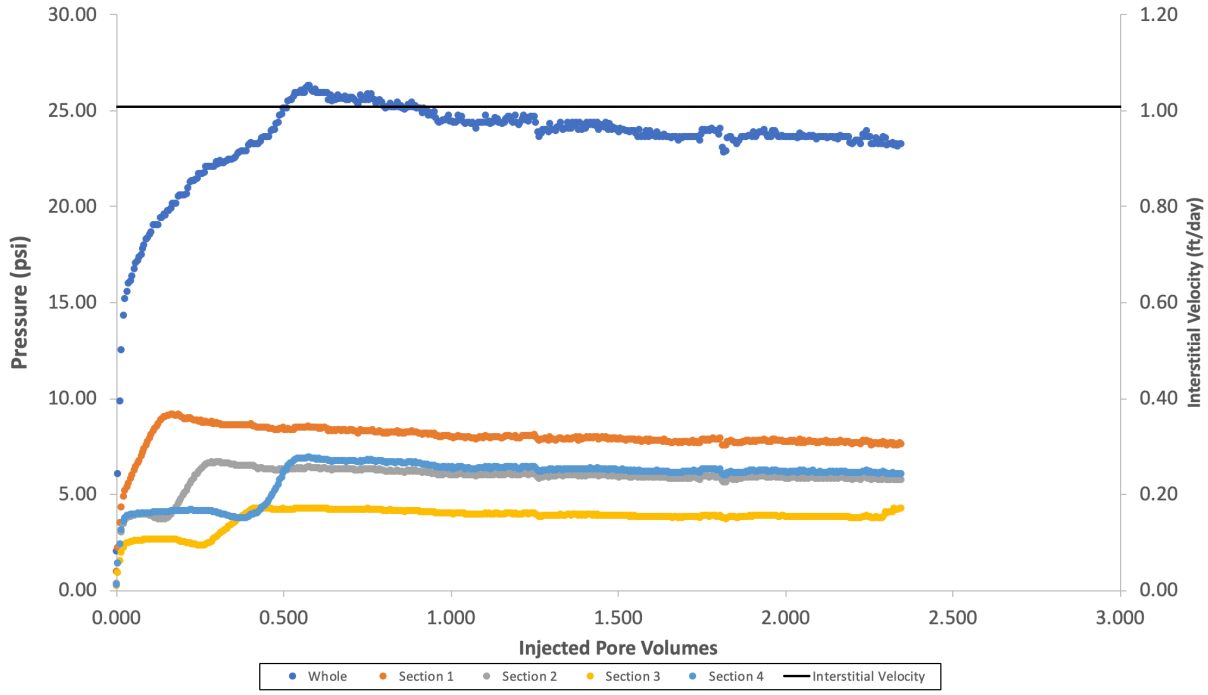


Figure 4.59: Pressure data during the third polymer flood (viscoelastic) in experiment #4.

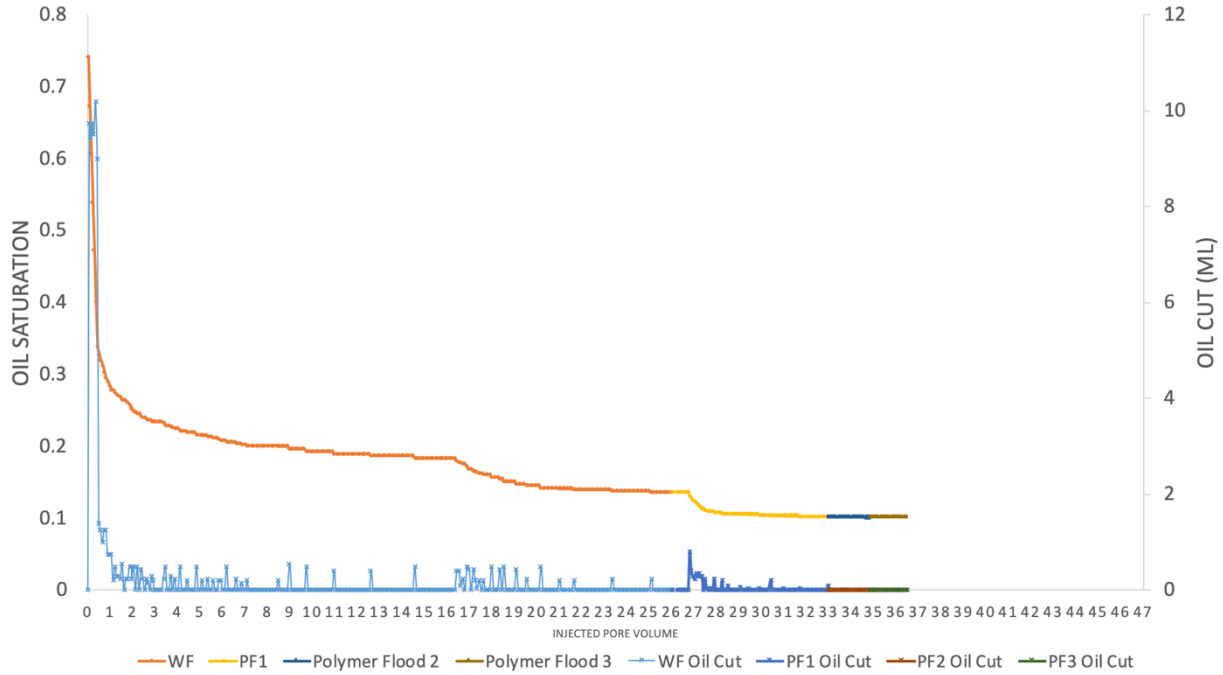


Figure 4.60: Oil Saturation after third polymer flood (viscoelastic) in experiment #4.

The cumulative oil recovery at the end of the polymer flood was 86.14% of the original oil in place. The maximum capillary number for the elastic polymer flood was 3.88 X $10^{-5}$, which was below the critical capillary number (1 X $10^{-4}$).

#### 4.5.4.4 Final Alternating Polymer Floods #4 and #5 and #6 (Inelastic, Viscoelastic, and Inelastic)

While there was minimal recovery of oil, there was still some minor amounts of oil being produced which is why another round of alternating inelastic and elastic polymer floods were chosen to be injected into the core. The final three floods of experiment #4 were an inelastic flood used to try to sweep any mobilized oil that the previous elastic flood had missed, and another additional elastic/inelastic flood cycle.

The high-salinity, inelastic, polymer was injected at a constant flow rate of 0.12 ml/min (0.96 ft/day) until steady state was reached and zero oil cut. Polymer flood was considered completed at zero oil cut, which was reached after almost 2PV. The pressure gradient (as seen in Figure 4.61) at steady state was similar to the previous flood, at 14 psi/ft. The equivalent shear rate at steady state was 35.96 $sec^{-1}$. The residual oil saturation decreased from 10.268% to 9.92% and the Deborah number was calculated at 1.84. Oil saturation and oil cut up to the fourth polymer flood (inelastic) are shown in Figure 4.62. The change in residual oil saturation barely decreased 0.348% from the inelastic polymer flood.

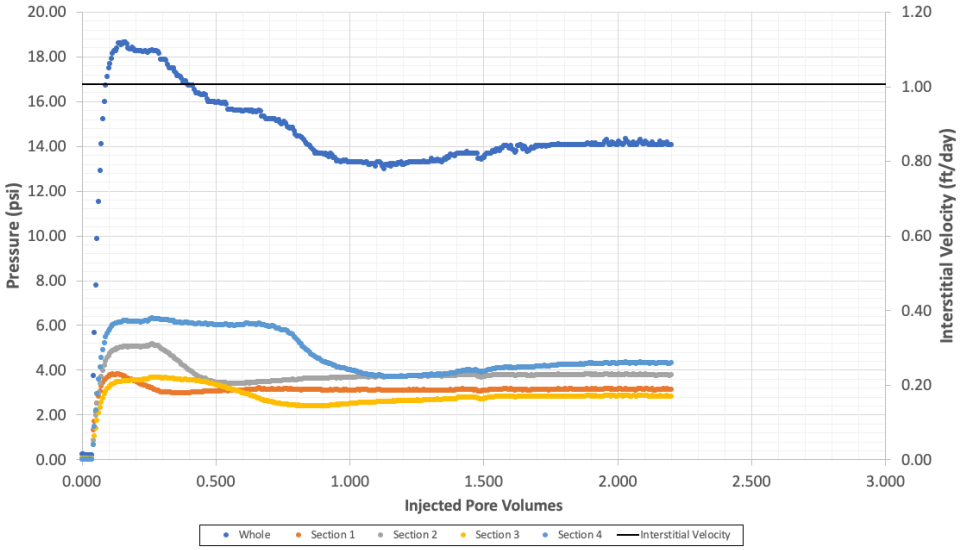


Figure 4.61: Pressure data for the fourth polymer flood (inelastic) in experiment #4.

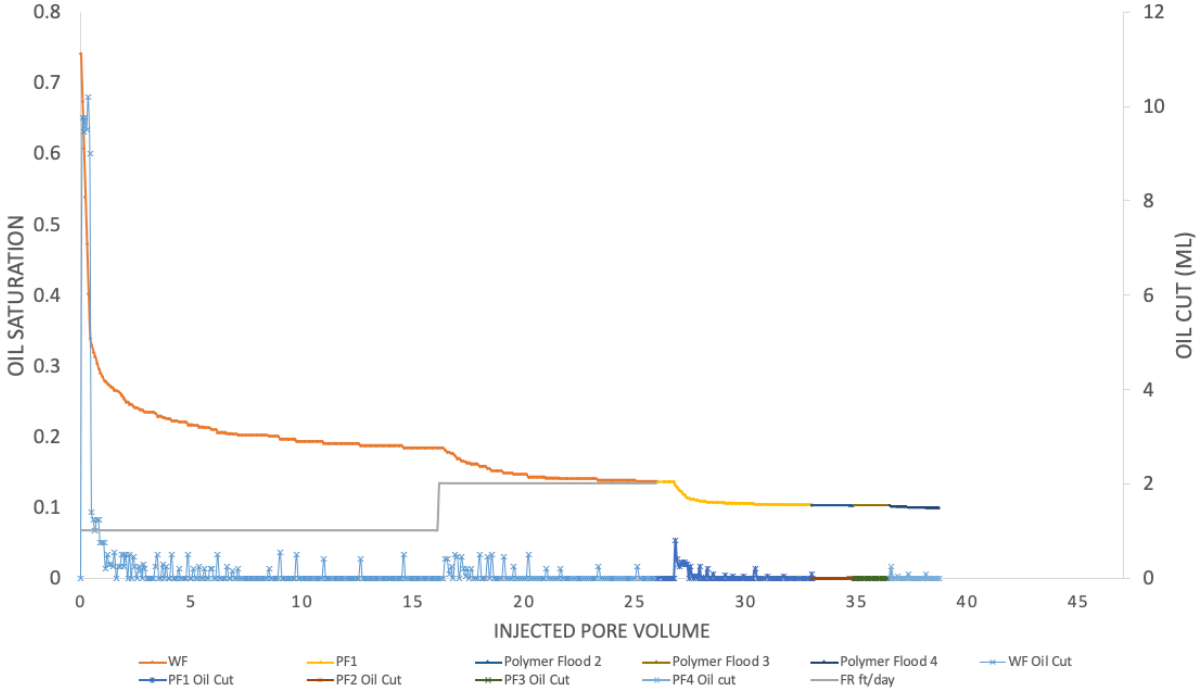


Figure 4.62: Oil saturation after fourth polymer flood (inelastic) in experiment #4.

The cumulative oil recovery at the end of the polymer flood was 86.6% of the original oil in place. The maximum capillary number for the elastic polymer flood was 2.47 X $10^{-5}$, which was below the critical capillary number (1 X $10^{-4}$).

As the polymer flood continued, it seemed as if there was still some oil potentially mobilized which is why another cycle of elastic and inelastic polymer floods were planned (Polymers 5 and 6 in Figure 4.54).

The low-salinity, elastic, polymer was injected at a constant flow rate of 0.1 ml/min (1 ft/day) until steady state was reached and zero oil cut. Polymer flood was considered completed at zero oil cut, which was reached after about 3 pore volumes. Pressure values are shows in Figure 4.63 and the oil saturation and oil cut up of all the polymer floods are shown in Figure 4.64. The pressure gradient at steady state was 14 psi/ft. The equivalent shear rate at steady state was 32.31 $sec^{-1}$. The residual oil saturation decreased from 9.92% to 9.74% and Deborah number was 41.51. The residual oil saturation decreased minimally 0.18%. The maximum capillary number for the elastic polymer flood was 2.47 X $10^{-5}$.

The final high-salinity, inelastic, polymer was injected at a constant flow rate of 0.1 ml/min (1 ft/day) until steady state was reached and zero oil cut. Polymer flood was considered completed at zero oil cut, which was reached after about 2 pore volumes. The pressure gradient at steady state stayed at 14 psi/ft. The equivalent shear rate at steady state was 32.13 $sec^{-1}$. The Deborah number was 1.64. The residual oil saturation did not significantly change and was considered the end of the flood. The maximum capillary number for the elastic polymer flood was 2.47 X $10^{-5}$. Pressure values are shows in Figure 4.63 and the oil saturation and oil cut up for all the polymer floods are shown in Figure 4.64.

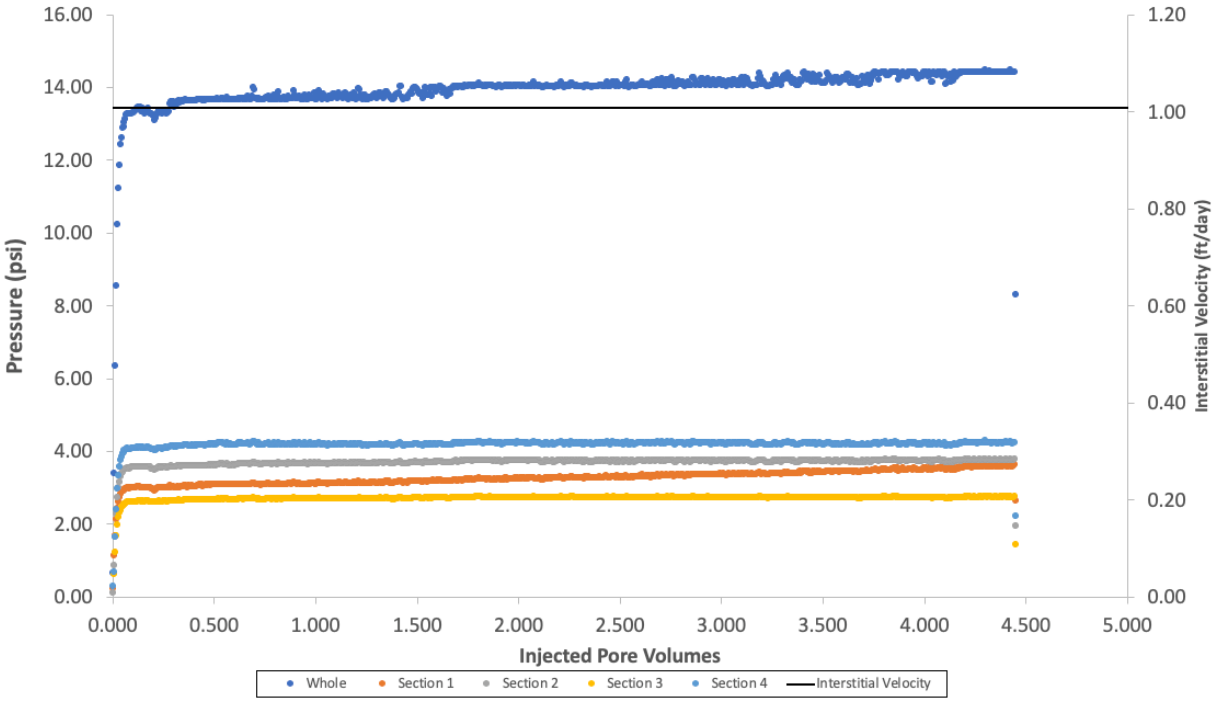


Figure 4.63: Pressure data for the final cycle of polymer flood (#5 and #6) in experiment #4.

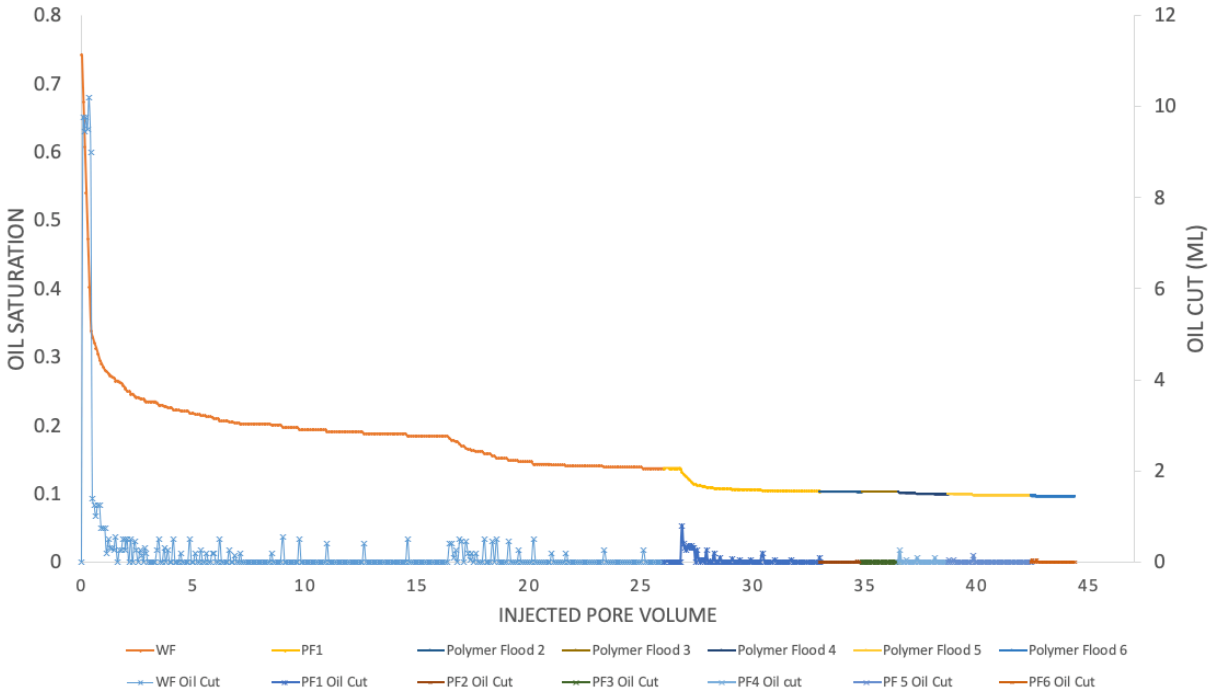


Figure 4.64: Final oil saturation after completion of polymer floods in experiment #4.

The final oil saturation of the coreflood was 9.74%. The main observation in this experiment was that the waterflood reduced the oil saturation to 18%, which was an already low saturation even before the polymer floods. A lot of brine had been injected prior to the any injection of polymer. A promising thing to note was that the immediate polymer flood following the waterflood produced oil to reduce the oil saturation 3.42%, even at that low saturation. The pressure gradients, while higher than those in the Boise sandstone experiments, remained relatively stable throughout the injections of polymers. All polymer floods remained below the critical capillary number. The starting oil saturation for this coreflood was only at 74.2%, and because of how long the waterflood was, it was noted that in the next experiment that the starting saturation should be higher to see if there would be a more noticeable effect of the polymer on reducing the oil saturation in the oil-wet core.

## 4.6 EXPERIMENT #5: OIL WET BENTHEIMER SANDSTONE CORE #2

### 4.6.1 Core Preparation and Conditioning

Experiment #5 was designed so that the starting oil saturation in the oil-wet Bentheimer core would be significantly higher than experiment #4. The core would be initially saturated at 100% oil prior to the waterflood.

The purpose of this coreflood was to again test the effect of viscoelastic polymer floods on residual oil saturation when a high-salinity polymer flood was performed following a low-salinity polymer flood and repeated these cycles until a steady state residual saturation was achieved. These floods were meant to be similar to the successful floods in experiment #1. The polymer floods were designed to try to keep the capillary number lower than the critical capillary

number in Bentheimer sandstone cores (~$1x10^{-5}$). Table 4.5 summarizes the general properties of the core and the brine and polymer fluids.

Table 4.5: Core and experimental fluid properties for experiment #5.

| | |
|---|---|
| **Core Name** | BT 1-2 |
| **Rock Type** | Bentheimer sandstone |
| **Brine permeability (mD)** | 1003 |
| **Crude Oil Viscosity (cP)** | 5 |
| **Temperature (°C)** | 23 |
| **Diameter (cm)** | 5.08 |
| **Length (cm)** | 30.48 |
| **Area ($cm^2$)** | 20.27 |
| **Bulk Volume (cc)** | 617.78 |
| **Pore Volume (mL)** | 126.0 |
| **Porosity** | 0.204 |
| **Bulk Density (g/cc)** | 2.00 |
| **Brine Composition** | 1000 ppm NaCl + 400 ppm $NaHCO_3$ + 400 ppm $Na_2S_2O_4$ |
| **Viscoelastic Polymer Composition** | 1000 ppm FP3630s HPAM polymer in 1000 ppm NaCl + 400 ppm $NaHCO_3$ aqueous solution |
| **Inelastic Polymer Composition** | 2200 ppm FP3630s HPAM polymer in 20,000 ppm NaCl + 400 ppm $NaHCO_3$ aqueous solution |

The Bentheimer sandstone core was dried in a 100°C oven overnight and then potted in epoxy to be prepared for core flooding, as discussed in Chapter 3. Because this core was going to be injected with organosilanes that would normally react with the polycarbonate end pieces, the end pieces were made from chemical resistant material (PEEK). The methods in preparing the core in epoxy was the same, but more care was taken to make sure the core was completely contained in the epoxy/PEEK so that no silanes would react or leak. Once in epoxy, the core was vacuum evacuated and underwent the chemical alteration of the wettability of the core as

detailed in Chapter 3. After the core was changed to oil-wet, it was cleaned with hexanes, and allowed to air dry at 23°C overnight to allow the hexane to fully dry. The core was then placed in a 100°C oven overnight to completely dry. Once completely dry, the core was then vacuum saturated at 25°C with the waterflood brine solution (1000 ppm NaCl + 400 ppm $NaHCO_3$ + 400 ppm $Na_2S_2O_4$). The estimated pore volume from brine imbibition was 125 mL. Once the core was saturated with this low salinity brine (0.0 normalized salinity), the high salinity iron reduction aqueous solution (4% $NaHCO_3$ + 1% EDTA + 1% $Na_2S_2O_4$) (1.0 normalized salinity) was injected at 2.5 ml/min to complete a salinity tracer test to calculate the pore volume and heterogeneity of the core. Figure 4.65 shows the salinity of the effluent samples increasing as the high salinity brine iron reduction aqueous displaced the low salinity brine solution previously existing in the core. The pore volume was calculated from the tracer test as 126 mL.

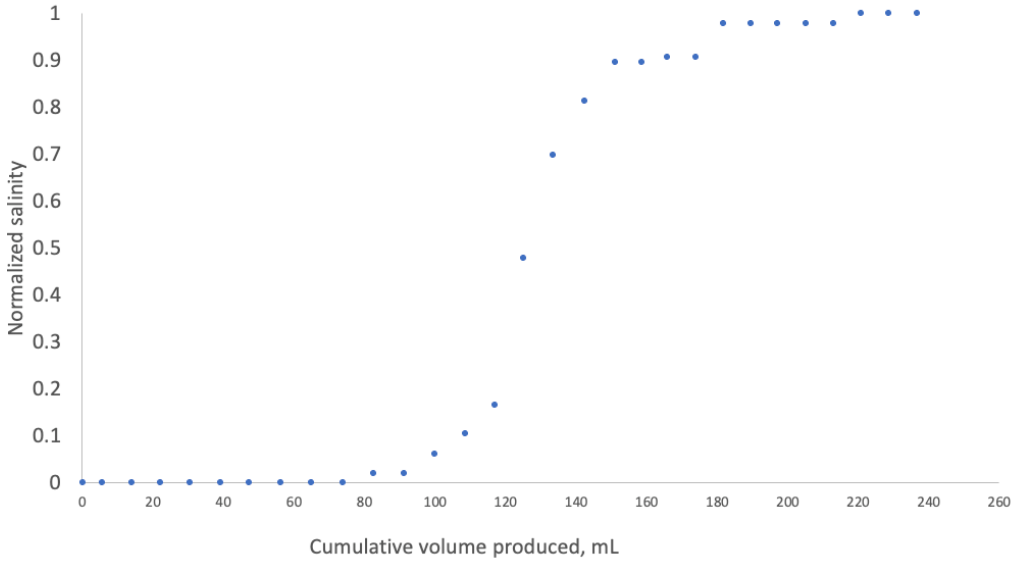


Figure 4.65: Salinity tracer test for oil wet Bentheimer core in experiment #5.

The core was continuously pumped with this iron reduction solution at 1ml/min (10.4ft/day) in order to reduce the amorphous oxidized iron in the core. The iron reducing fluid was injected at varying rates (1, 5, 10, 15, 20 ml/min) to determine permeability. The pressure readings during the brine injected in shown in Figure 4.66 and used to calculate brine permeability, which was estimated to be 1003 mD using Darcy's Law.

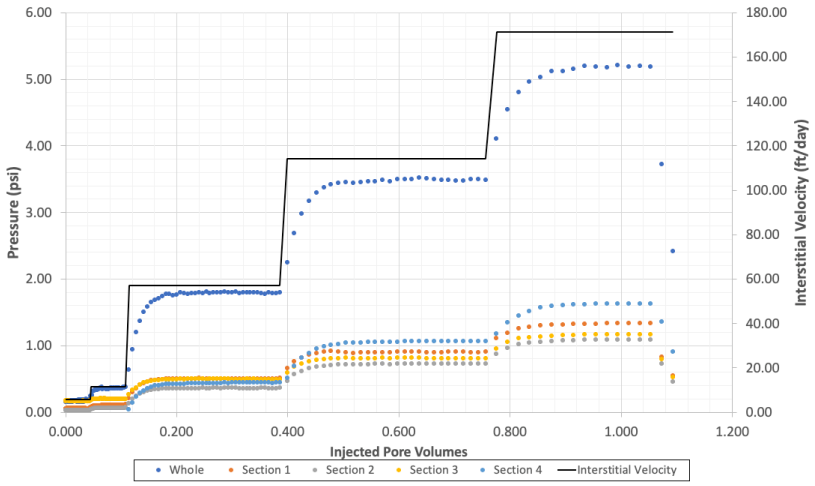


Figure 4.66: Pressure drop during brine injection experiment #5.

### 4.6.2 Oil Flood

Diluted dead crude oil (13% toluene) was filtered through 1.2 μm filter paper under 20 psi of air at 23°C. The diluted oil was found to have a viscosity of 5 cP. In order to saturate the core with 100% oil, the core was emptied of brine, completely dried in a 100°C oven overnight before being vacuum evacuated for at 5 hours. The core was then hooked up to a $CO_2$ tank, as well as the vacuum. The core was cycled between the vacuum and the $CO_2$ tank in order to get rid of as much oxygen as possible.

A stainless steel accumulator with a stainless steel piston was filled with the diluted low viscosity dead crude oil that had been filtered. The accumulator was attached to the core, and the pump was set at a constant pressure of 40psi. The starting pump value was noted in order to

calculate the total volume of oil injected. With the outlet closed, the oil was injected into the core at constant pressure of 40psi. Once the pressure stabilized, the pump was then set at a constant flow rate of 5 ml/min, and the outlet was opened. When oil began to be produced in the outlet, the ending pump value was recorded and this was subtracted from the starting pump value to obtain the total amount of oil injected. 126 mLs of oil was injected into the core to bring its starting oil saturation as close to 100% as possible.

### 4.6.3 Waterflood

An aqueous solution of 1000 ppm NaCl + 400 ppm $NaHCO_3$ + 400 ppm $Na_2S_2O_4$ was injected at constant flow rate of 0.09ml/min, (1 ft/day), 0.18 ml/min (2 ft/day), and then 0.45 ml/min (5 ft/day). This increase in flow rate was to maintain that the oil saturation after waterflood was truly residual oil saturation. This brine was injected until steady state pressure was reached and the oil cut was zero. Pressure values are shows in Figure 4.68 and the oil saturation and oil cut after the waterflood are shown in Figure 4.67.

Oil saturation after waterflood was calculated to be 49.9%, more than double the starting oil saturation after waterflood in experiment #3. The pressure gradient at steady state was recorded to be 0.27 psi/ft (1 ft/day), 0.5 psi/ft (2 ft/day), and 1.1 psi/ft (5 ft/day) (Figure 4.68).

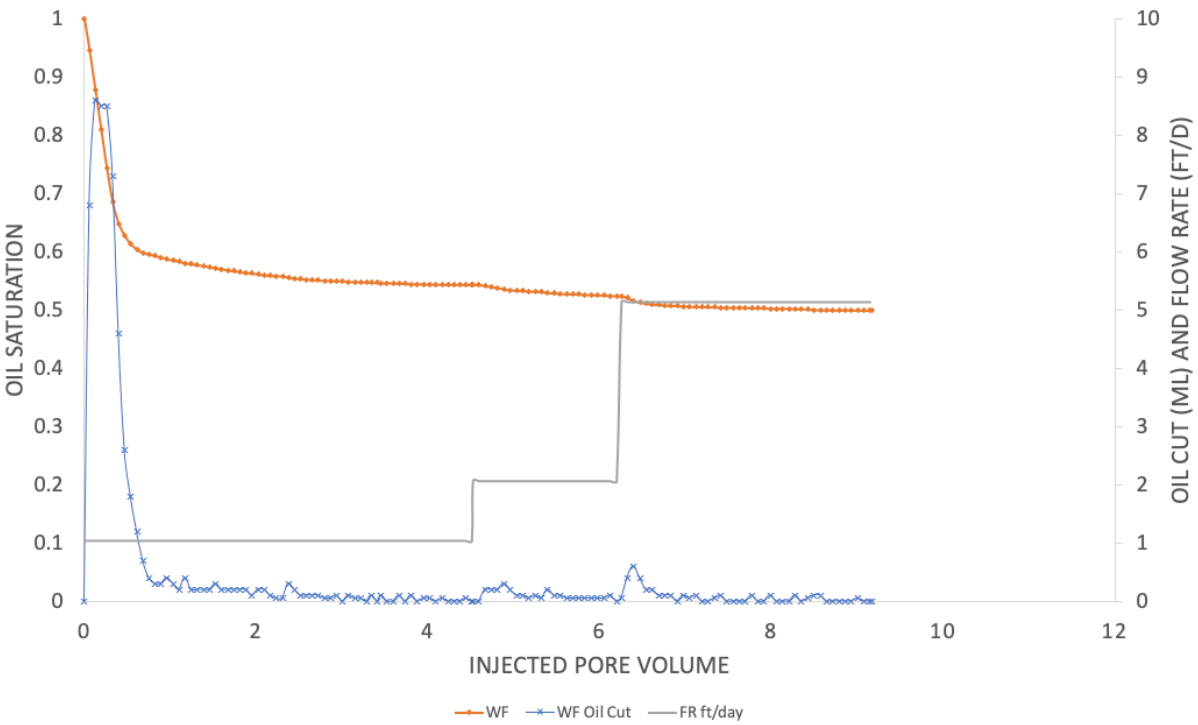


Figure 4.67: Oil saturation after waterflood in experiment #5.

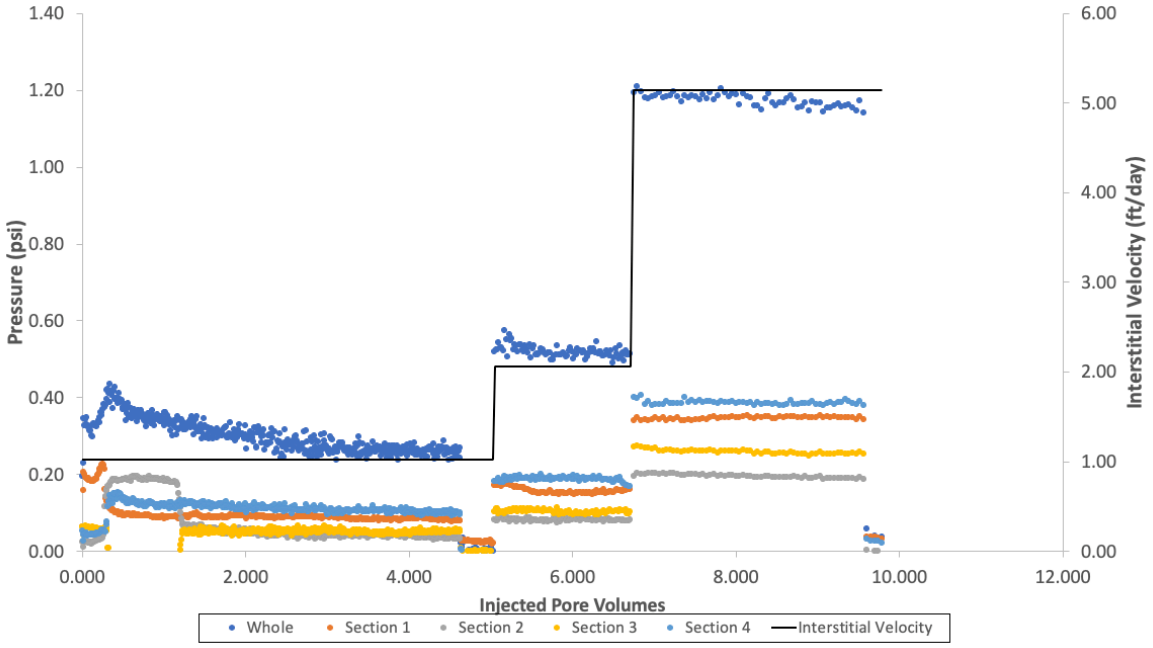


Figure 4.68: Waterflood pressure values in experiment #5.

Similar to experiment #4, the waterflood in this experiment, a large amount of brine was injected during the waterflood (10PV) because there was still small fractions of oil being produced even later in the flood. At the beginning of the waterflood, the oil fractions were almost 100%, although that reduced quickly within 1PV. However, the core consistently continued to produce almost 1mL in the fractions following the initial oil bank, which is why more brine was continued to be injected. Like in experiment #4, a bump in the waterflood rate was chosen after no oil was produced for almost 1 PV. As seen in Figure 4.67, even after the bump in injection rate to 5 ft/day, there was a period in which additional oil was being produced. Again, similar to the previous experiment, the waterflood was considered completed after all many pore volumes of brine was injected and increasingly smaller fractions of oil were being produced.

### 4.6.4 Polymer Floods for Experiment #5

The polymers used in this experiment are the same formulation as experiment #1 and experiment #4. A high molecular weight polymer (FP3630s) was prepared in the same low salinity brine as the waterflood (1000 ppm NaCl + 400 ppm $NaHCO_3$). This solution produced a polymer with a high relaxation time (1.2-1.4 sec) and referred to as the "elastic polymer flood". After hydrating for 24 hours, the solution was filtered under 15 psi of argon gas at 23$^{o}$C through a 1.2 μm filter paper. The same high molecular weight polymer (FP3630s) was prepared in high salinity brine (2200 ppm FP3630s HPAM polymer in 20,000 ppm NaCl + 400 ppm $NaHCO_3$) in a similar manner. This solution produced a polymer with a very low relaxation time (0.02-0.04 sec) and referred to as the "inelastic polymer flood." Multiple batches of these polymer solutions were made as the floods were planned to be alternated until steady state was reached. Polymer solutions 1, and 3 in Figure 4.69 were elastic and polymer 2 was an inelastic solution. The

dynamic frequency sweep test (DFST) was performed as previously discussed in Chapter 3 to determine relaxation times. The steady rate sweet test (SRST) was also performed as previously discussed in Chapter 3 to obtain the viscosity profiles of each polymer solution. The power-law viscosity region was used to fit an equation to create the power law model to obtain the constants for the solution.

The polymer solutions were compared to make sure that their viscosity at different shear rates were similar to avoid unstable displacement (Figure 4.69). It can be noted that the high salinity, inelastic polymer had slightly lower viscosities at lower shear rates, but were nearly identical at a shear rate of $20s^{-1}$, the rate at which the core floods were completed at. Each batch was tested on the rheometer for quality control.

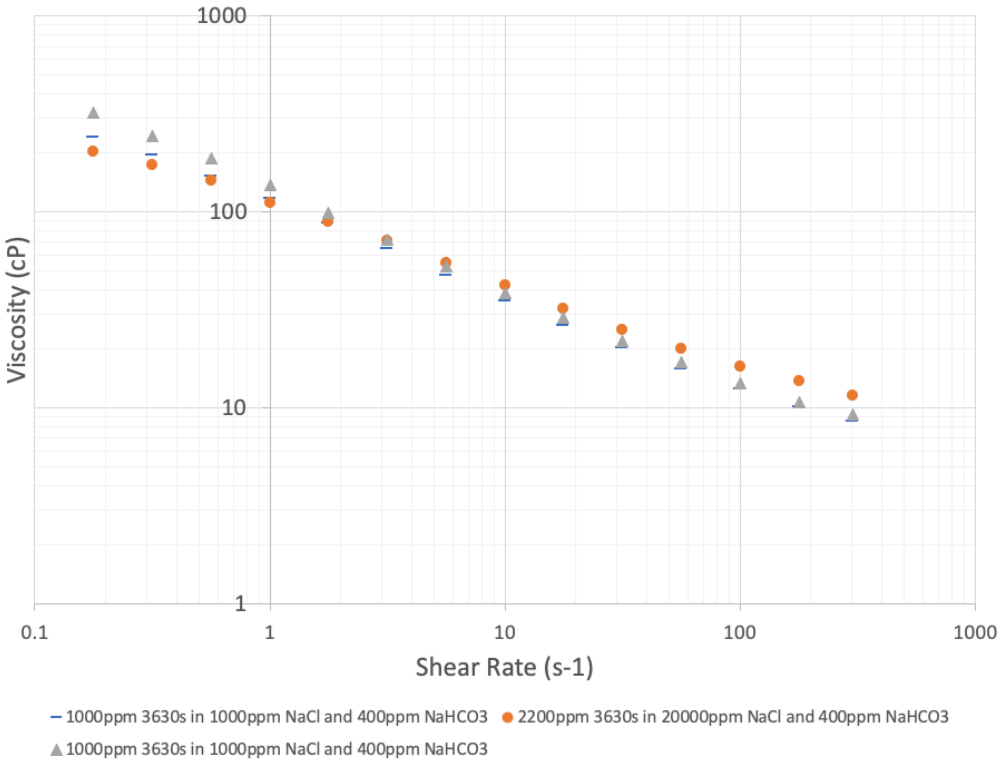


Figure 4.69: Polymer viscosities for experiment #5.

#### 4.6.4.1 Polymer Flood #1 (Viscoelastic)

The low-salinity, elastic, polymer was injected at a constant flow rate of 0.09 ml/min (1 ft/day) until steady state was reached and zero oil cut. Polymer flood was considered completed at zero oil cut, which was reached after almost 4 pore volumes. Pressure values are shows in Figure 4.70 and the oil saturation and oil cut up to the elastic polymer flood are shown in Figure 4.71. The pressure gradient at steady state was 14.78 psi/ft. The equivalent shear rate at steady state was 53.63 $sec^{-1}$. Residual oil saturation was decreased from 49.9% to 45%, and the corresponding Deborah number was 64.36. The change in residual oil saturation decreased 4.9% from the elastic polymer flood.

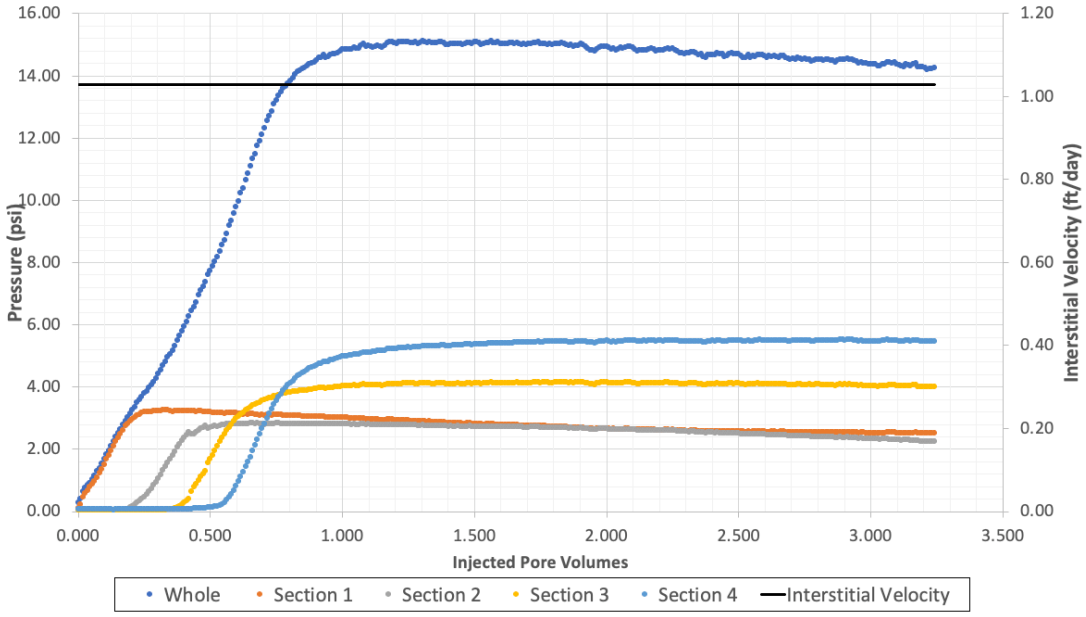


Figure 4.70: Pressure data during first polymer flood (viscoelastic) in experiment #5.

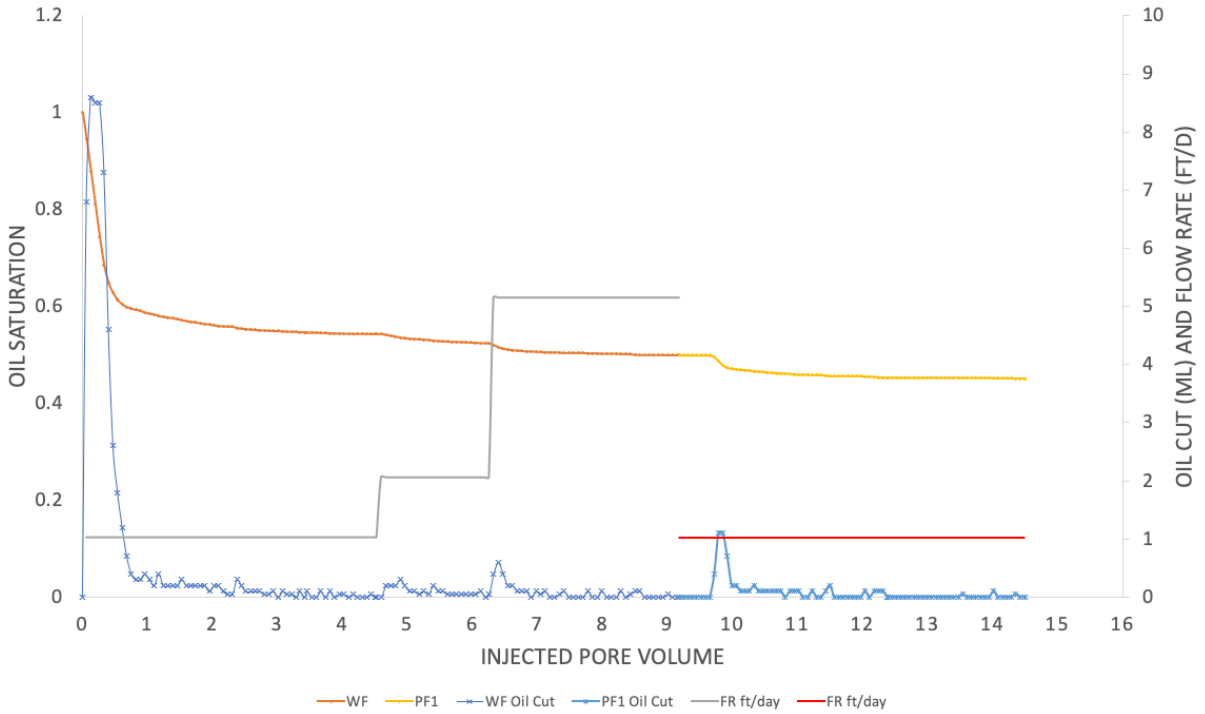


Figure 4.71: Oil saturation after the first polymer flood (viscoelastic) in experiment #5.

The cumulative oil recovery at the end of the polymer flood was 55% of the original oil in place. The maximum capillary number for the elastic polymer flood was 2.01 X $10^{-5}$, which was below the critical capillary number (1 X $10^{-4}$ ). Similar to the waterflood, the polymer flood was considered completed after significantly smaller fractions of oil were produced after multiple pore volumes of polymer were injected. As seen in Figure 4.71, the oil cut near the beginning of the polymer flood was a little over 10% of the effluent samples, which tapered off significantly after two pore volumes.

#### 4.6.4.2 Polymer Flood #2 (Inelastic)

The high-salinity, elastic, polymer was injected at a constant flow rate of 0.09 ml/min (1 ft/day) until steady state was reached and zero oil cut. Polymer flood was considered completed at zero oil cut, which was reached after almost 5 pore volumes. Pressure values are shows in Figure 4.72 and the oil saturation and oil cut up to the inelastic polymer flood are shown in

Figure 4.73. The pressure gradient at steady state was 10.5 psi/ft. The equivalent shear rate at steady state was 44.39 $sec^{-1}$. Residual oil saturation was decreased from 45.1% to 41.7%, and the corresponding Deborah number was 1.33. The change in residual oil saturation decreased 3.4% from the elastic polymer flood.

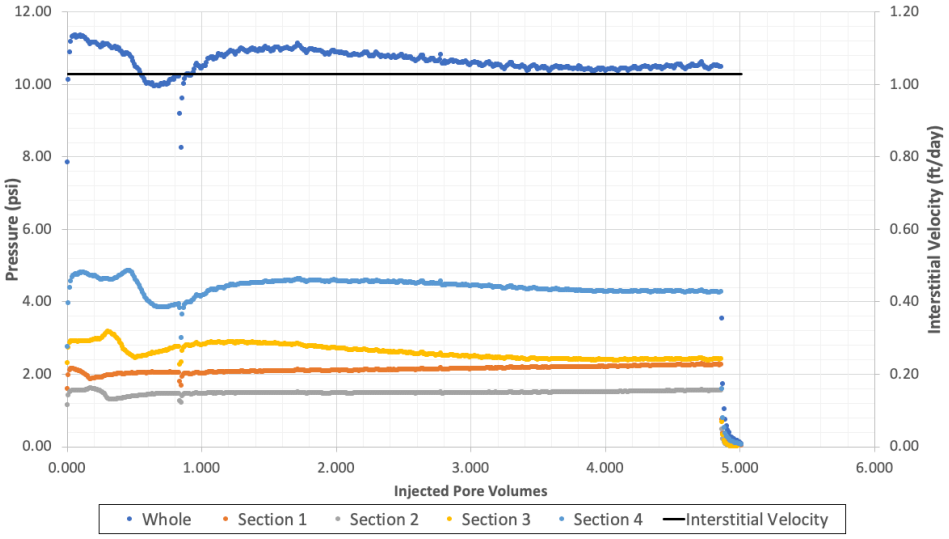


Figure 4.72: Pressure data during second polymer flood (inelastic) in experiment #5.

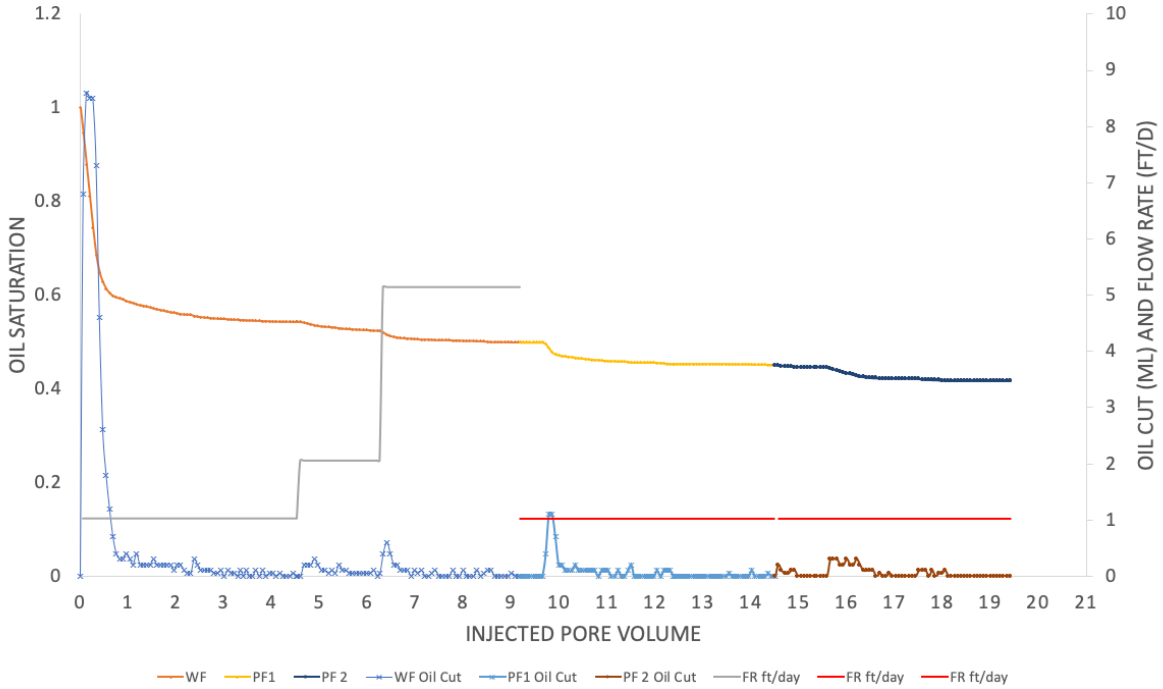


Figure 4.73: Oil saturation up to second polymer flood (inelastic) in experiment #5.

The cumulative oil recovery at the end of the polymer flood was 58.3% of the original oil in place. The maximum capillary number for the elastic polymer flood was 1.41 X $10^{-5}$, which was below the critical capillary number (1 X $10^{-4}$). Similar to the previous flood, the polymer flood was considered completed after significantly smaller fractions of oil were produced after multiple pore volumes of polymer were injected. As seen in Figure 4.73, the oil cuts tapered off after about 3.5 PV of polymer injected.

#### 4.6.4.3 Polymer Flood #3 (Viscoelastic)

The low-salinity, elastic, polymer was injected at a constant flow rate of 0.09 ml/min (1 ft/day) and 0.18 ml/min (2 ft/day). The flow rate was increased to see if the increase of rate (and subsequently pressure gradient) could increase the amount of oil produced. Pressure values are shows in Figure 4.74 and the oil saturation and oil cut up after all polymer floods are shown in Figure 4.75. At 1 ft/day, polymer flood reached a zero oil cut after 2.5 PV of polymer was injected. At 2 ft/day, the polymer flood began to produce more oil after an increase of pressure, and flow rate, but the oil production slowed down after 1.5 PV, as seen in Figure 4.75.

At 1ft/day, the pressure gradient at steady state was 15.5 psi/ft. The equivalent shear rate at steady state was 53.63 $sec^{-1}$. Residual oil saturation was decreased from 41.7% to 40.3%, and the corresponding Deborah number was 55.09. The change in residual oil saturation decreased 1.4% from the elastic polymer flood. At 2 ft/day, the pressure gradient at steady state was 27.9 psi/ft. The equivalent shear rate at steady state was 112.02 $sec^{-1}$. Residual oil saturation was decreased from 40.3% to 39.3%, and the corresponding Deborah number is 166.91. The change in residual oil saturation decreased an additional 1%. The total decrease in oil saturation after the third and final polymer flood was 2.4%.

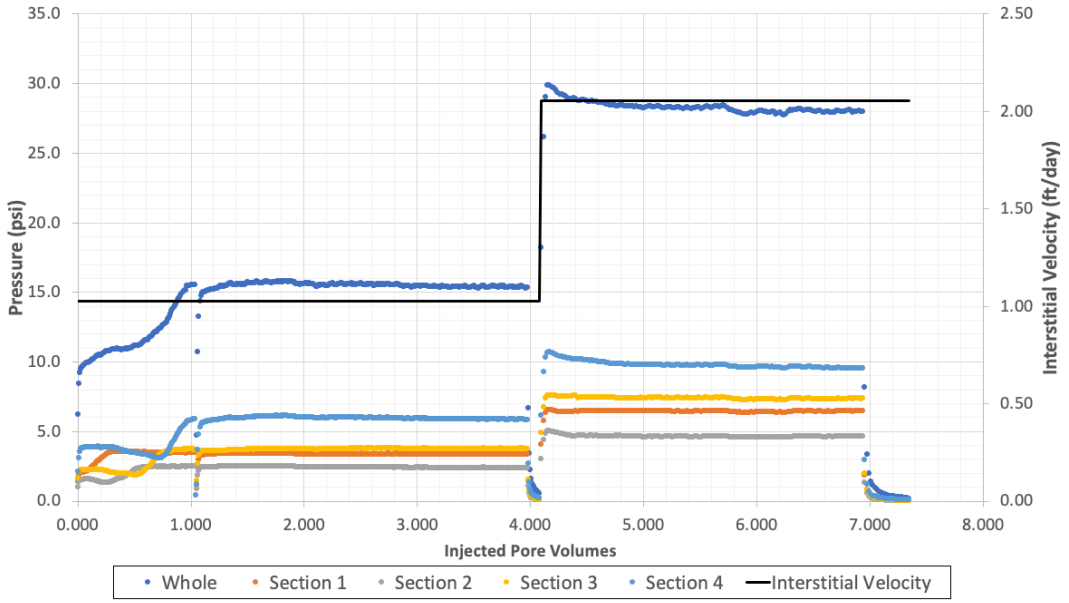


Figure 4.74: Pressure data of the third and final polymer flood in experiment #5. The polymer was injected at 1 ft/day and then increased to 2 ft/day.

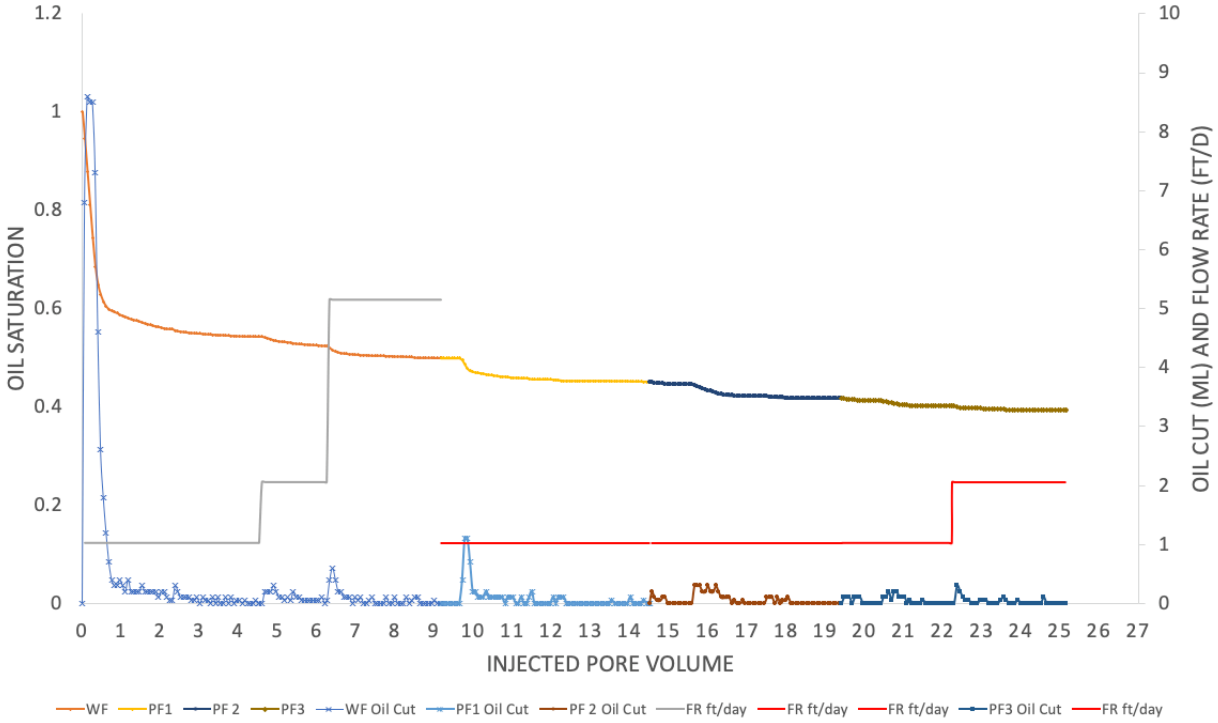


Figure 4.75: Oil saturation during the polymer floods in experiment #5.

The polymer floods were stopped after the third polymer flood. While more oil might have been produced, the amount of polymer needed to inject for the amount of oil produced is

not efficient. The final oil saturation of this experiment ended up being 39.3%. Each polymer injected reduced the residual oil saturation about 1-3%. The significant increase in pressure in the last elastic polymer flood did not significantly produce more oil, suggesting that perhaps a higher pressure gradient isn't necessarily the mechanism behind the viscoelastic effect of the polymer. The recovery of oil might not be attributed to capillary effects. Again, the pressure gradients, while higher than those in the Boise sandstone experiments, remained relatively stable throughout the injections of polymers. All polymer floods remained below the critical capillary number.

## 4.7 ANALYSIS OF THE EXPERIMENTS

A summary of the results of the five experiments are shown in Table 4.6. All experiments were completed using light (4-6cP) oil and no glycerin was injected because of the favorable mobility ratio to the waterflood. Brine was injected until the core was believed to be at residual oil saturation prior to the polymer floods.

Table 4.6: Summary of all six coreflood experiments completed in Chapter 4.

| **Experiments completed with light oils** | | | | | |
|---|---|---|---|---|---|
| **Core Experiment #** | **1** | **2** | **4** | **3** | **5** |
| Notes | | | Oil Wet | Repeat of Core #1 | 100% saturation |
| Rock Type | Boise | Boise | Bentheimer OW | Boise | Bentheimer OW |
| Diam (in) | 1.97 | 1.875 | 2 | 1.875 | 2 |
| Area (cm^2) | 19.665 | 17.814 | 20.268 | 17.814 | 20.268 |
| Length (in) | 11.3 | 11.9 | 12.0 | 11.9 | 12.0 |
| $\phi$ | 0.31 | 0.316 | 0.231 | 0.326 | 0.204 |
| k (mD) | 4400 | 3962 | 1322.7 | 3941 | 1003 |
| k($cm^2$) | 4.343E-08 | 3.910E-08 | 1.306E-08 | 3.890E-08 | 9.900E-09 |
| C | 4 | 4 | 4 | 4 | 4 |

Table 4.6: continued from previous page.

| Oil Flood | | | | | |
|---|---|---|---|---|---|
| Type | Light LDN diluted with 13% toluene | Light LDN diluted with 13% toluene | Light LDN diluted with 13% toluene | Light LDN diluted with 13% toluene | Light LDN diluted with 13% toluene |
| μoil (cP) | 4.5 | 6 | 4.5 | 5 | 5 |
| Injection Pressure (psi) | 30 | 28.1 | 30 | 40 | 40 |
| Soi | 0.657 | 0.654 | 0.7419 | 0.646 | 1 |
| Swr | 0.343 | 0.346 | 0.258 | 0.354 | 0.000 |
| $kro^o$ | 0.328 | 1.08 | 0.37 | 0.88 | |
| | | | | | |
| Waterflood | | | | | |
| Note | Low salinity waterflood | Low salinity waterflood | Low salinity waterflood | Low salinity waterflood | Low salinity waterflood |
| Solution | 1000 ppm NaCl 400 ppm NaHCO3 400 ppm NaS2O4 | 1000 ppm NaCl 400 ppm NaHCO3 400 ppm NaS2O5 | 1000 ppm NaCl 400 ppm NaHCO3 400 ppm NaS2O5 | 1000 ppm NaCl 400 ppm NaHCO3 400 ppm NaS2O5 | 1000 ppm NaCl 400 ppm NaHCO3 400 ppm NaS2O5 |
| μbrine(cP) | 0.95 | 0.95 | 0.95 | 0.95 | 0.95 |
| q* (ml/min) | 0.1 | 0.11 | 0.2 | 0.6 | 0.45 |
| v* (ft/d) | 0.96 | 0.883 | 2 | 5 | 5 |
| u (cm/s) | 8.48E-05 | 1.03E-04 | 1.64E-04 | 5.61E-04 | 3.70E-04 |
| Injected PV | 2.8 | 7.6 | 26 | 6.5 | 9 |
| Nc | 3.87E-06 | 1.16E-06 | 1.11E-06 | 3.15E-05 | 1.60E-05 |
| Swr* | 0.6592 | 0.787 | 0.86 | 0.7 | 0.5 |
| Remaining So | 0.3408 | 0.213 | 0.14 | 0.3 | 0.5 |
| $krw^o$ | 0.016 | 0.244 | 0.085 | 0.09 | 0.133 |
| | | | | | |
| □P (psi/ft) | 0.66 | 0.22 | 0.63 | 0.6 | 1.2 |
| | | | | | |

Table 4.6: continued from previous page.

| Secondary Flood | | | | | |
|---|---|---|---|---|---|
| Note | Low Salinity Polymer Flood | Low Salinity Polymer Flood | Low Salinity Polymer Flood | Low Salinity Polymer Flood | Low Salinity Polymer Flood |
| Solution | 1000 ppm HPAM 3630s 1000 ppm NaCl 400 ppm NaHCO3 | 825ppm FP6040 1000 ppm NaCl 400 ppm NaHCO3 | 1000 ppm HPAM 3630s 1000 ppm NaCl 400 ppm NaHCO3 | 1000 ppm HPAM 3630s 1000 ppm NaCl 400 ppm NaHCO3 | 1000 ppm HPAM 3630s 1000 ppm NaCl 400 ppm NaHCO3 |
| Power law Model Injected | K= 144.69 n=0.477 | K= 132.23 n=0.471 | K= 144.69 n=0.477 | K= 118.59 n=0.493 | K=113.58 n=0.509 |
| τ (s) Injected | 1.9 | 3 | 1.2 | 1.1 | 1.2 |
| q* (ml/min) | 0.12 | 0.06 | 0.1 | 0.12 | 0.09 |
| v* (ft/d) | 0.96 | 0.5 | 1 | 1 | 1 |
| u (cm/s) | 1.02E-04 | 5.61E-05 | 8.22E-05 | 1.12E-04 | 7.40E-05 |
| Remaining So | 0.2433 | 0.198 | 0.1 | 0.26 | 0.45 |
| k_r1$^o$ | 0.045 | 0.108 | 0.047 | 0.052 | 0.036 |
| Nc max | 3.96E-05 | 1.32E-05 | 2.47E-05 | 2.94E-05 | 2.01E-05 |
| □P (psi/ft) | 6.75 | 2.5 | 14 | 5.6 | 15 |
| NDe | 39.61 | 20.68 | 40.16 | 22.55 | 64.36 |
| μapp (cP) | 29.55 | 47.63 | 23.07 | 25.64 | 26.08 |
| C | 4 | 4 | 4 | 4 | 4 |
| ϒeq (s-1) | 20.85 | 6.89 | 33.46 | 20.5 | 53.63 |
| | | | | | |
| Third Flood | | | | | |
| Notes | High Salinity Polymer Flood | Low Salinity Polymer Flood - same salinity as previous flood | High Salinity Polymer Flood | Low Salinity Polymer Flood | Low Salinity Polymer Flood |

Table 4.6: continued from previous page.

| Solution | 2200 ppm HPAM 3630s 20000 ppm NaCl 400 ppm NaHCO3 | 1500 ppm HPAM 3330s 1000 ppm NaCl 400 ppm NaHCO3 | 2200 ppm HPAM 3630s 20000 ppm NaCl 400 ppm NaHCO3 | 900 ppm Scleroglucan 1000 ppm NaCl 400 ppm NaHCO3 | 2200 ppm HPAM 3630s 20000 ppm NaCl 400 ppm NaHCO3 |
|---|---|---|---|---|---|
| Power law Model Injected | K= 107.22 n=0.576 | K= 108.95 n=0.607 | K= 103.67 n=0.574 | K= 103.67 n=0.574 | K=108.18 n=0.49 |
| τ (s) Injected | 0.056 | 0.01918 | 0.02 | 0.07 | 0.03 |
| q* (ml/min) | 0.12 | 0.06 | 0.1 | 0.1 | 0.09 |
| v* (ft/d) | 0.96 | 0.5 | 1 | 1 | 1 |
| u (cm/s) | 1.02E-04 | 5.61E-05 | 8.22E-05 | 9.36E-05 | 7.40E-05 |
| Remaining So | 0.149 | 0.198 | 0.1 | 0.26 | 0.42 |
| k_r2$^{o}$ | 0.1 | 0.12 | 0.06 | 0.06 | 0.05 |
| Nc max | 2.05E-05 | 1.32E-05 | 2.47E-05 | 1.95E-06 | 1.14E-04 |
| □P (psi) | 3.5 | 2.5 | 14 | 3.7 | 10.5 |
| NDe | 0.73 | 0.12 | 0.64 | 1.34 | 1.33 |
| μapp (cP) | 36.05 | 52.32 | 23.63 | 21 | 15.63 |
| C | 4 | 4 | 4 | 4 | 4 |
| ϒeq (s-1) | 13.08 | 6.46 | 32.17 | 19.09 | 44.39 |
| | | | | | |
| Fourth Flood | | | | | |
| Notes | Low Salinity Polymer Flood | Low Salinity Polymer Flood - same salinity as previous flood | Low Salinity Polymer Flood | Low Salinity Polymer Flood | Low Salinity Polymer Flood |
| Solution | 1000 ppm HPAM 3630s 1000 ppm NaCl 400 ppm NaHCO3 | 825ppm FP6040 1000 ppm NaCl 400 ppm NaHCO3 | 1000 ppm HPAM 3630s 1000 ppm NaCl 400 ppm NaHCO3 | 1000 ppm HPAM 3630s 1000 ppm NaCl 400 ppm NaHCO3 | 1000 ppm HPAM 3630s 1000 ppm NaCl 400 ppm NaHCO3 |

Table 4.6: continued from previous page.

| | | | | | |
|---|---|---|---|---|---|
| Power law Model Injected | K= 140.97 n=0.484 | K= 129.79 n=0.471 | K= 124.47 n=0.57 | K= 113.58 n=0.509 | K=130.33 n=0.492 |
| τ (s) Injected | 1.44 | 1.9 | 1.2 | 1.02 | 1.49 |
| q* (ml/min) | 0.12 | 0.18 | 0.08 | 0.12 | 0.18 |
| v* (ft/d) | 0.96 | 1.5 | 1 | 1 | 2 |
| u (cm/s) | 1.02E-04 | 1.68E-04 | 6.58E-05 | 1.12E-04 | 1.48E-04 |
| Remaining So | 0.1 | 0.19627 | 0.1 | 0.25 | 0.393 |
| k_rp1$^{o}$ | 0.04 | 0.09 | 0.03 | 0.07 | 0.03 |
| | | | | | |
| Nc max | 4.23E-05 | 2.54E-05 | 39.93 | 2.37E-05 | 3.73E-05 |
| □P (psi) | 7.2 | 4.8 | 22 | 4.5 | 27.9 |
| NDe | 29.18 | 43.04 | 39.95 | 17.88 | 166.91 |
| μapp (cP) | 29.84 | 24.91 | 27.57 | 27.84 | 11.86 |
| C | 4 | 4 | 4 | 4 | 4 |
| ϒeq (s-1) | 20.26 | 22.65 | 33.29 | 27.52 | 112.02 |
| | | | | | |
| Fifth Flood | | | | | |
| Notes | High Salinity Polymer Flood | Low Salinity Polymer Flood - same salinity as previous flood after pause | High Salinity Polymer Flood | High Salinity Polymer Flood | |
| Solution | 2200 ppm HPAM 3630s 20000 ppm NaCl 400 ppm NaHCO3 | 825ppm FP6040 1000 ppm NaCl 400 ppm NaHCO3 | 2200 ppm HPAM 3630s 20000 ppm NaCl 400 ppm NaHCO3 | 2200 ppm HPAM 3630s 20000 ppm NaCl 400 ppm NaHCO3 | |
| Power law Model Injected | K= 90.74 n=0.593 | K= 129.76 n=0.471 | K= 114.37 n=0.572 | K=108.10 n=0.525 | |
| τ (s) Injected | 0.02 | 2 | 0.05 | 0.048 | |
| q* (ml/min) | 0.12 | 0.12 | 0.1 | 0.12 | |
| v* (ft/d) | 0.96 | 0.96 | 1 | 1 | |

Table 4.6: continued from previous page.

| | | | | | |
|---|---|---|---|---|---|
| u (cm/s) | 1.02E-04 | 1.12E-04 | 8.22E-05 | 1.12E-04 | |
| Remaining So | 0.055 | 0.19627 | 0.09918 | 0.25 | |
| k_rp1$^o$ | 0.08 | 0.09 | 0.05 | 0.1 | |
| Nc max | 2.35E-05 | 2.38E-05 | 2.47E-05 | 1.84E-05 | |
| □P (psi/ft) | 4 | 4.5 | 14 | 3.5 | |
| NDe | 0.28 | 45.25 | 1.65 | 0.7 | |
| μapp (cP) | 31.13 | 24.92 | 25.89 | 30.23 | |
| C | 4 | 4 | 4 | 4 | |
| ϒeq (s-1) | 13.86 | 22.63 | 32.16 | 14.64 | |
| | | | | | |
| Sixth Flood | | | | | |
| Notes | Low Salinity Polymer Flood | Low Salinity Polymer Flood - same polymer as previous exp. | Low Salinity Polymer Flood | Low Salinity Polymer Flood | |
| Solution | 1000 ppm HPAM 3630s 1000 ppm NaCl 400 ppm NaHCO3 | 1500 ppm FP3330s 1000 ppm NaCl 400 ppm NaHCO3 | 1000 ppm HPAM 3630s 1000 ppm NaCl 400 ppm NaHCO3 | 1000 ppm HPAM 3630s 1000 ppm NaCl 400 ppm NaHCO3 | |
| Power law Model Injected | K= 123.35 n=0.499 | K= 106.06 n=0.62 | K= 114.25 n=0.507 | K= 130.33 n=0.492 | |
| τ (s) Injected | 1.09 | 0.023 | 1.285 | 1.49 | |
| q* (ml/min) | 0.12 | 0.24 | 0.1 | 0.24 | |
| v* (ft/d) | 0.96 | 2 | 1 | 2 | |
| u (cm/s) | 1.02E-04 | 2.25E-04 | 8.22E-05 | 2.25E-04 | |
| Remaining So | 0.053 | 0.19216 | 0.09743 | 0.25 | |
| k_rp1$^o$ | 0.03 | 0.14 | 0.04 | 0.04 | |
| | | | | | |
| Nc max | 5.75E-05 | 2.75E-05 | 2.47E-05 | 4.36E-05 | |
| □P (psi/ft) | 9.8 | 5.2 | 14 | 8.3 | |
| NDe | 24.83 | 0.57 | 41.51 | 56.5 | |

Table 4.6: continued from previous page.

| | | | | | |
|---|---|---|---|---|---|
| μapp (cP) | 25.76 | 31.79 | 20.6 | 20.56 | |
| C | 4 | 4 | 4 | 4 | |
| Ɣeq (s-1) | 22.78 | 23.83 | 32.31 | 37.92 | |
| Sixth Flood | | | | | |
| Notes | | Low Salinity Polymer Flood - same as previous experiment | High Salinity Polymer Flood | | |
| Solution | | 1000 ppm HPAM 3630s 1000 ppm NaCl 400 ppm NaHCO3 | 2200 ppm HPAM 3630s 20000 ppm NaCl 400 ppm NaHCO3 | | |
| Power law Model Injected | | K= 130 n=0.488 | K= 114.37 n=0.572 | | |
| τ (s) Injected | | 1.2 | 0.0511 | | |
| q* (ml/min) | | 0.12 | 0.1 | | |
| v* (ft/d) | | 2 | 1 | | |
| u (cm/s) | | 1.12E-04 | 8.22E-05 | | |
| Remaining So | | 0.192 | 0.09743 | | |
| k_rp1$^{o}$ | | 0.12 | 0.05 | | |
| Nc max | | 2.43E-05 | 2.47E-05 | | |
| □P (psi/ft) | | 4.6 | 14 | | |
| NDe | | 31.22 | 1.64 | | |
| μapp (cP) | | 24.51 | 25.9 | | |
| C | | 4 | 4 | | |
| Ɣeq (s-1) | | 26.01 | 32.13 | | |
| | | | | | |
| Sixth Flood | | | | | |

Table 4.6: continued from previous page.

| | | | | | |
|---|---|---|---|---|---|
| Notes | | High Salinity Polymer Flood - inelastic | | | |
| Solution | | 2200 ppm FP3630s 20000 ppm NaCl 400 ppm NaHCO3 | | | |
| Power law Model Injected | | K= 103.67 n=0.574 | | | |
| τ (s) Injected | | 0.02 | | | |
| q* (ml/min) | | 0.18 | | | |
| v* (ft/d) | | 1.5 | | | |
| u (cm/s) | | 1.00E-03 | | | |
| Remaining So | | 0.192 | | | |
| k_rp1º | | 0.15 | | | |
| Nc max | | 1.85E-05 | | | |
| □P (psi/ft) | | 3.5 | | | |
| NDe | | 0.35 | | | |
| μapp (cP) | | 30.76 | | | |
| C | | 4 | | | |
| ϒeq (s-1) | | 17.32 | | | |
| | | | | | |

The main objective of this work is to determine different factors that influence the effect of viscoelastic polymers on residual oil saturations. Most elastic polymer floods had high Deborah numbers that corresponded with the floods. The majority of these results are consistent with similar studies (Ehrenfried, 2013; Qi, 2017) that viscoelastic polymers are capable of reducing residual oil saturation beyond inelastic fluids, such as brine or glycerin. The average residual oil saturation after waterflood is 0.298. The average residual oil saturation after the first

elastic polymer flood injection is 0.250, about a 4.77% decrease in residual oil saturation from the polymer flood. The average residual oil saturation after a second inelastic polymer flood was 0.2254, or about a 2.5% decrease in oil saturation. The average Deborah number of the elastic floods were 37.5 compared to the average Deborah number of inelastic floods, which was 0.83. All max capillary numbers were below the critical capillary number of Boise sandstones, and Bentheimer sandstones.

Oil breakthrough for the polymer floods were noted to require at least 1PV to see any recovery of oil. The elastic polymer floods had generally a higher maximum oil cut (1 mL versus 0.3-0.5 mL).

Experiment #1 replicated similar work done previously using viscoelastic polymers and alternating between elastic polymer floods and inelastic floods. Results in the first experiment showed extremely promising results in a heterogeneous Boise sandstone. After alternating between elastic and inelastic polymer floods, it decreased oil saturation to an low 6%. This was exciting because we were able to repeat the similar method of reducing oil saturation from past experiments. In an oil-wet Bentheimer (Experiment #3 and #4), there was also additional recovery after the elastic polymer flood.

These experiments were particularly designed to begin isolating variables that have been suspected to influence reduction in the residual oil saturation: such as high pressure gradients, changes in salinity, higher polymer relaxation times or higher Deborah numbers. These experiments were also completed in different sandstones, as well as different wettability. It was noted that while there was usually some reduction in oil saturation after the initial elastic polymer flood, continuous cycling between the elastic and inelastic polymer floods did not

provide significant returns. It was also observed it was important to allow a core to completely come to steady state before changing polymer floods.

In Qi (2018), an "elastic desaturation curve" (EDC) was established (Figure 2.21). By taking twenty corefloods from various corefloods in literature (Ehrenfried, 2013; Erincik et al., 2017; Qi, 2018), the residual oil saturation before and after a viscoelastic polymer flood were taken and compiled in Table 4.7 $S_{orw,\infty}$ is the residual oil saturation after waterflooding or before viscoelastic polymer flooding, and $S_{orp}$ is the residual oil saturation after viscoelastic polymer flooding.

Table 4.7: Core flood results after viscoelastic polymer flooding (from Qi 2018).

| | # | $N_{De}$ | $S_{orw,\infty}$ | $S_{orp}$ | $S_{orp}/S_{orw,\infty}$ |
|---|---|---|---|---|---|
| Viscous Oil | P1 | 16 | 0.26 | 0.19 | 0.72 |
| | P3 | 18 | 0.30 | 0.21 | 0.71 |
| | P4 | 1 | 0.31 | 0.31 | 1.00 |
| | P4(2) | 14 | 0.31 | 0.21 | 0.67 |
| | P5 | 27 | 0.21 | 0.18 | 0.87 |
| | P6 | 23 | 0.25 | 0.22 | 0.88 |
| | P7 | 17 | 0.29 | 0.28 | 0.96 |
| | RE-MZC | 302 | 0.36 | 0.22 | 0.62 |
| Light oil | G3 | 50 | 0.35 | 0.24 | 0.68 |
| | G4 | 424 | 0.38 | 0.34 | 0.88 |
| | G5 | 13 | 0.25 | 0.23 | 0.90 |
| | G7 | 12 | 0.32 | 0.27 | 0.83 |
| | B1 | 3 | 0.32 | 0.27 | 0.86 |
| Ehrenfried, 2013 | D-ben6 | 13 | 0.21 | 0.15 | 0.71 |
| | D-ben7 | 9 | 0.32 | 0.29 | 0.92 |
| Erincik et al, 2017 | M1 | 152 | 0.45 | 0.29 | 0.64 |
| | M2 | 100 | 0.38 | 0.29 | 0.76 |
| | M3 | 32 | 0.43 | 0.32 | 0.74 |
| | M4 | 254 | 0.44 | 0.34 | 0.77 |
| | M5 | 280 | 0.41 | 0.28 | 0.68 |

A correlation was established from Table 4.7 and is displayed in Figure 4.76.

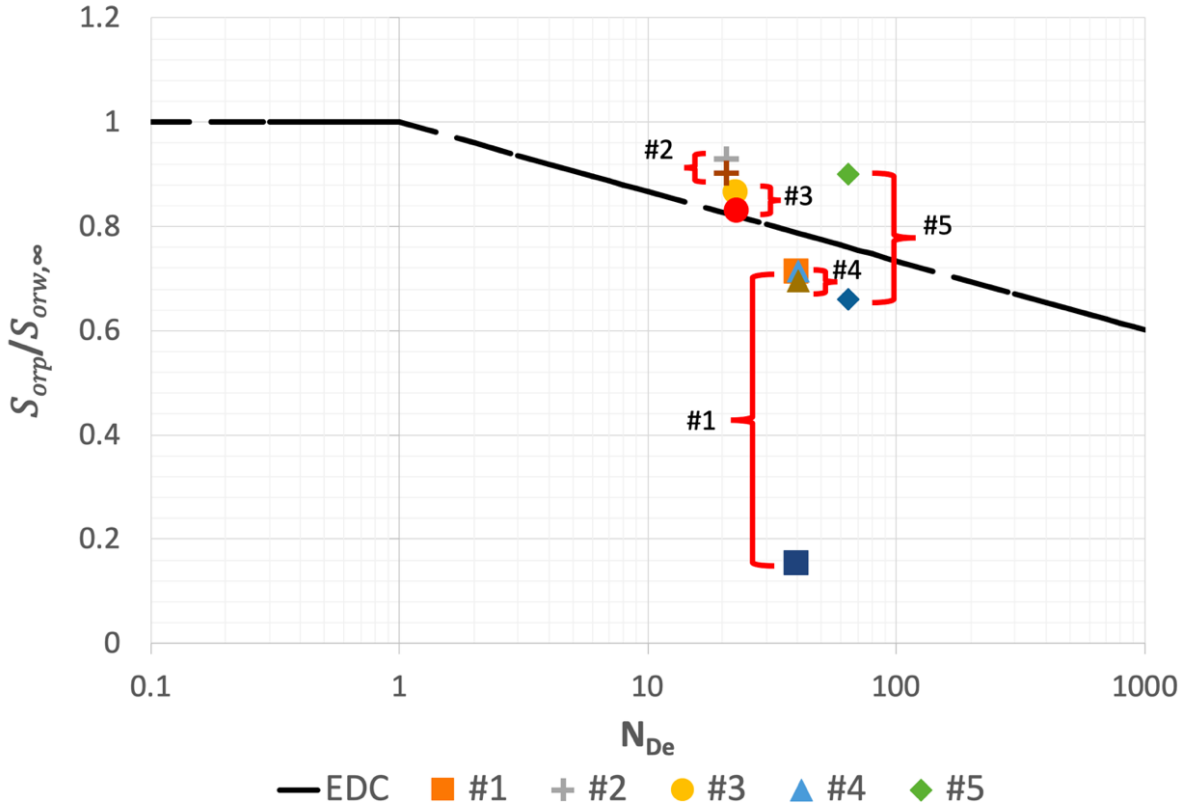


Figure 4.76: Residual oil saturation after polymer floods normalized to waterflood residual oil saturation in experiments #1 - #5. Final oil saturation is plotted below the residual saturation to the first viscoelastic polymer flood.

Applying the EDC correlation of the normalized oil saturation after viscoelastic polymer flooding to the five corefloods in this experiment, it is noted that the results from the experiment are close to the results given in the EDC (Table 4.8). Figure 4.76 shows the EDC from Qi (2018) along with the five points from the last five corefloods. Corefloods #1-3 were the Boise cores and corefloods #4-5 were the oil-wet Bentheimer cores. Each coreflood had their normalized residual oil saturation after viscoelastic polymer flood plotted versus their Deborah number. For comparison, the final saturation after alternating polymer floods normalized to residual saturation after waterflood was also plotted below each coreflood. The values after the initial viscoelastic polymer flood closely follows the elastic desaturation curve.

Table 4.8: Prediction of $S_{orp}$ using EDC and comparison to actual experimental values.

| Core Flood | $N_{De}$ | Ratio | $S_{orw\infty}$ | Predicted $S_{orp}$ | Actual Experimental $S_{orp}$ | Final $S_{orp}$ |
|---|---|---|---|---|---|---|
| #1 (Boise) | 39.61 | 0.7877 | 0.3408 | 0.2684 | 0.2433 | 0.053 |
| #2 (Boise) | 20.68 | 0.8252 | 0.213 | 0.1758 | 0.198 | 0.192 |
| #3 (Boise) | 22.55 | 0.8202 | 0.3 | 0.2461 | 0.26 | 0.25 |
| #4 (Oil Wet Bentheimer) | 40.16 | 0.7869 | 0.14 | 0.1102 | 0.1 | 0.0973 |
| #5 (Oil Wet Bentheimer) | 64.36 | 0.7596 | 0.5 | 0.3798 | 0.45 | 0.33 |

Looking at the actual experimental saturation values, they are mostly within 1-3% of the predicted saturation. The residual oil reduction in these five viscoelastic floods behaved in the same manner as other viscoelastic flood done by other researchers, suggesting a viscoelastic pattern correlating with the EDC given by Qi (2018).

One of the purposes of these experiments were to determine if there was a viscoelastic effect in rock types other than Bentheimer, such as Boise, or if the viscoelastic effect would work in oil-wet media. These experiments used three Boise cores and two oil-wet Bentheimer cores. In experiment #1, using a Boise core, the oil saturation decreased significantly from 65% to 5.3%. The other two floods showed a decrease in final $S_{or}$ to19.8% and 26.4%. While the multiple floods had varying results in final residual oil saturation, the initial viscoelastic polymer flood did reduce the residual oil saturation beyond the waterflood. Multiple injections of alternating viscoelastic and inelastic polymer floods did reduce residual oil saturation, although the efficiency of the floods had diminishing returns after multiple floods. However, these experiments did show that viscoelastic polymer floods can reduce residual oil saturation in different rock types. In addition, two oil-wet cores were used. The effect of viscoelasticity was inconclusive in the first oil-wet experiment, where the decrease in saturation was 4.3%, and it

was unknown if the saturation was residual oil saturation after the brine flood. As the saturation was only 14%, it was hard to see the effect of viscoelastic polymer on the remaining oil. In the second oil-wet core flood, the effect of viscoelastic polymer was more apparent, as the polymer recovered an additional 10.7%. The two corefloods showed that viscoelastic polymer can reduce residual oil saturation in oil-wet mediums, although the oil cuts from the experiment were very low so the amount of injectant was high. The mechanisms behind how the viscoelastic polymer reduces oil saturation in oil-wet cores are not completely clear.

Experiments were also designed to try to determine if the inelastic polymer floods that "chase" or "sweep" additional oil out because of an elasticity difference (change in Deborah number) or salinity change. The initial successful experiment with a Boise core (experiment #1) used the same polymer flood in the inelastic flood, but changed salinities to decrease the relaxation time. Some experiments had secondary polymer floods that did not have a change in salinity gradients. Experiments #2, and #3 used different polymers (lower weight polymers and scleroglucan) to maintain viscosity, but have a decrease in relaxation time without changing the salinity of the floods. There was not a significant change in residual oil saturation after those floods, although it is important to note that the polymers used between the floods were not the same, so it is not definitive if the change in salinity, the change in polymer, or the change in elasticity was the reason for the lack of decrease in saturation.

Another purpose was to test if increasing relaxation time, and subsequently Deborah number would make the viscoelastic polymer more effective. There was only one experiment that used a higher molecular weight polymer (experiment #2). The viscoelastic polymer did decrease the residual oil saturation initially, although the subsequent inelastic polymer flood

using the same salinity, but different polymer type, did not significantly "sweep" out any additional oil. In addition, that experiment was also conducted at lower pressure gradients (<3psi). However, as there was only one experiment completed, it was inconclusive to say if the higher molecular weight polymer was successful at reducing oil saturation. It is more difficult to observe the viscoelastic effects at lower pressure gradients, as the easiest way to achieve lower gradients is to lower injection rates (and subsequently lower Deborah number). While using the higher molecular weight polymer was not as promising as initially expected, there was still a small percentage of oil that was produced at a low pressure gradient, suggesting promise in using polymers with higher relaxation times, even at very low pressure gradients.

# Chapter 5: Conclusions and Future Work

## 5.1 CONCLUSIONS

Five coreflood experiments were completed using aqueous hydrolyzed polyacrylamide (HPAM) and scleroglucan (EOR-grade) polymer solutions. HPAM polymers were solubilized in low salinity brine which created viscoelastic solutions. All experiments were completed in high-permeability (>1000mD) Bentheimer and Boise sandstones. Two Bentheimer cores were chemically treated to be considered oil-wet. Three other water-wet Boise cores were also used. All experiments were completed using light (4-6 cP) oil and no glycerin was injected (as was done by Qi (2017) and Erincik (2018)), because of the favorable mobility ratio to the waterflood.

Four cores were saturated with brine, and then flooded with oil to reach initial oil saturation before being waterflooded. One oil-wet Bentheimer core was 100% saturated with oil first before proceeding with the waterflood. All experiments were completed using a low salinity (1000 ppm NaCl + 400 ppm $NaHCO_3$) brine. The low salinity brine was injected during the waterflood. The residual oil saturation was reached before the polymer was injected. All polymer flooding experiments were carefully designed so that capillary numbers would not exceed the critical capillary number.

The elastic polymer floods were formulated so that they would have high relaxation times, and therefore high Deborah numbers. Each elastic flood was followed by an inelastic polymer flood with a similar viscosity. For experiments #1, #3, and #4, the inelastic flood was conducted with HPAM 3630s in high salinity brine (20,000ppm NaCl + 400ppm $NaHCO_3$). For experiments #2, and #5, the inelastic flood was formulated with a different polymer in low

salinity brine. The polymer was either lower molecular weight (FP3330s), or a biopolymer (scleroglucan). The Deborah number for the inelastic polymer floods were less than or close to 1.

Following the success of Erincik (2017) experiments using alternating elastic and inelastic polymer floods in Bentheimer sandstones, these experiments were completed in different mediums to see if this phenomenon could be replicated under different circumstances. Experiment #1 replicated similar work completed using viscoelastic polymers and alternating elastic and inelastic floods. The results in coreflood #1 showed extremely promising results in the comparatively more heterogeneous Boise sandstone. After alternating between elastic and inelastic polymer floods, the residual oil saturation decreased to lower than 6%.

Further experiments were conducted to see if the saturation also decreases if the pressure gradients were significantly lower. While the pressure gradients in the original experiments were below the critical capillary number, experiment #2 was completed so that the pressure gradients would be below 3 psi/ft. In experiment #2, a high molecular weight polymer was used to create the viscoelastic solution with a higher relaxation time. This was chosen to try to maximize the Deborah number despite having very low pressure gradients. The initial elastic polymer did decrease the residual oil saturation after waterflood, but the subsequent inelastic and elastic floods did not yield significant recovery. It is promising that there was still oil recovery at lower pressure gradients. The effect of the viscoelastic polymer was still evident in the coreflood.

In oil-wet corefloods, the elastic polymer flood also decreased the residual oil saturation after waterflood. It was observed that after large amounts of brine had been injected, small amounts of oil came out of the core for a long time. This behavior was suspected to be due to the distribution of oil on the rock grains. As seen in Figure 2.2, the water prefers to be in the larger

pore spaces, while the oil likes to be in the smaller pore spaces in oil-wet media. As more water is injected, it slowly strips off oil droplets. It was also suspected that the polymer floods subsequent to the waterflood would produce oil in a similar fashion.

The hypothesis behind the additional recovery from the inelastic polymer flood following an elastic flood is that the inelastic flood "sweeps" out the residual oil that is mobilized by the preceding elastic flood. During the viscoelastic flood, some oil droplets are produced, some are remobilized into larger pore spaces, or some are trapped in new pores. It is hypothesized that the viscoelastic polymer has a stronger local turbulence and causes oscillations in the fluid flow. These oscillations can cause the oil droplets to leave the grain surface and transport to different pore spaces. When the inelastic polymer is injected, it can capture these oil droplets that have not been trapped or have been relocated into larger pore spaces. Microfluidic models (Qi, 2018) have shown evidence of an oscillating or turbulent fluid flow behavior, especially in areas of smaller pore space. This oscillation might also explain why some replicated corefloods are more successful than others, if the droplets are randomly transported to more accessible regions that can be accessed by the polymer.

The main conclusions of this work are summarized below:

1. Viscoelastic polymer flood using HPAM polymer (FP3630s) into Boise cores with low viscosity residual oil after water flood significantly decreased residual oil saturation. Polymer floods had relatively low frontal velocities (1 ft/day) and had pressure gradients from 3-9 psi/ft. The three floods showed a decrease in final $S_{or}$ to 5.3% and 19.8% and 26.4%. The results are similar to the results from Qi (2018) and Erincik (2017).

2. The viscoelastic polymer floods following a waterflood decreased residual oil saturation. In four of the five experiments, the residual saturation after viscoelastic polymer floods closely matched the predicted saturation given by the Elastic Desaturation Curve (EDC) developed by Qi (2018). Except for one flood, the actual experimental $S_{orp}$ values were within 1-3% of the predicted $S_{orp}$.
3. Using a higher molecular weight polymer (FP6040) resulted in a higher measured relaxation time (3.4 sec vs 1.2 sec) and in-situ Deborah number. However, this polymer did not result in higher recovery than the less elastic polymer (FP3630s). The higher molecular weight polymer was only used in one experiment, so no definitive conclusions can be made. Additional experiments should be conducted with higher molecular weight and viscoelastic polymers.
4. The effect of viscoelasticity was somewhat inconclusive in the first oil-wet Bentheimer experiment where the decrease in oil saturation was only 4.3% and it was unknown if the saturation was at residual after the brine flood. The oil saturation after brine flood was relatively low (14%) so it was hard to see the effect of viscoelastic polymer on the remaining oil. The residual saturation dropped from 14% to 9.7%. In a second experiment with oil-wet Bentheimer, the effect of viscoelasticity was more apparent and the flood recovered an additional 10.7% oil. The residual saturation dropped from 50% to 39.3%.
5. A high-salinity, inelastic polymer flood (FP3630s) after a low-salinity, viscoelastic polymer flood (also FP3630s) showed a significant additional oil recovery in a Boise core with a final oil saturation of 6%, which was remarkable for a polymer flood.

This result was consistent with similar findings by Qi (2018) and Erincik (2017), which were done in water-wet Bentheimer cores.

6. A low-salinity, inelastic polymer flood (Scleroglucan and FP3330s) after a low-salinity, viscoelastic polymer flood (FP3630s) did not show any additional recovery. The salinity of each flood remained constant. While there was only one experiment that used scleroglucan and one experiment that used FP3330s, these findings contradict the hypothesis that the change in elasticity is what causes significant additional recovery. An alternative hypothesis is that the change in salinity is what causes the additional recovery.
7. Alternating viscoelastic, low-salinity polymer floods (FP3630S) with a high-salinity, low elasticity polymer floods (also FP3630S) had some success but with diminishing returns.

## 5.2 FUTURE WORK

Further future work can be done to isolate the mechanisms between viscoelastic and inelastic floods. While it has been observed in different rock types (Bentheimer and, Boise) and different wettability, the process has not been fully optimized. In addition, even successful corefloods involved injecting many pore volumes of polymer solutions in the entire course of the coreflood, making it not a financially scalable option. Additional coreflood experiments will be useful to understand and optimize the use of viscoelastic polymers in the future.

1. Experiments done in a CT scanner from start to finish can help elucidate the mechanisms and fluid flow during a coreflood. CT imaging can provide visualization

of the changes of residual oil saturation during different floods. This was done once by Qi (2017).

2. Typical field pressure gradients (~ 1 psi/ft) are lower than those measured in our laboratory (3-20 psi/ft). Even though the experiments remain below the critical capillary number, it is still important to try to perform experiments at lower pressure gradients. It is more difficult to observe the effect of viscoelastic polymers at lower pressure gradients since the easiest way to achieve lower gradients is to lower injection rates (and is harder to maintain a high Deborah number at low velocities). While HPAM FP6040 was not as promising as we had initially expected, the small 1.5% decrease in oil saturation at lower pressure gradients (~2.5 psi/ft) suggested some promise in using polymers with much higher relaxation times. Additional formulations could help increase the relaxation time, although higher molecular weight polymers can be more difficult to implement in cores with low permeability.
3. Experiments in additional rock types are recommended. Most of experiments that study the viscoelastic effect to date have been completed in water-wet sandstones (Bentheimer, Boise, Berea). Bentheimer and Boise sandstones have a relatively high permeability, but obviously not all rocks have high permeability. However, it may be difficult to achieve high Deborah number in low-permeability media. Coreflood experiments with higher clay concentration, or a heterogeneous medium will be useful in testing the efficacy in viscoelastic polymers in complex sandstones.
4. Further studies on the optimization of the viscoelastic polymer solutions will be needed to increase their relaxation times. Hydrolysis of polymers in higher pH

conditions (>10) can help obtain very high Deborah numbers without significantly increasing the viscosity of the solution. This might be useful for lower molecular weight polymers that will not plug lower permeability rocks.

5. All these experiments were completed at room temperature (23$^{o}$C). This is not realistic for reservoirs. Doing corefloods in higher temperatures might show the feasibility of using viscoelastic polymers in the field. The higher temperature might help decrease the viscosity of polymer solutions, so higher weight polymers with higher relaxation times might be used.
6. Continued experiments with oil-wet cores will be necessary, as understanding how the viscoelastic polymer behave in different oil-trapping environments will be important. Two experiments were completed using oil-wet Bentheimer sandstones. One experiment was successful, while the other was inconclusive due to the lower starting residual oil saturation after waterflood. More experiments are necessary to confirm the results of the two experiments. Completing a coreflood in an oil-wet sandstone in the CT scanner can also help visualize the oil droplet distribution in comparison to the water-wet cores.
7. The single experiment using the biopolymer (scleroglucan) as the inelastic flood did not yield a significant decrease in residual oil saturation. The saturation between the preceding viscoelastic polymer flood before the scleroglucan flood was the same salinity, so more experiments should be done to determine if a decrease in oil saturation was due to the change in salinity or other factors, or rather a change in elasticity.

8. The brines used in this experiment lacked di-valent cations. Further work in using polymer solution with brines containing di-valent cations is important for understanding the effect of viscoelasticity on residual oil saturation.
9. Micromodel experiments can also help visualize more pore scale behaviors that might not be seen when doing corefloods, even in the CT. Micromodels might be able to give a closer look at how the viscoelastic polymer behaves in smaller pore spaces.

# Appendix A

Summary of Core Flood completed by Erincik (2017)

| Core # | 1 | 2 | 3 | 4 | 5 | 6 | 7 | 8 |
|---|---|---|---|---|---|---|---|---|
| Notes | High Nde using 3630s | Repeat of floor #1 of low sal to high sal | low sal, to high sal, lower v to 1ft/d | alternating salinities | alternating salinities with larger PV (1PV) | Completed by PPQ repeat of #3 | Completed by PPQ using low viscosity oil | Completed by PPQ using low viscosity oil and low MW |
| Rock Type | Bentheimer | Bentheimer | Bentheimer | Bentheimer | Bentheimer | Bentheimer | Bentheimer | Berea |
| Diam (in) | 2.016 | 2.016 | 2.157 | 2.157 | 2.02 | 1.966 | 1.953 | 2 |
| Area (cm^2) | 21.253 | 21.253 | 24.330 | 24.330 | 21.337 | 20.212 | 19.945 | 20.917 |
| Length (in) | 12.0 | 12.0 | 12.0 | 12.0 | 12.0 | 12.0 | 11.9 | 11.8 |
| $\phi$ | 0.22 | 0.24 | 0.25 | 0.24 | 0.24 | 0.24 | 0.25 | 0.24 |
| k (mD) | 1341 | 1483.5 | 1480 | 1604 | 1453 | 1277 | 1448 | 140 |
| k(cm2) | 1.324E-08 | 1.464E-08 | 1.461E-08 | 1.583E-08 | 1.434E-08 | 1.260E-08 | 1.429E-08 | 1.382E-09 |
| C | 4 | 4 | 4 | 4 | 4 | 4 | 4 | 4 |
| Core Reduction and Conditioning | | | | | | | | |
| Reducing Soln | 40000ppm $NaHCO_3$ 10000ppm $Na_4EDTA$ 10000ppm $Na_2S_2O_4$ | 40000ppm $NaHCO_3$ 10000ppm $Na_4EDTA$ 10000ppm $Na_2S_2O_5$ | 40000ppm $NaHCO_3$ 10000ppm $Na_4EDTA$ 10000ppm $Na_2S_2O_6$ | 40000ppm $NaHCO_3$ 10000ppm $Na_4EDTA$ 10000ppm $Na_2S_2O_7$ | 40000ppm $NaHCO_3$ 10000ppm $Na_4EDTA$ 10000ppm $Na_2S_2O_7$ | 40000ppm $NaHCO_3$ 10000ppm $Na_4EDTA$ 10000ppm $Na_2S_2O_8$ | 40000ppm $NaHCO_3$ 10000ppm $Na_4EDTA$ 10000ppm $Na_2S_2O_7$ | 40000ppm $NaHCO_3$ 10000ppm $Na_4EDTA$ 10000ppm $Na_2S_2O_8$ |
| final reduced [Fe+2/+3] | 0 | 0 | 0 | 0 | 0 | 0 | 0 | 0 |
| | | | | | | | | |
| Oil Flood | | | | | | | | |
| Type | Diluted with Decalin | Diluted with Decalin | Diluted with Decalin | Diluted with Decalin | Diluted with Decalin | Diluted with Decalin | | Diluted with Decalin |
| µoil (cp) | 124 | 126 | 114 | 129 | 137 | 128 | 9.6 | |
| Injection Pressure (psi) | 50 | 85 | 85 | 85 | 85 | 80 | 30 | 80 |
| Soi | 0.89 | 0.84 | 0.82 | 0.89 | 0.84 | 0.87 | 0.73 | 0.6 |
| Swr | 0.11 | 0.16 | 0.18 | 0.11 | 0.16 | 0.13 | 0.27 | 0.4 |
| kro° | 1.10 | 0.74 | 0.84 | 0.6 | 0.94 | 0.6 | 0.42 | NA |
| | | | | | | | | |
| Waterflood | | | | | | | | |
| Note | | | | | | | | |
| Solution | 1000ppm NaCl 1000ppm $Na_2S_2O_4$ | 1000ppm NaCl 1000ppm $Na_2S_2O_4$ | 1000ppm NaCl 1000ppm $Na_2S_2O_4$ | 1000ppm NaCl 1000ppm $Na_2S_2O_4$ | 1000ppm NaCl 400ppm NaHCO3 1000ppm $Na_2S_2O_4$ | 1000ppm NaCl 1000ppm $Na_2S_2O_4$ | 1000ppm NaCl 400ppm NaHCO3 400ppm $Na_2S_2O_4$ | 1000ppm NaCl 400ppm NaHCO3 400ppm $Na_2S_2O_4$ |
| µbrine(cp) | 0.95 | 0.95 | 0.95 | 0.95 | 0.95 | 0.95 | 0.95 | 0.95 |

| | | | | | | | | |
|---|---|---|---|---|---|---|---|---|
| q* (ml/min) | 1 | 0.5 | 0.5 | 0.5 | 0.5 | 0.204 | 0.103 | NA |
| v* (ft/d) | 10.3 | 4.7 | 4.7 | 4.8 | 4.8 | 2 | 1 | 5 |
| u (cm/s) | 7.84E-04 | 3.92E-04 | 3.43E-04 | 3.43E-04 | 3.91E-04 | 1.68E-04 | 8.61E-05 | NA |
| Injected PV | 5.0 | 5+ | 4+ | 6+ | 8+ | 7+ | 3.5+ | 3+ |
| Nc | 5.00E-05 | 3.50E-05 | 3.30E-05 | 5.20E-05 | 3.20E-05 | 2.90E-05 | 1.30E-06 | 2.80E-05 |
| Swr* | 0.52 | 0.605 | 0.55 | 0.537 | 0.561 | 0.57 | 0.617 | 0.68 |
| Remaining So | 0.48 | 0.395 | 0.45 | 0.463 | 0.439 | 0.43 | 0.383 | 0.32 |
| krw° | 0.1 | 0.09 | 0.09 | 0.08 | 0.1 | 0.03 | 0.11 | NA |
| Mo | 12.5 | 16.7 | 12.8 | 17.6 | 17.6 | 7.2 | 0.99 | NA |
| ΔP (psi/ft) | 4 | ~3 | ~2.75 | ~2.5 | ~2.5 | NA | NA | NA |
| | | | | | | | | |
| Secondary Flood | | | | | | | | |
| Note | 56cP | 46cP | 57cP | 60cP | 57cP | 60cP | no Glycerin flood Low sal high elast | no Glycerin flood Low sal high elast |
| Solution | 81wt% glycerin 19wt% brine (1000ppm NaCl, 400ppm NaHCO3) | 80wt% glycerin 20wt% brine (1000ppm NaCl, 400ppm NaHCO3) | 82wt% glycerin 18wt% brine (1000ppm NaCl) | 82wt% glycerin 18wt% brine (1000ppm NaCl) | 82wt% glycerin 18wt% brine (1000ppm NaCl 400ppm NaHCO3) | 82wt% glycerin 18wt% brine (1000ppm NaCl) | 1500ppm 3630s 1000ppm NaCl 400ppm NaHCO3 | 1500ppm 3330s 3000ppm NaCl 2000ppm NaHCO3 |
| Power law Model Pre Hydrolysis | - | - | - | - | - | - | - | - |
| τ (s) pre | - | - | - | - | - | - | - | - |
| Power law Model Injected | - | - | - | - | - | - | NA | NA |
| τ (s) Injected | - | - | - | - | - | - | 11.8 | NA |
| q* (ml/min) | 0.2 | 0.2 | 0.21 | 0.207 | 0.208 | 0.204 | 0.103 | NA |
| v* (ft/d) | 2.1 | 2.1 | 2 | 2 | 2 | 2 | 1 | 1 |
| u (cm/s) | 1.57E-04 | 1.57E-04 | 1.44E-04 | 1.42E-04 | 1.62E-04 | 1.68E-04 | 8.61E-05 | NA |
| Remaining So | 0.48 | 0.38 | 0.45 | 0.436 | 0.406 | 0.36 | 0.336 | 0.27 |
| k_r1° | 0.13 | 0.1 | 0.09 | 0.1 | 0.12 | 0.11 | NA | NA |
| Mo | 0.27 | 3.16 | 0.2 | 0.34 | 0.33 | 0.4 | NA | NA |
| Nc max | NA | NA | NA | NA | NA | NA | 6.90E-05 | 1.20E-05 |
| ΔP (psi/ft) | 23 | 26 | 34 | 30 | 26 | 34 | 35 | 66 |
| Nde | NA | NA | NA | NA | NA | NA | 280 | 3 |
| μapp (cp) | NA | NA | NA | NA | NA | NA | 60 | 18 |
| C | NA | NA | NA | NA | NA | NA | NA | NA |
| Yeq (s-1) | NA | NA | NA | NA | NA | NA | NA | 48.4 |
| | | | | | | | | |
| Third Flood | | | | | | | | |

| Notes | Low Salinity pH 8.49 Injected at three diff rates | Low Sal pH 8.71 high relax time | high MW low sal brine pH 8.5 | high MW low sal brine pH 8.2 inject for 0.48PV | high MW low sal brine pH 7.8 | high MW low sal brine | high salinity | high salinity |
|---|---|---|---|---|---|---|---|---|
| Solution | 2000ppm HPAM 3630s 1000ppm NaCl 400ppm NaHCO3 | 2000ppm HPAM 3630s 1000ppm NaCl 400ppm NaHCO3 | 2000ppm 3630s 1000ppm NaCl 400ppm NaHCO3 | 2000ppm 3630s 1000ppm NaCl 400ppm NaHCO3 | 2000ppm 3630s 1000ppm NaCl 400ppm NaHCO3 | 2000ppm 3630s 1000ppm NaCl 400ppm NaHCO3 | NA | 2800ppm 3330s 20,000ppm NaCl 10,000ppm Na2CO3 |
| Power law Model Pre Hydrolysis | - | - | - | - | - | - | - | - |
| τ (s) pre | - | - | - | - | - | - | - | - |
| Power law Model Injected | K=454 n=0.39 | K=411 n=0.4 | K=366 n=0.43 | K=507 n=0.37 | K=536 n=0.36 | NA | NA | NA |
| τ (s) Injected | 3.1 | 1.9 | 1.2 | 9.3 | 10.2 | 6.8 | NA | NA |
| q* (ml/min) | 0.194 | 0.213 | 0.106 | 0.103 | | 0.102 | 0.103 | NA |
| v* (ft/d) | 2 | 2 | 1 | 1 | | 1 | 1 | 1 |
| u (cm/s) | 1.52E-04 | 1.67E-04 | 7.26E-05 | 7.06E-05 | 0.00E+00 | 8.41E-05 | 8.61E-05 | NA |
| Remaining So | 0.29 | 0.29 | 0.31 | 0.342 | | 0.22 | 0.267 | 0.24 |
| k_r2° | ~0.1 | 0.11 | 0.114 | | | 0.12 | NA | NA |
| Mo | ~0.45 | 0.5 | 0.3 | | | 0.4 | NA | NA |
| Nc max | 8.30E-05 | 5.60E-05 | 4.60E-05 | | | 2.50E-05 | NA | 8.50E-06 |
| ΔP (psi) | 48 | 20 | 14 | | | 15 | 13 | 47 |
| Nde | 152.2 | 100.1 | 32.3 | | | 300 | 10 | 2 |
| μapp (cp) | NA | NA | NA | NA | NA | NA | 60 | 18 |
| C | 4 ± 0.2 | NA | NA | NA | NA | NA | NA | NA |
| Yeq (s-1) | 48 | 52.6 | 26.9 | | | NA | NA | NA |
| | | | | | | | | |

Fourth Flood

| Notes | High Salinity | High Sal | High Sal | High Sal pH 8.5 | High Sal pH 7.92 | | - | |
|---|---|---|---|---|---|---|---|---|
| Solution | 3800ppm HPAM 3630s 26,400ppm NaCl 300ppm NaHCO3 | 3400ppm HPAM 3630s 26400ppm NaCl 300ppmNaHCO3 | 3548ppm 3630s 24000ppm NaCl 300ppm NaHCO3 | 3547ppm 3630s 24000ppm NaCl 300ppm NaHCO3 | 3547ppm 3630s 24000ppm NaCl 300ppm NaHCO3 | 3548ppm 3630s 24000ppm NaCl 300ppm NaHCO3 | - | |
| Power law Model Pre Hydrolysis | - | - | - | - | - | - | - | |
| τ (s) pre | - | - | - | - | - | - | - | |
| Power law Model Injected | K=508 n=0.5 | K=205 n=0.54 | K=250 n=0.51 | K=342 n=0.46 | K=349 n=0.47 | NA | - | |
| τ (s) Injected | 0.19 | 0.12 | 0.24 | 1.03 | 0.45 | 1.3 | - | |
| q* (ml/min) | 0.388 | 0.426 | 0.106 | | | 0.102 | - | |

| | | | | | | | | |
|---|---|---|---|---|---|---|---|---|
| v* (ft/d) | 4 | 4 | 1 | | | 1 | - | |
| u (cm/s) | 3.04E-04 | 3.34E-04 | 7.26E-05 | 0.00E+00 | 0.00E+00 | 8.41E-05 | - | 0.00E+00 |
| Remaining So | 0.22 | 0.08 | 0.24 | | | 0.07 | - | |
| k_rp1º | 0.27 | 0.24 | 0.18 | | | 0.22 | - | |
| Mo | 0.67 | 1.6 | 0.5 | | | 0.8 | - | |
| Nc max | 4.50E-05 | 5.80E-05 | 2.40E-05 | | | 2.40E-05 | - | |
| ΔP (psi) | 26 | 30.6 | 7.75 | | | 9.5 | - | |
| Nde | 16.5 | 11 | 6.1 | | | 50 | - | |
| μapp (cp) | NA | NA | NA | NA | NA | NA | - | NA |
| C | NA | NA | NA | NA | NA | NA | - | NA |
| ϒeq (s-1) | 85 | 92 | 25.1 | | | NA | - | |
| | | | | | | | | |

# Appendix B

Summary of Core Flood completed by Qi (2018) Chapter 4 Core Floods

| Experiments completed with viscous oils (~120cp) | | | | | | | |
|---|---|---|---|---|---|---|---|
| **Core #** | **1** | **2** | **3a** | **3b** | **4** | **5** | **6** |
| Notes | | repeat of #1 but visualize on CT | repeat of #1 and #2 with low pressure grad (3psi/ft) | second half of #3 with second polymer flood higher grad and viscoelastic polymer | low sal brine flood pre oil flood | low sal brine flood pre oil flood | low sal brine flood pre oil flood |
| Rock Type | Bentheimer | Bentheimer | Bentheimer | Bentheimer | Bentheimer | Bentheimer | Bentheimer |
| Diam (in) | 1.98 | 2 | 1.97 | 2 | 1.95 | 1.95 | 2 |
| Area (cm^2) | 19.865 | 20.268 | 19.665 | 20.268 | 19.268 | 19.268 | 20.268 |
| Length (in) | 12.0 | 11.8 | 11.8 | 11.8 | 11.7 | 11.7 | 11.9 |
| $\phi$ | 0.22 | 0.22 | 0.22 | 0.22 | 0.22 | 0.22 | 0.22 |
| k (mD) | 2200 | 2140 | 2135 | 2135 | 2240 | 22445 | 2340 |
| k(cm2) | 2.171E-08 | 2.112E-08 | 2.107E-08 | 2.107E-08 | 2.211E-08 | 2.215E-07 | 2.310E-08 |
| C | 4 | 4 | 4 | 4 | 4 | 4 | 4 |
| Core Reduction and Conditioning | | | | | | | |
| Reducing Soln | 40000ppm $NaHCO_3$ 10000ppm $Na_4EDTA$ 10000ppm $Na_2S_2O_4$ | 40000ppm $NaHCO_3$ 10000ppm $Na_4EDTA$ 10000ppm $Na_2S_2O_5$ | 40000ppm $NaHCO_3$ 10000ppm $Na_4EDTA$ 10000ppm $Na_2S_2O_6$ | 40000ppm $NaHCO_3$ 10000ppm $Na_4EDTA$ 10000ppm $Na_2S_2O_7$ | 40000ppm $NaHCO_3$ 10000ppm $Na_4EDTA$ 10000ppm $Na_2S_2O_8$ | 40000ppm $NaHCO_3$ 10000ppm $Na_4EDTA$ 10000ppm $Na_2S_2O_9$ | 40000ppm $NaHCO_3$ 10000ppm $Na_4EDTA$ 10000ppm $Na_2S_2O_{10}$ |
| final reduced [Fe+2/+3] | 0 | 0 | 0 | 0 | 0 | 0 | 0 |
| | | | | | | | |
| Oil Flood | | | | | | | |
| Type | Heavy diluted with decalin | Heavy diluted with decalin | Heavy diluted with decalin | Heavy diluted with decalin | Heavy diluted with decalin | Heavy diluted with decalin | Heavy diluted with decalin |
| µoil (cp) | 120 | 120 | 120 | 120 | 120 | 120 | 120 |
| Injection Pressure (psi) | 80 | 80 | 80 | 80 | 80 | 80 | 80 |
| Soi | 0.85 | 0.86 | 0.9 | 0.9 | 0.89 | 0.9 | 0.91 |
| Swr | 0.15 | 0.14 | 0.1 | 0.1 | 0.11 | 0.1 | 0.09 |

| | | | | | | | |
|---|---|---|---|---|---|---|---|
| kro° | NA | NA | NA | NA | NA | NA | NA |
| | | | | | | | |
| Waterflood | | | | | | | |
| Waterflood Soln | 10,000ppm NaCl 1000ppm NaHCO3 | 10,000ppm NaCl 1000ppm NaHCO3 | 10,000ppm NaCl 1000ppm NaHCO3 | 10,000ppm NaCl 1000ppm NaHCO3 | 400ppm NaHCO3 | 400ppm NaHCO4 | 400ppm NaHCO5 |
| µbrine(cp) | 0.95 | 0.95 | 0.95 | 0.95 | 0.95 | 0.95 | 0.95 |
| q* (ml/min) | 6.8 | 5.75 | 6.75 | 6.75 | 6.8 | 6.3 | 1.5 |
| v* (ft/d) | 16 | 14 | 16 | 16 | 16 | 15 | 4 |
| u (cm/s) | 5.71E-03 | 4.73E-03 | 5.72E-03 | 5.55E-03 | 5.88E-03 | 5.45E-03 | 1.23E-03 |
| Injected PV | 9 | 6 | 6 | NA | NA | NA | NA |
| Nc | NA | NA | NA | NA | NA | NA | NA |
| Swr* | 0.7 | 0.63 | 0.65 | 0.65 | 0.782 | 0.712 | 0.642 |
| Remaining So | 0.3 | 0.37 | 0.35 | 0.35 | 0.218 | 0.288 | 0.358 |
| krw° | 0.11 | 0.09 | 0.11 | 0.11 | 0.09 | 0.08 | 0.07 |
| Mo* | ~17 | ~17 | | | | | |
| ΔP (psi/ft) | 10 | 10.4 | 10.1 | 10.1 | 11.7 | 11 | 3.1 |
| | | | | | | | |
| Glycerin Flood | | | | | | | |
| Solution | 81% glycerin in 10,000ppm NaCl 1000ppm NaHCO3 | 81% glycerin in 10,000ppm NaCl 1000ppm NaHCO4 | 81% glycerin in 10,000ppm NaCl 1000ppm NaHCO5 | 81% glycerin in 10,000ppm NaCl 1000ppm NaHCO6 | gly in (?) 400ppm NaHCO3 | gly in (?) 400ppm NaHCO4 | gly in (?) 400ppm NaHCO5 |
| µglycerin (cp) | 72.6 | 70 | 71 | 74 | 77 | 72 | 52 |
| q* (ml/min) | 0.101 | 0.081 | 0.100 | 0.100 | 0.050 | 0.025 | 0.033 |
| v* (ft/d) | 1.10 | 0.90 | 1.10 | 1.10 | 0.80 | 0.30 | 0.30 |
| u (cm/s) | 8.47E-05 | 6.66E-05 | 8.48E-05 | 8.22E-05 | 4.33E-05 | 2.16E-05 | 2.71E-05 |
| Max Oil Cut | ~0.55 | NA | NA | NA | NA | NA | NA |
| Remaining So | 0.26 | 0.31 | 0.31 | 0.31 | 0.21 | 0.252 | 0.29 |
| krgly° | 0.12 | 0.09 | 0.12 | 0.12 | 0.09 | 0.08 | 0.08 |

| | | | | | | | |
|---|---|---|---|---|---|---|---|
| Mo* | 0.2 | 0.17 | NA | NA | NA | NA | NA |
| Yeq (s-1) | 4 | NA | NA | NA | NA | NA | NA |
| ΔP (psi/ft) | 11 | 10 | 10 | 11 | 9.7 | 3.2 | 3.4 |
| | | | | | | | |
| Polymer Flood (1) | | | | | | | |
| Solution | 2100ppm HPAM 3630s 10000ppm NaCl 1000ppm NaHCO3 | 2100ppm HPAM 3630s 10000ppm NaCl 1000ppm NaHCO3 | 1800ppm HPAM 3630s 10000ppm NaCl 1000ppm NaHCO3 | 1800ppm HPAM 3630s 10000ppm NaCl 1000ppm NaHCO3 | 600ppm HPAM 3630s 400ppm NaHCO3 | 600ppm HPAM 3630s 400ppm NaHCO4 | 600ppm HPAM 3630s 400ppm NaHCO5 |
| τ (s) | 0.6 | 0.4 | 0.13 | 0.13 | 7.14 | 4.73 | 2.08 |
| | | | | | | | |
| Power law Model | K=143.9 n=0.52 | K=150.1 n=0.53 | K=105.83 n=0.56 | K=105.83 n=0.56 | K=166.0 n=0.34 | K=164.66 n=0.39 | K=106.58 n=0.44 |
| q* (ml/min) | 0.1 | 0.22 | 0.02 | 0.73 | 0.02 | 0.03 | 0.03 |
| v* (ft/d) | 1 | 2.4 | 0.2 | 7.9 | 0.2 | 0.3 | 0.3 |
| u (cm/s) | 8.39E-05 | 1.81E-04 | 1.70E-05 | 6.00E-04 | 1.73E-05 | 2.60E-05 | 2.47E-05 |
| Remaining So | 0.198 | 0.254 | 0.31 | 0.209 | 0.179 | 0.249 | 0.28 |
| k_rp1° | 0.048 | 0.096 | 0.057 | 0.173 | 0.067 | 0.102 | 0.053 |
| Mo | NA | NA | NA | NA | NA | NA | NA |
| Nc max | NA | NA | NA | NA | NA | NA | NA |
| ΔP (psi/ft) | 10 | 9.7 | 2.9 | 9.5 | 2.7 | 2.3 | 3.2 |
| Nde | 16.04 | 18.14 | 0.69 | 13.65 | 26.52 | 22.74 | 16.63 |
| μapp (cp) | 29.72 | 24.99 | 49.76 | 13.42 | 69.83 | 63.18 | 33.42 |
| C | 4 | 4 | 4 | 4 | 4 | 4 | 4 |
| Yeq (s-1) | 26.73 | 45.36 | 5.56 | 109.17 | 3.71 | 4.81 | 7.99 |
| | | | | | | | |
| Polymer Flood (2) | | | | | | | |
| Solution | - | - | 1800ppm HPAM 3630s 10000ppm NaCl 1000ppm NaHCO3 | - | - | - | - |
| | - | - | | - | - | - | - |

| | | | | | | | |
|---|---|---|---|---|---|---|---|
| τ (s) | - | - | 0.13 | - | - | - | - |
| Power law Model | - | - | K=105.83 n=0.56 | - | - | - | - |
| q* (ml/min) | - | - | 0.73 | - | - | - | - |
| v* (ft/d) | - | - | 7.9 | - | - | - | - |
| u (cm/s) | - | - | 6.19E-04 | - | - | - | - |
| Remaining So | - | - | 0.209 | - | - | - | - |
| k_rp1° | - | - | 0.173 | - | - | - | - |
| Mo | - | - | | - | - | - | - |
| Nc max | - | - | | - | - | - | - |
| ΔP (psi/ft) | - | - | 9.5 | - | - | - | - |
| Nde | - | - | 13.65 | - | - | - | - |
| μapp (cp) | - | - | 13.42 | - | - | - | - |
| C | - | - | 4 | - | - | - | - |
| Yeq (s-1) | - | - | 109.17 | - | - | - | - |

# Appendix C

Summary of Core Flood completed by Qi (2018) Chapter 6 Core Floods

| Experiments completed with light oils | | | | | | |
|---|---|---|---|---|---|---|
| **Core #** | **1** | **2** | **3** | **4** | **5** | **6** |
| Notes | | Repeat of #1 with neutral pH | increase relaxation time by reducing salinity | goal to investigate viscoelastic effect at high sal conditions | use of different rock (lower perm, more clay) | injection of glycerin post waterflood to make Mo close to 1 |
| Rock Type | Bentheimer | Bentheimer | Bentheimer | Bentheimer | Berea | Bentheimer |
| Diam (in) | 1.95 | 2 | 1.97 | 2 | 2.02 | 2.01 |
| Area (cm^2) | 19.268 | 20.268 | 19.665 | 20.268 | 20.676 | 20.471 |
| Length (in) | 11.7 | 12.0 | 11.9 | 12.0 | 12.0 | 11.9 |
| $\phi$ | 0.21 | 0.24 | 0.25 | 0.25 | 0.25 | 0.24 |
| k (mD) | 2188 | 1343 | 1448 | 1350 | 143 | 2538 |
| k(cm2) | 2.160E-08 | 1.326E-08 | 1.429E-08 | 1.332E-08 | 1.411E-09 | 2.505E-08 |
| C | 4 | 4 | 4 | 4 | 4 | 4 |
| Core Reduction and Conditioning | | | | | | |
| Reducing Soln | 40000ppm $NaHCO_3$ 10000ppm $Na_4EDTA$ 10000ppm $Na_2S_2O_4$ | 40000ppm $NaHCO_3$ 10000ppm $Na_4EDTA$ 10000ppm $Na_2S_2O_5$ | 40000ppm $NaHCO_3$ 10000ppm $Na_4EDTA$ 10000ppm $Na_2S_2O_6$ | 40000ppm $NaHCO_3$ 10000ppm $Na_4EDTA$ 10000ppm $Na_2S_2O_7$ | 40000ppm $NaHCO_3$ 10000ppm $Na_4EDTA$ 10000ppm $Na_2S_2O_8$ | 40000ppm $NaHCO_3$ 10000ppm $Na_4EDTA$ 10000ppm $Na_2S_2O_9$ |
| final reduced [Fe+2/+3] | 0 | 0 | 0 | 0 | 0 | 0 |
| | | | | | | |
| Oil Flood | | | | | | |
| Type | Light diluted with 17% toluene | Light diluted with 17% toluene | Light diluted with 17% toluene | Light diluted with 17% toluene | Light diluted with 17% toluene | Light diluted with 17% toluene |
| $\mu$oil (cp) | 9 | 9.6 | 9 | 9 | 9 | 9 |
| Injection Pressure (psi) | 20 | 20 | 20 | 20 | 20 | 20 |
| Soi | 0.716 | 0.71 | 0.73 | 0.747 | 0.614 | 0.723 |
| Swr | 0.284 | 0.29 | 0.27 | 0.253 | 0.386 | 0.277 |
| $kro^o$ | 0.704 | NA | NA | NA | NA | NA |
| | | | | | | |

| Waterflood | | | | | | |
|---|---|---|---|---|---|---|
| Note | Typical Sal Water Flood | Typical salinity water flood | Low salinity waterflood | High salinity waterflood (pH 10.3 to match polymer pH) | Typical salinity water flood | Typical salinity water flood |
| Solution | 10,000ppm NaCl 1000ppm NaHCO3 1000ppm Na2SO4 | 10,000ppm NaCl 1000ppm NaHCO3 | 1000ppm NaCl 400ppm NaHCO3 400ppm NaS2O4 | 60,000ppm NaCl 20,000ppm Na2CO3 10,000ppm Na2S2O4 | 3000ppm NaCl 2000ppm Na2CO3 400ppm Na2S2O4 | 10,000ppm NaCl 1000ppm NaHCO3 400ppm Na2S2O4 |
| μbrine(cp) | | | | | | |
| q* (ml/min) | 0.1 | 0.046 | 0.106 | 0.096 | 0.45 | 0.096 |
| v* (ft/d) | 1.1 | 0.5 | 1 | 0.9 | 4.3 | 0.9 |
| u (cm/s) | 8.65E-05 | 3.78E-05 | 8.98E-05 | 7.89E-05 | 3.63E-04 | 7.82E-05 |
| Injected PV | 3.6 | 2-3 | 3+ | NA | 3+ | 3+ |
| Nc | 6.71E-07 | 3.58E-07 | 4.44E-07 | 4.14E-07 | 2.67E-06 | 3.05E-05 |
| Swr* | 0.652 | 0.677 | 0.617 | 0.746 | 0.678 | 0.611 |
| Remaining So | 0.348 | 0.323 | 0.383 | 0.254 | 0.322 | 0.389 |
| krw° | 0.07 | 0.06 | 0.11 | 0.11 | 0.08 | 0.06 |
| Mo | 0.99 | NA | NA | NA | NA | NA |
| ΔP (psi/ft) | 0.23 | 0.2 | 0.23 | 0.23 | 14 | 9 |
| | | | | | | |
| Secondary Flood | | | | | | |
| Note | Typical Salnity Polymer Flood (pH 10.2) | Typical Salnity Polymer Flood Neutralized with HCl | Low Salinity Polymer Flood | High Salinity Polymer Flood | Typical Salinity Polymer Flood with lower MW | Typical Salinity Glycerin Flood (54cP) |
| Solution | 2600ppm HPAM 3630s 6000ppm NaCl 5000ppm Na2CO3 | 2413ppm HPAM 3630s 8455ppm NaCl 3268ppm NaHCO3 (post neutr) | 1500ppm HPAM 3630s 1000ppm NaCl 400ppm NaHCO3 | 2600ppm HPAM 3630s 60,000ppm NaCl 20,000ppm Na2CO3 | 1500ppm HPAM 3330s 3000ppm NaCl 2000ppm Na2CO3 | glyc in 10,000ppm NaCl 1000ppm NaHCO3 400ppm Na2S2O4 |
| Power law Model Pre Hydrolysis | K= 286.6 n=0.51 | - | K= 358.71 n=0.41 | K= 156.5 n=0.55 | - | - |
| τ (s) pre | 1.2 | - | 8.28 | 0.24 | - | - |
| Power law Model Injected | K= 407.48 n=0.43 | K= 229.6 n=0.518 | K= 483.73 n=0.35 | K= 383.73 n=0.50 | K= 48.67 n=0.696 | K= 175 n=0.468 |
| τ (s) Injected | 2.57 | 1.09 | 11.78 | 0.58 | 0.06 | 2.7 |
| q* (ml/min) | 0.1 | 0.042 | 0.103 | 0.096 | 0.09 | 0.1 |
| v* (ft/d) | 1.1 | 0.5 | 1 | 0.9 | 0.9 | 1 |
| u (cm/s) | 8.65E-05 | 3.45E-05 | 8.73E-05 | 7.89E-05 | 7.25E-05 | 8.14E-05 |
| Remaining So | 0.238 | 0.23 | 0.336 | 0.226 | 0.274 | 0.346 |

| | | | | | | |
|---|---|---|---|---|---|---|
| k_r1° | 0.11 | 0.07 | 0.05 | 0.11 | 0.04 | NA |
| Mo | NA | NA | NA | NA | NA | NA |
| Nc max | 3.07E-05 | 2.08E-05 | 6.61E-05 | 1.71E-05 | 1.26E-05 | NA |
| ΔP (psi/ft) | 10.5 | 11.6 | 34.2 | 9.5 | 50 | NA |
| Nde | 49.65 | 13.16 | 424.44 | 12.35 | 3 | 78 |
| μapp (cp) | 67.76 | 69.05 | 42.51 | 39.04 | 11.85 | NA |
| C | 4 | 4 | 4 | 4 | 4 | NA |
| ϒeq (s-1) | 19.32 | 12.1 | 36.03 | 21.44 | 104.26 | NA |
| | | | | | | |
| Third Flood | | | | | | |
| Notes | Typical salinity water flood | Low SalinityViscoelastic Polymer Flood | High Salinity Polymer Flood | Low Salinity Glycerin Flood (59cP) | High Salinity Polymer Flood with lower MW | Low Salinity Polymer Flood in low MW |
| Solution | 10,000ppm NaCl 1000ppm NaHCO3 1000ppm Na2SO4 | 6000ppm HPAM 3130s 10000ppm NaCl 1000ppm NaHCO3 | 3548ppm HPAM 3630s in 25000ppm TDS | 1000ppm TDS | 2800ppm HPAM 3330s 20,000ppm NaCl 10,000ppm Na2CO3 | 7000ppm HPAM 3130s 1000ppm NaCl 1000ppm NaHCO3 |
| Power law Model Pre Hydrolysis | - | - | - | - | - | - |
| τ (s) pre | - | - | - | - | - | - |
| Power law Model Injected | K=1 n=1 (brine) | K=117.8 n=0.75 | K=337.3 n=0.5 | K=62.0 n=1 (glycerin) | K=49.8 n=0.78 | K=54.0 n=1 |
| τ (s) Injected | 0 | 0.02 | 0.6 | 0 | 0.04 | 0.017 |
| q* (ml/min) | 0.1 | 0.046 | 0.1 | 0.1 | 0.1 | 0.096 |
| v* (ft/d) | 1 | 0.5 | 1 | 1 | 1 | 0.9 |
| u (cm/s) | 8.65E-05 | 3.78E-05 | 8.48E-05 | 8.22E-05 | 8.06E-05 | 7.82E-05 |
| Remaining So | 0.238 | 0.23 | 0.266 | 0.01 | 0.238 | 0.346 |
| k_r2° | NA | NA | NA | NA | NA | 0.042 |
| Mo | NA | NA | NA | NA | NA | NA |
| Nc max | NA | 1.40E-05 | 4.00E-05 | 3.60E-05 | NA | 3.39E-05 |
| ΔP (psi) | 0.4 | 8 | 14 | ~21 | 52 | 10 |
| Nde | - | 0.3 | 36 | 4 | 2 | 0.3 |

| | | | | | | |
|---|---|---|---|---|---|---|
| μapp (cp) | NA | NA | NA | NA | NA | 29.11 |
| C | 4 | 4 | 4 | 4 | 4 | 4 |
| Ɣeq (s-1) | NA | NA | NA | NA | NA | 29.12 |
| | | | | | | |
| Fourth Flood | | | | | | |
| Notes | High Salinity Glycerin Flood (61cP) | Typical Salnity Polymer Flood Neutralized with HCl | - | - | - | High Salinity Polymer Flood in low MW |
| Solution | Glycerin in 5% NaCl | 2413ppm HPAM 3630s 8455ppm NaCl 3268ppm NaHCO3 (post neutr) | - | - | - | 9000ppm HPAM 3130s 50,000ppm NaCl 1000ppm NaHCO3 |
| Power law Model Pre Hydrolysis | - | - | - | - | - | - |
| τ (s) pre | - | - | - | - | - | - |
| Power law Model Injected | K=62.0 n=1 (glycerin) | K=229.6 n=0.52 | - | - | - | K=117.8 n=0.75 |
| τ (s) Injected | 0 | 1.09 | - | - | - | 0.015 |
| q* (ml/min) | 0.1 | 0.1 | - | - | - | 0.096 |
| v* (ft/d) | 1 | 1 | - | - | - | 0.9 |
| u (cm/s) | 8.65E-05 | 8.22E-05 | - | - | - | 7.82E-05 |
| Remaining So | 0.07 | 0.2 | - | - | - | 0.346 |
| k_rp1º | NA | NA | - | - | - | NA |
| Mo | NA | NA | - | - | - | NA |
| Nc max | NA | 2.90E-05 | - | - | - | NA |
| ΔP (psi) | ~10.5 | 16 | - | - | - | 8 |
| Nde | 0 | 26 | - | - | - | ~0 |
| μapp (cp) | NA | NA | - | - | - | NA |
| C | 4 | 4 | - | - | - | 4 |
| Ɣeq (s-1) | NA | NA | - | - | - | NA |
| | | | | | | |
| Fifth Flood | | | | | | |
| Notes | - | Low SalinityViscoelastic Polymer Flood | - | - | - | Low Salinity Viscoelastic Polymer Flood in high MW |
| Solution | - | 6000ppm HPAM 3130s 10000ppm NaCl 1000ppm NaHCO3 | - | - | - | 1200ppm HPAM 3630s 1000ppm NaCl 400ppm NaHCO3 |

| | | | | | | |
|---|---|---|---|---|---|---|
| Power law Model Pre Hydrolysis | - | - | - | - | - | - |
| τ (s) pre | - | - | - | - | - | - |
| Power law Model Injected | - | K=117.8 n=0.75 | - | - | - | K=175 n=0.47 |
| τ (s) Injected | - | 0.015 | - | - | - | 2.7 |
| q* (ml/min) | - | 0.1 | - | - | - | 0.1 |
| v* (ft/d) | - | 1 | - | - | - | 1 |
| u (cm/s) | - | 8.22E-05 | - | - | - | 8.14E-05 |
| Remaining So | - | 0.2 | - | - | - | 0.341 |
| k_rp1º | - | NA | - | - | - | NA |
| Mo | - | NA | - | - | - | NA |
| Nc max | - | NA | - | - | - | NA |
| ΔP (psi/ft) | - | 13 | - | - | - | 10 |
| Nde | - | NA | - | - | - | 78 |
| μapp (cp) | - | NA | - | - | - | NA |
| C | - | 4 | - | - | - | 4 |
| Yeq (s-1) | - | NA | - | - | - | NA |
| | | | | | | |
| Sixth Flood | | | | | | |
| Notes | - | - | - | - | - | Low Salinity Low Viscoelastic Polymer Flood in low MW |
| Solution | - | - | - | - | - | 9000ppm HPAM 3130s 50,000ppm NaCl 1000ppm NaHCO3 |
| Power law Model Pre Hydrolysis | - | - | - | - | - | - |
| τ (s) pre | - | - | - | - | - | - |
| Power law Model Injected | - | - | - | - | - | K=116.1 n=0.77 |
| τ (s) Injected | - | - | - | - | - | 0.015 |
| q* (ml/min) | - | - | - | - | - | 0.1 |
| v* (ft/d) | - | - | - | - | - | 1 |
| u (cm/s) | - | - | - | - | - | 8.14E-05 |
| Remaining So | - | - | - | - | - | 0.336 |
| k_rp1º | - | - | - | - | - | NA |
| Mo | - | - | - | - | - | NA |

| | | | | | | |
|---|---|---|---|---|---|---|
| Nc max | - | - | - | - | - | NA |
| ΔP (psi/ft) | - | - | - | - | - | 8.1 |
| Nde | - | - | - | - | - | <0.5 |
| μapp (cp) | - | - | - | - | - | NA |
| C | - | - | - | - | - | 4 |
| Yeq (s-1) | - | - | - | - | - | NA |
| | | | | | | |

# Appendix D

## Polymer Rheology: Experiment #1 Boise

1000 ppm 3630s 1400 TDS

| Time | Shear rate | Viscosity | Viscosity | Angular frequency | Storage modulus | Loss modulus |
|---|---|---|---|---|---|---|
| s | 1/s | poise | cP | rad/s | dyne/cm² | dyne/cm² |
| 46.4607 | 0.100013 | 3.18691 | 318.691 | 0.1 | 0.174913 | 0.290526 |
| 81.5515 | 0.17785 | 2.88943 | 288.943 | 0.177828 | 0.27884 | 0.396611 |
| 116.641 | 0.316268 | 2.22095 | 222.095 | 0.316228 | 0.43883 | 0.528452 |
| 151.732 | 0.562413 | 1.6802 | 168.02 | 0.562341 | 0.615191 | 0.653175 |
| 186.822 | 1.00013 | 1.24203 | 124.203 | 1 | 0.868351 | 0.806286 |
| 221.915 | 1.77849 | 0.917372 | 91.7372 | 1.77828 | 1.15533 | 1.00119 |
| 257.005 | 3.16266 | 0.673107 | 67.3107 | 3.16228 | 1.51162 | 1.25238 |
| 292.092 | 5.62409 | 0.492762 | 49.2762 | 5.62341 | 1.94806 | 1.58946 |
| 327.181 | 10.0012 | 0.362833 | 36.2833 | 10 | 2.49429 | 2.05039 |
| 362.269 | 17.7849 | 0.272164 | 27.2164 | 17.7828 | 3.26696 | 2.83962 |
| 397.358 | 31.6266 | 0.210186 | 21.0186 | 31.6228 | 4.7194 | 4.14788 |
| 432.446 | 56.2409 | 0.163772 | 16.3772 | 56.2341 | 8.78481 | 5.67965 |
| 467.535 | 100.012 | 0.12878 | 12.878 | 100 | 17.922 | 0.0273514 |
| 502.623 | 177.849 | 0.103877 | 10.3877 | | | |
| 537.71 | 300.036 | 0.0881734 | 8.81734 | | | |

Previous 1000ppm 3630s in 1000ppm NaCl and 400ppm NaHCO3

K 137.1 n 0.485 tr 1.186

| Shear rate | Viscosity | Viscosity | Angular freq | Storage mod | Loss modulus |
|---|---|---|---|---|---|
| 1/s | Pa.s | cP | rad/s | dyne/cm² | dyne/cm² |
| 0.100013 | 0.354655 | 354.655 | 0.1 | 0.164785 | 0.315383 |
| 0.17785 | 0.322945 | 322.945 | 0.177828 | 0.287599 | 0.429252 |
| 0.316268 | 0.251915 | 251.915 | 0.316228 | 0.449404 | 0.557976 |
| 0.562412 | 0.191083 | 191.083 | 0.562341 | 0.663158 | 0.719376 |
| 1.00013 | 0.142143 | 142.143 | 1 | 0.927625 | 0.896304 |
| 1.77849 | 0.104284 | 104.284 | 1.77828 | 1.24931 | 1.11321 |
| 3.16266 | 0.075872 | 75.8719 | 3.16228 | 1.64832 | 1.38248 |
| 5.62409 | 0.055115 | 55.1145 | 5.62341 | 2.12001 | 1.74657 |
| 10.0012 | 0.040184 | 40.1835 | 10 | 2.74856 | 2.25206 |
| 17.7849 | 0.029663 | 29.6626 | 17.7828 | 3.64346 | 3.0535 |
| 31.6266 | 0.022468 | 22.468 | 31.6228 | 5.21695 | 4.35627 |
| 56.2408 | 0.017497 | 17.497 | 56.2341 | 9.33615 | 5.86014 |
| 100.012 | 0.013618 | 13.6176 | 100 | 18.5274 | 0.799134 |
| 177.849 | 0.010751 | 10.7509 | | | |
| 300.036 | 0.00887 | 8.86552 | | | |

SECOND INJ

2200ppm 3630s 20000ppm NaCl and 400ppm NaHCO3 2

K 103.67 n 0.574

Tr 0.02 s

| Shear rate | Viscosity | Viscosity |
|---|---|---|
| 1/s | poise | cP |
| 0.100013 | 1.6988 | 169.88 |
| 0.17785 | 1.59062 | 159.062 |
| 0.316262 | 1.37125 | 137.125 |
| 0.562412 | 1.24989 | 124.989 |
| 1.00015 | 1.02126 | 102.126 |
| 1.77848 | 0.809608 | 80.9608 |
| 3.16265 | 0.647686 | 64.7686 |
| 5.62409 | 0.507195 | 50.7195 |
| 10.0012 | 0.391422 | 39.1422 |
| 17.7849 | 0.30047 | 30.047 |
| 31.6266 | 0.231702 | 23.1702 |
| 56.2409 | 0.183988 | 18.3988 |
| 100.012 | 0.14982 | 14.982 |
| 177.849 | 0.123877 | 12.3877 |
| 300.036 | 0.107314 | 10.7314 |

THIRD INJ

1000ppm 3630s 1000ppm NaCl and 400ppm NaHCO3 2

K 140.97 n 0.484

Tr 1.440727 s

| Shear rate | Viscosity | Viscosity |
|---|---|---|
| 1/s | poise | cP |
| 0.100013 | 4.58246 | 458.246 |
| 0.17785 | 3.64049 | 364.049 |
| 0.316268 | 2.65617 | 265.617 |
| 0.562412 | 2.01205 | 201.205 |
| 1.00013 | 1.46908 | 146.908 |
| 1.77849 | 1.07313 | 107.313 |
| 3.16265 | 0.778331 | 77.8331 |
| 5.62408 | 0.563169 | 56.3169 |
| 10.0012 | 0.409923 | 40.9923 |
| 17.7849 | 0.303649 | 30.3649 |
| 31.6266 | 0.231383 | 23.1383 |
| 56.2409 | 0.178929 | 17.8929 |
| 100.012 | 0.139908 | 13.9908 |
| 177.849 | 0.112078 | 11.2078 |
| 300.036 | 0.0939906 | 9.39906 |

1000ppm 3630s 1000ppm NaCl and 400ppm NaHCO3

K 133.6 n 0.491

Tr 1.2991417 s

| Shear rate | Viscosity | Viscosity |
|---|---|---|
| 1/s | poise | poise |
| 0.100013 | 4.01922 | 401.922 |
| 0.17785 | 3.35082 | 335.082 |
| 0.316268 | 2.55486 | 255.486 |
| 0.562413 | 1.91507 | 191.507 |
| 1.00013 | 1.40359 | 140.359 |
| 1.77849 | 1.02024 | 102.024 |
| 3.16266 | 0.741548 | 74.1548 |
| 5.62408 | 0.538759 | 53.8759 |
| 10.0012 | 0.393827 | 39.3827 |
| 17.7849 | 0.293237 | 29.3237 |
| 31.6266 | 0.225087 | 22.5087 |
| 56.2408 | 0.174898 | 17.4898 |
| 100.012 | 0.137817 | 13.7817 |
| 177.849 | 0.111322 | 11.1322 |
| 300.036 | 0.0944853 | 9.44853 |

FOURTH INJ

2200ppm 3630s 20000ppm NaCl and 400ppm NaHCO3

K 90.738 n 0.593

Tr 0.0237138 s

| Shear rate | Viscosity | Viscosity |
|---|---|---|
| 1/s | poise | poise |
| 0.100013 | 1.51992 | 151.992 |
| 0.17785 | 1.45068 | 145.068 |
| 0.316267 | 1.21112 | 121.112 |
| 0.562413 | 1.00353 | 100.353 |
| 1.00013 | 0.868988 | 86.8988 |
| 1.77849 | 0.721855 | 72.1855 |
| 3.16265 | 0.585263 | 58.5263 |
| 5.62408 | 0.463864 | 46.3864 |
| 10.0012 | 0.361932 | 36.1932 |
| 17.7849 | 0.279725 | 27.9725 |
| 31.6266 | 0.217056 | 21.7056 |
| 56.2408 | 0.172584 | 17.2584 |
| 100.012 | 0.141536 | 14.1536 |
| 177.849 | 0.117386 | 11.7386 |
| 300.036 | 0.102137 | 10.2137 |

1000ppm 3630s 1000ppm NaCl and 400ppm NaHCO3

K 123.35 n 0.499

Tr 1.0869565 s

| Shear rate | Viscosity | Viscosity |
|---|---|---|
| 1/s | poise | poise |
| 0.100013 | 3.31025 | 331.025 |
| 0.17785 | 2.52321 | 252.321 |
| 0.316268 | 2.19601 | 219.601 |
| 0.562412 | 1.69102 | 169.102 |
| 1.00013 | 1.27494 | 127.494 |
| 1.77849 | 0.946071 | 94.6071 |
| 3.16265 | 0.695684 | 69.5684 |
| 5.62409 | 0.507827 | 50.7827 |
| 10.0012 | 0.373363 | 37.3363 |
| 17.7849 | 0.277717 | 27.7717 |
| 31.6266 | 0.212113 | 21.2113 |
| 56.2408 | 0.165855 | 16.5855 |
| 100.012 | 0.130554 | 13.0554 |
| 177.849 | 0.104999 | 10.4999 |
| 300.036 | 0.0889375 | 8.89375 |

# Appendix E

## Polymer Rheology: Experiment #2 Boise

First Inj

825ppm FP6040 in 1000ppm NaCl and 400ppm NaHCO3

| k | 132.23 | n | 0.471 | tr | 2.8235347 |
|---|---|---|---|---|---|
| Shear rate | Viscosity | Viscosity | Angular freq | Storage mod | Loss modulus |
| 1/s | Pa.s | cP | rad/s | dyne/cm² | dyne/cm² |
| 0.100013 | 0.314864 | 314.86 | 0.1 | 0.235 | 0.351246 |
| 0.17785 | 0.347723 | 347.72 | 0.177828 | 0.375 | 0.458856 |
| 0.316268 | 0.272063 | 272.06 | 0.316228 | 0.564 | 0.577141 |
| 0.562352 | 0.196291 | 196.29 | 0.562341 | 0.777736 | 0.70738 |
| 1.00021 | 0.140799 | 140.8 | 1 | 1.04723 | 0.849217 |
| 1.77849 | 0.0998691 | 99.87 | 1.77828 | 1.35831 | 1.02165 |
| 3.16275 | 0.0711265 | 71.13 | 3.16228 | 1.72266 | 1.23918 |
| 5.624 | 0.0508873 | 50.89 | 5.62341 | 2.14593 | 1.52373 |
| 10.0012 | 0.0369002 | 36.9 | 10 | 2.70057 | 1.97182 |
| 17.7849 | 0.027398 | 27.4 | 17.7828 | 3.50639 | 2.67058 |
| 31.6266 | 0.0208627 | 20.86 | 31.6228 | 5.04563 | 3.87443 |
| 56.241 | 0.0160199 | 16.02 | 56.2341 | 9.14189 | 4.87792 |
| 100.012 | 0.0124286 | 12.43 | 100 | 16.882 | -1.01961 |
| 177.849 | 0.00994 | 9.94 | | | |
| 300.036 | 0.00885 | 8.85 | | | |

Second Inj

1500ppm FP3330s in 1000ppm NaCl and 400ppm NaHCO3

| K | 108.95 | n | 0.607 | tr | 0.019182 |
|---|---|---|---|---|---|
| Shear rate | Viscosity | Viscosity | Angular freq | Storage mod | Loss modulus |
| 1/s | Pa.s | cP | rad/s | dyne/cm² | dyne/cm² |
| 0.100013 | 0.135689 | 135.689 | 0.1 | 0.0108928 | 0.117602 |
| 0.177851 | 0.123898 | 123.898 | 0.177828 | 0.0253066 | 0.204601 |
| 0.316268 | 0.117316 | 117.316 | 0.316228 | 0.0659804 | 0.345859 |
| 0.562412 | 0.109998 | 109.998 | 0.562341 | 0.159289 | 0.558289 |
| 1.00013 | 0.0985089 | 98.5089 | 1 | 0.330788 | 0.85849 |
| 1.77849 | 0.0856347 | 85.6347 | 1.77828 | 0.621252 | 1.2626 |
| 3.16265 | 0.0716363 | 71.6363 | 3.16228 | 1.06794 | 1.7737 |
| 5.62408 | 0.0589229 | 58.9229 | 5.62341 | 1.69329 | 2.40343 |
| 10.0012 | 0.0470556 | 47.0556 | 10 | 2.54586 | 3.22942 |
| 17.7849 | 0.0367724 | 36.7724 | 17.7828 | 3.72003 | 4.39346 |
| 31.6266 | 0.0283343 | 28.3343 | 31.6228 | 5.53732 | 6.20385 |
| 56.2408 | 0.0216785 | 21.6785 | 56.2341 | 9.3565 | 9.09056 |
| 100.012 | 0.0165827 | 16.5827 | 100 | 21.0822 | 9.6073 |
| 177.849 | 0.0129029 | 12.9029 | 177.828 | 37.5934 | 1.20535 |
| 300.036 | 0.0104302 | 10.4302 | 300 | 167.119 | -128.377 |

Third Inj

825ppm FP6040 in 1000ppm NaCl and 400ppm NaHCO3 1210

| K | 129.76 | n | 0.471 | tr | 1.9280751 |
|---|---|---|---|---|---|
| Shear rate | Viscosity | Viscosity | Angular freq | Storage mod | Loss modulus |
| 1/s | Pa.s | cP | rad/s | dyne/cm² | dyne/cm² |
| 0.100013 | 0.336342 | 336.34 | 0.1 | 0.2 | 0.336886 |
| 0.17785 | 0.316623 | 316.62 | 0.177828 | 0.325 | 0.434884 |
| 0.316268 | 0.250478 | 250.48 | 0.316228 | 0.487 | 0.559069 |
| 0.562412 | 0.185854 | 185.85 | 0.562341 | 0.705682 | 0.689955 |
| 1.00013 | 0.135981 | 135.98 | 1 | 0.962811 | 0.8592 |
| 1.77849 | 0.0971 | 97.14 | 1.77828 | 1.26971 | 1.04615 |
| 3.16265 | 0.0706 | 70.56 | 3.16228 | 1.64342 | 1.27268 |
| 5.62409 | 0.0506 | 50.59 | 5.62341 | 2.09519 | 1.58677 |
| 10.0012 | 0.0367 | 36.66 | 10 | 2.64042 | 2.06416 |
| 17.7849 | 0.027 | 26.97 | 17.7828 | 3.44081 | 2.83543 |
| 31.6266 | 0.0204 | 20.43 | 31.6228 | 4.92656 | 4.13402 |
| 56.2409 | 0.0157 | 15.67 | 56.2341 | 8.97121 | 5.64013 |
| 100.012 | 0.012 | 12.03 | 100 | 18.0401 | -0.162607 |
| 177.849 | 0.00939 | 9.39 | | | |
| 300.036 | 0.00781 | 7.81 | | | |

Fourth Inj

825ppm FP6040 in 1000ppm NaCl and 400ppm NaHCO3 01/09/2019 in column

| K | 132.54 | n | 0.468 | tr | 1.9084698 |
|---|---|---|---|---|---|
| Shear rate | Viscosity | Viscosity | Angular freq | Storage mod | Loss modulus |
| 1/s | Pa.s | cP | rad/s | dyne/cm² | dyne/cm² |
| 0.100013 | 0.442661 | 442.66 | 0.1 | 0.205648 | 0.330963 |
| 0.17785 | 0.369117 | 369.12 | 0.177828 | 0.333964 | 0.436855 |
| 0.316268 | 0.26762 | 267.62 | 0.316228 | 0.499589 | 0.55779 |
| 0.562411 | 0.190613 | 190.61 | 0.562341 | 0.713746 | 0.702826 |
| 1.00013 | 0.138872 | 138.87 | 1 | 0.972873 | 0.859753 |
| 1.77849 | 0.0997517 | 99.75 | 1.77828 | 1.29754 | 1.04648 |
| 3.16266 | 0.0716004 | 71.6 | 3.16228 | 1.66159 | 1.27775 |
| 5.62409 | 0.051341 | 51.34 | 5.62341 | 2.1086 | 1.60144 |
| 10.0012 | 0.0371362 | 37.14 | 10 | 2.66478 | 2.059 |
| 17.7849 | 0.0273439 | 27.34 | 17.7828 | 3.45628 | 2.82795 |
| 31.6266 | 0.0206923 | 20.69 | 31.6228 | 4.94536 | 4.13203 |
| 56.2408 | 0.0158911 | 15.89 | 56.2341 | 9.01046 | 5.60282 |
| 100.012 | 0.0121619 | 12.16 | 100 | 17.9009 | -0.060431 |
| 177.849 | 0.00945 | 9.45 | | | |
| 300.036 | 0.00796 | 7.96 | | | |

Fifth Inj

1500ppm 3330s in 1000ppm NaCl and 400ppm NaHCO3 01/22/2019 after filter

| K | 106.06 | n | 0.62 | tr | 0.0237138 |
|---|---|---|---|---|---|
| Shear rate | Viscosity | Viscosity | Angular freq | Storage mod | Loss modulus |
| 1/s | Pa.s | cP | rad/s | dyne/cm² | dyne/cm² |
| 0.100013 | 0.126091 | 126.09 | 0.1 | 0.0114446 | 0.119887 |
| 0.17785 | 0.119518 | 119.52 | 0.177828 | 0.028756 | 0.204914 |
| 0.316268 | 0.109198 | 109.2 | 0.316228 | 0.0753353 | 0.340364 |
| 0.562412 | 0.10446 | 104.46 | 0.562341 | 0.16923 | 0.549112 |
| 1.00013 | 0.0950969 | 95.1 | 1 | 0.336457 | 0.838628 |
| 1.77849 | 0.0837544 | 83.75 | 1.77828 | 0.618562 | 1.2294 |
| 3.16266 | 0.0714005 | 71.4 | 3.16228 | 1.04436 | 1.73112 |
| 5.62408 | 0.0589773 | 58.98 | 5.62341 | 1.64938 | 2.37031 |
| 10.0012 | 0.0473592 | 47.36 | 10 | 2.50251 | 3.20154 |
| 17.7849 | 0.0372343 | 37.23 | 17.7828 | 3.71897 | 4.36808 |
| 31.6265 | 0.0288535 | 28.85 | 31.6228 | 5.67473 | 6.11842 |
| 56.2409 | 0.0221967 | 22.2 | 56.2341 | 9.78969 | 8.62838 |
| 100.012 | 0.017108 | 17.11 | 100 | 20.8536 | 8.14882 |
| 177.849 | 0.0134581 | 13.46 | | | |
| 300.036 | 0.0108 | 10.83 | | | |

Sixth

1000ppm 3630s in 1000ppm NaCl and 400ppm NaHCO3 for boise1_4

| k | 130.55 | n | 0.488 | tr | 1.185767 |
|---|---|---|---|---|---|
| Shear rate | Viscosity | Viscosity | Angular freq | Storage mod | Loss modulus |
| 1/s | Pa.s | cP | rad/s | dyne/cm² | dyne/cm² |
| 0.100013 | 0.397067 | 397.07 | 0.1 | 0.164175 | 0.302898 |
| 0.17785 | 0.343356 | 343.36 | 0.177828 | 0.279647 | 0.413896 |
| 0.316268 | 0.254515 | 254.52 | 0.316228 | 0.432259 | 0.54455 |
| 0.562412 | 0.188865 | 188.87 | 0.562341 | 0.644631 | 0.69532 |
| 1.00013 | 0.136742 | 136.74 | 1 | 0.894791 | 0.866762 |
| 1.77849 | 0.0994975 | 99.5 | 1.77828 | 1.20746 | 1.07695 |
| 3.16266 | 0.0720528 | 72.05 | 3.16228 | 1.58762 | 1.33975 |
| 5.62408 | 0.052496 | 52.5 | 5.62341 | 2.0618 | 1.68514 |
| 10.0012 | 0.0383795 | 38.38 | 10 | 2.64643 | 2.19102 |
| 17.7849 | 0.0285142 | 28.51 | 17.7828 | 3.46803 | 2.99635 |
| 31.6266 | 0.0217275 | 21.73 | 31.6228 | 4.95414 | 4.37643 |
| 56.2408 | 0.0169571 | 16.96 | 56.2341 | 8.93012 | 6.17905 |
| 100.012 | 0.013188 | 13.19 | 100 | 18.6078 | 1.33812 |
| 177.849 | 0.0104049 | 10.4 | | | |
| 300.036 | 0.00903 | 9.03 | | | |

# Appendix F

## Polymer Rheology: Experiment #3 Boise

1000ppm 3630s in 1000ppm NaCl and 400ppm NaHCO3

| | time | 1.49335086 | | | |
|---|---|---|---|---|---|
| **Shear rate** | **Viscosity** | **Viscosity** | **Angular freq** | **Storage mod** | **Loss modulus** |
| **1/s** | **Pa.s** | **cP** | **rad/s** | **dyne/cm²** | **dyne/cm²** |
| 0.100013 | 0.365731 | 365.731 | 0.1 | 1.85E-01 | 0.316846 |
| 0.17785 | 0.320537 | 320.537 | 0.177828 | 3.11E-01 | 0.426589 |
| 0.316268 | 0.245421 | 245.421 | 0.316228 | 0.475802 | 0.54534 |
| 0.562412 | 0.1871 | 187.1 | 0.562341 | 0.668787 | 0.694786 |
| 1.00013 | 0.136742 | 136.742 | 1 | 0.929847 | 0.851872 |
| 1.77849 | 0.0994898 | 99.4898 | 1.77828 | 1.24206 | 1.04799 |
| 3.16266 | 0.0722806 | 72.2806 | 3.16228 | 1.61001 | 1.30226 |
| 5.62408 | 0.0525393 | 52.5393 | 5.62341 | 2.06168 | 1.62904 |
| 10.0012 | 0.0384695 | 38.4695 | 10 | 2.63155 | 2.13001 |
| 17.7849 | 0.028703 | 28.703 | 17.7828 | 3.46015 | 2.92693 |
| 31.6266 | 0.022044 | 22.044 | 31.6228 | 5.00539 | 4.19942 |
| 56.2409 | 1.71E-02 | 17.14 | 56.2341 | 8.97599 | 5.66509 |
| 100.012 | 1.34E-02 | 13.35 | 100 | 17.7219 | 0.940322 |
| 177.849 | 1.06E-02 | 10.62 | | | |
| 300.036 | 9.28E-03 | 9.28 | | | |

900ppm Scleroglucan in 1000ppm NaCl and 400ppm NaHCO3

| | | | 0.0789266 | | |
|---|---|---|---|---|---|
| Shear rate | Viscosity | Viscosity | Angular freq | Storage mod | Loss modulus |
| 1/s | Pa.s | cP | rad/s | dyne/cm² | dyne/cm² |
| 0.100013 | 0.120958 | 120.958 | 0.1 | 8.08E-03 | 0.1141 |
| 0.17785 | 0.12185 | 121.85 | 0.177828 | 2.93E-02 | 0.190402 |
| 0.316267 | 0.11051 | 110.51 | 0.316228 | 0.0725204 | 0.314234 |
| 0.562413 | 0.0952312 | 95.2312 | 0.562341 | 0.14574 | 0.511322 |
| 1.00013 | 0.0833389 | 83.3389 | 1 | 0.301532 | 0.79239 |
| 1.77849 | 0.0711238 | 71.1238 | 1.77828 | 0.590007 | 1.16656 |
| 3.16266 | 0.0579432 | 57.9432 | 3.16228 | 1.03998 | 1.60142 |
| 5.62409 | 0.0447785 | 44.7785 | 5.62341 | 1.66385 | 2.09337 |
| 10.0012 | 0.0331454 | 33.1454 | 10 | 2.50392 | 2.65295 |
| 17.7849 | 0.0238049 | 23.8049 | 17.7828 | 3.61691 | 3.40081 |
| 31.6266 | 0.0167627 | 16.7627 | 31.6228 | 5.44929 | 4.57608 |
| 56.2409 | 0.0117218 | 11.7218 | 56.2341 | 9.92276 | 5.83756 |
| 100.012 | 0.00829 | 8.29 | 100 | 19.3825 | -2.88357 |
| 177.849 | 0.00601 | 6.01 | | | |
| 300.036 | 0.00462 | 4.62 | | | |

1000ppm 3630s in 1000ppm NaCl and 400ppm NaHCO3

| Shear rate | Viscosity | Viscosity | Angular freq | Storage mod | Loss modulus |
|---|---|---|---|---|---|
| 1/s | Pa.s | cP | rad/s | dyne/cm² | dyne/cm² |
| 0.100013 | 0.333909 | 333.909 | 0.1 | 0.121891 | 0.261315 |
| 0.177848 | 0.291812 | 291.812 | 0.177828 | 0.226558 | 0.369093 |
| 0.31627 | 0.216033 | 216.033 | 0.316228 | 0.36886 | 0.478491 |
| 0.562413 | 0.170123 | 170.123 | 0.562341 | 0.544371 | 0.618393 |
| 1.00013 | 0.125461 | 125.461 | 1 | 0.76922 | 0.776875 |
| 1.77849 | 0.0892434 | 89.2434 | 1.77828 | 1.06311 | 0.973959 |
| 3.16265 | 0.0659319 | 65.9319 | 3.16228 | 1.3942 | 1.22024 |
| 5.62408 | 0.0481411 | 48.1411 | 5.62341 | 1.82462 | 1.53754 |
| 10.0012 | 0.0354194 | 35.4194 | 10 | 2.36122 | 2.01538 |
| 17.7849 | 0.0262852 | 26.2852 | 17.7828 | 3.15189 | 2.77568 |
| 31.6266 | 0.0200442 | 20.0442 | 31.6228 | 4.73206 | 4.00233 |
| 56.2408 | 0.0156919 | 15.6919 | 56.2341 | 8.78648 | 5.12876 |
| 100.012 | 0.012274 | 12.274 | 100 | 16.5579 | 0.300734 |
| 177.849 | 0.00974 | 9.74 | | | |
| 300.036 | 0.00832 | 8.32 | | | |

2200ppm 3630s in 20000ppm NaCl and 400ppm NaHCO3 #2

| | time | 0.04845431 | | | |
|---|---|---|---|---|---|
| **Shear rate** | **Viscosity** | **Viscosity** | **Angular freq** | **Storage mod** | **Loss modulus** |
| **1/s** | **Pa.s** | **cP** | **rad/s** | **dyne/cm²** | **dyne/cm²** |
| 0.100013 | 0.191594 | 191.594 | 0.1 | 3.28E-02 | 0.164255 |
| 0.17785 | 0.188581 | 188.581 | 0.177828 | 8.21E-02 | 0.260944 |
| 0.316268 | 0.160682 | 160.682 | 0.316228 | 0.167156 | 0.402098 |
| 0.562412 | 0.132408 | 132.408 | 0.562341 | 0.317407 | 0.572037 |
| 1.00013 | 0.106307 | 106.307 | 1 | 0.507668 | 0.794327 |
| 1.77849 | 0.0855878 | 85.5878 | 1.77828 | 0.797508 | 1.06891 |
| 3.16266 | 0.067683 | 67.683 | 3.16228 | 1.18063 | 1.40418 |
| 5.62409 | 0.0527098 | 52.7098 | 5.62341 | 1.6674 | 1.83339 |
| 10.0012 | 0.0406193 | 40.6193 | 10 | 2.32451 | 2.42518 |
| 17.7849 | 0.0311873 | 31.1873 | 17.7828 | 3.26637 | 3.31304 |
| 31.6266 | 0.0241451 | 24.1451 | 31.6228 | 4.92557 | 4.7329 |
| 56.2408 | 1.94E-02 | 19.36 | 56.2341 | 8.94924 | 6.38301 |
| 100.012 | 1.58E-02 | 15.75 | 100 | 18.2964 | 2.87384 |
| 177.849 | 1.31E-02 | 13.06 | | | |
| 300.036 | 1.15E-02 | 11.45 | | | |

# Appendix G

## Polymer Rheology: Experiment #4 Oil Wet Bentheimer

PF1

1000ppm 3630s in 1000ppm NaCl and 400ppm NaHCO3

| k | | n | | tr | 1.24361404 |
|---|---|---|---|---|---|
| **Shear rate** | **Viscosity** | **Viscosity** | **Angular freq** | **Storage mod** | **Loss modulus** |
| **1/s** | **Pa.s** | **cP** | **rad/s** | **dyne/cm²** | **dyne/cm²** |
| 0.100013 | 0.328155 | 328.155 | 0.1 | 0.163848 | 0.292156 |
| 0.17785 | 0.315308 | 315.308 | 0.177828 | 0.275625 | 0.397054 |
| 0.316267 | 0.241489 | 241.489 | 0.316228 | 0.425877 | 0.520751 |
| 0.562412 | 0.177947 | 177.947 | 0.562341 | 0.619822 | 0.663178 |
| 1.00013 | 0.13144 | 131.44 | 1 | 0.869877 | 0.834751 |
| 1.77849 | 0.0968801 | 96.8801 | 1.77828 | 1.16743 | 1.0362 |
| 3.16266 | 0.0709011 | 70.9011 | 3.16228 | 1.53757 | 1.29205 |
| 5.62409 | 0.0518919 | 51.8919 | 5.62341 | 1.98391 | 1.62885 |
| 10.0012 | 0.0381934 | 38.1934 | 10 | 2.56121 | 2.13079 |
| 17.7849 | 0.0286036 | 28.6036 | 17.7828 | 3.4091 | 2.93632 |
| 31.6266 | 0.0220122 | 22.0122 | 31.6228 | 5.00537 | 4.19127 |
| 56.2409 | 0.0170531 | 17.0531 | 56.2341 | 8.92491 | 5.39964 |
| 100.012 | 0.0132774 | 13.2774 | 100 | 17.44 | 0.728594 |
| 177.849 | 0.0107313 | 10.7313 | | | |
| 300.036 | 9.97E-03 | 9.97E+00 | | | |

PF2

2200ppm 3630s in 20000ppm NaCl and 400ppm NaHCO3

| k | | n | | tr | 0.02628826 |
|---|---|---|---|---|---|
| **Shear rate** | **Viscosity** | **Viscosity** | **Angular freq** | **Storage mod** | **Loss modulus** |
| **1/s** | **Pa.s** | **cP** | **rad/s** | **dyne/cm²** | **dyne/cm²** |
| 0.100013 | 0.201576 | 201.576 | 0.1 | 0.0361555 | 0.16297 |
| 0.17785 | 0.178987 | 178.987 | 0.177828 | 0.0791715 | 0.256628 |
| 0.316268 | 0.154202 | 154.202 | 0.316228 | 0.159152 | 0.394912 |
| 0.562412 | 0.12474 | 124.74 | 0.562341 | 0.294945 | 0.566295 |
| 1.00013 | 0.103355 | 103.355 | 1 | 0.495152 | 0.791011 |
| 1.77849 | 0.0832727 | 83.2727 | 1.77828 | 0.781933 | 1.06666 |
| 3.16266 | 0.0665576 | 66.5576 | 3.16228 | 1.16464 | 1.41265 |
| 5.62409 | 0.0520681 | 52.0681 | 5.62341 | 1.65826 | 1.85467 |
| 10.0012 | 0.0402889 | 40.2889 | 10 | 2.30973 | 2.4582 |
| 17.7849 | 0.031036 | 31.036 | 17.7828 | 3.225 | 3.36453 |
| 31.6266 | 0.024066 | 24.066 | 31.6228 | 4.8038 | 4.83729 |
| 56.2409 | 0.0192767 | 19.2767 | 56.2341 | 8.68239 | 6.82796 |
| 100.012 | 0.0156933 | 15.6933 | 100 | 18.5785 | 3.86965 |
| 177.849 | 0.0128942 | 12.8942 | | | |
| 300.036 | 0.0115464 | 11.5464 | | | |

PF3

2750ppm 3630s in 50000ppm NaCl and 400ppm NaHCO3

| k | | n | | tr | 0.06216586 |
|---|---|---|---|---|---|
| **Shear rate** | **Viscosity** | **Viscosity** | **Angular freq** | **Storage mod** | **Loss modulus** |
| **1/s** | **Pa.s** | **cP** | **rad/s** | **dyne/cm²** | **dyne/cm²** |
| 0.100013 | 0.209944 | 209.944 | 0.1 | 0.046905 | 0.191845 |
| 0.17785 | 0.198894 | 198.894 | 0.177828 | 0.093306 | 0.301989 |
| 0.316267 | 0.178563 | 178.563 | 0.316228 | 0.197146 | 0.46223 |
| 0.562413 | 0.152605 | 152.605 | 0.562341 | 0.363965 | 0.658883 |
| 1.00013 | 0.122561 | 122.561 | 1 | 0.603118 | 0.91676 |
| 1.77849 | 0.0982854 | 98.2854 | 1.77828 | 0.933105 | 1.21777 |
| 3.16266 | 0.0778739 | 77.8739 | 3.16228 | 1.37074 | 1.58979 |
| 5.62409 | 0.0601084 | 60.1084 | 5.62341 | 1.94087 | 2.06619 |
| 10.0012 | 0.0460544 | 46.0544 | 10 | 2.67058 | 2.72331 |
| 17.7849 | 0.0351982 | 35.1982 | 17.7828 | 3.71025 | 3.68937 |
| 31.6266 | 0.0272407 | 27.2407 | 31.6228 | 5.51035 | 5.19812 |
| 56.2408 | 0.0219441 | 21.9441 | 56.2341 | 9.63868 | 7.13105 |
| 100.012 | 0.0178754 | 17.8754 | 100 | 20.0925 | 3.92619 |
| 177.849 | 0.0150565 | 15.0565 | | | |
| 300.036 | 0.0133559 | 13.3559 | | | |

PF4

2200ppm 3630s in 20000ppm NaCl and 400ppm NaHCO3

| k | | n | | tr | 0.05111926 |
|---|---|---|---|---|---|
| **Shear rate** | **Viscosity** | **Viscosity** | **Angular freq** | **Storage mod** | **Loss modulus** |
| **1/s** | **Pa.s** | **cP** | **rad/s** | **dyne/cm²** | **dyne/cm²** |
| 0.100013 | 0.198139 | 198.139 | 0.1 | 0.039137 | 0.172719 |
| 0.17785 | 0.20457 | 204.57 | 0.177828 | 0.0861274 | 0.277549 |
| 0.316268 | 0.170688 | 170.688 | 0.316228 | 0.176056 | 0.42505 |
| 0.562412 | 0.133577 | 133.577 | 0.562341 | 0.32142 | 0.61768 |
| 1.00013 | 0.111985 | 111.985 | 1 | 0.543275 | 0.861937 |
| 1.77849 | 0.0895801 | 89.5801 | 1.77828 | 0.848675 | 1.15731 |
| 3.16266 | 0.0715295 | 71.5295 | 3.16228 | 1.27968 | 1.51831 |
| 5.62409 | 0.055709 | 55.709 | 5.62341 | 1.81135 | 1.9866 |
| 10.0012 | 0.0430123 | 43.0123 | 10 | 2.52333 | 2.61664 |
| 17.7849 | 0.0330007 | 33.0007 | 17.7828 | 3.52311 | 3.55198 |
| 31.6266 | 0.0254245 | 25.4245 | 31.6228 | 5.21789 | 5.00598 |
| 56.2409 | 0.0200764 | 20.0764 | 56.2341 | 9.17951 | 6.94404 |
| 100.012 | 0.0163775 | 16.3775 | 100 | 19.164 | 4.19868 |
| 177.849 | 0.0135184 | 13.5184 | | | |
| 300.036 | 0.0123292 | 12.3292 | | | |

PF5

1000ppm 3630s in 1000ppm NaCl and 400ppm NaHCO3

| k | | n | | tr | 1.28542305 |
|---|---|---|---|---|---|
| **Shear rate** | **Viscosity** | **Viscosity** | **Angular freq** | **Storage mod** | **Loss modulus** |
| **1/s** | **Pa.s** | **cP** | **rad/s** | **dyne/cm²** | **dyne/cm²** |
| 0.100013 | 0.333592 | 333.592 | 0.1 | 0.145204 | 0.27325 |
| 0.17785 | 0.309965 | 309.965 | 0.177828 | 0.257277 | 0.373594 |
| 0.316268 | 0.223321 | 223.321 | 0.316228 | 0.400624 | 0.489026 |
| 0.562412 | 0.165185 | 165.185 | 0.562341 | 0.576478 | 0.622392 |
| 1.00013 | 0.11966 | 119.66 | 1 | 0.814362 | 0.767487 |
| 1.77849 | 0.0877404 | 87.7404 | 1.77828 | 1.08246 | 0.961089 |
| 3.16266 | 0.0644267 | 64.4267 | 3.16228 | 1.42989 | 1.18855 |
| 5.62408 | 0.0474149 | 47.4149 | 5.62341 | 1.83134 | 1.51024 |
| 10.0012 | 0.0350485 | 35.0485 | 10 | 2.36162 | 1.99136 |
| 17.7849 | 0.0263943 | 26.3943 | 17.7828 | 3.15187 | 2.75377 |
| 31.6266 | 0.0204254 | 20.4254 | 31.6228 | 4.68978 | 3.94488 |
| 56.2408 | 0.0159826 | 15.9826 | 56.2341 | 8.62667 | 5.054 |
| 100.012 | 0.0124888 | 12.4888 | 100 | 16.3899 | 0.560016 |
| 177.849 | 0.0101312 | 10.1312 | | | |
| 300.036 | 9.17E-03 | 9.17E+00 | | | |

# Appendix H

## Polymer Rheology: Experiment #5 Oil Wet Bentheimer

2200ppm 3630s in 20000ppm NaCl and 400ppm NaHCO3

| | | 0.04688408 | | | |
|---|---|---|---|---|---|
| **Shear rate** | **Viscosity** | **Viscosity** | **Angular freq** | **Storage mod** | **Loss modulus** |
| **1/s** | **Pa.s** | **cP** | **rad/s** | **dyne/cm²** | **dyne/cm²** |
| 0.100013 | 0.22042 | 220.42 | 0.1 | 4.49E-02 | 0.176313 |
| 0.17785 | 0.202589 | 202.589 | 0.177828 | 9.46E-02 | 0.276135 |
| 0.316268 | 0.173194 | 173.194 | 0.316228 | 0.184659 | 0.413069 |
| 0.562411 | 0.144606 | 144.606 | 0.562341 | 0.328618 | 0.597031 |
| 1.00013 | 0.112037 | 112.037 | 1 | 0.53374 | 0.82367 |
| 1.77849 | 0.0895581 | 89.5581 | 1.77828 | 0.833282 | 1.09796 |
| 3.16265 | 0.0708503 | 70.8503 | 3.16228 | 1.21951 | 1.43512 |
| 5.62408 | 0.0548056 | 54.8056 | 5.62341 | 1.74228 | 1.87724 |
| 10.0012 | 0.042019 | 42.019 | 10 | 2.40093 | 2.4707 |
| 17.7849 | 0.0321642 | 32.1642 | 17.7828 | 3.33541 | 3.38055 |
| 31.6266 | 0.0249077 | 24.9077 | 31.6228 | 4.96687 | 4.84298 |
| 56.2408 | 2.00E-02 | 20.01 | 56.2341 | 9.00135 | 6.73714 |
| 100.012 | 1.63E-02 | 16.29 | 100 | 18.8788 | 3.35528 |
| 177.849 | 1.37E-02 | 13.71 | | | |
| 300.036 | 1.16E-02 | 11.57 | | | |

1000ppm 3630s in 1000ppm NaCl and 400ppm NaHCO3

| | time | 1.49335086 | | | |
|---|---|---|---|---|---|
| **Shear rate** | **Viscosity** | **Viscosity** | **Angular freq** | **Storage mod** | **Loss modulus** |
| **1/s** | **Pa.s** | **cP** | **rad/s** | **dyne/cm²** | **dyne/cm²** |
| 0.100013 | 0.365731 | 365.731 | 0.1 | 1.85E-01 | 0.316846 |
| 0.17785 | 0.320537 | 320.537 | 0.177828 | 3.11E-01 | 0.426589 |
| 0.316268 | 0.245421 | 245.421 | 0.316228 | 0.475802 | 0.54534 |
| 0.562412 | 0.1871 | 187.1 | 0.562341 | 0.668787 | 0.694786 |
| 1.00013 | 0.136742 | 136.742 | 1 | 0.929847 | 0.851872 |
| 1.77849 | 0.0994898 | 99.4898 | 1.77828 | 1.24206 | 1.04799 |
| 3.16266 | 0.0722806 | 72.2806 | 3.16228 | 1.61001 | 1.30226 |
| 5.62408 | 0.0525393 | 52.5393 | 5.62341 | 2.06168 | 1.62904 |
| 10.0012 | 0.0384695 | 38.4695 | 10 | 2.63155 | 2.13001 |
| 17.7849 | 0.028703 | 28.703 | 17.7828 | 3.46015 | 2.92693 |
| 31.6266 | 0.022044 | 22.044 | 31.6228 | 5.00539 | 4.19942 |
| 56.2409 | 1.71E-02 | 17.14 | 56.2341 | 8.97599 | 5.66509 |
| 100.012 | 1.34E-02 | 13.35 | 100 | 17.7219 | 0.940322 |
| 177.849 | 1.06E-02 | 10.62 | | | |
| 300.036 | 9.28E-03 | 9.28 | | | |

2200ppm 3630s in 20000ppm NaCl and 400ppm NaHCO3 #2

| | time | 0.04845431 | | | |
|---|---|---|---|---|---|
| **Shear rate** | **Viscosity** | **Viscosity** | **Angular freq** | **Storage mod** | **Loss modulus** |
| **1/s** | **Pa.s** | **cP** | **rad/s** | **dyne/cm²** | **dyne/cm²** |
| 0.100013 | 0.191594 | 191.594 | 0.1 | 3.28E-02 | 0.164255 |
| 0.17785 | 0.188581 | 188.581 | 0.177828 | 8.21E-02 | 0.260944 |
| 0.316268 | 0.160682 | 160.682 | 0.316228 | 0.167156 | 0.402098 |
| 0.562412 | 0.132408 | 132.408 | 0.562341 | 0.317407 | 0.572037 |
| 1.00013 | 0.106307 | 106.307 | 1 | 0.507668 | 0.794327 |
| 1.77849 | 0.0855878 | 85.5878 | 1.77828 | 0.797508 | 1.06891 |
| 3.16266 | 0.067683 | 67.683 | 3.16228 | 1.18063 | 1.40418 |
| 5.62409 | 0.0527098 | 52.7098 | 5.62341 | 1.6674 | 1.83339 |
| 10.0012 | 0.0406193 | 40.6193 | 10 | 2.32451 | 2.42518 |
| 17.7849 | 0.0311873 | 31.1873 | 17.7828 | 3.26637 | 3.31304 |
| 31.6266 | 0.0241451 | 24.1451 | 31.6228 | 4.92557 | 4.7329 |
| 56.2408 | 1.94E-02 | 19.36 | 56.2341 | 8.94924 | 6.38301 |
| 100.012 | 1.58E-02 | 15.75 | 100 | 18.2964 | 2.87384 |
| 177.849 | 1.31E-02 | 13.06 | | | |
| 300.036 | 1.15E-02 | 11.45 | | | |

Low Sal Elastic Polymer 3630s

| Shear rate | Viscosity | Viscosity | Angular freq | Storage mod | Loss modulus |
|---|---|---|---|---|---|
| 1/s | Pa.s | cP | rad/s | dyne/cm² | dyne/cm² |
| 0.100013 | 0.333909 | 333.909 | 0.1 | 0.121891 | 0.261315 |
| 0.177848 | 0.291812 | 291.812 | 0.177828 | 0.226558 | 0.369093 |
| 0.31627 | 0.216033 | 216.033 | 0.316228 | 0.36886 | 0.478491 |
| 0.562413 | 0.170123 | 170.123 | 0.562341 | 0.544371 | 0.618393 |
| 1.00013 | 0.125461 | 125.461 | 1 | 0.76922 | 0.776875 |
| 1.77849 | 0.0892434 | 89.2434 | 1.77828 | 1.06311 | 0.973959 |
| 3.16265 | 0.0659319 | 65.9319 | 3.16228 | 1.3942 | 1.22024 |
| 5.62408 | 0.0481411 | 48.1411 | 5.62341 | 1.82462 | 1.53754 |
| 10.0012 | 0.0354194 | 35.4194 | 10 | 2.36122 | 2.01538 |
| 17.7849 | 0.0262852 | 26.2852 | 17.7828 | 3.15189 | 2.77568 |
| 31.6266 | 0.0200442 | 20.0442 | 31.6228 | 4.73206 | 4.00233 |
| 56.2408 | 0.0156919 | 15.6919 | 56.2341 | 8.78648 | 5.12876 |
| 100.012 | 0.012274 | 12.274 | 100 | 16.5579 | 0.300734 |
| 177.849 | 0.00974 | 9.74 | | | |
| 300.036 | 0.00832 | 8.32 | | | |

Polymer A

| Shear rate | Viscosity | Viscosity | Angular freq | Storage mod | Loss modulus |
|---|---|---|---|---|---|
| 1/s | Pa.s | cP | rad/s | dyne/cm² | dyne/cm² |
| 0.100013 | 0.329399 | 329.399 | 0.1 | 0.111196 | 0.240051 |
| 0.177851 | 0.319389 | 319.389 | 0.177828 | 0.202147 | 0.337715 |
| 0.316267 | 0.238425 | 238.425 | 0.316228 | 0.32391 | 0.45781 |
| 0.562411 | 0.175918 | 175.918 | 0.562341 | 0.496753 | 0.595368 |
| 1.00013 | 0.131028 | 131.028 | 1 | 0.716307 | 0.760679 |
| 1.77849 | 0.0938095 | 93.8095 | 1.77828 | 0.993486 | 0.961302 |
| 3.16266 | 0.0685657 | 68.5657 | 3.16228 | 1.34019 | 1.20917 |
| 5.62408 | 0.0492754 | 49.2754 | 5.62341 | 1.75136 | 1.55254 |
| 10.0012 | 0.0361962 | 36.1962 | 10 | 2.29984 | 2.02788 |
| 17.7849 | 0.0268731 | 26.8731 | 17.7828 | 3.10251 | 2.80425 |
| 31.6266 | 0.020501 | 20.501 | 31.6228 | 4.6645 | 4.02312 |
| 56.2409 | 0.0160218 | 16.0218 | 56.2341 | 8.60349 | 5.1782 |
| 100.012 | 0.0125028 | 12.5028 | 100 | 16.5168 | 0.543081 |
| 177.849 | 0.00992 | 9.92 | | | |
| 300.036 | 0.00859 | 8.59 | | | |

1000ppm 3630s in 1000ppm NaCl and 400ppm NaHCO3

| | | | | | for BT |
|---|---|---|---|---|---|
| | | | | k | 130.33 |
| | time | 1.49335086 | | n | 0.492 |
| Shear rate | Viscosity | Viscosity | Angular freq | Storage mod | Loss modulus |
| 1/s | Pa.s | cP | rad/s | dyne/cm² | dyne/cm² |
| 0.100013 | 0.365731 | 365.731 | 0.1 | 1.85E-01 | 0.316846 |
| 0.17785 | 0.320537 | 320.537 | 0.177828 | 3.11E-01 | 0.426589 |
| 0.316268 | 0.245421 | 245.421 | 0.316228 | 0.475802 | 0.54534 |
| 0.562412 | 0.1871 | 187.1 | 0.562341 | 0.668787 | 0.694786 |
| 1.00013 | 0.136742 | 136.742 | 1 | 0.929847 | 0.851872 |
| 1.77849 | 0.0994898 | 99.4898 | 1.77828 | 1.24206 | 1.04799 |
| 3.16266 | 0.0722806 | 72.2806 | 3.16228 | 1.61001 | 1.30226 |
| 5.62408 | 0.0525393 | 52.5393 | 5.62341 | 2.06168 | 1.62904 |
| 10.0012 | 0.0384695 | 38.4695 | 10 | 2.63155 | 2.13001 |
| 17.7849 | 0.028703 | 28.703 | 17.7828 | 3.46015 | 2.92693 |
| 31.6266 | 0.022044 | 22.044 | 31.6228 | 5.00539 | 4.19942 |
| 56.2409 | 1.71E-02 | 17.14 | 56.2341 | 8.97599 | 5.66509 |
| 100.012 | | 13.35 | 100 | 17.7219 | 0.940322 |
| 177.849 | 1.06E-02 | 10.62 | | | |
| 300.036 | 9.28E-03 | 9.28 | | | |

# Bibliography


1. Abidin AZ, Puspasari T, Nugroho WA. Polymers for Enhanced Oil Recovery Technology. *Procedia Chem*. 2012;4:11-16. doi:10.1016/j.proche.2012.06.002.

2. Afsharpoor, A., Balhoff, M. T., Bonnecaze, R., & Huh, C. (2012). CFD modeling of the effect of polymer elasticity on residual oil saturation at the pore-scale. Journal of Petroleum Science and Engineering, 94, 79-88.

3. Alvarado V, Manrique E. Enhanced oil recovery: An update review. *Energies*. 2010;3(9):1529-1575. doi:10.3390/en3091529.

4. Anderson, W. G. (1986, October 1). Wettability Literature Survey- Part 1: Rock/Oil/Brine Interactions and the Effects of Core Handling on Wettability. Society of Petroleum Engineers. doi:10.2118/13932-PA

5. Azad, M.S., Trivedi., J.J., (2019) Quantification of the Viscoelastic Effects During Polymer Flooding: A Critical Review., SPE 195687.

6. Cannella, W.J., Huh, C., Seright, R.S. 1988. Prediction of Xanthan Rheology in Porous Media. Proc. SPE Annu. Tech. Conf. Exhib. doi:10.2523/18089-MS

7. Clarke, A., Howe, A. M., Mitchell, J., Staniland, J., Hawkes, L., and Leeper, K. 2015. Mechanism of anomalously increased oil displacement with aqueous viscoelastic polymer solutions, Soft Matter, 11, 3536.

8. Clarke, A., Howe, A. M., Mitchell, J., Staniland, J., & Hawkes, L. A. (2016). How viscoelastic-polymer flooding enhances displacement efficiency. SPE Journal, 21(03), 675–687.

9. Chatzis, I., & Morrow, N. R. (1984). Correlation of Capillary Number Relationships for Sandstone. Society of Petroleum Engineers Journal, 24(05), 555–562. https://doi.org/10.2118/10114-PA

10. Delshad, M., Kim, D.H., Magbagbeola O.A., Huh, C., Pope, G.A., and Tarahhom, F. 2008. Mechanistic Interpretation and Utilization of Viscoelastic Behavior of Polymer Solutions for Improved Polymer Flood Efficiency. SPE 113620.

11. Ehrenfried, D. 2013.Impact of Viscoelastic Polymer Flooding on Residual oil Saturation in Sandstones, MS Thesis. Austin, Texas: University of Texas at Austin.

12. Erincik, M. Z., Qi, P., Balhoff, M. T., & Pope, G. A. (2017, October). New Method to Reduce Residual Oil Saturation by Polymer Flooding. In SPE Annual Technical Conference and Exhibition. Society of Petroleum Engineers.

13. Erincik, M. Z., (2017) New Method to Reduce Residual Oil Saturation by Polymer Flooding. Masters Thesis, UT Austin.

14. Garrouch, A.A. 1999. A Viscoelastic Model for Polymer Flow in Reservoir Rocks. Paper SPE 54379 presented at the 1999 SPE Asia Pacific Oil and Gas Conference and Exhibition, Jakarta, Indonesia, 20-22 April.

15. Green, D., and Willhite, P. (1998). Enhanced Oil Recovery. Richardson, TX: SPE Textbook Series Volume 6.

16. Green, D. W., & Willhite, G. P. (2018). *Enhanced oil recovery* (Second edition). Richardson, Texas, USA: Society of Petroleum Engineers.

17. Huh, C., & Pope, G. A. (2008, January). Residual oil saturation from polymer floods: laboratory measurements and theoretical interpretation. In SPE Symposium on Improved Oil Recovery. Society of Petroleum Engineers.

18. Humphry, K.J., Suijkerbuijk, M.J.M., van der Linde, H.A., Pieterse, S.G.J., Masalmeh, S.K., Impact of Wettability on Residual Oil Saturation and Capillary Desaturation Curves. *Petrophysics.* 2014;55, 4:313-318.

19. Jin, M. (1995). *A Study of Nonaqueous Phase Liquid Characterization and Surfactant Remediation*. PhD, Dissertation, The University of Texas at Austin

20. Jung JC, Zhang K, Chon BH, Choi HJ. Rheology and polymer flooding characteristics of partially hydrolyzed polyacrylamide for enhanced heavy oil recovery. *J Appl Polym Sci.* 2013;127(6):4833-4839. doi:10.1002/app.38070.

21. Kamal, M.S., Sultan. A. S., Al-Mubaiyedh, U. et al. 2015. Review on Polymer Flooding: Rheology, Adsorption, Stability and Field Applications of Various Polymer Systems. Polym Rev. 55(3): 491-530. https://doi.org/10.1080/15583724.2014.982821.

22. Koh, H. 2015. Experimental Investigation of the Effect of Polymers on Residual oil Saturation, Ph.D. Dissertation. Austin, Texas: University of Texas at Austin.

23. Kokal S, Al-Kaabi A. Enhanced oil recovery: challenges and opportunities. *Glob Energy Solut*. 2010:64-69. http://www.world-petroleum.org/docs/docs/publications/2010yearbook/P64-69_Kokal-Al_Kaabi.pdf.

24. Kumar, N., Gaur, T., & Mandal, A. (2017). Characterization of SPN Pickering emulsions for application in enhanced oil recovery. Journal of Industrial and Engineering Chemistry, 54, 304-315.

25. Lake, L. 1989. Enhanced Oil Recovery. Upper Saddle River, NJ: Prentice - Hall.

26. Masuda, Y., Tang, K.-C., Miyazawa, M., & Tanaka, S. (1992). 1D Simulation of Polymer Flooding Including the Viscoelastic Effect of Polymer Solution. Society of Petroleum Engineers. https://doi.org/10.2118/19499-PA.

27. Meter, D. M., & Bird, R. B. (1964). Tube flow of non-Newtonian polymer solutions: PART I. Laminar flow and rheological models. AIChE Journal, 10(6), 878-881.

28. Needham RB, Doe PH. Polymer Flooding Review. *J Pet Technol*. 1987;39(12):1503-1507. doi:10.2118/17140-PA.

29. Nilsson MA, Kulkarni R, Gerberich L, et al. Effect of fluid rheology on enhanced oil recovery in a microfluidic sandstone device. *J Nonnewton Fluid Mech*. 2013;202:112-119. doi:10.1016/j.jnnfm.2013.09.011.

30. Owens, W. W., & Archer, D. L. (1971, July 1). The Effect of Rock Wettability on Oil-Water Relative Permeability Relationships. Society of Petroleum Engineers. doi:10.2118/3034-PA

31. Peters, E. J. (2012). *Advanced petrophysics* (1st ed). Austin, TX: Live Oak Book Company.

32. Pope, G. A., Wu, W., Narayanaswamy, G., Delshad, M., Sharma, M. M., & Wang, P. (2000). *Modeling Relative Permeability Effects in Gas-Condensate Reservoirs With a New Trapping Model*. SPE Reservoir Evaluation & Engineering, *3*(02), 171–178. https://doi.org/10.2118/62497-PA

33. Qi, P. 2018.*Impact of Viscoelastic Polymer Flooding on Residual oil Saturation in Sandstones*, PhD Thesis. Austin, Texas: University of Texas at Austin.

34. Qi, P., Ehrenfried, D. H., Koh, H., & Balhoff, M. T. (2017). Reduction of Residual Oil Saturation in Sandstone Cores by Use of Viscoelastic Polymers. Society of Petroleum Engineers. https://doi.org/10.2118/179689-PA.

35. Ranjbar, M., Rupp, J., Pusch, G., and Meyn, R. 1992. Quantification and Optimization of Viscoelastic Effects of Polymer Solutions for Enhanced Oil Recovery. Paper SPE 24154 presented at the SPE/DOE Eighth Symposium on Enhanced Oil Recovery, Tulsa, Oklahoma, 22-24 April.

36. Sheng, J., 2010. Modern Chemical Enhanced Oil Recovery: Theory and Practice. Gulf Professional Publishing.

37. Sorbie, K. S. 1991. Polymer Improved Oil Recovery. Glasgow & London: Blackie and Son Ltd.

38. Stegemeier, G. L. (1977). *MECHANISMS OF ENTRAPMENT AND MOBILIZATION OF OIL IN POROUS MEDIA*. In Improved Oil Recovery by Surfactant and Polymer Flooding (pp. 55–91). Elsevier. https://doi.org/10.1016/B978-0-12-641750-0.50007-4

39. Vermolen, E.C.M., van Haasterecht, M.J.T., Masalmeh, S.K., 2014. A Systematic Study of the Polymer Visco-Elastic Effect on Residual Oil Saturation by Core Flooding. Paper SPE-169681-MS

40. Wang, D., Xia, H., Yang, S. et al. 2010. The Influence of Visco-Elasticity on Micro Forces and Displacement Efficiency in Pores, Cores and in the Field. Presented at the SPE EOR Conference at Oil and Gas West Asia, Muscat, 11–13 April. SPE-127453-MS. https://doi.org/10.2118/127453-MS.

41. Wreath, D.G. 1989. A Study of Polymer Flooding and Residual Oil Saturation. Master's Thesis, University of Texas at Austin, Austin, Texas.

42. Ziauddin, M., Montaron, B., Hussain, H., Habashy, T., Seleznev, N., Signer, C., & Abdallah, W. (2007). Fundamentals of Wettability. Schlumberger Oilfield Review.